Preparation of Nano-Structured Macro-Porous Materials

A thesis submitted to the Newcastle University for the degree of Doctor of Philosophy

by

Rozita Mohamed

School of Chemical Engineering and Advanced Materials

Newcastle University

November 2011

Disclaimer

The candidate confirms that the work submitted is her own and that appropriate credit has been given where references have been made to work of others. This is all her work and does not necessarily represent the view of the Newcastle University or any other party.

Abstract

This research reveals a catalyst development towards achieving catalysts with hierarchical porous structures with enhanced mechanical properties by using nano-structured macro-porous PolyHIPE polymer. This work can be divided into two parts: the fabrication and its characterisation of hierarchical metal structure using PHP and other fibre materials; and the fabrication and characterisation of PHP with silica particles and glass wool, further coated with silane material as templates. A catalyst system was successfully fabricated forming a 3D-interconnecting network of pore size, ranging from tens of micrometers and gradually reducing finally to nanometer scale. An electroless deposition flow through method using Ni-B bath solution was performed on the templates and was subsequently heat treated to obtain porous metallic structures, thus providing accessibility for reactants to the surface and for products away from the surface. Meanwhile, silanated templates were produced by surface treatment. This was performed by submerging templates directly into the silanes solution at room temperature (24°C) using a water-ethanol based solution of the silanes. The polymer-metal/alloy or silica functionalized based composite demonstrated a high impact strength. The results showed that not only hierarchical pore structure was formed, but it was also demonstrated that silica particles were totally and uniformly covered/coated by metal deposit and had good adhesion. When used on glass wool, silanation had greatly improved the bond strengths of metal deposits to the templates. SEM micrographs revealed that the formation of cracks were tremendously reduced and exhibited higher bond strengths due to silanated glass surface. It is expected to be more efficient and robust in the case of an enhanced surface area, and most desirable in catalyst applications.

Acknowledgements

In the name of Allah, Most Gracious, Most Merciful. First of all, I would like to express immense gratitude to my supervisor Prof. Galip Akay for giving me the opportunity to work under his supervision and providing me with constant intellectual motivation and continuous guidance. Prof. Akay's commitment and endless support over the years, both academically and personally, have been invaluable and I have been fortune to have worked with him.

I wish to acknowledge and express my sincere appreciation and heartiest gratitude to my husband Mohd. Fauzi for being patient, enduring, making sacrifices, and making it financially possible for me to continue my studies. Most of all, I would like to thank him for being the guardian of our four little angels, Aisyah, Muhamad Azri, Muhammad Azhad and Afiah. To my little angels I would like to say that you have been such fun and so loving, and you have made it possible for mummy to have the courage to complete this thesis. To my parents, Abah, Mak, my siblings and my in-laws I would like to say thank you for your unconditional love, care, tolerance, encouragement and continuous prayer for the success of my PhD program.

This thesis would never have been completed without the support of many individuals. I would like to thank all those that contributed to the work presented in this thesis, especially the CEAM technicians Stewart Latimar, Rob Dixon, Paul Sterling, Simon Daley, Jimmy Banks, Brian Grover and Iain Strong. I would like to thank Vincent Scott and Daniel Padgett for their IT help, and SEM personnel Pauline Carrick and Grant Straines, who captured the best SEM image ever. Last but not least I would like to thank Dr Kath Liddel for the XRD analysis and the entire PIM research group.

Alhamdulillah, thank you Allah for giving me the strength and determination to continue.

TABLE OF CONTENTS

LIST OF FIGURES

LIST OF TABLES

CHAPTER 1

INTRODUCTION

1.1 Overview

Several different approaches are required to fabricate a wide range of nano-structured macro porous materials. The past decade has seen a number of significant breakthroughs in the design and processing of novel porous materials, driven by the rapid growth of emerging applications especially in chemical engineering such as energy conversion and storage and bioprocess engineering such as tissue engineering and DNA sequencing. The emergence of such new technological applications requires a higher level of control over the properties of porous structure. Although catalysis accelerates reaction rates and chemical conversions, accessibility of the reactants to, and removal of products from the catalytic sites are important to realize the full potential of catalysts. Supported catalyst systems are intended for these provisions. The fabrications of catalysts with hierarchical pore structure are either through deposited as a thin film on a support or fabricated as pellets. However these two conventional techniques have certain drawbacks: in coated systems, catalyst adhesion can be non-uniform and weak while the accessibility of the active sites within the interior of the catalyst is hindered due to low porosity, small pore size and connectivity. Therefore, when the reactions are transport limited, even these systems can not provide adequate accessibility of the catalytic sites, since the support materials themselves restrict transport processes. In recent years, the so called ‘structured catalysts’ have become available in order to address these problems.

The accessibility of the nano-sized catalytic sites is achieved most effectively by a hierarchical channel or pore network structures which are ubiquitous in nature (Coppens, 2001; Coppens, 1997), such as the cardio-vascular system or organs (liver,

kidney, lung), and a plant nutrient cycle system. In these systems, the main biophysical-chemical processes are principally controlled at the molecular/nano scale, as many of these processes are transport limited, while the continuous supply and removal of reactants/products is achieved through capillaries/pores of ever increasing diameter. Such a system provides an optimum architecture, incorporating micro-nano scale bio-physically/chemically functional features within the macro-system (organ) through a functional connectivity network (cell-cell communication) at an optimum surface area (for catalytic conversion) per unit organ volume. Such hierarchically structured catalyst systems with fractal-like meso- to macropore size distribution (Coppens and Maschmeyer, 2001) can be expected to be more efficient and robust due to enhanced surface area and accessibility, as well as the fact that the catalyst material also forms the overall structure, providing physical strength and integrity. However, it still remains a challenge to fabricate nanostructured macroporous materials with controlled morphology and interconnected pore structure.

1.2 Scope of the Thesis

The scope of this research is the fabrication of a robust template base material from high internal phase emulsion, production of a PolyHIPE polymer (PHP) having hierarchical pore structure, a template that can be characterized by meso and macropores, a method of depositing metal on a template by an electroless deposition flow through method, and fabrication of a novel material on a template with silica particles and functionalized with silane material, together with other non-metal bondage materials and characterisations.

1.3 Thesis Layout

This thesis is organized in seven chapters which describes the research in a sequential order. Chapter 1 introduces the research background on fabrication of nano-structured macro porous materials, problems encountered by the conventional porous materials and underlined objectives and scope of thesis. The introduction is followed by Chapter

2, an overview of the preparation of materials with hierarchical nanostructures. Also, a description of the fabrication of porous template based methods is given to provide a basis to the procedures used in this thesis. Chapter 3 explains the formation of the PolyHIPE Polymer, its characteristic and application. In Chapter 4, the electroless deposition process is described. Special attention is given to the electroless deposition of Ni-B, its characteristic and its properties. The mechanism of electroless deposition on non-metal substrate is also discussed in this chapter. Chapter 5 details the experimental procedures and describes all the methods and apparatus used. In Chapter 6, a detailed study of the preparation and characterization is presented and results are discussed. Chapter 7 gives the general conclusion and related perspectives, and successful preliminary experiments performed to obtain nano-structured macroporous materials are presented.

CHAPTER 2

LITERATURE REVIEW: FABRICATION OF CATALYSIS WITH HIERARCHICAL PORE STRUCTURE

2.1 Overview

This chapter reviews various template techniques for catalysts system with emphasis on characterisation of fabricated nano-structure macro-porous materials. Also, the methods developed as template strategies are described.

2.2 Introduction

Porous materials with hierarchical pore structure containing both interconnected mesoporous and macroporous structures have recently attracted a great deal of research interest (Yuan and Su, 2005). These materials were reported to have enhanced properties (Kaucic, 2009) over ordered materials porous or single-sized pore materials due to its ability to increase mass transfer and thus prevent fouling when use as catalysts or catalysts substrate. Much effort had devoted to the synthesis, characterisation and applications of uniform mesoporous materials over the last decade, and progress had made in structural, compositional and morphology control for emerging application in catalysis, adsorption, sensors and biotechnology. Practical applications require mesoporous materials having hierarchical pore structure at different length scales in order to achieve highly organised functions, since the limited diffusibility of substrates through confined ordered structure can be a problem. Therefore, to improve the activity of mesoporous catalysts, secondary larger pores have been introduced (Yu et al., 2003). These materials were interesting and useful for catalysis and engineering pore systems since the micropores and mesopores can

enhance the selectivity and surface area, while the macropores can increase mass transfer and reduce transport limitations (Yuan and Su, 2005). The templating technique is a method to create these materials that involves the fabrication of the template with a specific porous structure, followed by coating with desired metal materials and finally removal of the template, leaving a metal structure resembling the original template. The fabrication of these materials were prepared by using a self assembly surfactant or amphiphilic block copolymer species with regards to macrotemplates, for instance colloidal crystal (Lu and Eychmuller, 2008), polymer foams (Colombo, 2008) , bio-cellulose (Wang et al., 2002), emulsions (Akay, 2005), inorganic salt (Zhai and Chang, 2008), and ice crystal (Yokota et al., 2001), or by macroscopic phase separation (Xianglin et al., 2008). These nano-structured macro-porous materials have found a number of applications including HPLC separation, catalysis, fuel cells, biomaterials engineering and microreactors. However, it still remains a challenge to fabricate nano-structured macroporous materials with controlled morphology and interconnected pore structure.

2.3 Preparation of Porous Materials with Hierarchical Pore Structure: Template Based Approached

The template method has become a very simple yet powerful process for the synthesis of nanomaterials (Hulteen and Martin, 1997). To enable the design of hierarchical pore structure materials, coordination of several variations of mesopore structures within the macroporous materials is introduced. For instance, self-assembled molecular aggregates or supramolecular assemblies are usually employed to determine mesostructure. While colloidal crystals, polymer foams, bio-celluloses, emulsions, vesicles, inorganic salts and ice crystals are utilised to obtain macroporous structure.

2.3.1 Colloidal Crystal Templating

According to Liew et al. (2006), the procedure for this templating method can be summarised into four different stages: 1) the assembly of particles into a 3D colloidal

crystal matrix, allowing aggregation in a regular manner; 2) infiltration of organic precursors and surfactant micellar solution within the sphere/particles; 3) solidification of materials; 4) the removal of the template by high-temperature calcination or solvent extraction, leading to the formation of 3D ordered meso-macroporous materials.

Since the particles are spherical in shape, the pores found in this method are typically spherical and can be modified using particles of different shape. The pore structure can be manipulated by varying the size of the colloidal particles (Velev and Lenhoff, 2000). This method is versatile and pore dimension can easily be controlled. Work by Sen et al. (2004) demonstrates a series of hierarchically ordered porous silica composites with three different scale pore size. A variety of porous materials can be produced by colloidal crystal templating, both organic and inorganic, using a wide range of materials, typically latex and silica microspheres (Xia et al., 2000; Velev et al., 1998). Other hierarchical materials that have been reported include titania, niobia and silica-alumina (Yuan and Su, 2005). Yang et al. (1998) reported a fabrication of hierarchically ordered structures ranging from ten nanometers to several micrometers using polystyrene spheres and corporative assembly of hydrolyzed inorganic species and amphiphilic surfactant, while Danumah et al. (2001) present an eggshell type macrostructure with an MCM-48 type cubic mesophase by adding a mixed solution of cetyltrimethylammonium chloride/hydroxide and tetraethylorthosilicate with latex spheres.

Although this method appears to be compatible, inexpensive and controllable, calcination or solvent extraction often destroy the pore dimension, thus it is impossible to control the length scale of the solid porous skeleton containing the 3D array of pores (Liew et al., 2006).

2.3.2 Emulsions

The emulsion templating process is relatively simple and cheap, and emulsion droplets can be easily produced. The pore structure can be tailored by using different emulsion

conditions according to the requirement. Thus, the final pore structure can be controlled to different diffusion and reaction conditions. With this method, a wide variety of inorganic porous materials can be produced using metal oxide (Roger et al., 1994) and organic polymer gel (Zhang and Cooper, 2005). The oil droplets produced during polymerization is highly deformable, allowing the inorganic metal oxide to accommodate large shrinkage which prevents cracking and pulverization during ageing and drying. Templates using a rigid sphere, by contrast, tend to break into small pieces. The templates are usually removed by evaporation, dissolution or heat treatment.

Imhof and Pine (1997) first reported the use of emulsion droplets as templates to produce crystal–like assembles, followed by depositing of material through a sol-gel process for the formation of porous titania, zirconia and silica. It was a breakthrough and important development in terms of the methods used to construct hierarchical pore structure. Further investigation was made by Akay and co workers, who reported the fabrication of nanostructure micro-porous materials using polymerization of a high internal phase emulsion as a template in bioprocess-chemical process intensification (Akay, 2006), agro process intensification (Burke, 2008) and tissue engineering (Akay, 2005). A macro-mesoporous silica material was studied by Sen et al. (2003) using an oil-in-water emulsion containing cetyltrimethylammonium bromide as a surfactant. This material produced a three dimensional interconnected pore structure with a surface area of about 800 m^2/g^{-1}. In addition, Cooper and co-worker studied the fabrication of hierarchical porous emulsion-templated polymer/silica composite beads by polymerization of a high internal phase emulsion (Cooper and Holmes, 1999). Besides the oil and aqueous phase fraction, other factors that contribute to the structural change must also be taken into consideration, as described in Chapter 3. As demonstrated by Carn et al. (2004), a porous silica monolith with hierarchical pore structure can be produced with emphasis on the pH condition. Other researchers have also reported having produced materials with low bulk density < 0.01 gcm^{-3}, high mesopore volume > $2cm^3\ g^{-1}$ and high surface area >1000 $m^2\ g^{-1}$, attributed to good control over the properties (Suzuki et al., 2003).

2.3.3 Natural Biological Template

The use of natural biological materials as templates to construct novel hierarchical inorganic materials is an emerging area because of their unique and complex structure. Among the typical examples of natural biological templates there are natural cellulose matrices such as filter papers, fabrics, cotton (Su et al., 2007), plant leaves, wood (Li et al., 2008), eggshell membranes, insect wings (e.g. butterfly), and bacterial thread. These materials comprise an irregular open cell shape, formed from interconnected wire-like fibres. Davis et al. (1997) reported a fabrication of ordered macroporous fibres of either amorphous silica or ordered mesoporous silica mesophase using bacteria consisting of a thread of co-aligned multicellular filaments arranged in a hexagonal packing. The pore size was determined by the diameter of the bacteria filaments and was difficult to control. The structural morphology was influenced by the silica sol which was infiltrated through the bacteria thread initially, and subsequently followed by heat treatment to remove the template. The template produced tended to shrink as a result of sintering and the long and tedius time required to achieve the complete infiltration for the mineralization process, thus limiting its application.

Since natural cellulose matrices have anisotropic cellulose structures, they can be used as a hierarchical template to produce hierarchically porous structure materials. Through mineralization of wood cellular structure using a surfactant-templated sol-gel solution at different pH values, porous ceramic was successfully produced (Shin et al., 2003), replicating the hierarchical structure of the wood cellulose. Since wood was also used as a carbon precursor, further investigation was undertaken by mineralizing wood with silica in acidic condition, followed by carbothermal reduction in argon. This resulted in the formation of hierarchical SiC with wood cellular structure (Shin et al., 2005). However, there is no control over the pore structure as these dimensions are determined by the morphology of the original templates.

2.3.4 Other Techniques

In order to fully utilize available resources, other techniques were employed for the fabrication of nanostructure microporous materials. Inorganic salt plays an important role in the formation of the meso-macro silica structures that are grown at the interface of inorganic salt solution droplets (Yuan and Su, 2005). Depending on the evaporation rate of the solvent, the pore range that is controlled by the size of the salt solution can be adjusted accordingly. Additionally, Zhao et al. (1999) reported on a formation of sponge-like silica membrane with 3D meso-macrostructures produced by a multiphase process in the presence of inorganic salt and a mesoscopically ordered block copolymer/silica phase that macroscopically separates from an electrolyte phase. This result in hierarchically organized composite structures whose different characteristic length scales can be independently adjusted.

On the other hand, micrometer-size ice crystals were used as template to prepare ordered macroporous silica, silica gel microhoneycomb, by Nishihara et al. (2005). Basically, their method involved immersing the hydrogels, hydrosols or aqueous slurries of metal oxide or polymer in a cold bath. The quick freeze led to the growth of micrometer ice spheres inside their matrices, which was due to thermal induced phase separation. These ice spheres then acted as templates forming a 3D interconnected macroporous metal oxide or polymer. The pore size could be controlled by changing the immersion rate into a cold bath and the freezing temperature without changing the micro and mesoporosity of their honeycomb walls.

2.4 Method to Incorporate Metal inside the Hierarchical Pore System

Since metallic nanostructured materials are one of the most active fields owing to their unique potential application in chemical, biomedical electronics and energy storage (Huczko, 2000), a lot of methods have been employed to prepare metallic nanostuctured materials such as inert gas condensation, plasma processing, physical and chemical vapour deposition, electrodeposition, mechanical alloying, sol gel, micro emulsion and

severe plastic deformation (Suryanarayana, 2002). Although the use of many such techniques is limited to laboratory scale, inert gas condensation, mechanical alloying and electrodeposition are among the methods that are available for commercial use (Bera et al., 2004). In this section, methods commonly used for the preparation of metallic nanostructure are presented.

2.4.1 Deposition Technique

Many metal depositions require special reaction conditions influence by various parameters including applied temperature, concentration and the reduction potential of the reducing agent. As the consequences, the whole system use needs to exhibit a sufficient physical and chemical stability toward suitable conditions for metal deposition. Therefore, certain aspects need to be considered, for instance the wetability, pore blockage and template stability.

2.4.1.1 Electrochemical deposition

Electrodeposition of a template is carried out by coating a metal film onto one surface of the template and then using this metal film as a cathode for electroplating (Martin, 1996). The volume of the pore is continuously filled up beginning from the bottom pore. Hence, the length of the nanostructure can be controlled by varying the amount of material deposited (Huczko, 2000). Both metal and conductive polymers can be metal deposited using this method. While Bera et al. (2004) have reported synthesizing metallic nanomaterials with controlled shape and sizes using template-assisted electrodeposition, Tsai et al (2006) have investigate an improved electrodeposition technique for preparing platinum and platinum–ruthenium nanoparticles on carbon nanotubes directly grown on carbon cloth for methanol oxidation.

2.4.1.2 Electroless Deposition

Electroless deposition is a convenient method to obtain metal deposits at any surface and need not be electrochemically conductive at a low cost. This method uses a solution that contains a reducing agent and complex metal ions as the source of the metal. Self-assembly was successfully used in the electroless deposition of metals to achieve the selectivity of catalyst species (Xu et al., 2005; Dressick et al., 1994). There is further discussion on this matter in Chapter 4.

2.4.1.3 Sol-gel deposition

The sol–gel process involves a precursor in the form of a solution undergoing gelation by evaporation of the solvent, subsequently being cured or sintered to produce the desired product (Duran et al., 2007). The process typically involves preparation of a solution of a precursor molecule to first obtain a suspension of colloid particles (the sol). Then a gel composed of aggregated sol particles is thermally treated to yield the desired nanostructure within the pores of the template (Huczko, 2000). Nakamura et al. (2000) have reported Ni/SiO_2 catalyst with hierarchical pore structure prepared by phase separation in sol-gel process silica gel without PEO (Polyethylene oxide). It was found that Ni was selectively incorporated into a gel skeleton as fine particles in the system.

2.4.1.4 Chemical Vapour Deposition

This technique is the surface solidification of required metals resulting from their gas-phase chemical transformation, or processes that involve depositing a solid material from a gaseous phase. In general, deposition of metal on three dimensional templates remains a challenge and is limited to surfaces that are exposed to a deposition source. Incomplete metal catalyst coverage leads to insufficient coverage on the template areas that do not face the catalyst deposition source; for instance, deposition on complex substrates such as foams, meshes or fibre cloths. With this method, thermal decomposition of the gas occurs throughout the pores, resulting in the deposition of

metal along the wall and within the pore. According to Pierson (1999), this technique can be utilised to grow a wide variety of nanostructures on microstructured surfaces having arbitrary topography, giving templates with hierarchical microscale and nanoscale surface features. Carbon nanofiber and nanotube have been produced using chemical vapor deposition (CVD) by synthesising carbon within the pores of an alumina template membrane with or without a Ni catalyst (Che et al., 1998)

However, the chemical vapour deposition (CVD) process requires very high process temperatures (900–1000 °C), which may deform the template. Furthermore, entrapped particles from deposits may be observed, thus reducing the beneficial properties of the deposited metal.

2.5 Application of Hierarchical Nanostructured Materials

A great deal of interest has been made to the fabrication of hierarchically structured materials with meso-macropores due to its unique structures and properties. While the mesopores would be helpful for adsorption and the desorption process, the macropores on the other hand would enhance diffusion of the reactants. The structural features of these meso–macroporous materials have potential application as catalysts supports and catalysts in heterogeneous catalyses where diffusion of reactant molecules could be facilitated. A controlled multiporosity network with a high surface area, a wide variety of oxide compositions, and the ability for homogeneous or selective doping of active sites are all in high demand for improved catalytic activity (Liew et al., 2006).

Silica-supported nickel catalysts with both macropores and mesopores has been reported by Nakamura et al. (2000) in the presence of poly(ethylene oxide) (PEO). Ni/SiO system has been used in various catalytic processes such as reductive alkylation, methanation, heterogeneous hydrogenation of aromatic compounds and methane reformation. In this study, it was found that interconnected macroporous morphology was formed and is expected to be used in various catalytic reactions in a monolithic body. In addition, recent work by Kim et al. (2006) has described the preparation of

porous materials with mesoporous silica monoliths having macropores inter-connected 3-dimensionally system by using polystyrene with sub-micrometer size as a template. It has been demonstrated that these bimodal structured porous silicates have been used as supports for asymmetric kinetic resolution of racemic epoxides to synthesize optically pure epoxide (Kim et al., 2006).

Ocampo et al. (2009) have reported a new generation of structured catalysts produced by a combination of supramolecular templating methods (systems that are created suitable for reaction to progress that is not possible to use on a macroscopic scale) followed by conventional self-assembly of template cations and silica species. By introducing the microporosity within the macro-mesopore materials, it exhibited enhanced diffusional properties which would enhanced mass transport properties by improving the selectivity of light olefins in the important *n*-hexane cracking reaction. Chmelka and co-workers proposed procedures for producing meso–macroporous aluminosilicas (Si/Al = 72) of centimetre size (Chiu et al. 2004). Mechanically stable monoliths with interconnected macropores whose walls were comprised of ordered mesopores by combining oil-in-water (O/W) emulsion and block-copolymer templating were investigated for the Friedel–Crafts alkylation properties of single-ring aromatic compounds, including toluene, ethylbenzene, cumene, and styrene, with benzyl alcohol. Meso-macroporous meta oxides prepared by surfactant-assisted spontaneous assembly also have potential application in catalysts (Maekawa et.al. (2003).

Considering the extremely widespread use of hierarchically structured materials with meso-macropores in most chemical applications involving catalysis, it is a challenge for researches to take the advantage of this emerging field.

CHAPTER 3

LITERATURE REVIEW: POLYHIPE POLYMER

3.1 Overview of PolyHIPE

PolyHIPE Polymers (PHP) are microporous materials prepared by polymerising the continuous phase of a High Internal Phase Emulsion (HIPE). Emulsions usually contain two immiscible liquids, with one liquid dispersed in the other in the form of droplets (Zhang and Cooper, 2005). This is referred to as the dispersed, discontinuous or internal phase, while the dispersing medium is known as the continuous or external phase containing (Lissant, 1984). Generally emulsion systems can be classified as oil-in-water (O/W) or water-in-oil (W/O) depending on the nature of the external phase. When an internal phase volume fraction (ϕ) is greater than 74% relative to the total emulsion volume, the emulsion is categorised as High Internal Phase Emulsion. This ϕ value, which can be as high as 0.99, represents the maximum volume ratio of uniform non-deformable spheres when packed in the most efficient manner (Cameron, 2005). At these high volume fractions, the droplets of the internal phase become overcrowded and they can no longer be spheres but take the shape of deformed polyhedral droplets with relatively large contact areas, surrounded by a continuous phase and stabilized by thin surfactant films. The formation of PolyHIPE Polymer is shown in Figure 3-1. This produces a highly porous material with a pore volume fraction that can be as high as 0.99. In addition, it possesses an open cellular structure, in which each cavity is connected to its neighbours (Cameron, 1996).

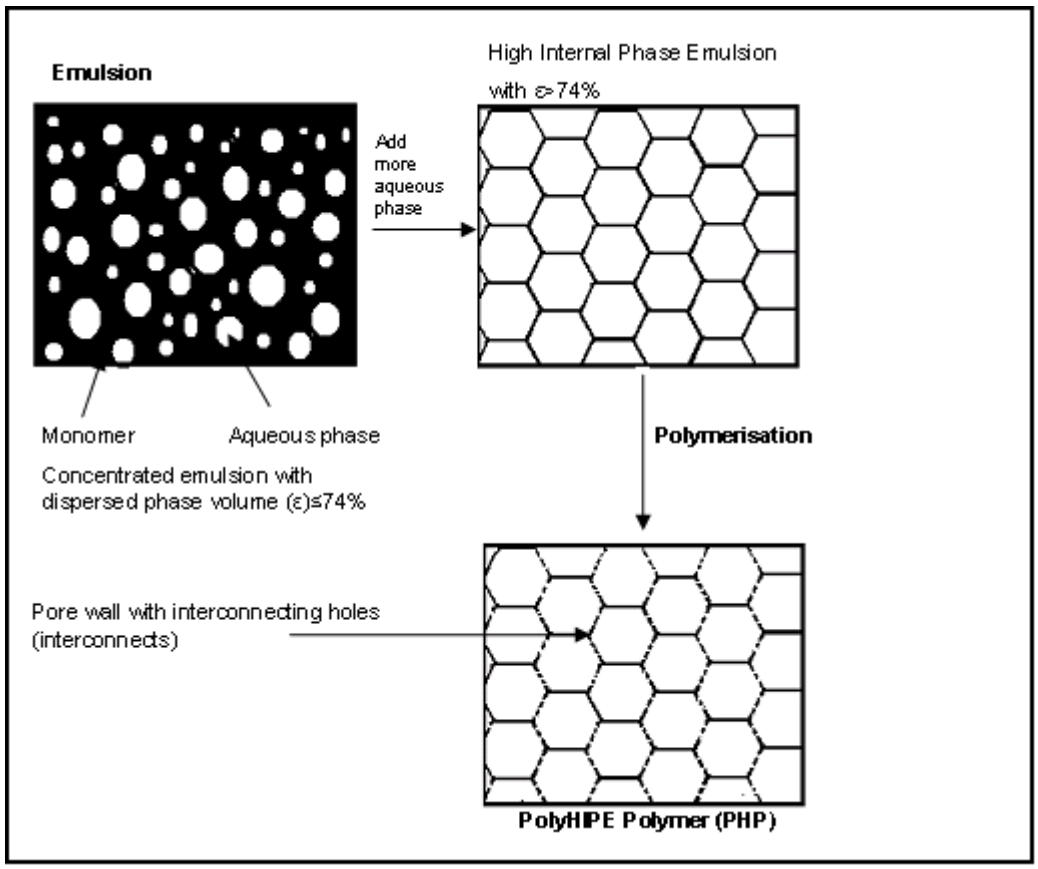

Figure 3-1: Schematic Diagram of PolyHIPE Polymer Formation (Akay, 2005)

This production of PHP can be tailor-made to meet certain specifications according to their applications. William et al. (1989) have reported that highly porous interconnected monolithic PolyHIPE materials can be produced with an open-cell, well-defined and uniform microstructure with very low dry density of approximately 0.1g/m^3. These materials can be prepared over a wide range of pore sizes and can be classified into 4 types: (1) coalescence pore D, (0.5 μm<D<5000 μm) – this is the stable pore structure, the size of which is determined at the emulsification stage of PHP formation. The dispersed phase droplets in the emulsion are coalesced by the addition of water soluble polymers into aqueous phase (2) interconnect pore size, d (0 < d/D<0.5.), depending on the conditions of the starting emulsions – the type of pore architecture is obtained through the controlled of the type 1 pores during polymerization. ; (3) primary pore size – it is possible to obtain a network of pores within type 1 and 2 pores. Primary pores are

smaller compared with the coalescence pore (type 1) ; and (4) nano-scale pore size – the walls of microporous PHP can be made nano-porous by using suitable fillers in the oil phase so that after polymerization, the filler can be removed by solvent extraction (Akay et al. 2000). The structure of a typical PolyHIPE Polymers is shown in Figure 3-2. According to (Akay and Vickers, 2003), pores of a size greater than 200 μm are obtained through a coalescence polymerization technique. In addition, adding small quantities of water-miscible organic species to the HIPE aqueous phase promotes Ostwald ripening which leads to a controlled coalescence (Hayman et al., 2004). Furthermore, by varying the surface chemistry of materials against which the HIPE are polymerized, the porosity of a PHP's surface can be controlled, allowing asymmetric materials to be produced (Akay, 2006).

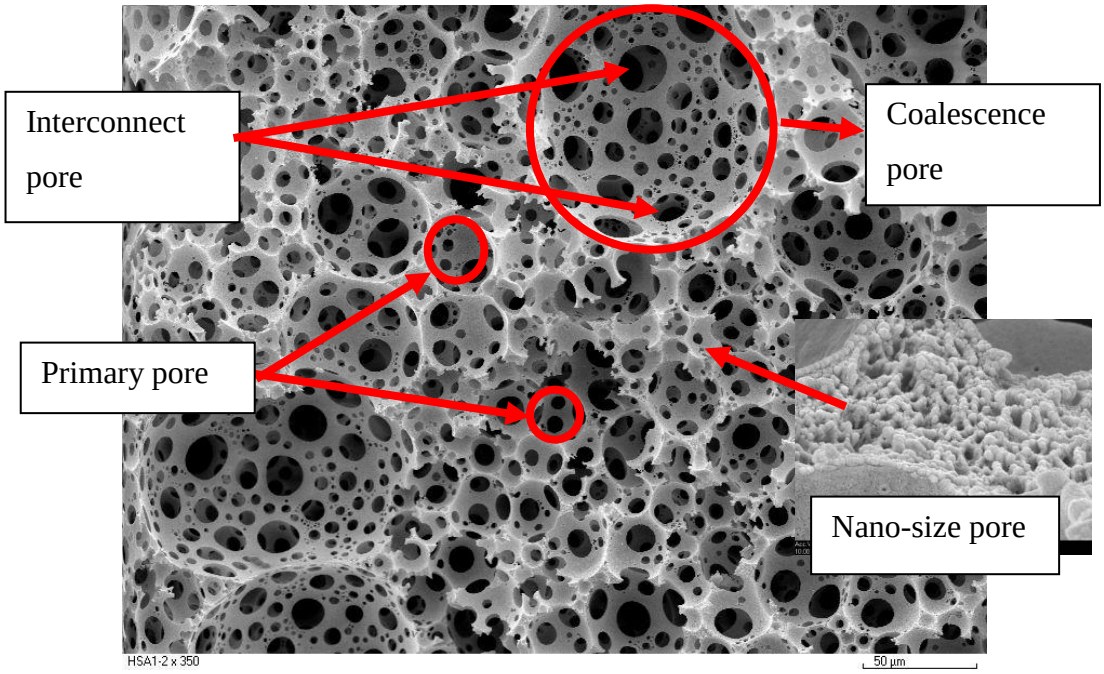

Figure 3-2: Structure of a Typical PolyHIPE Polymer

Due to their unique characteristics, structures and properties, HIPEs have found their way into applications such as food preparation, cosmetics, oil recovery and many others (Lissant, 1974). Besides this, PHP are utilised in diverse fields of intensified processes, especially in biology; examples include the discovery of several size-dependent

bioprocesses (Akay et al., 2004b; Akay et al., 2002) and tissue engineering (Akay, 2005; Akay et al., 2004; Bokhari et al., 2003; Akay et al., 2002), and other intensified bioprocesses (Akay et al., 2005; Erhan et al., 2004).

Currently, these materials (both hydrophilic and hydrophobic versions) have also been employed in intensified demulsification processes (Akay et al., 2005; Noor et al., 2005; Akay and Vickers, 2003), gas-liquid separation (Calkan et al., 2005; Dogru and Akay, 2004) and metal ion removal in water treatment (Fuat and Akay, 2006; Wakeman et al., 1998). In addition, PHPs have also been utilised in other intensified processes such as in foam and filtration fabrications (Tai et al., 2001b; Walsh et al., 1996; Bhumgara, 1995), metal plating (Akay, 2005; Calkan et al., 2005; Brown et al., 1999; Sotiropolous et al., 1998) and organic chemistry processes (Deleuze et al., 2002).
In order for the PHP to be utilised in the applications mentioned in the previous section, the preparation and modification/optimisation of the materials has to be able to (Noor, 2006):

- produce PHP with a required internal architecture or morphology for instances of specific pore/interconnect sizes and/or presence of arterial channels;
- form monolithic structures;
- chemically/biologically functionalise/optimise the PHP for a particular application;
- ensure the production and modification of PHP is sustainable

3.2 PolyHIPE Preparation

The preparation of high internal phase emulsion has been extensively investigated over the past few decades and has been discussed in detail by Lissant (1974). Barby and Haq (1985) reported the process for the preparation of HIPE in which the monomers are polymerised in the form of a water-in-oil high internal phase emulsion comprising, as the internal phase, at least 90% by weight of the emulsion of water. Several other related methods of producing PHP have also been reported (Elmes et al., 1988; Edwards et al., 1987; Haq, 1985). Several new procedures have recently reported to synthesize

PHP (Butler et al., 2001; Barbetta et al., 2000; Cooper and Holmes, 1999). While Mezzengga et al.(2003) describes a solvent based technique without the need of polymerization, Akay et al. have established a system based on a highly porous (up to 97%) cross-linked polymeric foam which reflects their own processing history (Akay, 2005; Akay et al., 2004; Akay et al., 2002; Akay et al., 1995).

The process of preparing PolyHIPE is relatively simple. The continuous phase of emulsion contains monomers, cross-linking agents, suitable surfactants and, in certain cases, oil-phase soluble polymerization initiators as well as additives/fillers are added (Akay, 2005). The disperse phase can involve low molecular weight compounds such as light oil or distilled water, with the addition of a polymerisation initiator such as potassium persulphate or lauryl peroxidecan and/or additional additives/fillers. The continuous phase is generally disperse dropwise in a solution of monomer, cross linker and surfactant so that an emulsion of up to 90% oil in a monomer bath can be obtained and subsequently polymerized (Tai et al., 2001; Cameron and Sherington, 1997; Bhumgara, 1995; Hainey et al., 1991; Sherington, 1991). The polymerisation reaction of styrene and divinylbenzene to obtain PolyHIPE polymer is shown in Figure 3.3.

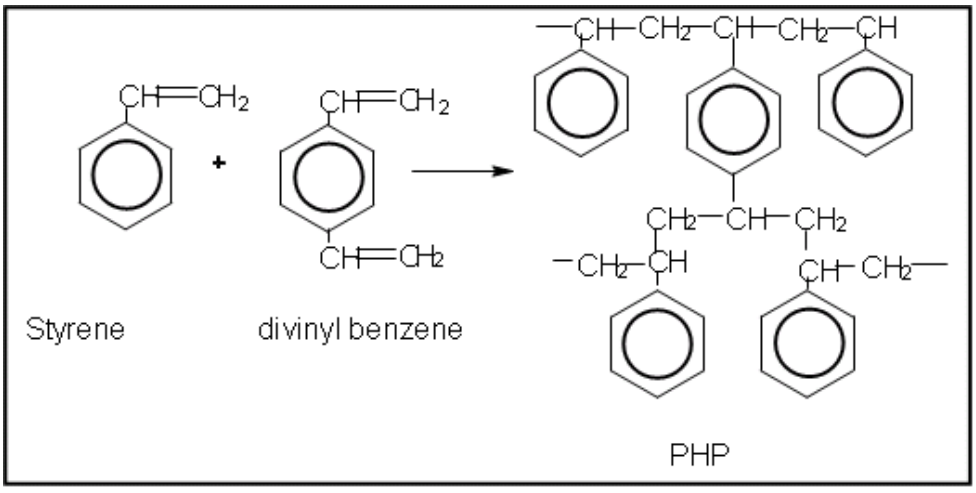

Figure 3-3: The polymerization reaction between styrene and divinyl benzene (Bokhari, 2003)

The processing of HIPE can be divided into two stages. In the first stage, the dispersed (aqueous) phase is continuously dosed into the continuous (oil) phase, which is already placed in the mixing vessel. The addition of the aqueous phase also creates mixing and therefore care is taken to minimize jet mixing of the phases. Owing to the rotation of the impellers during dosing, there is a reduction in the aqueous phase droplet size. The second stage of processing starts after the completion of dosing, when further mixing can be carried out in order to reduce the aqueous phase droplet size (i.e. the size of the pores after polymerization), and HIPE with narrow droplet size distribution can be obtained.

The relative dosing rate which has the dimension of the deformation rate is used to characterize the dosing rate of the aqueous phase:

$$R_D = \frac{V_A}{t_D V_O} \qquad \text{Eq. 3. 1}$$

where:

R_D = Relative dosing rate, ml/s

V_A = Volume of aqueous phase,

t_D = Period of time which the aqueous phase is dosed,

V_O = Volume of the oil phase placed in the batch mixer

The total mixing time t is defined as

$$t = t_D + t_H \qquad \text{Eq. 3. 2}$$

where:

t_D = Period of time which the aqueous phase is dosed

t_H = Homogenization time

The mixing rate is defined as:

$$R_M = \frac{D_I}{D_O}\Omega \qquad \text{Eq. 3. 3}$$

where:

D_O = Diameter of the batch mixer, m

D_I = Diameter of the impellers, m

Ω = Rotational speed of the impellers, rpm

If the dosing rate is very low, there will be no need for the additional mixing (homogenization) stage. If the relative dosing rate is very large and the mixing rate is small, HIPE does not form; rather a dilute (low) internal oil-in-water (O/W) emulsion is obtained (Bokhari, 2003). When HIPE is stable, it can be polymerized without phase separation.

Styrene-divinylbenzene (DVB) PolyyHIPE are the most extensively used monomers and can be polymerized by a free radical polymerization process (Barbetta and Cameron, 2004; Cameron, 1996; Tai et al., 1991). Since styrene is immiscible in water, water-in-oil (W/O) HIPEs are prepared to create styrene-based PolyHIPEs. In order to enhance the structural stability, other hydrophobic monomer(s)/crosslinkers, such as divinylbenzene (DVB), are usually added in varying quantities. According to Sherrington (1998), if styrene is polymerized in a mixture with divinylbenzene (DVB) then the latter becomes a constituent of two polymer chains, effectively linking the chains together to form infinite network connectivity (Figure 3.4).

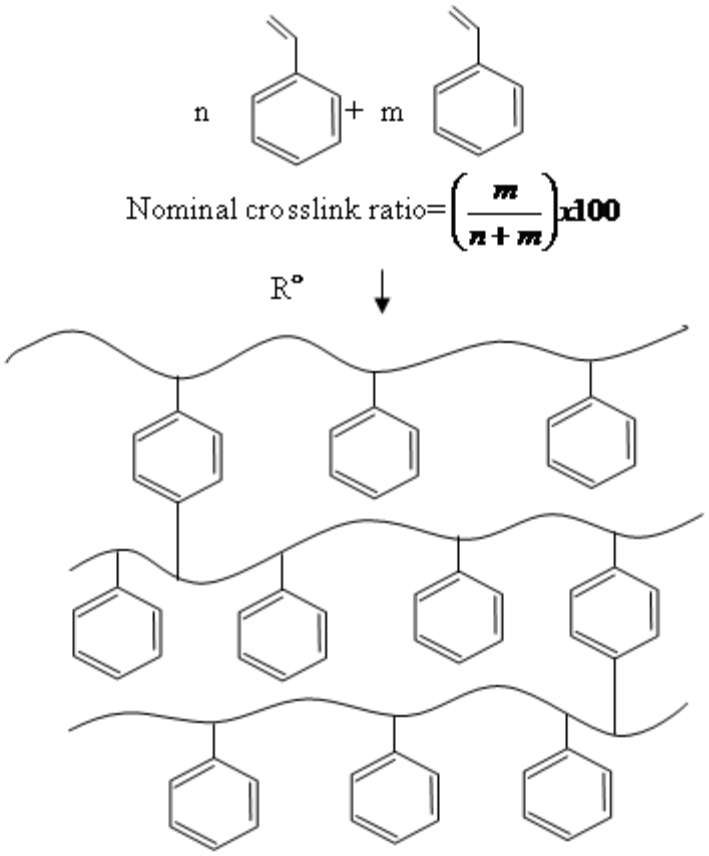

Figure 3-4: Polymerisation of Styrene and Divinylbenzene to form an Infinite Polymer Network (Sherrington, 1998)

Other useful cross linking hydrophobic monomers include 2-ethylhexyl acrylate (2-EHA), methyl acrylate (MA), butyl acrylate (BA) and isoboryl acrylate (IBA). In order to produce homogeneous PolyHIPEs from W/O HIPEs, the organic continuous phase must be sufficiently hydrophobic (Cameron, 2005). Similarly, hydrophilic PHP can be prepared from oil-in water (o/w) HIPEs. With the aid of a hydrophilic surfactant such as sodium dodecyl sulfate (SDS), hydrophobic organic liquids such as kerosene, paraffin, ether, petrol and cyclohexane can be emulsified in an aqueous solution of polyacrylamide or poly(acrylic acid). Other materials that have been used to prepare hydrophilic PHP include urea and formaldehyde (Elmes et al., 1988). Recently, the PIM (Process Intensification and Miniaturisation) research group from Newcastle University have successfully produced several batches of relatively hydrophilic homogenous

polyHIPE by adding vinyl pyridine, which acts as the hydrogen donor/acceptor in the organic continuous phase (Noor, 2006).

3.3 PolyHIPEs Morphology

Generally, morphology of PHP depends much on the controllability of the internal architecture (pore and interconnect structures), the fabrication, and the chemical modifications of their walls. They are complex and basically have open cellular with spherical cavities known as pores or voids. PHP can be tailored to have a wide range of pore size from 0.1μm to 5000μm. In addition, the dimensions of the material can be adjusted from thin membranes to very large well-organised monolithic articles. PHP are currently being widely utilised in a variety of areas, where each different application requires different material properties (morphology, physical, mechanical, thermal, etc.).

3.3.1 Factors Affecting PolyHIPE Polymers Morphology

Workers from Unilever Gregory et al. (1989); William and Wrobleski (1988) were the first to investigate the factors that determine the cellular condition of the material. It has been discovered that although internal phase volume ratio (ϕ) does have some influences, surfactant concentration is by far the most important in determining the cellular nature of PHP.

3.3.1.1 Internal Phase Volume Ratio

In a study conducted by Williams and co-workers (1990), it was discovered that the ratio of styrene/DVB, used in the preparation of a styrene/DVB HIPE from 0 to 100% DVB, plays an important role in determining the character of the resulting PHP. It was noticed that emulsions with DVB blend easier and more uniformly compared to those with styrene alone. Therefore, an increased ratio of styrene/DVB in a HIPE results in increased emulsion stability, which consequently leads to a decrease in average pore size diameter from 15 to 5μm. Furthermore, the above researchers also observed that

small increases in the amount of surfactant were effective in reducing the pore size, although 50% and beyond surfactant concentration (w/w) relative to the monomer content) yielded crumbly, weak polyHIPE materials.

3.3.1.2 Surfactant Parameter

The amount of surfactant is crucial to the type of structure that will be formed. There are three main factors pertaining to surfactant parameters that can obviously determine the final cellular structure, namely the Hydrophile-lipophile balance (HLB), surfactant level, and surfactant concentration. Surfactants used to form HIPEs must have a low HLB value (between 2 and 6) (Barby and Haq, 1982) and the optimum surfactant was found to be Sorbitan Monooleate (Span 80), which has an HLB value of 4.3. Another study reported that a surfactant level of at least 4% volume relative to the total oil phase was required for PolyHIPE formation (Cameron, 1996). Surfactant levels between 4%-5% volume have been found to result in closed-structure material, whereas 7%-50% produce an open cell structure with an entirely interconnected microstructure (William, 1988). However, surfactant concentration has been found to be more important than the internal phase volume (William, 1988). This occurrence can be explained by the fact that by increasing the surfactant concentration, the monomer films that separate the adjacent emulsion droplets became thin. At a particular critical film thickness, windows between adjacent droplets appear during polymerisation.

Akay et al. (1995) suggests a mechanism that explains the relationship between the surfactant and the pore structure of the PHP. According to the proposed mechanism, during polymerization the surfactant molecules (which can not become part of the polymer chain) form a separate phase at the interface region between the polymerizing monomer and the aqueous internal phase of the HIPE. Steric attraction between the tails of surfactant molecules that are opposite each other (Figure 3-5(A)) would cause the surfactant molecules to agglomerate into a separate phase (Figure 3-5(B)). Any excess surfactant that does not occupy a place at the interface exists as micellular droplets in the oil phase, and therefore will also become part of the separate surfactant phase. The

agglomerated surfactant molecules form areas in the external phase and are reduced in the polymerised material. Once the surfactant is removed these areas then become pores between the cells. However, if too much surfactant is used to produce the HIPE, the surfactant agglomerates begin to attach together, break up the wall like structure, and cause the PHP to collapse.

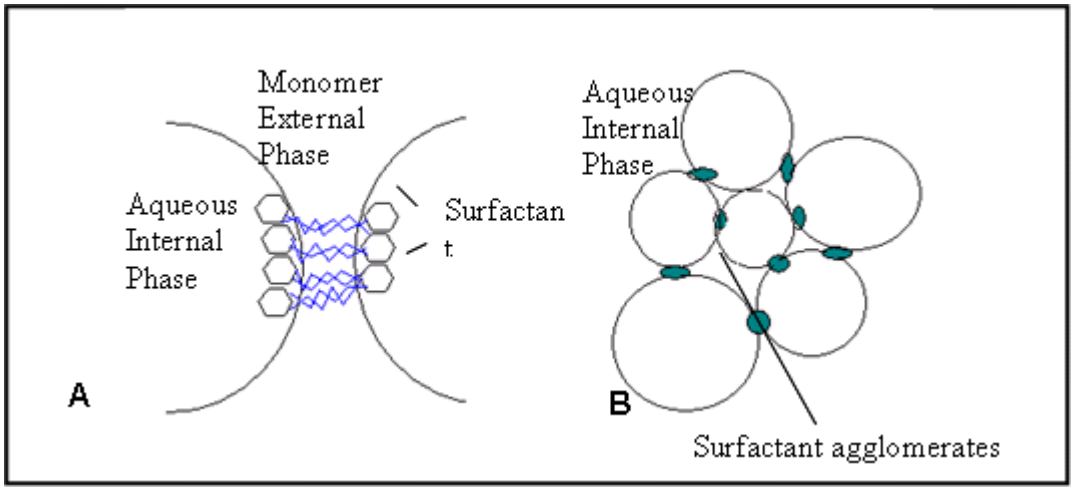

Figure 3-5: Schematic diagrams illustrating the formation of pores in PHP (Akay et al., 1995)

3.3.1.3 Electrolyte Content

Research carried out by Cameron (2005) demonstrates that there is a significance influence of electrolyte concentration in the aqueous phase on average pore size diameter. The pore diameter is reduced up to 10 fold when the salt concentration of aqueous solution with azobisisobutyronitrile (AIBN) as an initiator is increased from 0 to 10g/100 ml. By increasing electrolyte concentration, the propensity for Ostwald ripening is reduced. Hence, limiting the Ostwald ripening leads to a more stable emulsion with a smaller average droplet diameter. Other researchers have demonstrated that the addition of electrolyte has been known to affect emulsion stability by reducing the interfacial tension, and hence the final structure of the PolyHIPE (Aronson and Petko, 1993; Gregory et al., 1989).

3.3.1.4 Composition of HIPE Continuous Phase

It was further investigated that the composition of HIPE continuous phase can influence pore size (Cameron, 2005). PolyHIPE prepared by VBC(4-vinylbenzyl chloride) and DVB had smaller average droplet diameter than those prepared from the mixture of styrene and DVB (Barbetta et al., 2000). In addition, by increasing VBC content, the pore diameter decreases to less than 5μm (Cameron and Barbetta, 2000). Cameron and Barbetta (2000) suggested that VBC was co-adsorbing at the emulsion interface with surfactant, thus lowering the interfacial tension resulting in a smaller average droplet size. A similar effect was observed when a non-polymerisable solvent is used (Cameron, 2005).

3.3.1.5 Mixing Time/Dosing Time

There are several factors that contribute to the stability of HIPEs. Like other emulsions, the stability of HIPE is highly dependent on the preparation parameters, namely shear stress (i.e. mixing speed) and the duration of the mixing time. Mixing an emulsion to high mixing speed can easily and uniformly break it down into small emulsion droplets, thus producing more stable emulsion. Prolonged mixing time also has a similar effect, as shown in a study by Walsh and co-workers in 1996. It was demonstrated that with increased mixing time there was a reduction in water cavity size and an increase in the number of windows, resulting in more micro-size open structure materials. Extensive studies were performed by Bokhari (2003) to determine the effect of mixing and dosing time on the structure of PHP. They had established parameters for mixing and dosing time of 120 seconds and 60 seconds respectively. It was found that these parameters produce an open pore PHP with large pore size. Figure 3-6 shows that as the mixing time increased, the average pore size decreased.

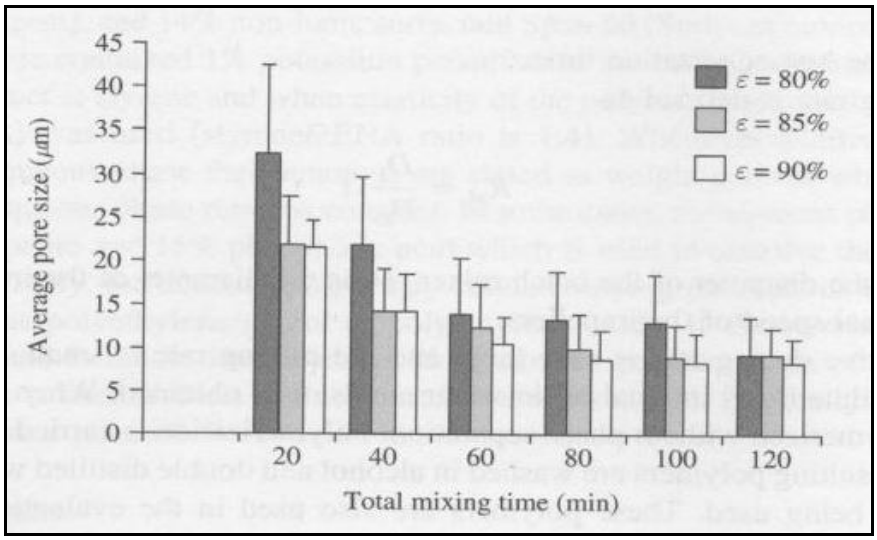

Figure 3-6: Variation of average pore size (D) with total mixing time (t) as a function of dispersed phase volume fraction (ε). Dosing time = 10 min, impeller speed Ω = 300 rpm, emulsification temperature T = 25 ºC. Pore size is evaluated from scanning electron micrographs of the polymers (Bokhari, 2003)

3.3.1.6 Emulsification Temperature

Several studies have analysed the effect of emulfication temperature on pore size. By operating at high temperature, it was found that larger pores are created (Bokhari et al., 2003). Since emulsion produced by the phase invasion technique did not go through a homogenization stage, a wide pore size distribution PHP was obtained by operating at high temperature (Akay, 2005). This is because the numbe of oil particle which contain water reduces after each homogenization stage (Akay, (1998). Figure 3-7 shows that PHP with larger average pore sizes (D) can be produced as the emulsification temperature is increased from 30 ºC to 80 ºC. In an attempt to exploit PolyHIPE Polymer as a biomaterial, Akay et al (2004) used different emulfication temperature to obtain the optimum pore size for the specific application. It was found that largest pore sized polymer (100μm) showed the most rapid cell penetration into the polymer whereas more cells were observed in the layers below the surface of the 40μm pore-sized PHP compared to other pore size (Bokhari, 2003).

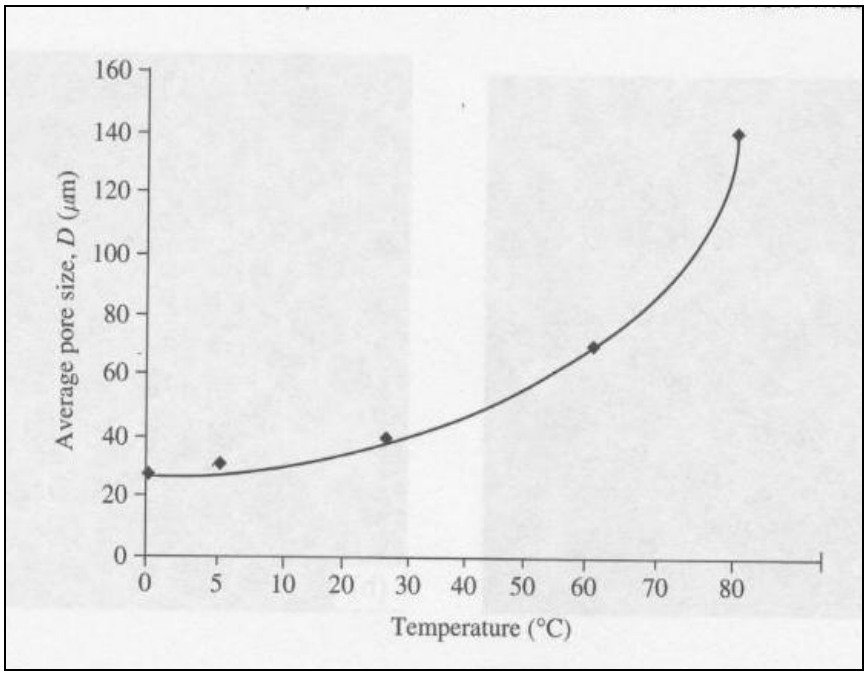

Figure 3-7: Variation of average pore size with emulsification temperature when dosing time = 40 s, total mixing time = 100 s, impeller speed = 300rpm, phase volume = 90 % (Akay, 2005)

3.3.1.7 Moulding Type

Typically, PolyHIPE materials are polymerized inside a suitable container, which acts as a mould that can vary in shape and type. Some evidence shows that the nature of the mould substrate has a significant influence on its surface morphology and degree of adhesion to the mould (Cameron, 2005; Akay et al., 1995). It was found by Cameron (2005) that when glass mould is used, it causes surface bonding with PolyHIPE and shows a different morphology between the contact surface and the inner surface. Further investigation has found that the stability of HIPEs is hindered by the use of PVC (polyvinyl chloride) mould due to leaching of the plastic container. Although the use of a polypropelene container does not result in adhesion, the structure of the contact surface has been found to be a closed cell structure. Furthermore, preferential wetting of the mould surface by either phase of the emulsion can cause phase separation. As a result, the monomer film becomes a surface skin upon polymerisation (Cameron, 2005).

PTFE mould does not produce adhesion, exhibiting open-cell morphology at the PolyHIPE-mould interface (Cameron, 2005; Akay et al., 1995). PTFE has shown promising results and therefore other types of mould may also be utilized by spraying the surface of the mould with a PTFE spray. Other mould types have been used by other researchers, such as aluminium foil and falcon tube, but no significant effect on morphology of PHP produce was reported (Gitli and Silverstein, 2008; Menner et al., 2008).

3.4 PolyHIPEs Properties

3.4.1 Surface Area

Despite having highly permeable interconnected walls, the surface area of polyHIPE materials prepared in the manner described in section 3.2 is considerably low, with 3-20 m^2/g being the typical range (Noor, 2006). This can be explained by looking at the pore sizes of these materials, which are relatively large at up to 10s of microns. Nevertheless, certain applications of polyHIPE materials, such as chromatographic support (Kreutzer, 2005), require a much higher surface in the order of hundreds of meters square per gram. However, there are ways to significantly enhance the surface area of these materials.

According to work carried out by Hainey and co-workers (1991), the polyHIPEs surface area can be dramatically increased by substituting one of the monomers with organic porogenic solvent and adding a high amount of cross linker (i.e. DVB) in the continuous phase. By doing this, it is possible to produce monoliths with a surface area up to 350 m^2/g. Unfortunately, one drawback of this method is that the mechanical properties of the resulting polyHIPEs are seriously affected. The monoliths structure is easily collapsed when subjected to moderate low to moderate stress, and to the flow through of liquid. The nature of the porogen has a strong influence on the surface area, and this is strongly related to the solvent type. Better solvents for the growing network give rise to higher surface areas. This spurred Cameron (2005) and Barbetta (2004) to conduct

studies to find the best alternative porogenic solvents to obtain high surface area polyHIPE materials which have the same level of mechanical performance as those with low surface areas. They have found that by changing the solvent from toluene (T) to chlorobenzene (CB) to 2-chloroethylbenzene (CEB), BET (Brunauer, Emmett and Teller theory) surface area is increased from 350 to 550m^2/g.

Although by using CEB the area was increased even further, a change in the morphology of the resulting material was also noticeable. Under SEM (scanning electron micrscospoce), the produced polyHIPE material was observed as not having a similar morphology compared to the standard polyHIPE structure with significantly large windows. In addition, despite the large surface area, the mechanical properties were not improved. A further study by one of the researchers (Cameron, 2005) found that a 1:1 (volume:volume) mixture of CEB and CB not only yielded a material with the same value of surface area (550 m^2/g), but also maintained the original polyHIPE morphology. Although the material was claimed to be more robust it was discovered that this specific type of polyHIPE was not as durable as those prepared using the combination of styrene/DVB (Noor, 2006).

3.4.2 Mechanical Properties

In order to produce a commercially attractive product, PolyHIPE Polymers of superior strength can be developed. The mechanical properties of polymeric materials are of great importance in technological applications. Various methods can be employed to increase the toughness and modify the properties of polymeric material through a combination of different factors. The choice of monomers and crosslinker have a strong effect on mechanical properties; for instance, PolyHIPEs based on styrene and divinlbenzene are brittle and chalky (Cameron, 2005; Williams, 1990; Williams and Wrobleski, 1988), whereas bisphenol-A-polycarbonate has outstanding mechanical properties (Cameron and Sherrington, 1997). This is believed to be a consequence of hindered motion of the main-chain phenyl groups in bisphenol-A-polycarbonate, which tend to micro segregate in contrast to the freedom of rotation of the main-chain phenyl

groups. Therefore, the monomer chemical structure has an important bearing on the properties of the final product.

On the other hand, PolyHIPE polymers produced using high internal phase emulsions can be rigid or elastomeric (Cameron and Sherington, 1997). By adjusting the ratio of styrene to divinyl benzene to 2-ethylhexyl acrylate (2-EHA) by use of a hydrophobic elastomer, the final polymer can be made in an elastomeric form. Alternatively, the base material itself can be changed to be highly rigid by changing methyl to methacrylate or resorcinol-formaldehyde (Cameron and Sherington, 1997). Here the toughening mechanisms are complex as a result of the superposition of the physical properties of the components and the effect of supramolecular organization (Sherrington, 1998; Cameron and Sherington, 1997). However, a large amount of cross-linking can cause embrittlement similar to styrene-divinylbenzene system (Hainey et al., 1991).

Adding filler does not only modify the morphological features of PolyHIPE materials but also improves the mechanical properties of PolyHIPE materials. Loading poly (styrene/DVB) HIPEs with short fibre fillers can lead to significant improvements in flexural and compressive modulus and toughness. In particular, it has been found that Kevlar fibres bond particularly well to the matrix, leading to enhanced properties (Cameron, 2005).

Recent studies have proved that introducing a suitable reinforcement within the polymerized organic phase is a promising alternative to enhancing mechanical properties. Haibach et al. (2006) have demonstrated that by reinforcing the polymer phase with nano-sized silica particles, the Young's modulus as well as the crush strength of foams is further increased by 280% and 218% respectively in comparison to foams without reinforcement. Moreover, Menner et al. (2009) report that by reinforcing PolyHIPEs with titania in the organic phase or oxidised carbon nanotubes in the aqueous internal phase, an improvement in mechanical performance is achieved without having to increase their density, enabling a wide range of PolyHIPE applications, such as scaffolds for tissue engineering and filters.

Besides mechanical reinforment of PHP, silica particles have been used to stabilized the properties of oil in water emulsions (Binks and Lumsdon, 1999). Binks and Whitby (2005) reported that emulsion is stabilised by particles of larger diameter consisted of drops ranging from macroscopic to microscopic in size. Other researches have developed and synthesized novel polymer foams with improved structural and mechanical properties and permeabilities when compared to conventional polyHIPEs which involved silica particles as stabilizer (Ikem et al., 2008).

3.5 Chemical Modification of PolyHIPE Polymers

Chemical modification of PolyHIPE materials can be carried out by using the phenyl rings of polystyrene as reactive sites. The production of PHP with reactive branches allows further synthetic elaboration, which results in changes in the chemistry of the porous material. DVB-crosslinked large cylindrical PHP monoliths can be adjusted by electrophilic aromatic substitution to yield sulpho-, nitro-, phosphor- and bromo-substituted materials (Cameron, 2005).

3.5.1 Sulphonation

Besides using different kinds of monomers in the oil phase to create hydrophobic or hydrophilic materials, the chemistry of PHP can be varied in another manner, resulting in modification of the chemistry of the materials. By substituting aromatic electrophilic (preserving aromaticity of the ring system) into the phenyl rings of styrene, a sulphonic acid material can be achieved. This process is called sulphonation. Sulphonation is used to attach the sulphonic acid functional group ($SO^{3-}H^{+}$) to a molecule of an organic compound via a chemical bond. Aromatic sulphonation is a substitution organic reaction in which a hydrogen atom of an arene organic compound is replaced by a $SO^{3-}H^{+}$ functional group through electrophilic aromatic substitution (Figure 3-8). However a sulphonation degree of 100% is impossible to achieve due to internal stresses in the polymer matrix. Haq (1985) had reported that sulphonation degree of 68 % to 80 % was

achieved whilst Calkan et al. (2005) proved that the degree of sulphonation increased with increasing time and reached a plateau value at ca. 60%. The degree of sulphonation on the PHP represented its hydrophilic characteristic (Akay and Vickers, 2003).

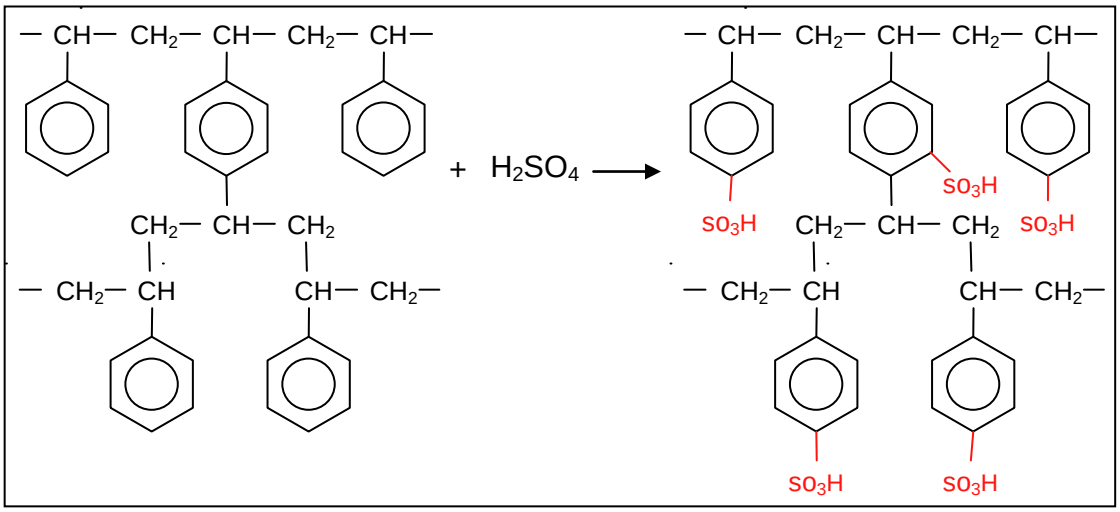

Figure 3-8: Chemical structure of 100 % sulphonated polyHIPE (Calkan, 2006)

Sulphonated form polymer is the most widely used functionalised PolyHIPE Polymer due to its capability for metal ion removal. These materials are highly water adsorbent both in acid form or salt form (often sodium salt). The sulphonation of PHP techniques involve the simple heating of the acid containing polymer where the sulphonation temperature is dependent on the acid concentration. Several methods have been proposed in trying to sulphonate PolyHIPE Polymer. Although the sulphonated form of cross linked styrene-DVB copolymer PHP has been widely used where hydrophilic material is required, current available methods of sulphonation (Akay and Vickers, 2003; Cameron, 1996; Wakeman and Akay, 1996; Williams and Wrobleski, 1988; Haq, 1985) are less than ideal because of the generation of excessive waste acid after the sulphonation. The conventional method by Miller et al. (1963) demonstrated that the use of concentrated sulphuric result in inability of acid to infiltrate the material, therefore not suitable for the sulphonation of thick monolithic structures. Moreover since sulphuric acid is a very strong sulfonating reagent, it is not compatible with cross linked polystyrene. Other sulphonation reagent that was investigated includes

chlorosulfonic acid in chlorinated solvents (Su et al., 1994) and sulphur trioxide (Thaler, 1983). On the other hand, a uniform sulfonation was achieved by using acetyl in 1, 2 dicloro-ethane (DCE) and lauroyl sulphate in cyclohexane (Cameron, 1996). Sulphonation was performed after polymerisation.

Recently, the PIM research group at Newcastle University have discovered a novel sustainable and efficient method of sulphonation (Calkan, 2007; Calkan, 2006; Akay et al., 2005). In their proposed technique, sulphonated PHP material is produced using the internal phase during the emulsification stage. Since sulphuric acid is already present within the pores of the polymer, the use of excess acid and the need for it to penetrate the pores are eliminated. This technique is employed in some parts of PHP modification conducted in this study. Figure 3-9 shows the typical structure of sulphonated PHP. As indicated by the SEM micrographs, the coalescence pores are dominant because of the presence of sulphuric acid which destabilises the emulsion during polymerisation. As a result, water droplet coalescence and cross-linking reaction occurs simultaneously, leading to the formation of coalescence pores dispersed into the primary pores. This implies that the size and volume fraction of coalescence pores depends on the size of the primary pores as well as the rate of polymerisation and temperature.

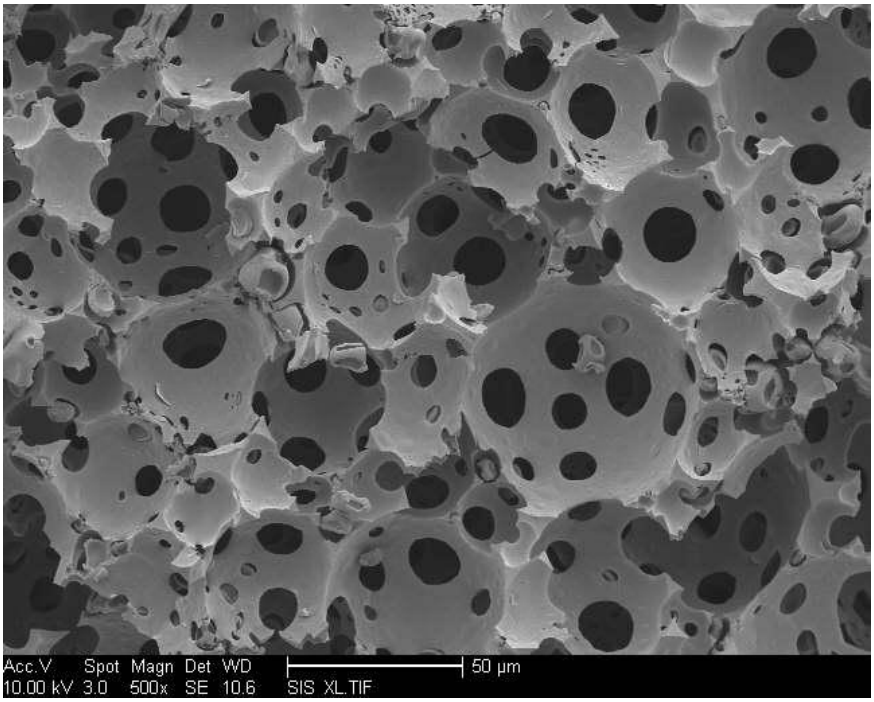

Figure 3-9: SEM micrograph of microwave irradiated PHP (MWD-7) at low magnification. MW irradiation time, t = 4 min

It was found that when these polymers are sulphonated using thermal methods (with or without acid present at the emulsification stage, using concentrated or dilute acid), surface area is reduced drastically (to ca. 3 m^2g^{-1}). Surface area is also reduced by the addition of 2-Vinyl Pyridine.

An intensified method proposed by Akay (2006) and Mohamed et al. (2006) in which PolyHIPE Polymers are sulphonated or nitrated using sulphuric and nitric acid respectively. It is also possible to carry out simultaneous sulphonation and nitration using a mixture of these acids. Accordingly, upon polymerization of the HIPE emulsion (which typically contains 10 wt% acid in the dispersed phase) in cylindrical container, samples in the form of disks were cut and soaked in concentrated sulphuric acid for two hours. This was followed by irradiation in a microwave oven for a preset length of time for sulphonation or nitration. Some of the samples were dried under vacuum at 60°C in order to increase the sulphuric acid concentration from 10% to 70% before sulphonation

so as to accelerate the rate of sulphonation. Due to the increase in temperature within the samples during microwave irradiation, radiation was intermittent with air cooling. Typically, irradiation time of t_i is followed by a cooling period of $t_c = t_i / 2$. This was repeated N times so that the total irradiation time was $t_T = Nt_i$. The average sulphonation temperature was 40°C. After sulphonation, samples were washed in a mixture of water/iso-propanol to remove all the residual monomer/crosslinker, initiator and excess acid. Polymer disks were then dried under vacuum and stored for examination and for determination of the degree of sulphonation using the method described in (Akay et al., 1995). Figure 3-10 show a schematic diagram for the preparation of functionalized PolyHIPE Polymer. It was found that when the polymer was sulphonated through microwave irradiation, surface area increased from 3.52 m^2g^{-1} to 243 m^2g^{-1} (Mohamed et al., 2006).

.

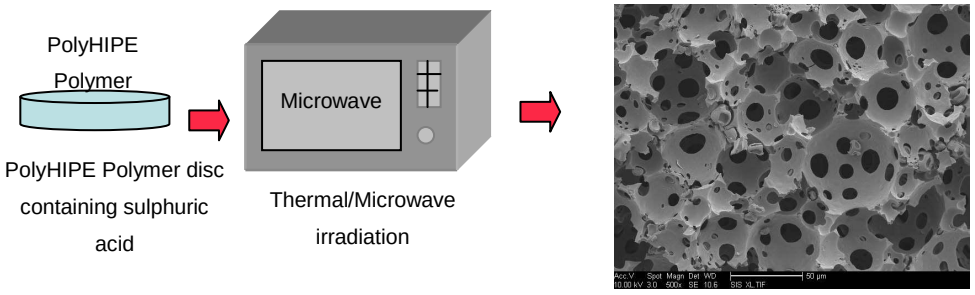

Figure 3-10: Schematic Diagram for the Preparation of Functionalised PolyHIPE Polymer

3.5.2 Silanation

It is important to understand the mechanisms that mediate metal interactions with polymer surfaces so as to promote the required environment in order to improve metal penetration. The surface chemistry of the template may be the key to metal adhesion. On a poorly adhesive surface, metal may attach so weakly that no interaction can be obtained and therefore no deposition occurs. The conditions for a metal to attach have to

be favourable. The challenge is to design a polymer or other media with a suitable environment that can increase metal adhesion.

Silane coupling agents are among others used as an alternative to surface treatment and have the possibility of working as adhesion promoters between template and metal. Silane coupling agents belong to a class of organosilane compounds having at least two active groups of different types bonded to the silicon atom in a molecule. One of the reactive groups of different types, such as methoxy, ethoxy and silanolic hydroxyl groups, is reactive with various inorganic materials, such as glass, metals, silica sand and so forth, to form a chemical bond with the surface of the inorganic material (Goyal, 2006). The other reactive groups, such as vinyl, epoxy, methacryl, amino and mercapto groups, is reactive with various kinds of organic materials or synthetic resins to form a chemical bond. As a result of possessing these two types of reactive groups, silane coupling agents are capable of providing chemical bonding between an organic material and an inorganic material.

These unique properties of silane coupling agents have played an important role in the fast growing field of advanced materials. They act as adhesion promoters, coupling agents and surface primers (Walker, 1992). In addition, silanes are utilized widely in applications for surface treatment of glass fiber products, performance improvement of fiber-reinforced plastics by direct admixture to the synthetic resin, improvement of paints and other coating materials and adhesives, modification of surface properties of inorganic fillers, and surface priming of various substrate materials. Much work has been performed to achieve the mechanisms for the properties enhancement induced by these compounds (Pizzi and Mittal, 1994; Silberzan et al., 1991).

Organosilane coupling agents are represented by R'- Si $-(OR)_3$, where R' is a short hydrocarbon chain (usually 3-6 backbone carbons long) with an appropriate organic functional group such as an amine or epoxy group, and OR is a hydrolysable alkoxy group such as $-OC_2H_5$-OCH_3.

Schematic presentations of silane deposition are as follows (Lindberg et al., 1998):

- Hydrolysis of molecule

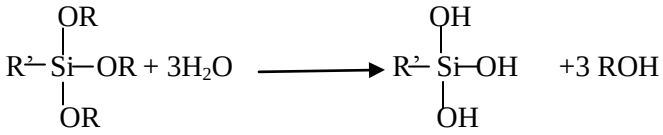

- Productionof silanols through hydrolysis of alkoxy groups.
- The formation of oligomers by condensation reaction of the hydrolysed molecules to form siloxane bond

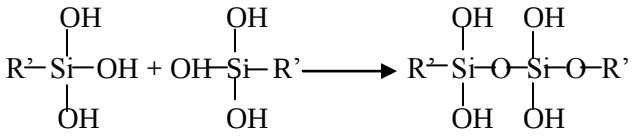

- The hydrolysed.molecules can also bind to the silica or silicate surface by reaction condensation to form siloxane bond.

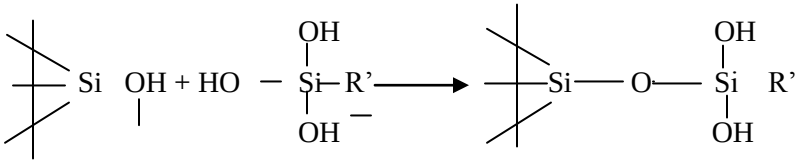

3.5.2.1 Utilising Silane Applications

Silane can be utilized in various applications by three basic method: 1) as surface treatment; 2) as additive; 3) as crosslinker whereby each of these methods requires special consideration. According to Witucki (1993) surfaces can be silanated from alcohol solution. A 2% silane solution can be prepared in the alcohol of choice

(methanol, ethanol or isopropanol) and followed by wiping, dipping or spraying the solution onto the surface. Before the surface treatment, silane is subjected to hydrolysis process where a reactive silanol group is formed followed by condensation with other silanol groups from either the surface of siliceous fillers or other oxides (nickel, aluminum, zirconium, tin, titanium). It is necessary to provide sufficient amount of water to enhance the degree of hydrolysis which may be present on the substrate surface, or from the atmosphere. When silane is used as additive, it becomes a component of the coating from which it diffuses or migrates to the inorganic substrate and reacts. Silane are generally effective in concentrations ranging from 0.05 to 1.00% of the coating (Plueddemann, 1983). Silane can also react with organic polymers to attach the trialkoxysilyl group onto the polymer backbone. The silane is then available to react with moisture to crosslink the silane into a stable, three-dimensional siloxane structure.

An organic-inorganic hybrid open-cell foams was successfully prepared by Tai et al (2001) through copolymerizing MPS (a vinylsilane) and styrene in HIPEs. The combination of vinyl radical polymerization with trimethoxysilane hydrolysis and condensation in a HIPE was expected to yield an organic-inorganic hybrid foam, possessing unique properties, including higher thermal stability (Tai et al., 2001). Menner et al. (2006) have reported an attempt to enhance the mechanical properties of PolyHIPE Polymer. Methacryloxypropyltrimethoxysilane was added to the continuous phase to ensure that the silica particles were covalently bonded into the inorganic polymer network formed by the hydrolytic condensation of the silane groups (Menner et al., 2006). Although the stability of the emulsion was not affected, upon polymerisation the polyFoams did not possess the characteristic open porous network structure. On the other hand, nanoporous polymer nanocomposites synthesized within high internal phase emulsions was reported by Silvertein and Normatov (2007). Their study proposed procedures to obtain nanocomposite polyHIPE with 3D hybrid nanostructures using silane from vinyl group added to organic phase (Silverstein and Normatov, 2007).

Glass fibre based composite materials have become very attractive materials in many industrial applications because of their excellent mechanical performances/cost ratio. The structure depends mainly on the coating applied to the fibre surface before association with another matrix (Zinck et al., 2001). In most cases, the latter is an organofunctional alkoxysilane which can react at the glass surface with the silanol groups and which favour chemical coupling with the sizing as well as with the polymer matrix in order to promote interfacial adhesion (Zhou et al., 2005; Pleudemann, 1982).

One of other applications of silanes is to improve adhesion of organic coatings to metals. Films of vinyl-triethoxy silane (VTES) on iron (Fe/VTES system) were used to study the effect of exposure to air on protective properties and on chemical transformations of silane films. It was found that apart from improving adhesion, silanes also play an important role in protecting against corrosion (Fils and Kanova, 2006)

3.5.2.2 Applying Silanes

Substrates are treated with either neat silane or a solution of silane in water and/or alcohol. With a neat silane, the absorbed waster on the substrate surface is often sufficient to hydrolyze the alkoxysilane and simultaneously bond the silane to the substrate surface. It is imperative to use an intensive mixing to obtain a uniformly coated silane. To remove the byproduct of alcohol and water, substracts are further heat treated and hence complete the bonding of the silane surface. Other methods were also employed depending on nature of the substrates. Bulk deposition onto powders is used for treatment that is accomplished by a spray on method. The powder is placed in a high intensity solid mixer, e.g. twin cone mixer with intensifier and known as most effective method used. An integral blend method is performed in composite formulation. In this method the silane is used as a simple additive. Composites can be prepared by the addition of alkoxysilanes to dry-blends of polymer and filler prior to compounding. Generally 0.2 to 1.0 weight percent of silane (of the total mix) is dispersed by spraying the silane in an alcohol carrier onto a preblend. The mix is dry-blended briefly and then

melt compounded. Vacuum devolatization of byproducts of silane reaction during melt compounding is necessary to achieve optimum properties. Additionally, anhydrous liquid phase deposition of chlorosilanes, methoxysilanes, aminosilanes and cyclic azasilanes is preferred for small particles and nano-featured substrates. This method involves a direct nucleophilic displacement of the silane by the surface silanol

CHAPTER 4

LITERATURE REVIEW: ELECTROLESS DEPOSITION

4.1 Overview

This section consists of three subsections that review the literature published on one of the key areas of the present research: a) The concept of elctroless deposition b) The electroless deposition and c) Electroless films Formations Mechanism on Non-Metal Substrate. It also outlines a framework for the later chapter obtained in this study.

4.2 Electroless deposition

Electroless deposition is the formation of a metallic coating on a metallic or nonmetallic surface by means of a chemical reaction between metal ions and a reducing agent in an aqueous solution in the absence of external electric current (Durkin and Steinecker, 2004). Also known as autocatalytic plating, in this process the substrate develops a potential when it is submerged in electroless solution which contains a source of metallic ions, reducing agent, stabilizer and other components (Delaunois and Lienard, 2002). Due to the developed potential, both positive and negative ions are attracted towards the substrate surface and release their energy through a charge transfer process. Each process parameter has a specific role in the process and influences the process response variables (Oraon et al., 2007). The reduced metal atom is absorbed on the substrate surface, which is followed by the formation of metal film. Eventually it acts as a catalyst when the metal film covers the whole substrate and subsequently helps increase the thickness (Watanabe, 2004). Temperature initiates the reaction mechanism which controls the ionization process in the solution and charge transfer process from

source to substrate. The basic chemical reactions for electroless plating are given by the following expressions (Riedel, 1991):

$$R^{n+} \rightarrow R^{(n+z)} + ze$$
$$Me^{+z} + ze \rightarrow Me \qquad \text{Eq 4-1}$$

where 'R' indicates the reducing agent and 'Me' indicates the metal to be deposited on a substrate, 'z' indicates number of electron released and 'e' indicates number of electrons. Electroless deposition has the advantages of simplicity and feasibility over other method such as chemical vapour deposition and electroplating (Oraon, 2007).

Generally, metals obtainable by an electroless plating method and their reducing agent are listed in Table 4-1 . The quantity of these alloying elements depends on the concentration of reducing agent, pH and solution temperature.

Table 4-1: Reduced metals by electroless plating methods and their reducing agent (Watanabe, 2004)

Metal	**Reducing Agent**
Ni	$NaHPO_2$, DMAB, $NaBH_4$, KBH_4, NH_2NH_2 ,HCHO
Co	NaH_2PO_2, DMAB, $NaBH_4$, KBH_4, NH_2NH_2, HCHO
Pd	NaH_2PO_2, $NaHPO_2$, NaHPO, NH_2NH_2
Cu	HCHO, DMBA, KBH_4
Ag	DMBA, KBH_4
Au	DMBA, KBH_4, NaH_2PO_2, $NaHPO_2$, CH_4N_2S, $C_6H_8O_6$
Pt	NaH_2PO_2, $NaHPO_2$
Pb	$SnCl_2$
Rh	NH_2NH_2
Ru	$NaBH_4$

4.3 The Electroless Nickel Deposition

Electroless nickel plating has become a practical and popular finish since its discovery by Brenner and Riddel in 1946 on chemically deposited metal coatings formed by hypophosphite reduction of nickel and cobalt ions from aqueous solution. The alloy coatings so produced were observed to possess many superior properties, such as high hardness and low porosity, when compared to conventional electrodeposited nickel (Narayanan et al., 2003; Riedel, 1991; Weightman and Pearlstein, 1974). Electroless nickel plating is used to deposit nickel alloy on a substrate that can be either nickel-phosphorus or nickel-boron.

Applications of electroless nickel was reported in many industries, including the petroleum, chemical, plastics, optics, aerospace, nuclear, electronic, computer and printing industries (Delaunois and Lienard, 2002) due to its excellent corrosion and wear resistance properties.

4.3.1 The Components of Electroless Nickel Plating Bath

The principal parameters controlling an electroless bath in an electroless nickel system are the nickel ion concentration, the complexing agent concentration, temperature, pH, stabilizer concentration, bath age, bath loading and agitation (Riedel, 1991; Mallory, 1990). According to Mallory (1990), a typical nickel plating bath generally includes:

- A source of nickel ions
    - There are three main nickel ion sources used in electroless nickel plating. The most widely used nickel ion source is nickel sulphate. Having found fewer applications, the other nickel sources are nickel chloride and nickel acetate.

- A reducing agent to supply electrons for the reduction of nickel.
    - There are a number of different reducing agents available in electroless plating. These are sodium hypophosphite, sodium borohydride, dimethylamine borane, hydrazine and formaldehyde. The similarity between all structures shown in Figure 4-1 is that all five chemicals contain two or more reactive hydrogen.
    - It is believed that nickel reduction is a result of catalytic dehydrogenation of the reducing agent; hence the reduction of nickel is always accompanied by liberation of hydrogen gas. It is very important to understand the mechanism of the reactions between nickel ions and reducing agents. It will lead to a more accurate control of the plating rate and a better control of the amount of phosphorus and boron, since the quantity of phosphorus and boron is one of the main factors that determine the properties of the deposit. Nickel deposits, reduced by hypophosphite or boron containing reducing agents, also contain codeposited phosphorus or boron

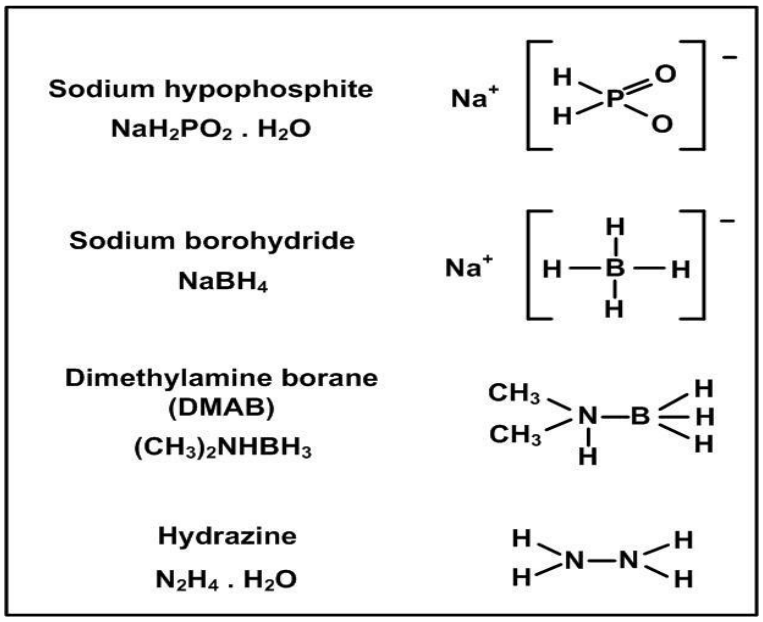

Figure 4-1: Reducing agents for electroless deposition (Mallory, 1990)

● Complexing agents to determine the amount of free nickel

- Complexing agents are generally added to electroless nickel plating baths in order to prevent rapid decrease in the pH of the bath, to prevent the precipitation of the nickel salts and to reduce the concentration of free nickel ions. Apart from these functions, complexing agents control the reaction so that it occurs only on the catalytic surface. They also affect the deposition reaction and hence the resultant nickel deposit. They are usually organic acids or their salts.

● Stabilizors (inhibitors) to control the reaction

- Stabilizers are chemical agents used to prevent the spontaneous decomposition of the entire plating bath. Decomposition of the bath is generally caused by an increase in the volume of the hydrogen gas evolved and the formation of a finely divided black precipitate (nickel phosphide or nickel boride depending on the reducing agent) throughout the bulk of the solution (Mallory, 1990).

● Buffering agents to keep pH in the required range

● Accelerators

- Accelerators are used to regulate the rate of reaction. An addition of complexing agents sometimes causes the plating speed to become uneconomically slow. This problem can be overcome by adding small amounts of organic additives, called accelerators Succinic acid is the most commonly used accelerator in hypophosphite reduced solutions (Fields et al., 1982).

4.4 Electroless Ni-P Deposition

The chemical reducing agent most commonly used is sodium hypophosphite (NaH_2PO_2). Compared to other reducing agents it is much cheaper and easier to control. In general, the electroless deposition of Ni–P alloy can be classified into three categories according to phosphorus content: low (1–5 wt.%), medium (5–8 wt.%), and

high (9 wt.% and above) phosphorus deposits (Gu et al., 2005). In a system containing NaH_2PO_2 the following reaction sequence has been observed to occur (Mallory, 1990):

$$H_2PO_2^- + H_2O \rightarrow H_2PO_3^- + 2H^+ + 2e^- \quad \text{Eq 4-2}$$

Nickel ions at the catalytic surface are reduced by the absorbed active hydrogen:

$$Ni_+^+ + 2e^- \rightarrow Ni \quad \text{Eq 4-3}$$

The liberation of hydrogen gas in the catalytic nickel reduction is the recombination of the hydrogen atoms:

$$2H^+ + 2e^- \rightarrow H_2 \quad \text{Eq 4-4}$$

Another reaction between some of the absorbed hydrogen and a small amount of hypophosphite ion at the catalytic surface produces water, hydroxyl ions and elemental phosphorus:

$$H_2PO_2^- + 2H^+ + e^- \rightarrow P + 2H_2O \quad \text{Eq 4-5}$$

It was reported that this reaction occurs independently of the deposition of nickel and phosphorus hence causing the low efficiency of electroless nickel solutions

$$(H_2PO_2)^{2-} + H_2O \rightarrow H^+ + (HPO_3)^{2-} + H_{2-} \quad \text{Eq 4-6}$$

It has been reported that factors affecting the phosphorus content of electroless Ni-P are the pH of the plating solution, the concentration of hyphosphite ions, the concentration of free nickel ions, and the temperature of the reaction (Allen and Vance Sande, 1982). Ni-P bath solution is formulated as an alkaline solution and can be operated at low temperatures, making it suitable for plating on PolyHIPE materials.

It was also reported that the morphology and structure of Ni-P deposits depends upon the content of phosphorus. It was found that above 7 wt% the structure is amorphous, and below it is microcrystalline. However, recent findings of Kumar and Nair (1994) claim that a mixture of microcrystalline and amorphous was found in Ni-P deposits, with phosphorus content between 4.4 to 9.1wt%. The effect of heat treatment results in modification of their structure (Hirth and Speckhardt, 1972). It was also reported that the deposits become metallic nickel containing nickel phosphide crystallites, Ni_3P. The degree of crystallization is influenced by the temperature, length of exposure, phosphorus content and composition (Huang and Cui, 2007; Liu et al., 2006; Qiao et al., 1995; Allen and VanderSande, 1982). Ni-P deposits have been found to result in improved properties such as high corrosion resistance, high wear-resistant, good lubricity, high hardness and acceptable ductility (Gu et al., 2005, Lin and He, 2005).

4.5 Electroless Ni-B

Although electroless nickel–phosphorus (Ni–P) has gained maximum attention in electroless plating processes (Riedel, 1991), Ni-B has received widespread acceptance due to properties that are uniquely advantages. A nickel-boron electroless deposition is designed when extreme hardness, ductility, wear, lubricity, elevated operating temperature and corrosion characteristics are required. Electroless Ni-B deposits can be produced using either sodium borohydride ($NaBH_4$) or amine borane compounds as a reducing agent (Watanabe, 2004; Riedel, 1991). Sodium borohydride is one of the most powerful reducing agents. It has a higher reducing efficiency than hypophosphites and other boron-containing reducing agents.

In a system containing $NaBH_4$, the following reaction sequence has been observed to occur (Mallory, 1990):

$$BH_4^- + 8OH^- \rightarrow B(OH)_4^- + 4H_2O + 8e^- \qquad \text{Eq 4-7}$$

$$4Ni^{+2} + 8e^- \rightarrow 4Ni^0 \qquad \text{Eq 4-8}$$

The overall reaction would be:

$$4Ni^{+2} + BH_4- + 8OH- \rightarrow B(OH)_4^- + 4H_2O + 4Ni^0 \qquad \text{Eq 4-9}$$

The plating bath produced by using sodium borohydride as a reducing agent is a highly alkaline solution. The deposition solution is operated at a pH ranging from 12 to 14 and temperature 90 to 95°C to prevent decomposition (Delaunois et al., 2000). These bath tend to be less stable because of their alkalinity and bath decomposition may occur if the pH falls below 12 (Henry, 2007). In acid or neutral solutions, hydrolysis of borohydride ions is very rapid. If there are nickel ions in the solution, nickel boride will form spontaneously. However, if the pH of the plating bath is maintained between 12 and 14, nickel boride formation is suppressed and the product of the reaction is elemental nickel. Deposition of nickel and rate of decomposition of sodium borohydride increases as the temperature of the bath increases (Lo and Hwang, 1994). Hence, an optimal operation temperature must be taken into account for the electroless nickel bath. Borohydride reducing agent may consist of any water soluble borohydride having a good degree of solubility and stability in aqueous solutions. As it is more cost effective than amine boranes and it can be used efficiently in a low temperature electroless bath, it can be applied to metalize polymer materials which can not tolerate high temperatures (Lo and Hwang, 1994).

.

The utilization of aminoboranes in electroless plating is generally limited to two chemicals, namely dimethyamine borane (DMAB) and diethyamine borane (DEAB). Although DMAB is readily soluble in aqueous solutions, DEAB has to be mixed with a short chain aliphatic alcohol in advance in order to be dissolved in the electroless plating bath.

The operating temperatures for aminoborane baths have a typical range of 40 to 90 ºC. The possibility to operate these baths as low as 30ºC makes them ideal for plating over plastic and non-metal surfaces. Unlike borohydrides, aminoborane reduced electroless

plating solutions have wide pH ranges, although the baths are generally optimized between 6 and 9.

Amineboranes are covalent compounds although borohydrides such as Na+ BH4- are completely ionic, that is Na + BH_4^- = Na^+ + BH_4^-. Despite the fact that aminoboranes do not ionize, one of the atoms has a greater affinity for electrons than the other and thus the bond will be polar (Mallory, 1990):

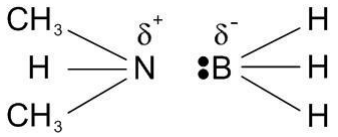

Displacing towards the boron atom, the electrons give boron atom excess negative charge whereas the nitrogen atom displays excess positive charge. The electrical polarity of a molecule plays an important role in the reactions of covalent compounds. Since DMAB has three active hydrogen atoms bonded to the boron atom, theoretically it should reduce three nickel ions for each DMAB molecule consumed. Then the reduction of nickel ions with DMAB can be described by the following equations:

$$Ni^{+2} + (CH_3)2NHBH_3 + 3H_2O \rightarrow 3Ni^0 + (CH_3)2NH^{2+} + H_3BO_3 + 5H^+ \quad \text{Eq 4-10}$$

$$2[(CH_3)_2NHBH_3] + 4Ni^{+2}\ 3H_2O \rightarrow Ni_2B + 2Ni0 + 2[(CH_3)_2NH^{2+}] + H_3BO_3 + 6H+ + ½H_2 \quad \text{Eq 4-11}$$

However, the experimental results do not support the theoretical expressions. Mallory (1971) reported that the molar ratio of nickel ions reduced to DMAB molecules consumed is approximately 1:1.

The deposits obtained from these electroless system; Ni-P and Ni-B exhibit many different characteristic especially dependency of both phosphorous and boron content. Different properties can be achieved depending on the alloyed quantity of the deposit. Nickel boron (B) alloy deposits can provide other additional properties and

characteristics with the change of boron content (Baudrand, 1995). Deposit characteristics of Ni–B coatings change with boron content similar to Ni–P coatings and the boron content in electroless Ni–B coatings varies between 1% and 10% in weight (Mallory, 1990). Higher concentrations of boron containing alloys are very hard and wear resistant, although the cost of producing these deposits is many times greater than newer, lower phosphorus deposit formulations capable of similar hardness and wear properties (Narayanan et al., 2003). Ni-B amorphous coating (16-25% of boron) is used in the manufacture of tools and products for electronic and mechanical engineering as it demonstrates a low contact resistance and is good in terms of plated hardness and wear resistance. Lower concentration boron deposits provide high electrical conductivity, which means they are suitable for use in the electronics industry because of their electrical and physical qualities (Prusov and Makasov, 2005). Ni-B polycrystalline (1-6% of boron) is used in the manufacture of printed circuit-boards (Flacker et al., 1995). It has been found to have many uses as it can reduce or eliminate the usage of gold in the electronic industry. According to Duncan and Arney (1984), electroless coatings are more wear resistant than tool steel and hard chromium coatings and they can replace the use of gold in electronic industries.

The main advantages of electroless Ni–B coatings are that they have high hardness and superior mechanical wear resistance properties (Oraon et al., 2008; Dervos et al., 2004; Narayanan et al., 2003; Delaunois and Lienard, 2002; Ivanov, 2001). In the as-deposited condition, microhardness of borohydride reduced coatings range from 650 to 750 HV100 (Narayanan et al., 2003). After 1h heat treatment between 350°C and 400 C, hardness values of about 1200 HV100 can be produced (Bandrand, 1994). Studies by Delaunois and Lienard (2002) demonstrated that the Knoop microhardness of Ni-B after bath reaches $759hk_{100}$ and after treatment can increase microhardness up to more than $1000hk_{100}$. Long term heat treatment for about 30–40 weeks between 200°C and 300 C can produce hardness between 1700 and 2000 HV100 (Ziyuan et al., 2004).

The study on corrosion rate of Ni–B coatings has been seen to be greater than that of Ni–P coatings for as-deposited condition (Ziyuan et al., 2004). It is also known to be

more ductile and have better adhesion. The columnar structure of Ni-B coatings is useful in retaining lubricants under conditions of adhesive wear that lead to a Nickel-boron surface with a low coefficient of friction (Mc Comas, 2002). It wears longer and most importantly is more cost effective than hard chrome. Due to its resistance to oxidation, these types of deposits will solder or braze well and show good shelf life solderability (Katsuhiko et al., 2002). A study by Tomlinson et al. (1989) showed that Ni-P deposit oxidized approximately 1000 times faster than pure nickel, while the addition of boron decreased the amount of oxidation and tended to retard the formation of oxides on the surface of the deposit.

In addition, the melting point of Ni-B deposits is found higher than that of Ni-P deposits (1080°C for Ni-B (5% B) in comparison to 890°C for Ni-P) (Dervos et al., 2005). The different melting temperatures of electroless nickel deposits depend on the amount of boron alloyed in the deposit. In general, the melting point is about 1200°C for deposits from processes with approximately 7-9% boron. This temperature corresponds to the melting point of nickel boride, which precipitates during heating of electroless nickel deposits (Saito et al., 1999). The 0.25% B deposit has a melting point of 1,455°C (Baudrand and Bengston, 1995), which makes it suitable for high temperature catalyst.

The structure of Ni-B deposits is mainly determined by boron content; deposits with high boron content tend to form amorphous phase while deposits with low boron content tend to form semi-crystal (Rao et al., 2005). The quantity of amorphous phase increases with boron content (Watanabe, 2004; Narayanan et al., 2003). According to Watanabe and Tanabe (1975) the microstructures of Ni–B deposits are a mixture of microcrystalline nickel and amorphous Ni–B phases in the as-deposited condition. On the other hand, as deposited electroless Ni-B deposits formed grains that are in a columnar manner and the grains is perpendicular to the substrate surface (Riddle and Bailer, 2005). The columnar grain growth leads to semi-hemipherical (nodular) caps at the exposed surface of the as plated deposits. A study presented by Di Gaimpaolo et al. (1997) has produced a continuous film of uniform thickness deposition. Nickel-boron deposits a dense, uniform and continuous deposition through the substrate.

4.6 Electroless films Formation Mechanism on Non-Metal Substrate

Watanabe (2004) has described the formation of metal film, starting from the migration of metal ions toward the substrate surface via diffusion through to the metal-ion gradient with the aid of solution agitation. Since the substrate surface acts as a catalyst for the reducing agent, it is consequently oxidized and generates electrons. These electrons are incorporated with incoming metal ions and neutral metal atoms. Upon a physical or chemical adsorption on the substrate surface, neutral atoms become adatoms, which is followed by the formation of an electroless film. However, the substrate needs to be catalytic active to initiate metal deposition.

Initially, a metal layer was formed as a flat island on the substrate surface. Due to heat evolution and violent solution movement caused by the reaction, the edge of the metal island is highly activated. Hence, the edge region is spread through preferentially and expands laterally in two dimensions until it reaches a critical thickness where a layer of low metal-ion concentration is generated at the solution-island interface. However, the film cannot grow beyond the critical thickness until the layer of low metal-ion concentration is destroyed by solution agitation and replaced with a fresh solution of high metal-ion concentration from the bulk electrolyte. Consequently, the second layer is formed when the high metal-ion concentration solution comes in contact with the first layer. The growth process is repeated in the same manner for the next additional layer. Accordingly, the growth rate of electroless films is controlled by the thickness, agitation speed and solution temperature (Watanabe, 2004; Dennis and Such, 1972). This process is illustrated in Figure 4-2. However when a film grows without agitation, the layer formed represent a trace of compositional modulation induced by a change in solution pH and temperature.

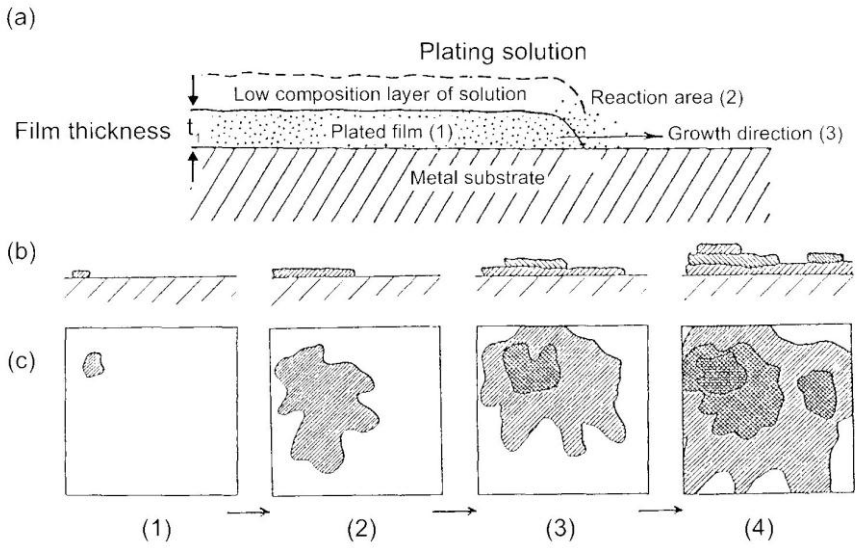

Figure 4-2: A schematic diagram showing a mechanism of elecroless film formation.

a) at the edge of the metal island,

b) in the cross-sectional view,

c) from the top view (Watanabe, 2004)

Electroless films can grow expetaxially on metal substrate by forming a metal-metal bond (Watanabe and Tanabe, 1976). The bond strength corresponds to the maximum adhesive force of the film to the substrate. However, for a non-metal substrate, a proper surface treatment is necessary prior to metal deposition by etching to create microscopic pores on the substrate. Contrary to the catalytic metal substrate, no chemical bond exists between an electroless metal film and a non-metallic substrate. Thus, there is no adhesion between them. The initial deposit is embedded and anchored inside the pores and a large amount of force is required to separate the film from the substrate. This anchoring force is mechanical in nature and represents the adhesive strength of electroless films and non-metallic substrate, depending on the shape, depth and density of the pores. Therefore, proper control over the geometry of the pore is essential and must be structurally non-uniform. Figure 4.3 a schematic diagram illustrating how an electrless film grows on a non-metallic substrate.

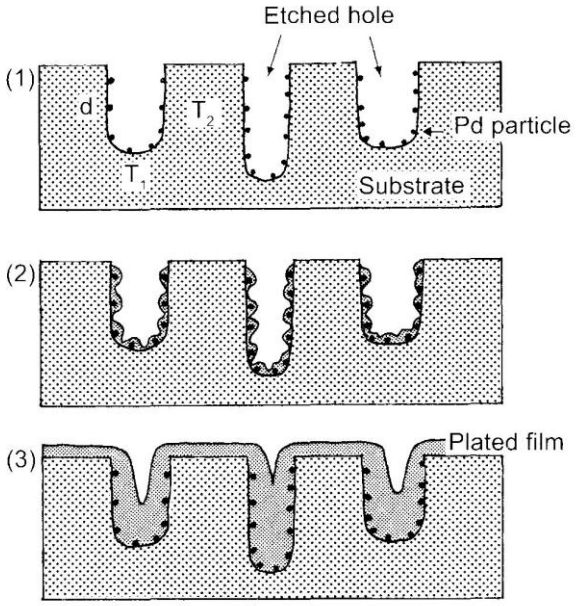

Figure 4-3: Film formation processes of electroless metals on an etched/activated non-metallic substrate(Watanabe, 2004)

CHAPTER 5

EXPERIMENTAL PROCEDURE APPARATUS and ANALYTICAL METHOD

5.1 Overview

This chapter is presented in three main categories:

i. Preparation of PHP templates – which includes the preparation of PHP with with hierarchical pore structure and preparation of materials from other porous material.
ii. Metallization with Ni-B/P of PHP and other porous materials and its characterisation – which consists of the operation condition that includes concentration of bath solution, nickel source and reducing agent used, as well as operating cell temperature and deposition solution flow rate. The morphological structural was observed through a Scanning Electron Microscope (note that some micrographs result in blurry images This explained that when taking images of unconducting samples at low vacuum, the resolution is not as good at high magnification as when taking images of conducting (on gold/carbon coated) samples at high vacuum. Also at high magnification some unconducting samples charge up and 'move' in the beam making focusing difficult and slow scans impossible) and X-ray Diffraction Analysis
iii. Silanation of template for better surface metal deposition– which includes the preparation and silanation on templates that demonstrates poor adhesion between metal deposition and template.

5.2 Preparation of Porous Materials with Hierarchical Pore Structure

5.2.1 Preparation of standard PHP (Coded as PHP 1)

High internal phase emulsions (HIPEs) is used in the design of a highly porous materials (PolyHIPEs) with hierarchical and interconnect pore size and used them as template. These polymers are prepared either in particulate form or monoliths with any size and shape due to their capacity of being moulded at the emulsion stage. Droplets of dispersed phase during polymerization leaves each cell connected to all its neighbouring cells. Therefore it is necessary to control the property of the emulsion ie pore size (the diameter of the dispersed droplets in emulsion) such as disperse phase volume (ε), concentration of the surfactant, co-monomers and the cross-linking agent (Byron, 2000a).

In this study, we are concerned with the production of PolyHIPE polymer having pore sizes that can penetrate metal deposition, therefore the pore sizes should fall within the size of metal grain use. It was reported from previous studies that pore sizes ranging between 40µm-60µm was successfully metal deposited using Ni-P eletroless deposition system having grain size ranging 5-15µm (Calkan, 2006). For our experiments we are going to develop PHP with pore sizes in the range of 20-60 µm, in order to obtain full metal deposition penetration as we are using Ni-B electroless deposition system having the grain size in the range of 0.25-2 µm. This section's main objective is to produce PHPs that are suitable for metal deposition which entailed making the polymer with hierarchical pore structure.

Materials

The polymer used in this study is derived from a styrene based oil phase containing styrene and aqueous phase containing potassium per-sulphate. PolyHIPE Polymer is produced by the polymerization of a high internal phase emulsion (HIPE) formed from the two phases, the compositions of which are described in the next section:

For these experiments the composition for PHP is made up as shown below:

Oil phase

78 % styrene (monomer) cross linked with

8 % divinyl benzene (cross linking agent) and to this add

14% Span 80 (surfactant)

Aqueous phase

1%wt of potassium persulphate (polymerization initiator)

Made-up with deionised water (1 litre)

These chemicals were purchased from Aldrich Chemicals and used as received.

Experimental Procedure

The PHP used in this study was produced on a laboratory scale using apparatus as shown in the schematic diagram in Figure 5.1. This set up produced PHP with large pore sizes ranging from 20-60 µm suitable for metal deposition.

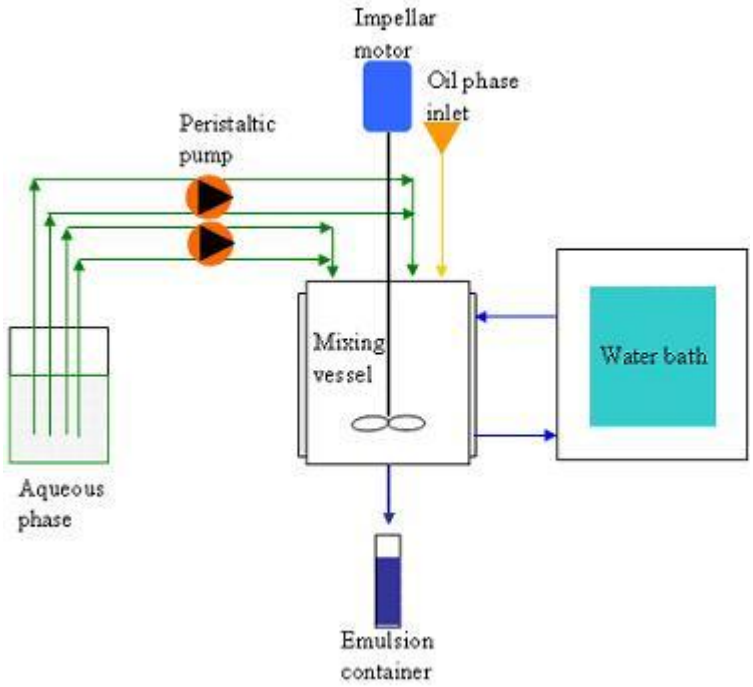

Figure 5-1: Schematic diagram of the production of PHP

The mixing of oil phase and aqueous phase was carried out using jacketed stainless steel mixing vessel with 12 cm in diameter and water bath was used to circulate hot water through the vessel at 60°C (Figure 5-2). The phase volume was kept as 80% to ensure an open pore structure. The total volume of oil phase and aqueous phase used in each experiment was 225ml. The oil phase was initially dosed through a funnel inlet into the mixing vessel followed by aqueous phase (heated at 60°C) that was pumped using two peristaltic pumps via four feed points at a constant rate for the duration of the dosing time. The dosing of the aqueous phase was within 2 min intervals and another 1 minute was allowed for mixing.

Figure 5-2 : Mixing vessel used for emulsification

The mixing vessel consisted of 2 flat impellers that were stacked at right-angles to each other (Figure 5-3). The bottom end of the impeller was placed 1 cm from the bottom of the vessel to obtain homogenous mixing. The impeller was set to a mixing speed of 300rpm..

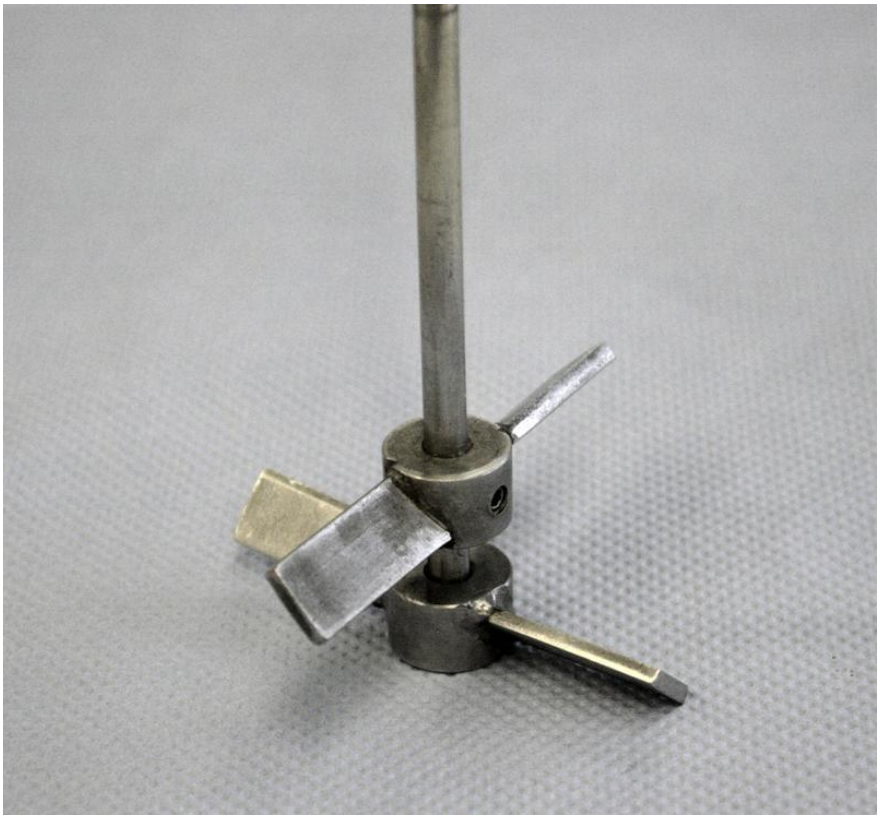

Figure 5-3: The two flat impeller:s used to mix the emulsion

After emulsification, the emulsion was transferred to cylindrical containers with an internal diameter of 26 mm and polymerized at 60°C for at 8 hours. After polimerization, PHP samples were cut into 26mm in diameter and 4 mm thick disks ((Figure 5.4). Samples were then dried in fume hood for 2-3 days

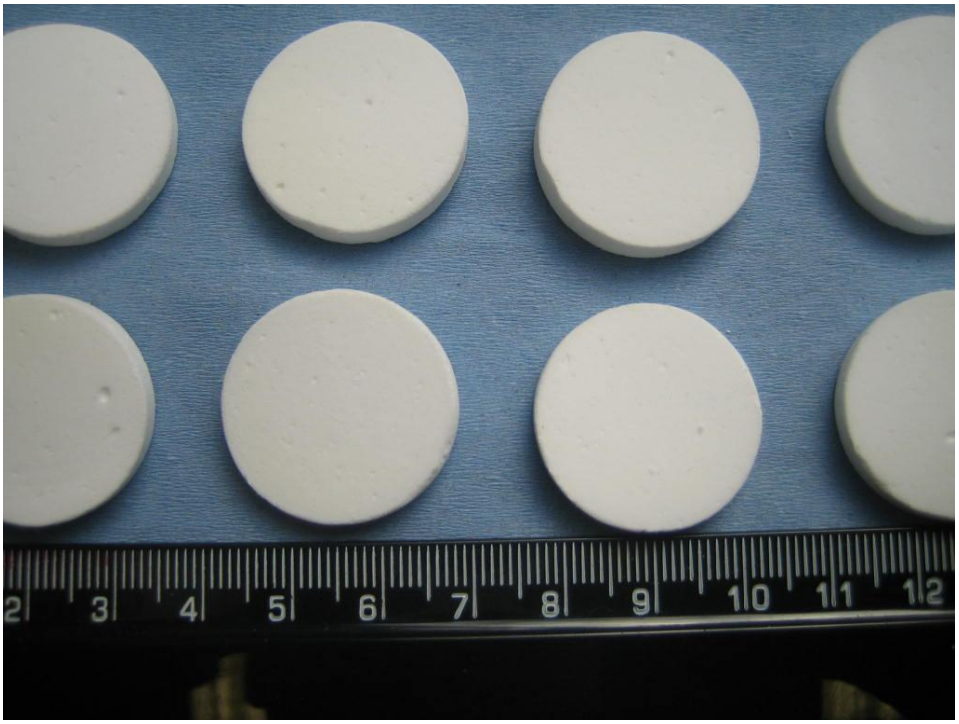

Figure 5-4: PHP samples were cut to size of 26mm diameter and 4 mm thickness after polymerization

5.2.1.1 Washing of PHP

A soxhlet system (Figure 5-5) was used to wash the PHP samples in order to remove as much residual surfactant, toxic monomer and electrolytes from the polymer. This was carried out by washing the PHP samples in iso-propanol for three hours and with distilled water another 3 hours. All samples were then dried overnight in a vaccum oven to evaporate the remaining iso-propanol and water.

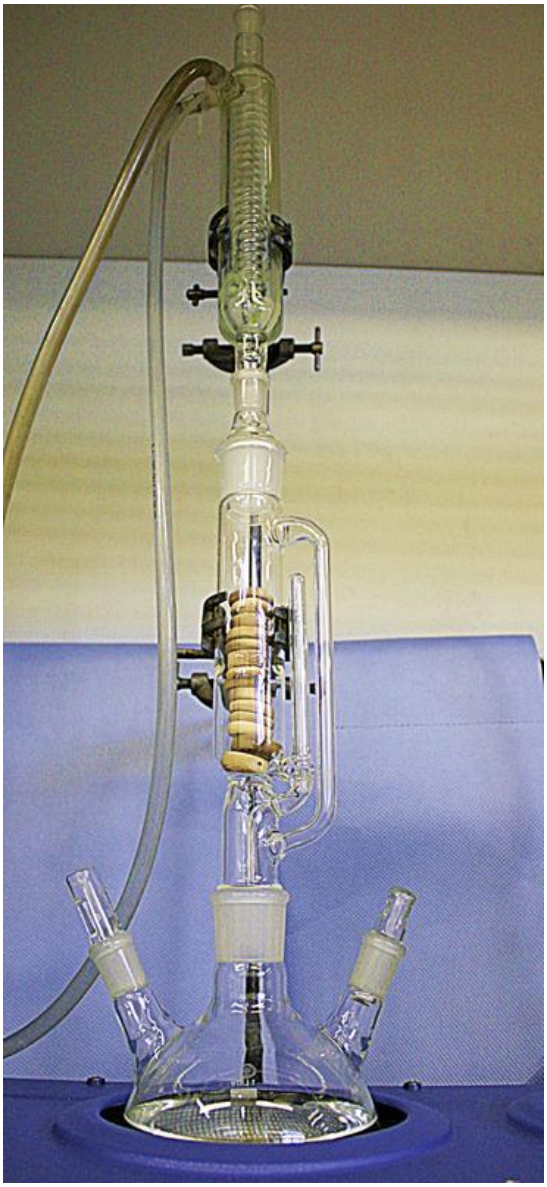

Figure 5-5: Soxhlet System - apparatus used in the washing of PHP

5.2.1.2 Determination of Pore and Interconnect Size Distribution

In order to determine the uniformity of the emulsion, it is therefore necessary to calculate the distribution of the pore sizes within the polymer (Byron, 2000a). All polymers were analysed by SEM and each polymer sample was micrograph at a suitable magnification to obtain at least 10 pores. The diameters of the pores and interconnects were measured by the program IMAGE. The average of the pore size and interconnects

were calculated from raw data and this was taken as the pore and interconnect size of each polymer. This was carried out three times on independent samples of the same experiment to give better spread of pore and interconnect size. It is assumed that the polymer is fractured through the centre of the sphere. However the result cannot be taken as an absolute reflection of the porosity since the fracturing technique employed will go through the weakest point of the structure and the weakest point of the pore, this therefore may not be the centre of the sphere (Byron, 2000).

5.2.1.3 Analytical Method

Scanning Electron Microscope

The SEM equipment used in this work was an environmental SEM model Hitachi S2400 Scanning Electron Microscope fitted with an Oxford Instrument Isis 200 Ultra Thin Window X-ray detector. Since the SEM operation uses vacuum conditions and electrons to form an image, special preparations are essential. Before each sample can be analysed, all water, solvents or other materials that may vaporise while in a vacuum must be removed using a vacuum oven at 60°C for 4 hours before the next step.

Samples were prepared to withstand the vacuum inside the column. Samples were broken/cut into small pieces and were glued onto an aluminium stub with carbon cement (Figure 5-7). In order for the sample to withstand the vacuum, the samples were left overnight for the carbon to dry off. It is very important to be cautious about the detail of the mounting procedure so as to obtain quality results. Since the samples were analysed in an environment SEM, non-conductive samples could be examined without being coated with a conductive material. However, to obtain better clarity, a few samples were coated with a very thin layer of gold using a gold sputter coater.

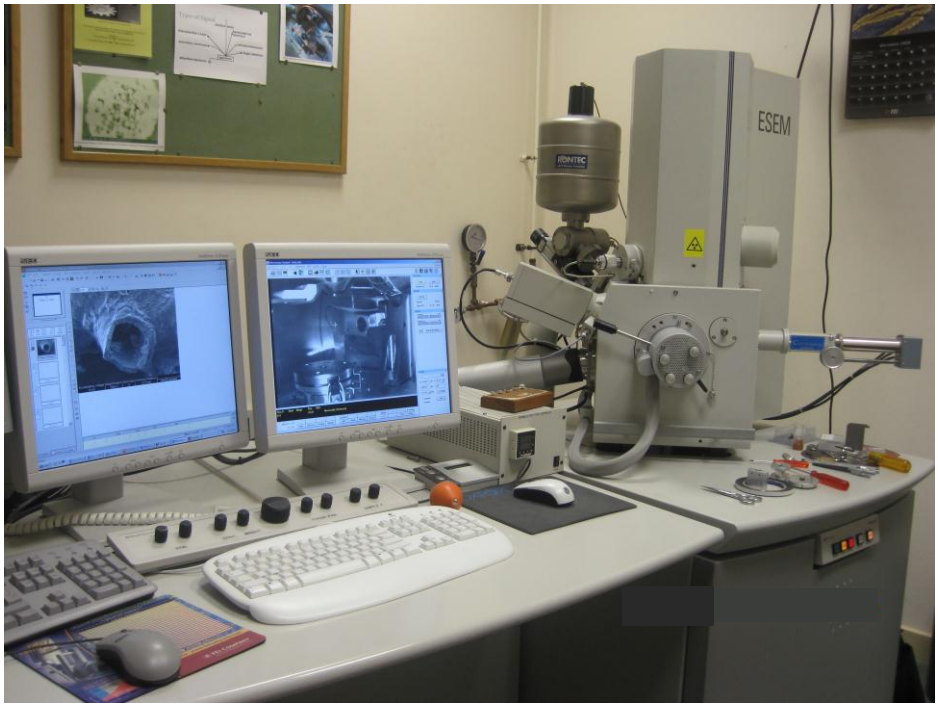

Figure 5-6: SEM used from the research

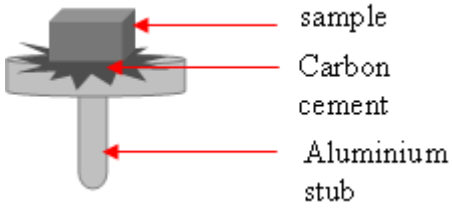

Figure 5-7: Sample glued on aluminium holder with carbon cement

EDX

The equipment used in this work was the same SEM equipment as described in previous section where the Rontec Quantax system was employed in SEM for local elemental analysis identification (EDX). The instrument was fitted with light element analysers to detect and quantify elements from Beryllium upwards. Images were provided in various digital formats, from about 20 times up to 300 000 times magnification, when the patterns were successfully interpreted by the control computer and analysis software

(Dyson, 2004). Imaging modes included secondary electron emission, backscattered electron and cathodoluminescence. Samples were prepared as described in section 5.2 or the same samples that were used to obtain the SEM micrograph were simultaneously used to obtain compositional analysis. Samples were analysed as distribution maps, and area average and spot analysis was considered.

X-ray ***Diffraction***

The X-ray diffraction equipment used in this work was PANalytical X'Pert Pro diffractometer, fitted with an X'Celerator (Figure 5-8). The X'Celerator is a relatively new attachment to the X'Pert and has the effect of giving a good quality pattern in a fraction of the time of a traditional diffractometer. Samples were usually made to powder and place on a stub before analysis.

Figure 5-8: Image of PANalytical X'Pert Pro diffractometer, fitted with an X'Celerator

Surface Area Measurement

The equipment used in this research to measure surface area of samples from section 5.2 was a Coulter SA 3100 analyzer (Figure 5-9), manufactured by the Beckman-Coulter Ltd. This analyser is a bench-top surface area and pore size analyser with built–in vacuum pumps. It measures surface areas, pore size distributions and pore volume parameters of powdered, pelleted or solid piece samples. There are six steps with regards to preparing and analysing samples as follows (COULTER-manual, 1996):

- Weighing the sample tube assembly
- Adding sample to the sample tube
- Logging-in the sample
- Weighing the outgassed sample
- Analysing the sample

Before each sample could be analysed, tubes and samples were kept dry to enhance the outgassing procedure. Depending on the estimated surface area value of each sample, tubes and samples were weighed accordingly. In this work, samples fall into two categories: low surface area and high surface area. For low surface area samples, samples were weighed up to 1 g per analysis and for a high surface area samples they were weighed to reach 0.1 g. Samples were cut or smashed into small pieces and fitted into the sample tube. An insert tube was inserted into the sample tube to reduce the free volume inside the sample tube, increasing the sensitivity and accuracy. Glass wool was used to cover the tip of the tube to prevent samples from being sucked back through the equipment during vacuum operation. Samples were outgased for 6 hours, which was followed by the analysing procedure. Sample analysis took approximately 20 min, whereby the freespace measurements and isotherm measurements were performed. The freespace data displayed the volume in the tube and accurately measured the quantity of gas absorbed, while the isotherm measurement calculated the surface area of the sample. Results were then displayed on the screen.

Figure 5-9: Coulter SA 3100 analyser

5.2.2 Preparation of PHP via Two Feed Points (Coded as PHP 2)

Previous work has shown that feed points of the aqueous phase had a profound effect on pore size of PHP (Akay et al., 2000). While Akay et al. (2000) has established the dosing of aqueous phase from the bottom via sixteen feed points, Bokhari et al. (2003) dosed the aqueous phase from the top of the mixing vessel by four multiple feed point that resulted in the production of large pores and interconnects. For this section, the aqueous phase was dosed from the top via two feed point.

Materials and experimental procedures

All materials, apparatus and experimental procedures were as described in section 5.2. However the aqueous phase was dosed into the mixing vessel from the top using peristaltic pump via two feed points instead of four feed points.

5.2.3 Preparation of PHP with High Surface Area (Codes as PHP 3)

In order to enhance surface area of PHP, Hainey and co-workers (1991) substituted one of the monomers with organic porogenic solvent and adding a high amount of cross linker (i.e. DVB) in the continuous phase. However it was reported that the mechanical properties of the resulting polyHIPEs are seriously affected. Further studies was carried out by Barbetta (2004) and Cameron (2005) and found that by changing the solvent from toluene (T) to chlorobenzene (CB) to 2-chloroethylbenzene (CEB), BET surface area is increased from 350 to 550m^2/g. Although the polyHIPE produced have the same level of mechanical performance as those with low surface areas, it was observed as not having a similar morphology compared to the standard polyHIPE structure with significantly large windows. Additionally, (Cameron, 2005) found that a 1:1 (volume: volume) mixture of CEB and CB not only yielded a material with the same value of surface area (550 m^2/g), but also maintained the original polyHIPE morphology. Nonetheless Noor (2006) discovered that polyHIPE was not as durable as those prepared using the combination of styrene/DV. Therefore, for this research 1:1 CEB and CB was added in the continous phase while other materials remain the same. For these experiments the compositions for PHP were made up as shown below:

Materials

Oil Phase Composition*:*

8% Styrene (monomer)

33% Divinyl benzene (DVB) crosslinker

17% Span 80 (surfactant)

21% CEB

21% CB

***Aqueous Phase**:*

1.11 wt% $CaCl_2.2H_2O$

0.22 wt% Potassium persulphate

Deionised water

Experimental Procedures: Experimtental procedures were carried out as described in previous section (refer to section 5.2.2)

5.2.4 Preparation of Nano-structured Micro-porous Silica Materials (Coded as PHP 4)

A functional PolyHIPE Polymer is described in this section whereby functional 'filler' is added to the aqueous phase of a high internal phase emulsion and subsequently concentration of the filler in the oil phase is restricted due to the low volume of the oil phase. Consequently, nano-pores are formed within the pore walls of the larger micron sized pores when filler is added to the continuous or disperse phase. These nano-pores are useful for many applications. The material constitutes a silica-polymer composite providing a very large surface area, mainly provided by the silica.

Materials

Oil Phase

67 wt% monomer (styrene) cross linked with

20 wt% cross linking agent (divinyl benzene). To this

12 wt% surfactant (Span 80) was added and

1 wt% of Lauryl peroxide as an oil initiator.

Aqueous Phase

Deionised water

Bindzil CC30 - 7nm particle size (Silane coated colloidal silica content is 30%) or Bindzil CC40 -12nm particle size (Silica coated colloidal silica content is 40%).

Experimental procedures

The preparation of PHP with silica as an additive was carried out using apparatus as described in section 5.2.1. Experimental procedures were performed as dscribed in section 5.2.1 except the dosing of the aqueous phase was within 10 min intervals and another 30 minutes was allowed for mixing. Another addition to the previous section was that during polymerization, samples were shaken every 15 minutes in the first 4 hours until gelling occurred in order to obtain a more uniform sample across the tube (this was due to the high density difference between the oil and aqueous phases) and to prevent from separation.

5.2.5 Preparation of Compressed PHP

Preparation of compressed PHP was performed using preformed PHP (prepared as described in section 5.2). Samples were compressed using two tonne hydraulic press under 60°C heat for 10 seconds (Figure5-10). The PHP discs were compressed to a final size of 26 mm φ x 1mm thickness.

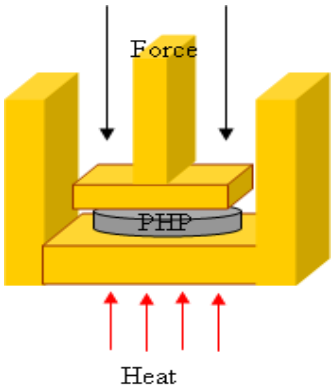

Figure 5-10: Schematic diagram of hydraulic press used to produce compressed PHP (reproduced from (Byron, 2000)

5.2.6 Preparation of Other Porous Materials

The present research dealt with not only the above mentioned templates but also other fibres materials. Porous materials used in this research were referred to as any substrate through which fluids can easily permeate under normal conditions. These include, for example, paper, textiles, woven or non-woven fabrics, solid foams, membranes, and similar materials exhibiting permeability properties. Analysis of deposited metal was made on natural fibres and manmade fibres made from synthetic polymers and inorganic fibres. For this research, nylon fibre, cotton wool, glass wool and carbon felt were used as sources of other porous materials that categorized from natural and manmade fibres.

5.2.6.1 Nylon Fibre

The nylon fiber used in this work was an ordinary washing-up pad scourer commercially known as Scotch-Brite™ Heavy Duty Flat Scourer obtained from Tesco. Figure 5-11 showed a magnified sample that contained an irregular filament like shape with diameter average of 50µm. The sample was commercially sold as cut strip in varies sizes. In order to use it as the template, the sample was measured and cut to fit the size of the depositing cell; disc 26 mm φ x 4 mm thickness. This was followed by

rinsing thoroughly with deionised water, drying-up and weight immediately after. The samples were then ready to be deposited by method mention in section 5.3.

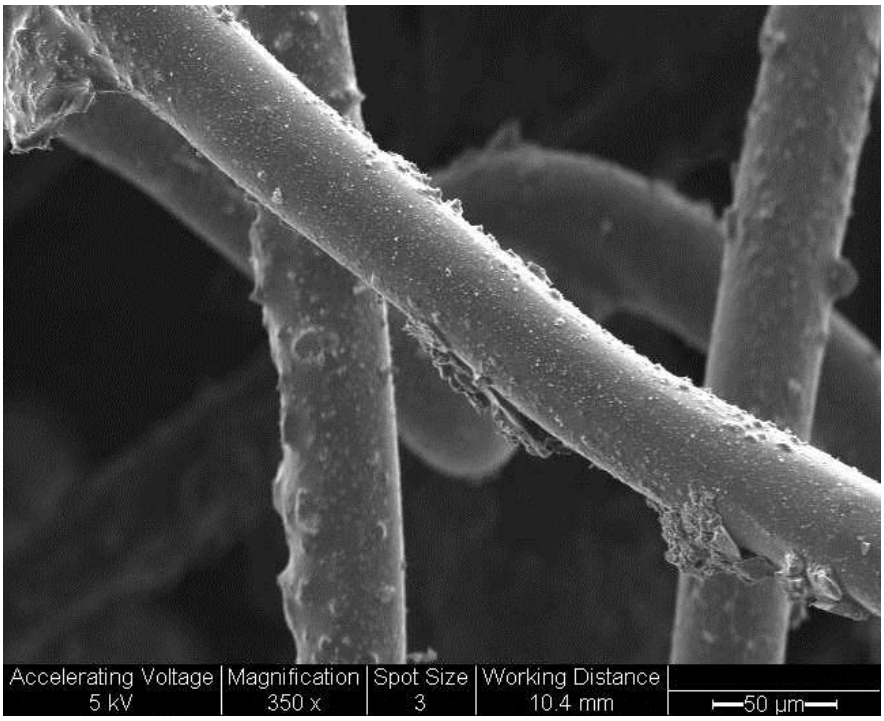

Figure 5-11: Micrograph of a nylon fibre (at x350 magnification)

5.2.6.2 Carbon Felt

Carbon felt used in this work was supplied by Fibres Material Inc., who offers a variety of widths and thicknesses to meet a wide range of applications. The felt used was obtained as a sample, having a thickness of 1 cm. In order to use it as the template, carbon felt was cut to fit the deposition cell. This was followed by rinsing thoroughly with deionised water, drying-up and weighing immediately after. The samples were then ready to be deposited by the method mentioned in section 5.3. The felt was compressed through the deposition cell to obtain the maximized thickness disc of 0.4cm. The general view of the carbon felt is shown in Figure 5-12 and it can be seen that it had a flexible continuous filament like shape with a diameter in the range of 10-15 µm.

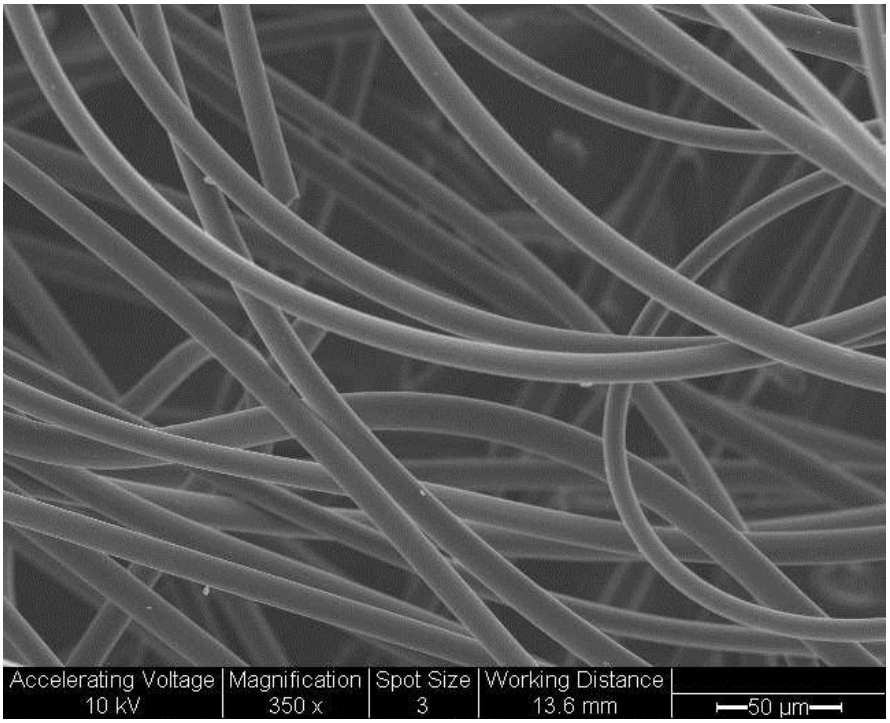

Figure 5-12: A micrograph Carbon felt (at x350 magnification)

5.2.6.3 Glass Wool

The glass wool used in this research was glass wool for laboratory use obtained from Sigma-Aldrich (18421). Figure 5-13 shows a general view of the glass wool. It was formed as continuous filament although flock (or a velvet likeness) was observed. Unlike carbon felt, glass wool is more rigid and difficult to handle. In order to use it as a template, the glass wool was cut to fit the deposition cell. This was followed by rinsing thoroughly with deionised water, drying-up and weighing immediately after. The samples then went through the silanation process described in section section 5.4 before ready to be deposited by the method mentioned in section 5.3.

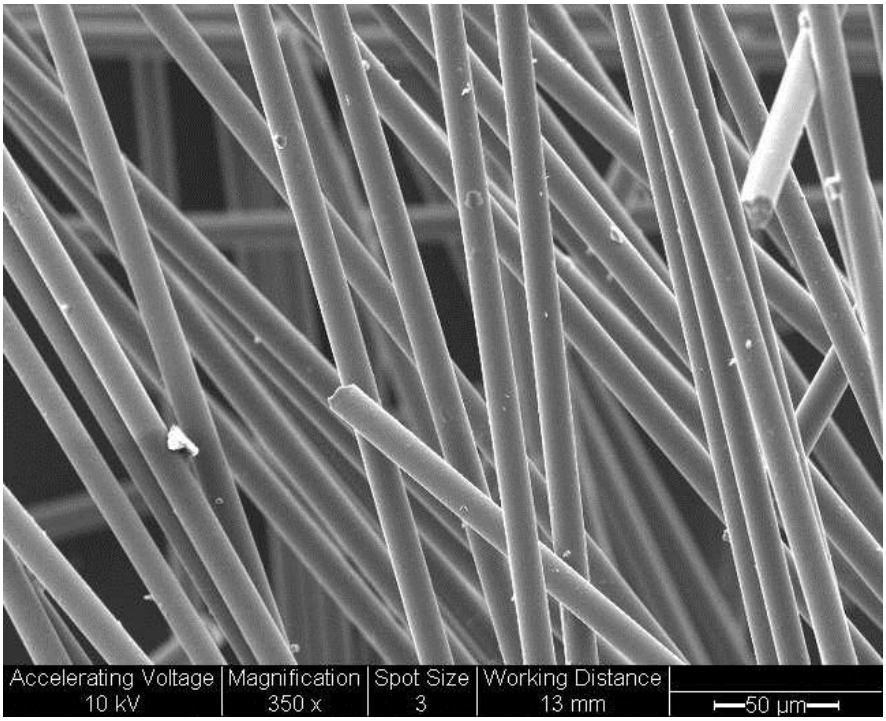

Figure 5-13: A micrograph image of glass wool (at x350 magnification)

5.2.6.4 Cotton Wool

Cotton wool used in this work was a product refined from a cotton plant in its raw state and produced for cosmetic purposes. The cotton wool used in this research was cosmetic cotton obtained from Boots. The morphology of the cotton wool can be seen in Figure 5-14. The strands exhibited an irregular shape with some flat and hollow sections. They also spanned in almost all directions. Since it was not a circular shape the size was taken as width of the strand rather than the diameter and in the range of 10-25 µm width. In order to use it as the template, the cotton wool was cut to fit the deposition cell. This was followed by rinsing thoroughly with deionised water, drying-up and weighing immediately after. It was ready to be deposited using the method mentioned in section 5.3.

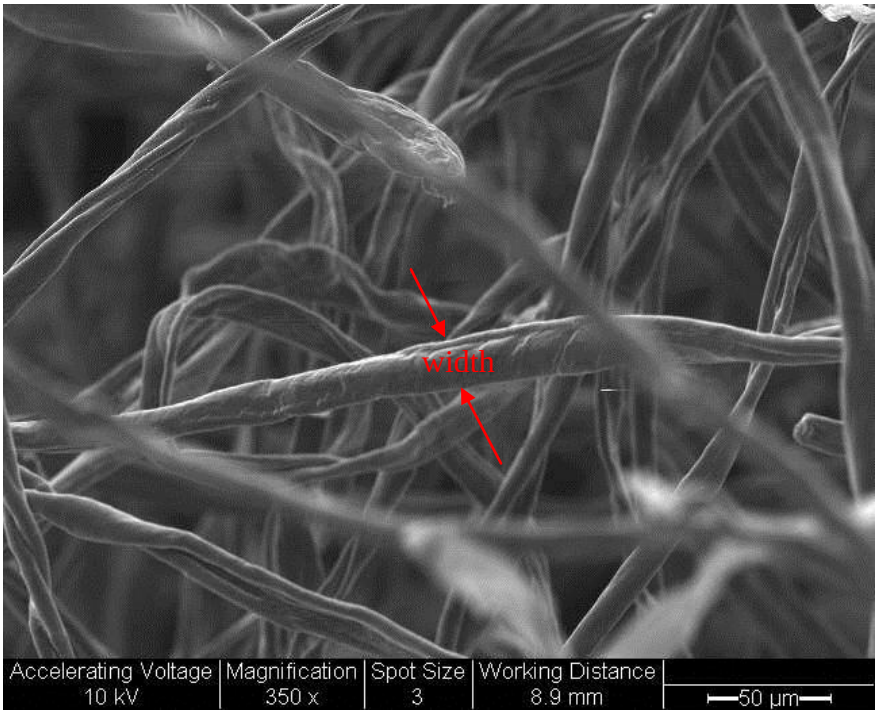

Figure 5-14: A Micrograph image of Cotton Wool (at x350 magnification)

5.3 Metal Deposition of PHP and other Fibrous Materials

This section describes an electroless deposition method using a flow-through system to produce nano-structured macro-porous material with hierarchical pore structure. Previous study on nickel incorporation into a microporous polymer by Akay et al. (1998) produced an outer surface coating which did not penetrate significantly into the interior of the polymer. Method proposed was by submerging templates/samples into deposition solution. Earlier investigation by Calkan, B (2006) on the designs of deposition cell had failed to achieve the required metal penetration through the template. However a modified deposition cell made of brace was eventually set up and problems such as unwanted heating of the plating solution, unwanted metal deposition in the flow channels even before reaching the template, thus clogging the channels or deposition only on the surface of the template disks rather than depositing in the pores, were overcame (Calkan, B, 2006).

Parallel studies were performed together with the former researcher using the same apparatus whereby metal was uniformly deposited using the deposition cell onto the template and subsequently heat treated to obtain metal hierarchical pore structure.

Materials

To produce a Ni-B deposition, dimethyamine borane and sodium borohydride were used as reducing agents. The bath solution was prepared by dissolving the following chemicals with 600 ml of deionised water

Dimethylamine Borane as reducing agent

- 0.19 M Nickel Chloride – The source of nickel ions
- 0.38 M Dimethylamine Borane – Reducing Agent
- 0.27 M Sodium acetate – Complexing Agent
- 3.88 10^{-4}M Sodium Lauryl Sulphate- Stabilizer

And sodium borohydride used as reducing agent

- 0.19 M Nickel Chloride – The source of nickel ions
- 0.02 M Sodium Borohydride – Reducing Agent
- 0.22 M NaOH - Complexing Agent
- 0.0037 M $H_2NCH_2CH_2NH_2$ - Stabilizer

In order to produce the Ni-P deposition, sodium hypophosphate was used as the reducing agent. The bath solution was prepared by dissolving the following chemicals in deionised water.

- 0.13 M nickel chloride
- 0.63M sodium hypophosphite hydrate
- pH set to 11.5 with ammonium hydroxide (35% concentration)

All chemicals was received and purchased form Adrich.

Experimental Procedures

The metallised templates were produced on a labarotary scale using the apparatus outlined in Figure 5-15. The system layout includes a syringe pump, a stirrer, a deposition cell, a water bath and a temperature controller.

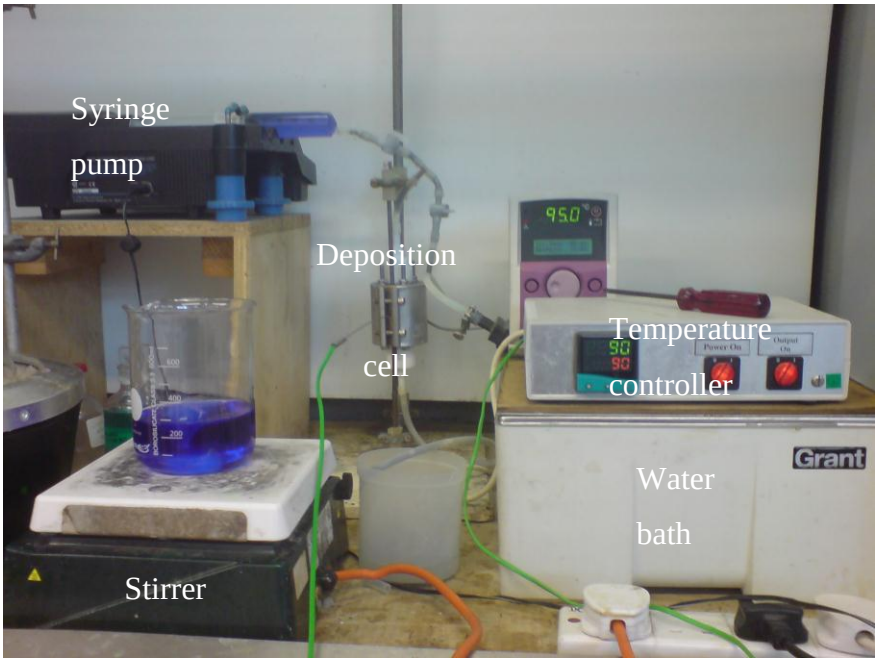

Figure 5-15: Layout of apparatus used for metal deposition

Metal deposition was carried out at various temperatures (30°-90°C) using the deposition cell that was electrically heated using a band heater. Thermocouple was used to monitor the temperature and was place in direct contect with the samples. The deposition cell itself consists of three different parts (Figure 5-16):

- inlet/outlet tips A,B,C (PTFE)
- heating holder, D (brass cylindrical hollow section)
- Flow distributor, E

and samples were sandwich between the flow distributors.

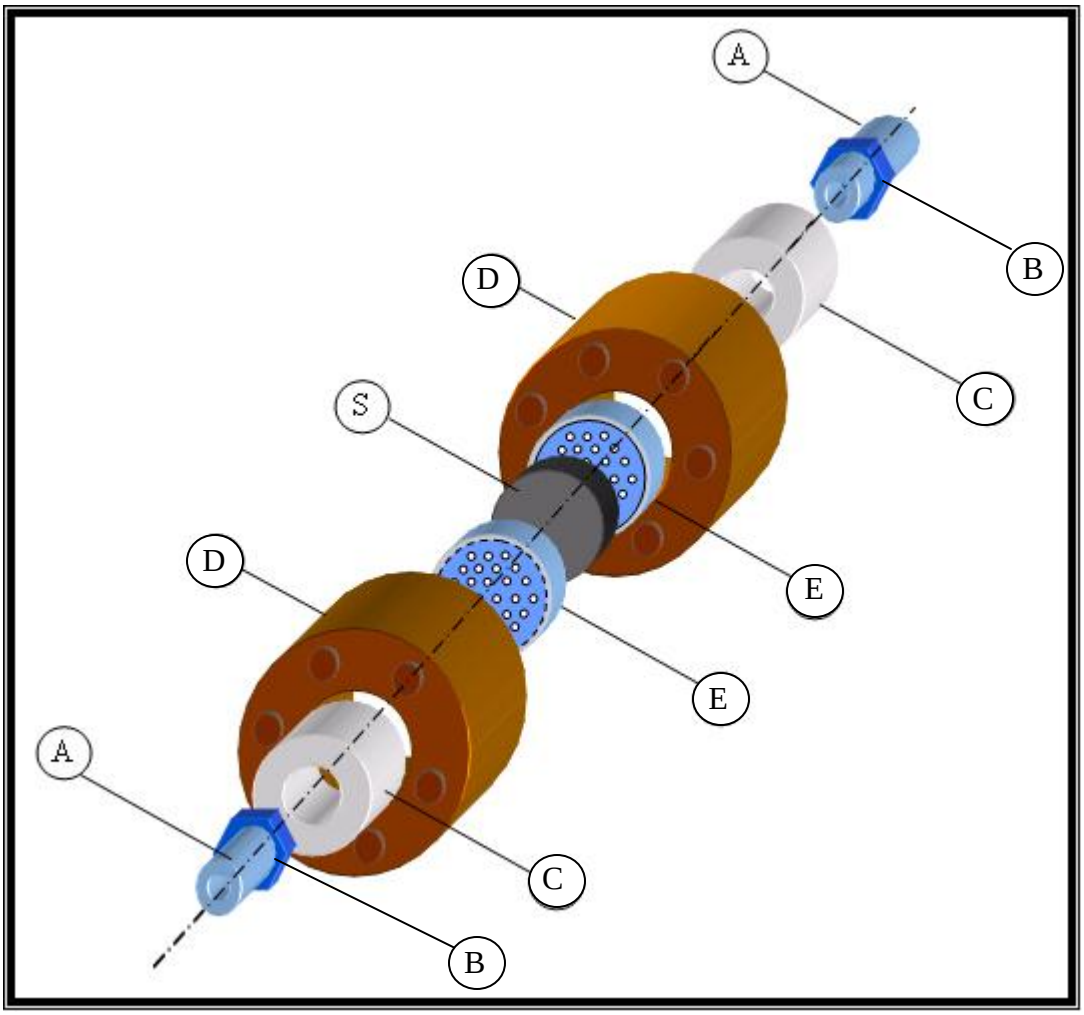

Figure 5-16: Exploded diagram of deposition cell consist of : A,B,C – inlet/outlet PTFE tips; D- heating holder; E – flow distributor, S - sample

In order to prevent metal deposition in the flow channels, all parts of the flow cell which were in direct contact with the metal bath solution were made of PTFE. Note also that the brass holder used is to provide direct heating to the templates.

Initial Preparation

In each experiment the amount of bath solution prepared using the specific composition was typically 600ml. The bath solution was continuously stirred using the stirrer and kept at room temperature to prevent precipitation all throughout the experiment until all

the solution was utilised. Once the bath solution was prepared, using a 60ml syringe, 50ml of the bath solution was taken and placed on the syringe pump. The syringe pump was set to drive the solution at a rate of 2ml/min. Simultaneously; the water bath was set at a temperature slightly higher than the deposition cell temperature. The samples were fixed in the deposition cell and the temperature was set using the temperature controller connected to the thermocouple at the desired temperature. In each experiment, the temperature set-up from the temperature controller was used as the deposition cell temperature. All tubes and .fitters were connected accordingly as shown in schematic diagram (see Figure 5-17). The items were connected using tubes, two 2-way valves, V1, V2 and a t-juction.

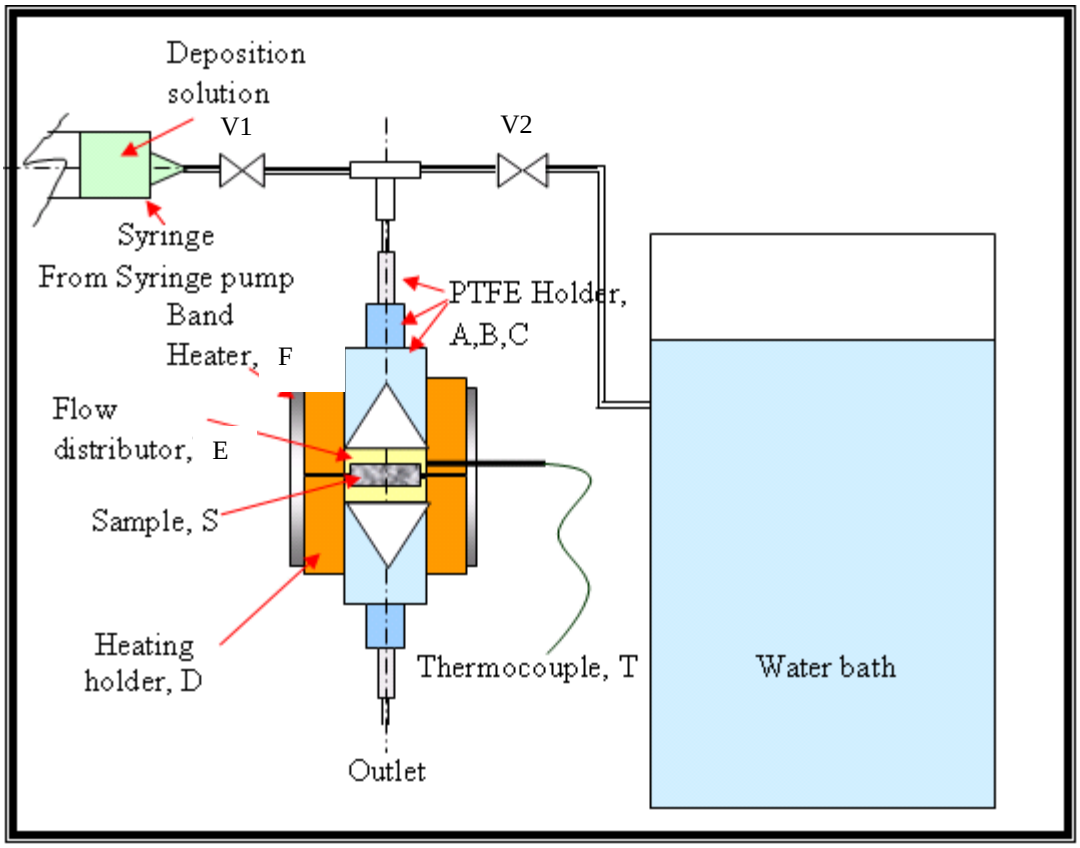

Figure 5-17: Schematic diagram of apparatus used for metal deposition

Deposition Process

Prior to metallization, 200ml of heated deionised water from the water bath was pumped in through the deposition cell to provide better operating conditions for the deposition environment of the sample. This was followed by pumping of the bath solution from the syringe pump. After the entire 50ml solution was pumped through the deposition cell, the cell was reversed in the opposite direction to achieve a more uniform and optimum amount of metal deposition. Then 80ml of heated deionised water from the water bath was flushed through the deposition cell to wash the excessive hydrogen evolution, and hence providing a better deposition environment. The cycle was repeated until all the bath solution was finally utilized. After metalization, the cell was cooled down to room temperature and the sample was dismantled. Sample was then left to dry in fume hood for 2-3 days and weight subsequently. All parts of the deposition cell were dismantled, cleaned in diluted nitric acid to remove deposited metal, and rinsed with deionised water to wash off excessive acid.

5.3.1 Determination of Grain Size

All PolyHIPE polymner that was metal deposited was analysed by SEM in order to determine the grain size of deposited metal. It is imperative to calculate the distribution of the grain size within the polymer. Each sample was micrograph at a suitable magnification to obtain the min and max size of metal grain. The diamters of 10 metal grains were measured by the program IMAGE. The average of the metal grain was calculated and this was carried out three times on independent samples of the same samples.

5.3.2 Metal Deposition of Compressed Polymer

The bath solution was prepared using chemicals as discussed in section 5.3. In each experiment the amount of bath solution prepared was 100ml. Using a 50 ml beaker, 10

ml of bath solution was dispensed into the beaker containing the compressed PHP that was glued initially at the bottom of the beaker as shown in Figure 5-18.

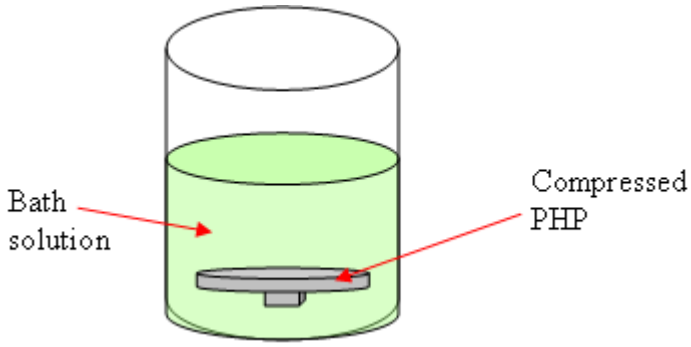

Figure 5-18: Metal deposition of compressed PHP

To initiate the deposition process, the beaker was submerged in a water bath to provide a constant temperature. The water bath was set at the desired temperature (70˚C and 90˚C). The process was stopped when all the metal salt was reduced to metal. To obtain an optimised metal deposition the beaker was cleaned and the sample was rinsed with deionised water. The cycle was repeated until all the 100 ml solution was utilised. The samples was taken out, rinsed with deionised water and dried at room temperate and weigh immediately after.

5.4 Silanation

This section describes a method of treating samples that demonstrate poor adhesion between metal deposition and samples. Generally, silane agents are typically used for surface treatment. Silanes are monomeric silicon compounds with four substituent groups attached to the silicon atom. These substituent groups can be from any combination of nonreactive, inorganically reactive, or organically reactive groups. Due to silicon versertility, silicon will bond strongly to other inorganics such as glass and steel and to organic polymers. The choice of which silane to use in a particular application is determined by the nature of the desire requirement. In this experiment, an organo reactive silane namely vinyltrimethoxysilane was chosen to provide a chemical bondage to reactive sites that present in the samples, hence providing better

metal/sample adhesion. There are a number of methods used to deposit silane to substrate and most common are describe as follow and used in this experiment.

5.4.1 Silane from water

According to Weetal and co workers, silanazation procedures using X_3SiR reagents were initially conducted in organic solvent but most recently reactions in aqueous media was used due to its longer-wearing surface result (Untereker, 1977). Deposition from aqueous solution is employed for most commercial fiberglass systems. In this method, the alkoxysilane is dissolved at 0.5-2.0% concentration in water. It is not necessary to ulitized distilled water, but water containing fluoride ions must be avoided According to study by Witucki (1993), it was found that poor solubility parameters limit the use of long chain alkyl and aromatic silanes by this method. Stability of aqueous silane solutions varies from 2-12 hours for the simple alkyl silanes.

.

Materials

Deionized water
0.1M Acetic Acid
98% Vinyltrimethoxysilane

Experimental Procedure

An aqueous solution from deionized water was prepared to make-up a 100 ml aqueous solution. The solution was adjusted to reach pH=4 with 0.1M acetic acid. This was followed by 5ml of Vinyltrimetyloxysilane and stirred with a magnetic stirrer for 15 min to allow for hydrolysis and silanol formation. The sequences are shown in schematic diagram Figure 5-19. Sample was dipped into the solution and left for 12 hours. Sample was then dry in fume hood for 1-2 days.

5.4.2 Silane from Alcohol Solution

Deposition from aqueous alcohol solutions is the simplest method for preparing silanated surfaces. A two percent silane solution was prepared in the alcohol of choice (methanol, ethanol, and isopropanol are typical choices). Adhesion are improved by applying silanes from this method (Pleudemann, 1982).

Material

Deionized water

0.1M Acetic Acid

98% Vinyltrimethoxysilane

98% Ethanol

Experimental Procedure

Method for this section was as discussed in section 5.4.1 except that the aqueous alcohol solution was prepared from 95% ethanol and 5% water solution that made-up a 100 ml aqueous alcohol solution.

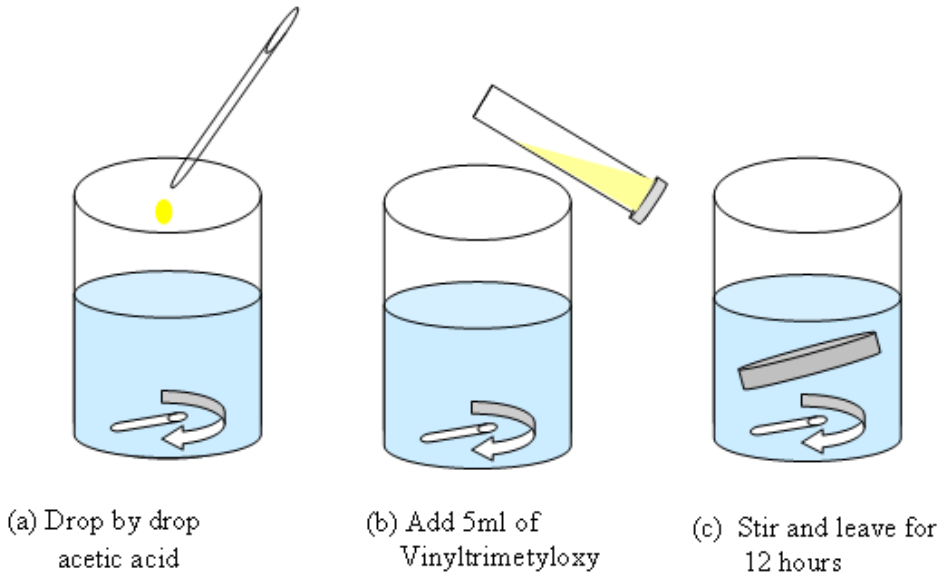

.Figure 5-19: Schematic diagram of silanation procedure

CHAPTER 6

RESULTS AND DISCUSSION

6.1 Overview

This chapter discusses the interpretation and significance of the results obtained from the experimental research described in Chapter 5. The layout of this chapter is presented in three subsections. The main discussion in section 6.2 covers the production of PHP and pore size distribution. Section 6.3 covers the development of metal deposition structure on PHP, grain size and morphology in response to the various operating conditions adopted in this work, both in the as deposited condition and following heat treatment. Section 6.4 concentrates on characterisation of metal deposition on different templates other than PHP. The relationship between the observed morphology and different templates is discussed in this section. The surface treatment effect carried out by the silanation process on templates with weak metal bondage, both as deposited and heat treated, is discussed in section 6.5.

6.2 Production of PHP and pore size distribution

The first part of this chapter dealt with the preparation of PHP that formed hierarchical pore structure and appeared suitable for metal deposition penetration hence catalysts application. Experiment were carried out to produce sets of PHP coded as PHP1, PHP2, PHP 3 and PHP 4 that has hierarchical pore structure according to specific parameters. All experiments were carried out three times.

6.2.1 Architectural Structure of PHP Produced

SEM was used to determine the PHP structure. The PHPs produced in this experiment exhibited an open structure. The pore and interconnect architecture was well defined and evenly distributed for all four types of PHPs (PHP1, PHP2, PHP3 and PHP4) as shown in Figure 6-1(a) to (d). The resulting PHPs revealed a hierarchical pore structure: coalescence pores that were created from the HIPE droplets; interconnect pore within each coalescence pore and its neighbours; primary pore, a network of pores between coalescence pores and interconncet pores, and nanopores that covered within the polymer walls.

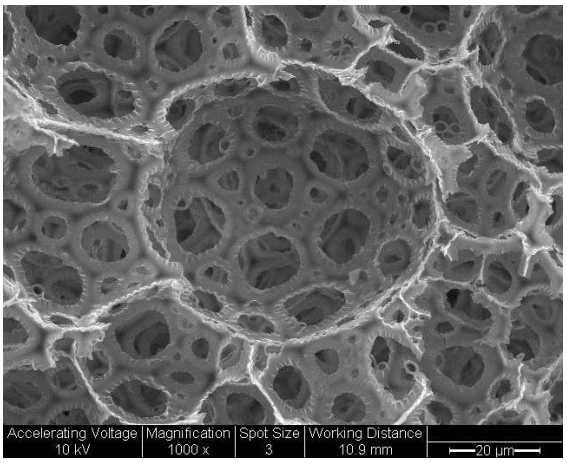

(a) PHP1 x1000 magnification

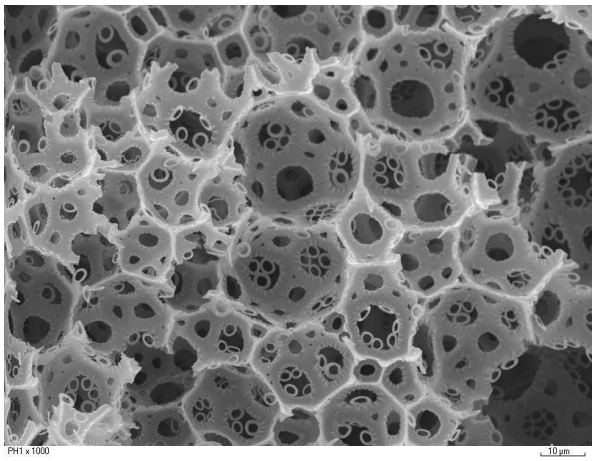

(b)PHP2 x1000 magnification

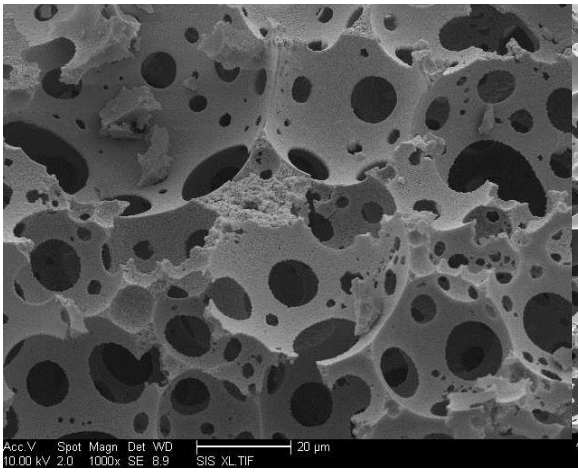

(c) PHP3 x1000 magnification

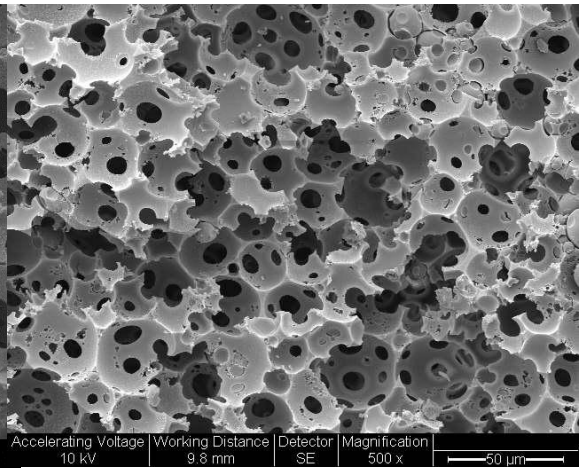

(d) PHP4 x 500 magnificationn

Figure 6-1: SEM micrograph showing the morphology of PHP produced namely: a.)PHP1 b) PHP2 c) PHP3 d) PHP4

As shown from SEM images Figure 6-1 and Table 6-1, pores are between 7µm - 58µm in diameter and homogenous structure observed. The range of pore size distribution for the PHPs produce was as below:

Table 6-1: The range of pore size distribution for PHPs produced.

PHP code	Range
PHP1	16µm-58µm
PHP2	7µm-45µm
PHP3	7µm-30µm
PHP4	7µm-26µm

The experiments were carried out to observe the effect of multiple feed points while other parameters remained the same on the morphological structure of the resulting porous polymer that appeared to affect the structure of PHP significantly. The production of PHP with large pores and interconnect using multiple feed point is known to be an important factor influencing the morphology of PolyHIPEs (Akay et al., 2000). However much less is known about the use of two feed points. Therefore PHP1 and PHP2 were prepared (as discussed in section 5.2) using four feed points and two feed points respectively. Both PHPs exhibited a homogeneous structure and good mechanical stability (see Figure 6.2 and Figure 6.3).

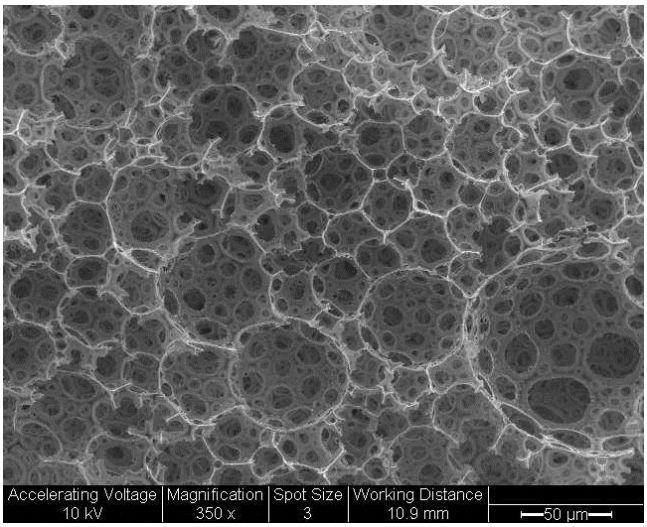

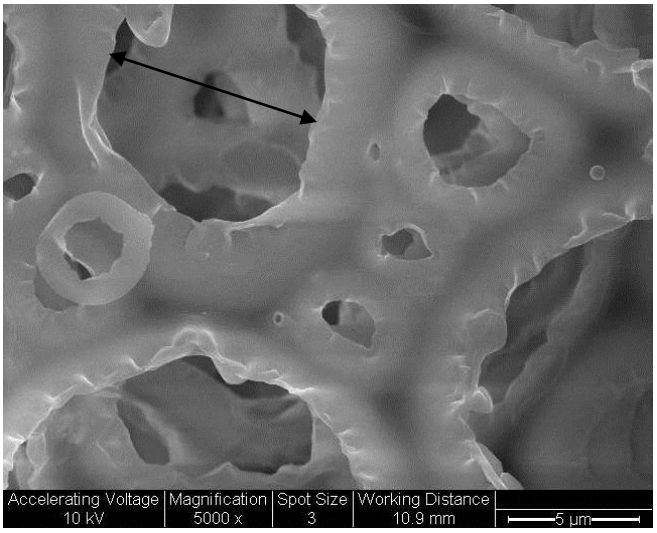

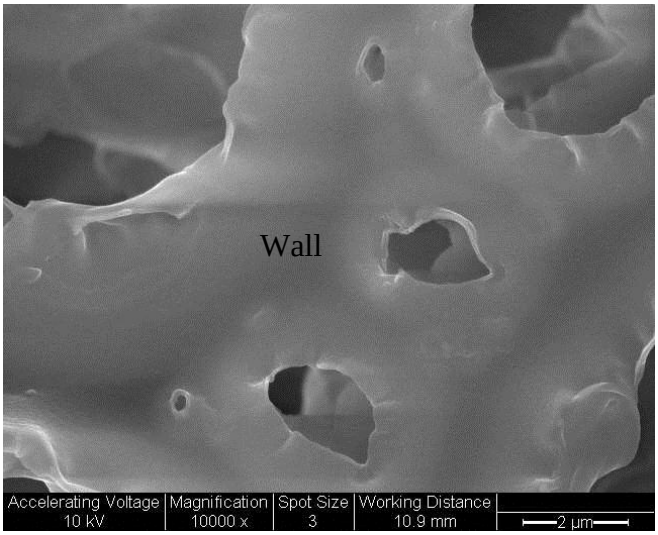

Figure 6-2: SEM micrograph of PHP1 SEM micrographs of PHP 1: Dosing rate=1.78ml/s, Mixing rate: 60s, Impeller speed=:300 rpm, uisng 4 feed points where the highly interconnected pore network can clearly be seen and shown at different magnification a) general view of PHP2 x350 b) pore and interconnect x5000 (black arrow) (c) PHP3 wall produced smooth surface x10000

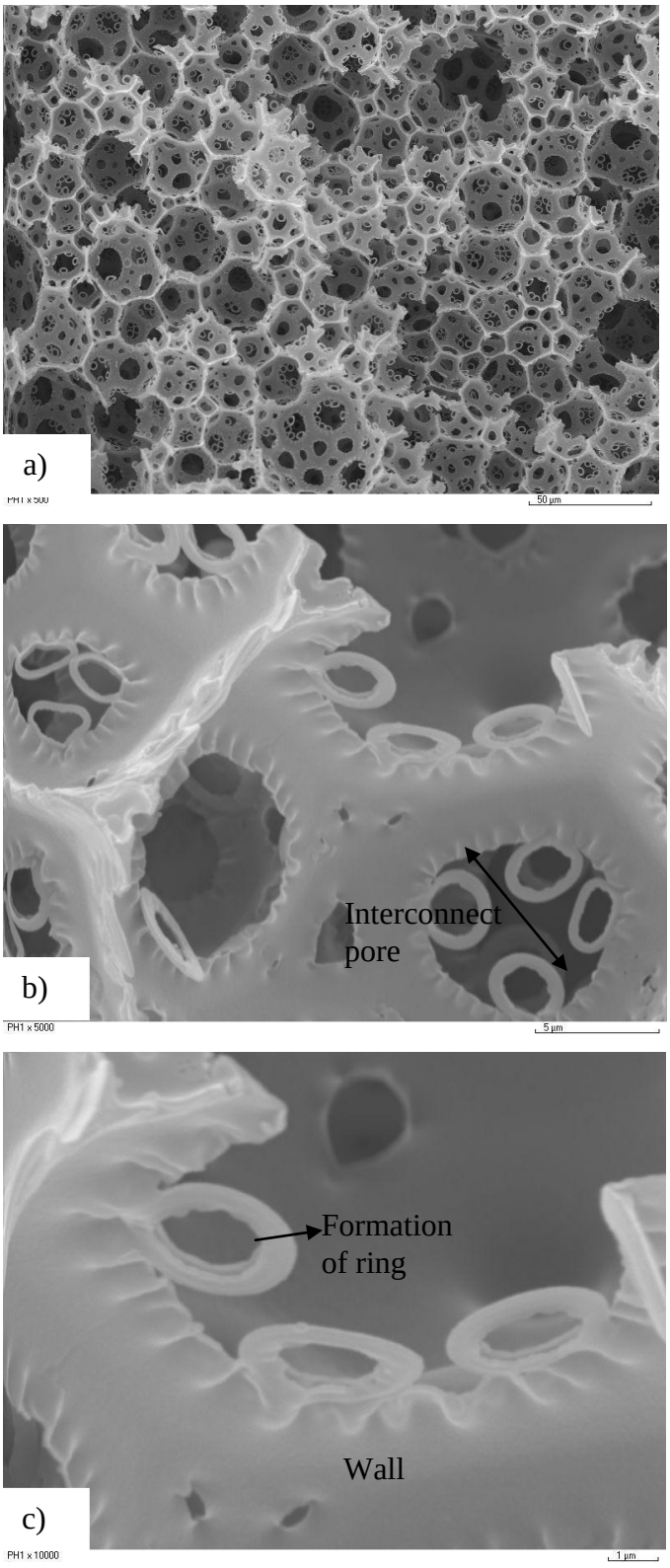

Figure 6-3: SEM micrograph of PHP2 that was produced: Dosing rate=1.78ml/s, Mixing rate: 60 s: Impeller speed=300 rpm, using two feed point and shown at different magnification: a) general view of PHP2 x350 b) pore and interconnect x5000 (black arrow) (c) PHP3 wall produced smooth surface x10000

SEM micrograph analysis (using IMAGE software) was used to determine the pore size distribution and the diameters measured from the images were underestimates of the actual values since the pores are not seen at equatorial positions (Menner et al., 2006b). From TabIe 6-1, it was observed that the pore size of PHP1 was larger and interconnect pore for four feed point was twice the size of two feed points. The interconnect pores for PHP1 were closed to each other, densed and separated by thin wall while interconnect pores for PHP2 were separated by thicker wall and less dense than PHP1. Rings were observed to formed at the inner side of the interconnect pore creating a flower-like formation for PHP2. This was due to a lower emulsion stability and subsequent water droplet formation during polymerization. The effect of four feed points resulted in more than a fold increase of min value of average pore size (see Table 6-1). On the other hand, min average pore size for PHP2, PHP3 and PHP4 showed the same value of 7µm when two feed points were used.

For catalysts application, a polymer with high surface area and maintaining the mechanical strength are an advantage. According to Cameron (2005), a mixture of 1:1 CEB and CE in oil phase increases the surface area to 550 m^2/g. Although the polymer produced maintains its original polyHIPE morphology, the mechanical strength could not be compromised. Therefore CEB and CE were added in the oil phase to enhance the surface area and mechanical property in preparation of PHP3. The addition of CEB and CE had a profound effect on the surface area that increased from ca 4 m^2/g to ca.230 m^2/g (see Table 6-3). Addition of silica showed an increased of the surface area to ca 150 m^2/g. From Figure 6-2 and Figure 6-3, it was observed that the pore size was in the range of 7µm-30µm and 7µm-26µm respectively. PHPs produced gave more stable emulsions and therefore PolyHIPEs with more homogeneous pore size distribution. Addition of salt concentration and Bindzil in the aqueous for PHP3 and PHP4 respectively was to provide an emulsion with kinetic stability during polymerization (Cameron, 2005). The wall formed was much broader and nanopore structure were observed (see Figure 6-4 (c) and Figure 6-5 (c)). Howerver no significant difference with regards to surface area for PHP1=3.69m^2/g, PHP2= 5.68 m^2/g) and smooth wall surface was observed (see Figure 6.3 (c) and Figure 6.4 (c))

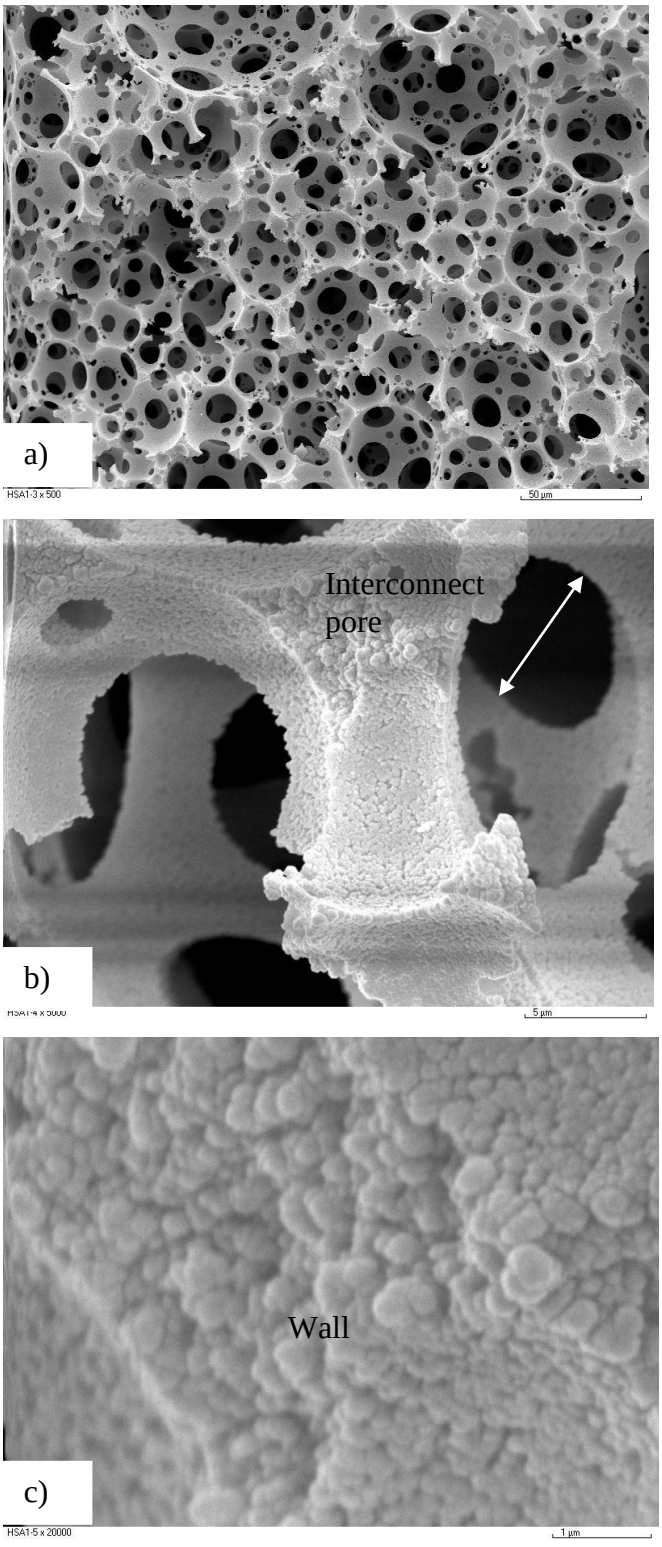

Figure 6-4: SEM micrograph of PHP 3: Dosing rate: 1.78ml/s, Mixing rate: 60s, Impeller speed=300 rpm, using 2 feed point with additional of CE and CEB in oil phase and shown at different magnification: a) general view of PHP3 x350 b) pore and interconnect x5000 (white arrow) (c) PHP3 wall produced nanopores x10000

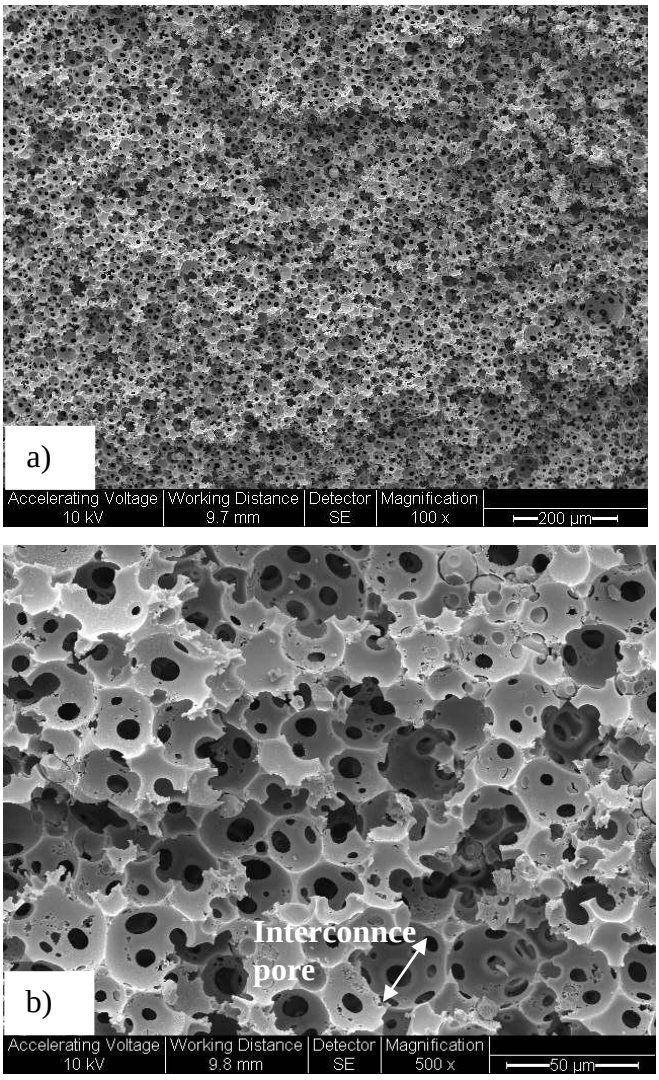

Figure 6-5: SEM micrograph of Benzil CC30 coated PolyHIPE Polymer: Dosing rate=0.36ml/s, Mixing rate=1800s, Impeller speed=, using 2 feed point. shown at different magnification (a) general view of PHP4 x350 b) pore and interconnect x5000 (white arrow) (c) PHP3 wall produced nanopores x10000

6.2.2 Pore size Distribution of PHP

Pore size and interconnect pore were determine from PHP morphology as described in section 5.2.1.2. However to simplify pore sizes in term of terminology used, pore size was measured from the coalescence pore (as described in section 3.1) and interconnect was measured from interconnect pore (as described in section 3.1). Therefore the range of pore size was determine from the interconnect pore and coalescence pore ie. the minimum value was an average interconnects value and the maximum value was an average of pore size value.

Table 6-2: Average pore and interconnectg sizes determined from the PHP produced. Each PHP code was calculated from three independent experiments where 10 pores were measeured from each sample.

PHP Code	Average Pore Size (µm)	Average Interconnect (µm)
PHP 1	58±15	16±5
HP 2	45±10	7±5
PHP 3	30±7	7±2
PHP 4	26±6	7±3

6.2.3 Surface Area Measurement

Table 6-3: BET surface area analysis for PHP1, PHP2, PHP3 and PHP4 determined by Beckman Coulter BET Gas Adsorption Analyser (Type SA310 Plus)

PHP Code	Surface Area (m^2/g)
PHP 1	3.69 ± 0.16
PHP 2	5. 68 ± 0.15
PHP 3	229.03 ± 7.61
PHP 4	146.02 ± 6.01

6.2.4 Summary

- Nano-structured macro porous materials with hierarchical pore structure were successfully developed. The hierarchical structure developed on each template had a pronounced effect on the surface area and morphologies.
- PHPs were produced with pore and interconnect pore sizes ranging from 7µm-58µm.
- Nanopores were also produced on wall of PHP3 and PHP4.

6.3 Deposition and Characterisation

The technique employed to metalize PHP in this research is the Ni-B electroless flow through method; a technique used to filterate the bath solution into the pores of porous material and subsequently metal deposit on the material. Materials were then heat treated to obtain hierarchical pore structure.The metal attachment to templat is the key process of metal-surface interactions and this affects subsequent catalytic activity. Template suitability remains the focus for template materials application in catalyst. Therefore the aim for this session is to assess the compatibility of PHP (Code 1-4) and other fibrous materials (scoth brite, cotton wool, carbon felt, glass wool) as nano structured material suitable for catalyst application.

6.3.1 Development of Ni-B Deposition on PolyHIPE Polymer Template

A 600ml of deposition solution was used as electroless Ni-B deposition (as describe in section 5.3) to ensure the walls of PHPs were totally covered with Ni-B particles. After electroless plating treatment, the hierarchical structure of PHP still remained its original structure together with the continuous metal depositions that was attributed from the growth and coalescence of the particles. An average plain polymer disk (4mm thick and 26 mm in diameter) were weighed. 0.08 g before metal deposition and it made up to 40 times of its original weight of metal deposits and generally reaching a final disk weight of around 3.2g.

Figure 6-6 showed SEM micrograph of metallised PHPs after heat treatmetn. These result suggest that all PHPs coded as PHP1, PHP2, PHP3 and PHP4 are suitable for metal deposition hence for catalyst application. Adhesion of metal to PHPs and other materials is considered as indicator to compatibility. Nucleation of metal grain on PHPs is the first process of metal-surface interactions.

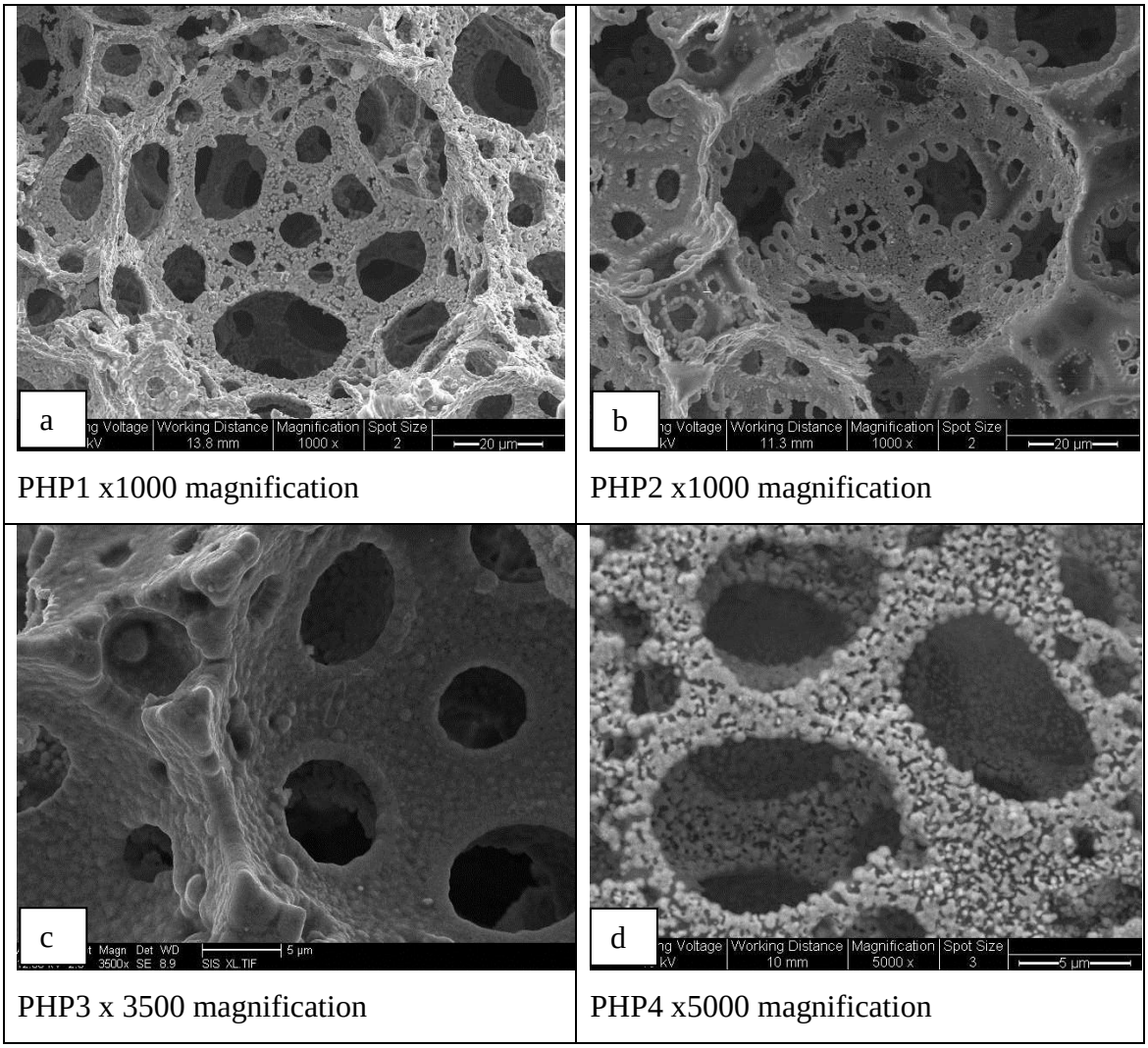

PHP1 x1000 magnification

PHP2 x1000 magnification

PHP3 x 3500 magnification

PHP4 x5000 magnification

Figure 6-6: PHPs after metal deposition using Ni-B electroless system DMAB as reducing agent: a.)PHP1 b) PHP2 c) PHP3 d) PHP4

The stages of metal deposition on PHPs are shown in Figures 6.7, Figure 6.8, Figure 6.9 and Figure 6.10. It presented the deposition behaviour of Ni-B deposits on PHPs using deposition bath containing nickel chloride as the nickel source and dimethylamine borane as chemical reducing agent (see secion 5.3). From the SEM micrograph Figure 6.-7, it was observed that grains first nucleate in the region surrrounding the pore and interconnect that lay perpendicular to the direction of flow. The initial Ni-B deposits were as small as tens of nanometers. The preferential of nucleation in this region shows the interconnect pores that provide the flow channel. It is evident that the metal deposition to the walls is affected by the flow conditions. Since the deposition was carried out by the flow through deposition method, the solution flowed faster at the uneven surface than at the surrounding area, therefore accelerating the deposition rate at the surface (Watanabe, 2004).

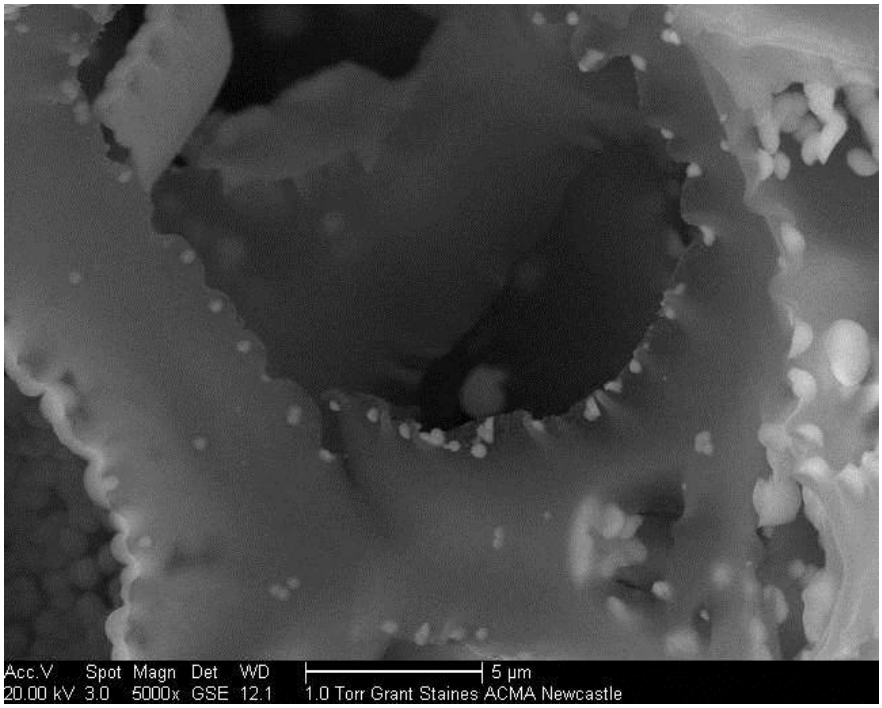

:

Figure 6-7: Initial nucleation of Ni-B grain on PHP

As the deposition process sustained and due to the autocatalytic nature of the metal reduction, metal grains continued to grow enlarging their sizes from tens to hundreds of nanometers (Figure 6.8). Various sizes of Ni-B deposits were observed on the polymer wall, generally spherical shapes.

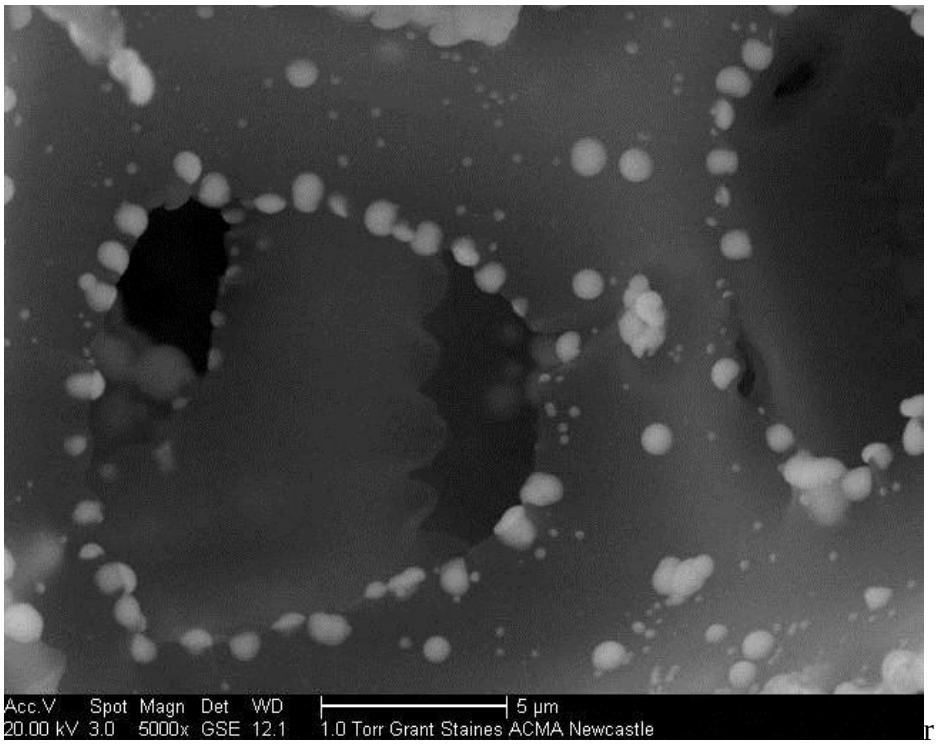

r

Figure 6-8: Ni-B deposition at the early stages

Due to heat evolution and violent movement by the reaction, the edge of PHP pore and interconnect pore is highly activated (Watanabe, 2004). Thereofore metal grains continue to grow and expand until it reached a critical grain size and formed a new layer of metal grain covering the walls of PHP (Figure 6.9).

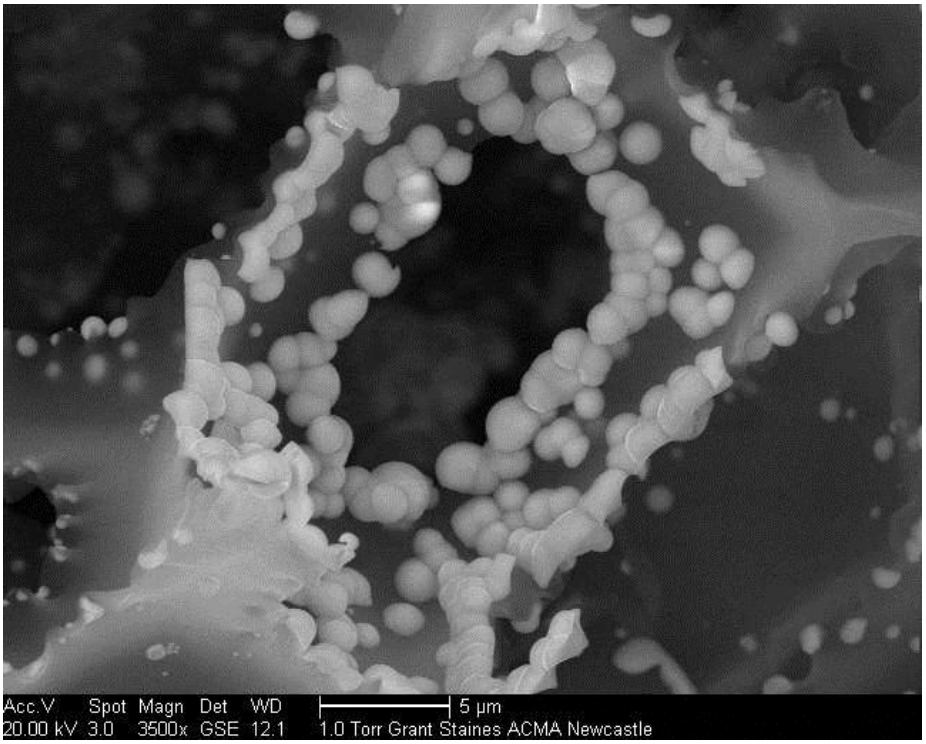

Figure 6-9: As deposition preceded the Ni-B deposits enlarged in size and started covering PHP walls

On the other hand, it was also observed that there were high and low/non deposition regions. This indicates that surface exposed to the solution flow or that are in direct contact with the solution results in a high deposition region. Figure 6-10 shows the high and low deposited region and clearly indicate no metal deposition occur on side.

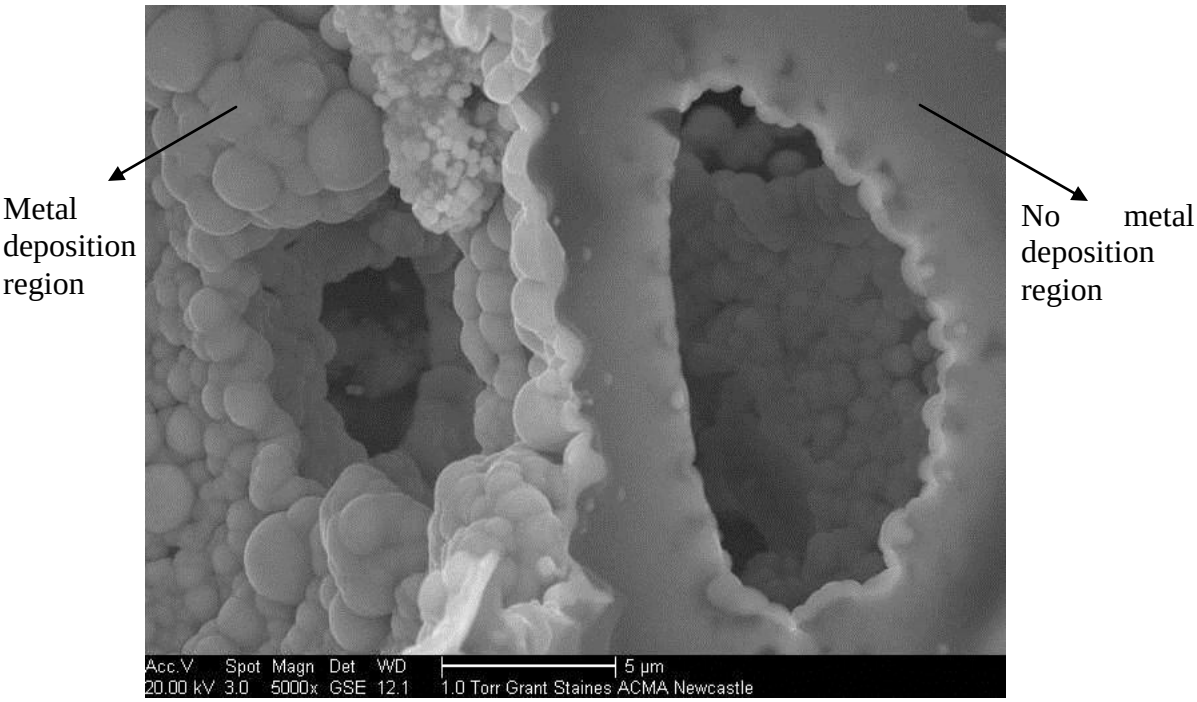

Figure 6-10: The high and low deposition region

When there was a sufficient amount of deposition, the Ni-B deposits totally covered the wall of the polymer (Figure 6-11). Although it is known that no chemical bond exists between an electroless metal film and and non-metallic substrate (Watanabe, 2004), however due to nano pore structure of PHP wall, etching and particle activated site is not necessary as it provide a natural deposition environment. The initial deposits were embedded and anchored inside the pores whereby achoring force provides the adhesion strength between the deposits and PHP templates. Therefore fully metallised templates showed a strong bond and prevent it from collapse. Figure 6-12 showed a final appearance of a hard bond Ni-B deposit and template. This is one advantage PHP has that no other porous material can offer.

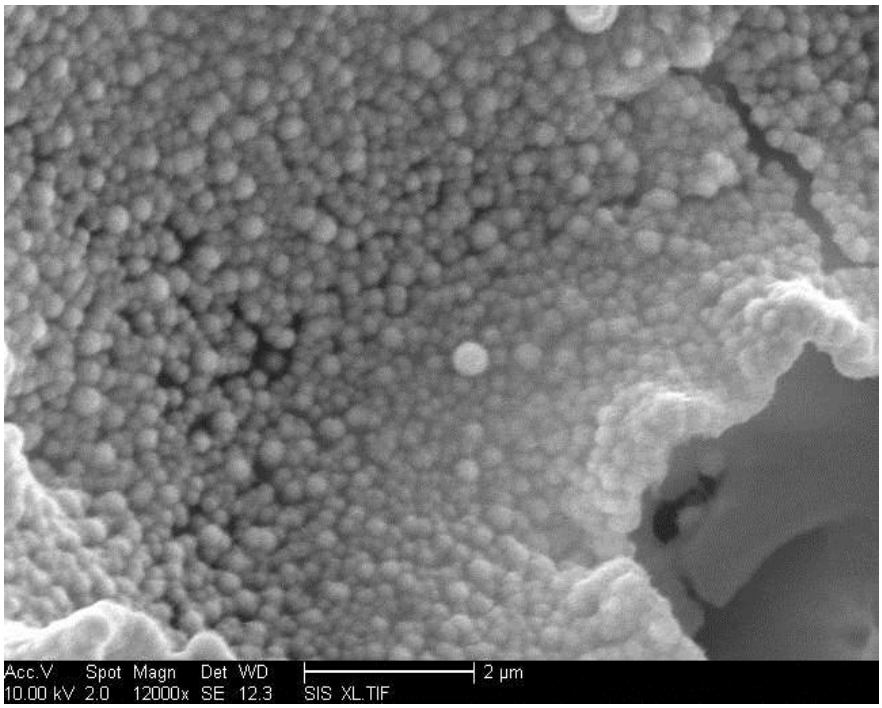

Figure 6-11: Fully deposited polymer wall with Ni-B deposits

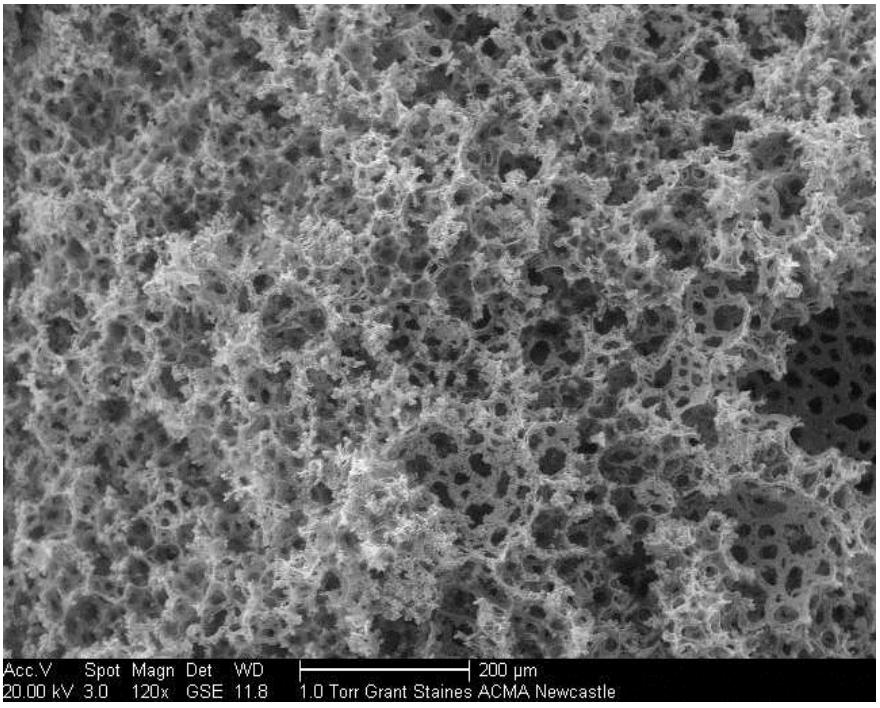

Figure 6-12: Final appearance of Ni-B deposits on PHP

A cross section line scan EDX analysis was performed on metallised PHP disk to evaluate the distribution of metal in Ni-B deposits on PHP and to identify the elemental composition of the disk. Metalized PHP disc was cut cross sectionally (see Figure 6-13). Figure 6-14 showed SEM micrograph image of a cross section metalized PHP disc.

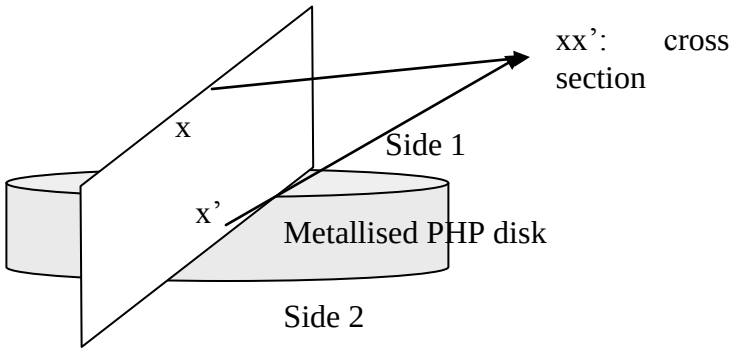

Figure 6-13: Metalized PHP disc cut cross sectionally

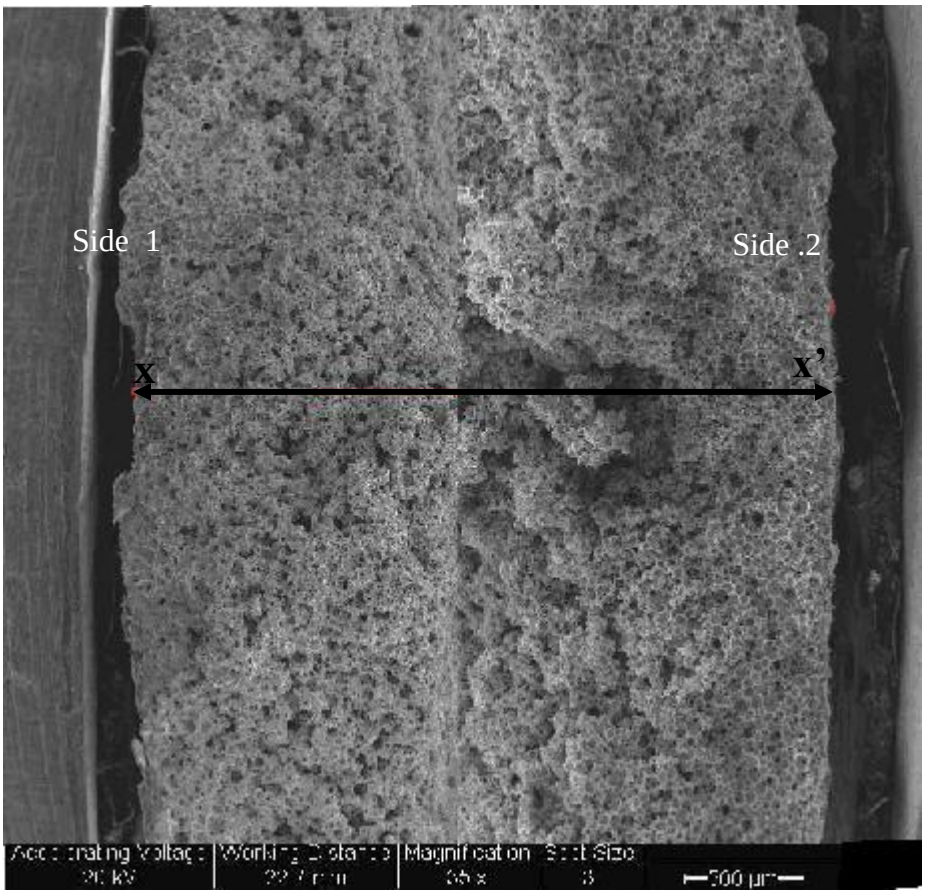

Figure 6-14: Cross-section of a metal disk that was produced by using nickel chloride as the nickel source and DMAB as reducing agent

A number of spots were taken on the axis illustrated with the arrow on the cross-section of the metal disk as indicated in Figure 6-15. Each spot corresponse to the depth of template. EDX analysis was performed for each spot on the axis to obtain the distribution of nickel and oxygen along the cross-section of the metal disk (see Figures 6-16). From Figure 6-18, it was observed that metal deposition from side 1 to side 2 presented a uniformly distributed Ni and O along the disk. The highest concentration value of Ni atomic percentage was traced having 99.98% at side 1 and 99.97% at side 2 for the metallised PHP disk. Thus, this showed an efficient and effective metallisation method for porous materials. However, it was difficult to map boron by EDX; hence comparison with previous studies using Ni-P system was not possible.

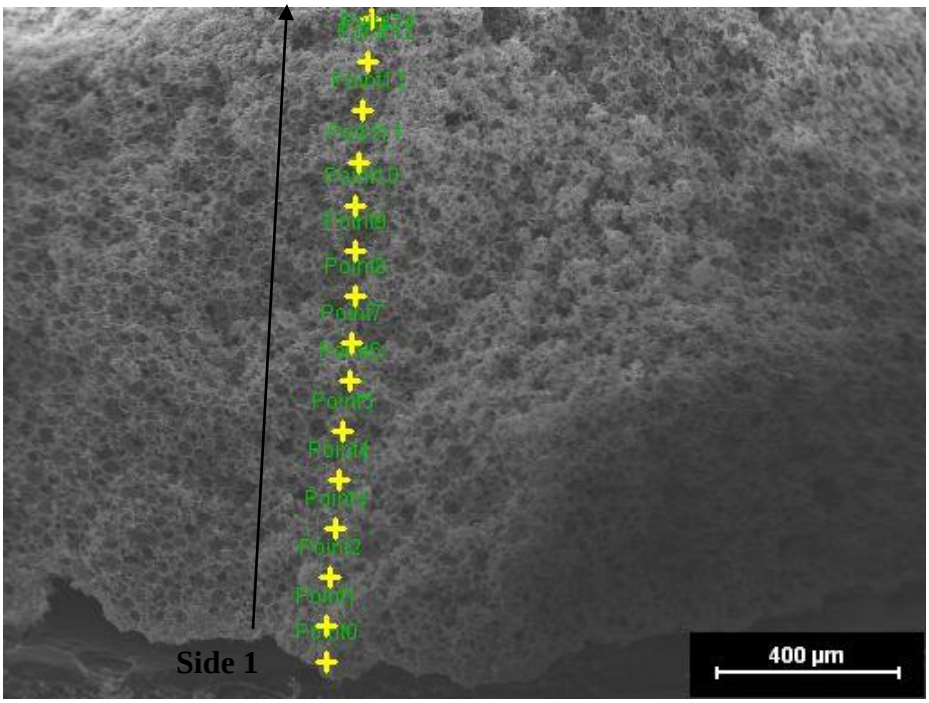

Figure 6-15: A number of spots (*points 1- n*) were taken on the cross-section from side 1 to mid point of metalized disc

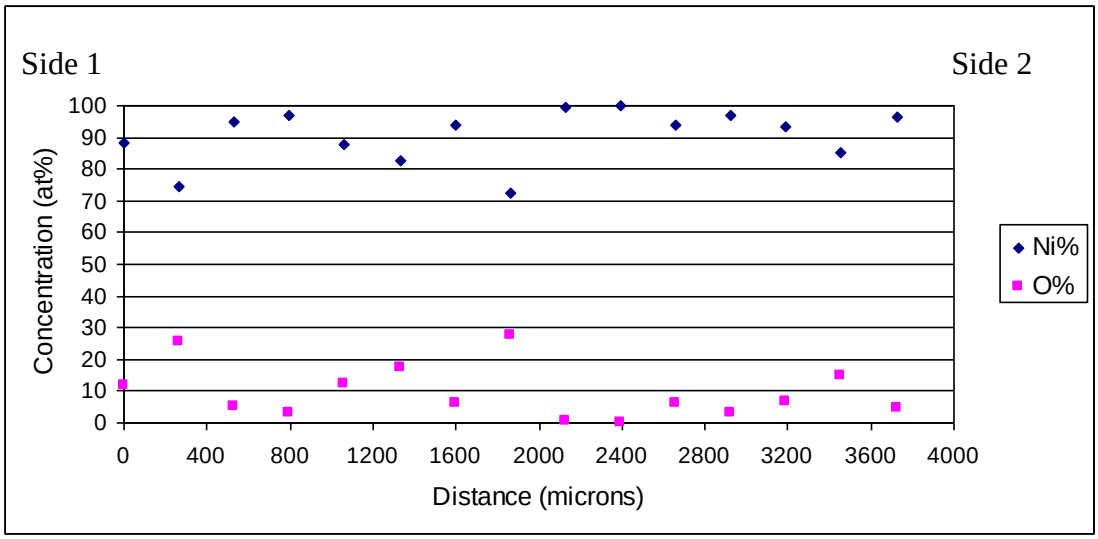

Figure 6-16: Concentration of Ni and O along the cross-section of a sample

6.3.2 Effect of of Nickel-Boron Ratio on Grain Size

The effect of nickel / boron ratio is illustrated when the deposition temperature is 90°C. As the nickel / boron ratio is decreased from 0.5 µm to 0.2 µm, deposition appears to be more uniform and the size of the metal grains is reduced as a result of reduced agglomeration The grain size of Ni-B deposits at different [Ni] / [B] ratio measured as deposited are shown in Figure 6-17 and Figure 6-18. The results clearly show that deposits made from a higher [Ni] / [B] ratio exhibits larger grain size. Figure 6-17 grain size .made with higher [Ni] / [B] ratio formed large grains. In comparison, nickel grain size from lower [Ni] / [B] ratio still remained in small size as shown in Figure 6-18. This is with agreement from studies conducted by Chou et al. (2007). However, these are only qualitative and are intended to serve us as a guide to optimising the processing conditions and plating bath composition.

Table 6-4 : Average of grain size deterrmined in relation to [Ni]/[B] ratio

[Ni]/[[B]	Grain size
0.2	0.15 ± 0.02
0.5	0.40 ± 0.06

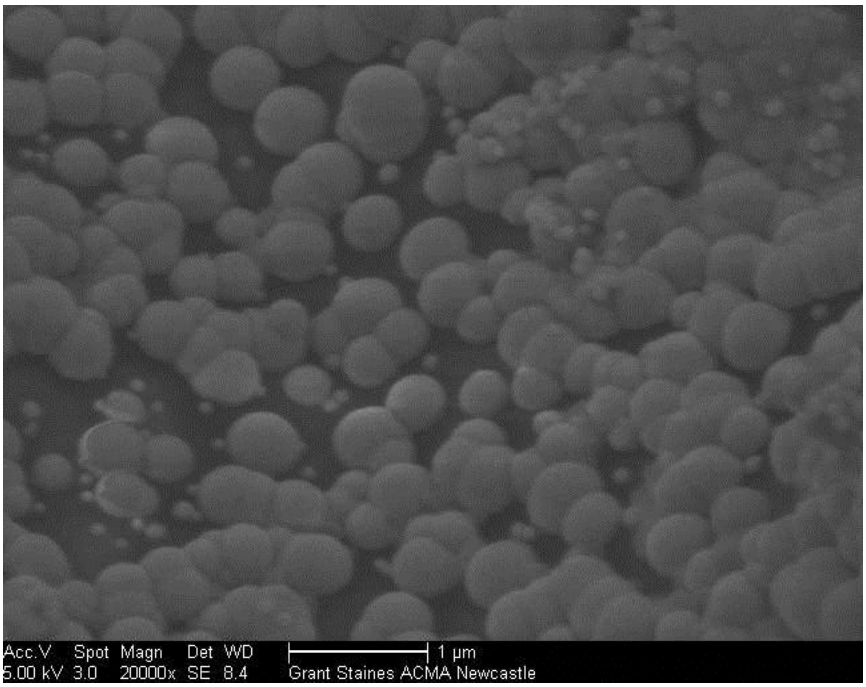

Figure 6-17: The effect of Ni/B molar concentration ratio on the metal deposition quality when T= 90°C; grain appearance when [Ni]/[B] = 0.5

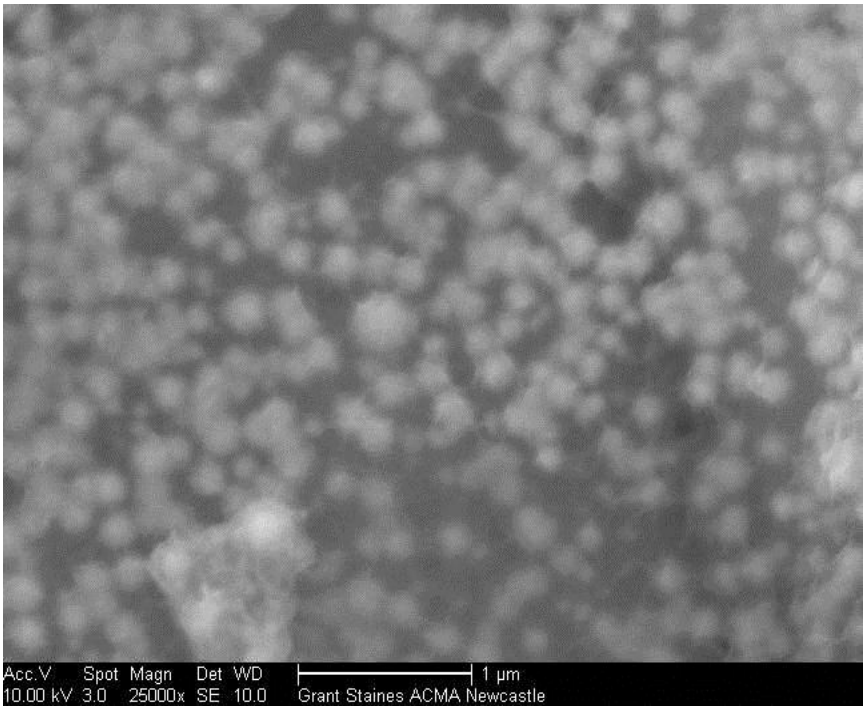

Figure 6-18: The effect of Ni / B molar concentration ratio on the metal deposition quality when T= 90°C; grain appearances when [Ni]/[B] = 0.2

6.3.3 Effect of Cell Temperature on Grain Size

Cell temperature can also be referred to as the solution temperature, as described in earlier section. Initial solution temperature was room temperature before entering the cell and solution temperature was controlled by a band heater set at the desired temperature. The effect of cell temperature on grain size is shown in Table 6-5. As the deposition temperature decreased, the nickel-boron system appeared similar to the nickel-phosphorus system, but with metal grain size of 0.26-2.0 μm, as opposed to 5-15 μm encountered in the nickel-phosphorus system.

Table 6-5: Average grain size in relation to cell temperature

Cell Temperature °	Average Grain Size, μm
35	0.26±0.01
50	0.40±0.04
75	0.6 ±0.09
90	2.0 ± 0.38

The connectivity in nickel-boron alloy was far better than that obtained for nickel-phosphorous systems. The main reason for these differences was the size of the metal deposit attained at the deposition stage. Although the initial deposits were small (ca. 0.25 μm), they appeared to agglomerate to form larger grains with size 1-2 μm. The grain size increased as the solution temperature increased. The structure was formed by small metal grains of a size less than a micrometer when the deposition temperature was low (35°C or 50°C), while larger agglomerated grains formed the skeletal structure when the deposition temperature was higher (75°C and 90°C). These results are shown in Figure 6.19 (a)–(d). This phenomena is due to the increased diffusivity that allows a single atom to migrate a long distance over the template, thus producing large grains (Watanabe, 2004).

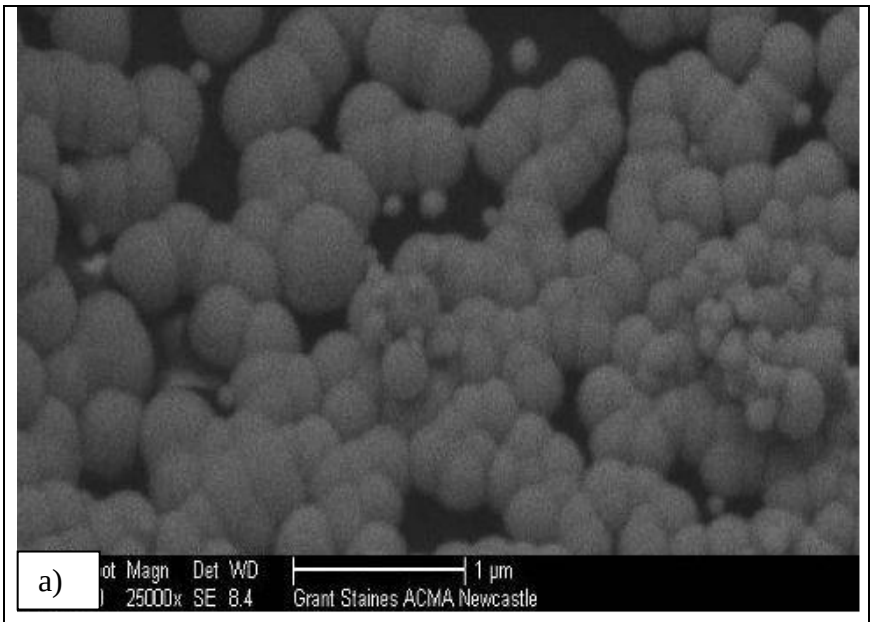

(a) Grain size deposited at 35°C

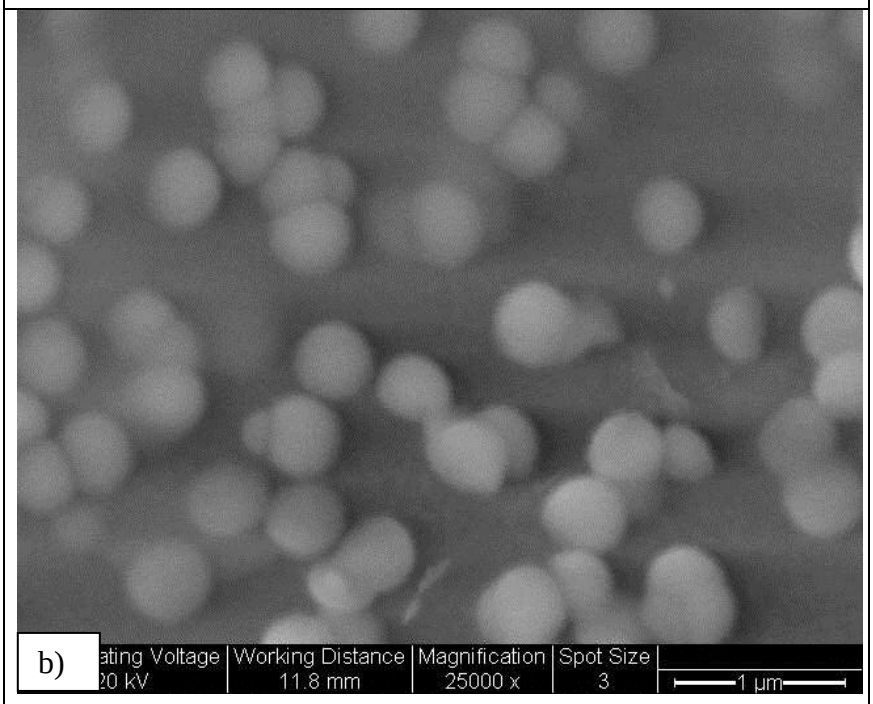

(b) Grain size deposited at 50°C

(Continue next page)

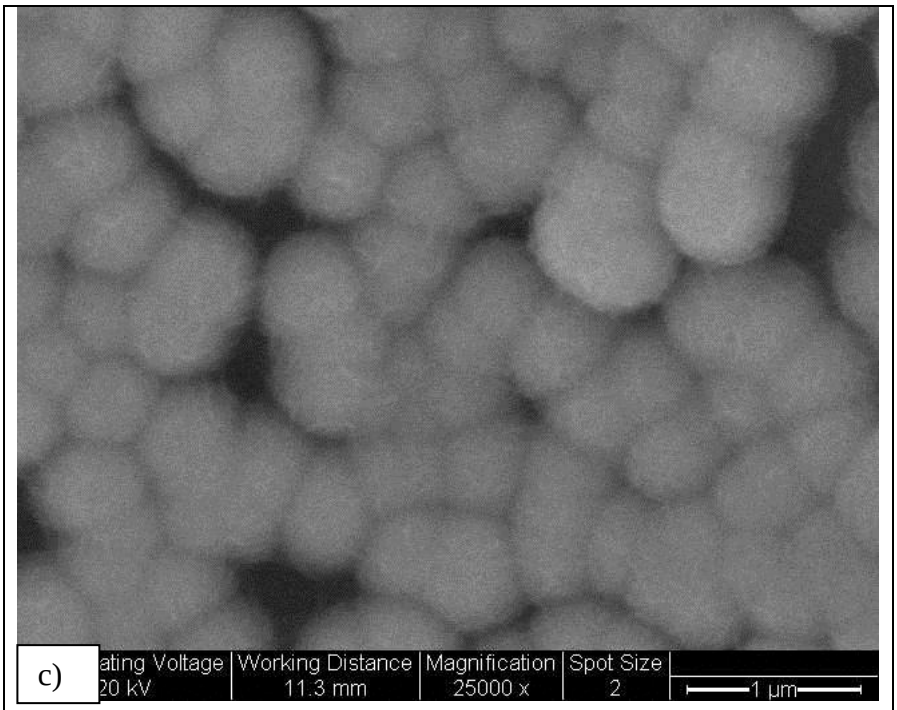

(c) Grain size deposited at 75°C

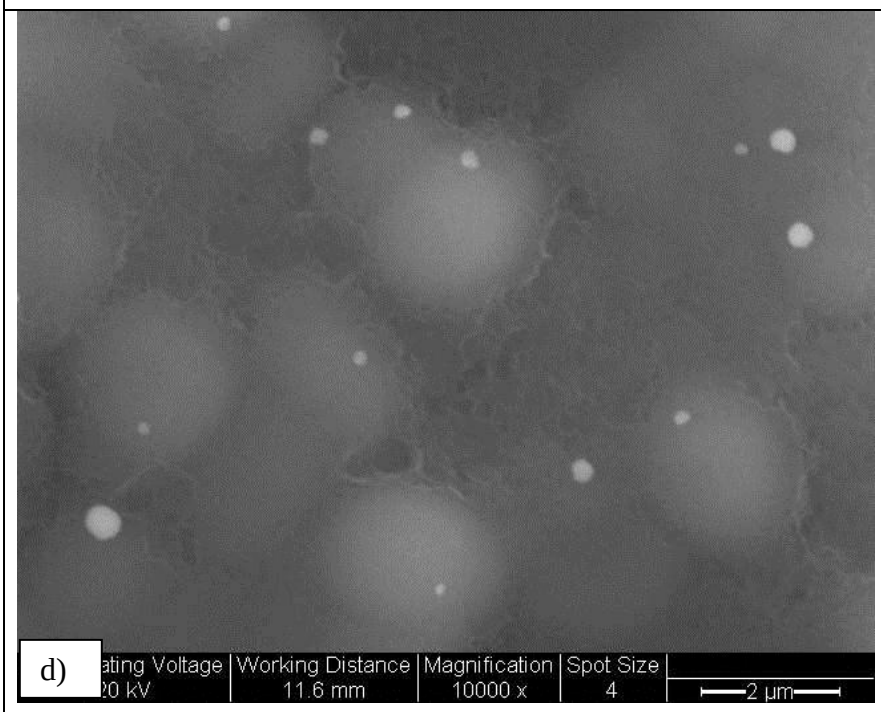

(d) Grain size deposited at 90°C

Figure 6-19 (a)-(d): Effect of cell temperature on grain size in Ni-B electroless deposition using DMAB as reducing agent.

The results from X-ray diffraction patterns of the electroless Ni-B deposition on PHP as deposited are shown in Figure 6.20, Figure 6.22, Figure 6.24, and Figure 6.26. The samples of PHP containing the electroless Ni-B metal deposits in the as deposited condition clearly exhibited a single broad peak occurred at 2Θ=45°, indicating the amorphous nature of the metal deposits and suggesting that the size of Ni-B deposits apparently is fine grain particles. Many studies have confirmed that as deposited Ni-B deposits on metal substrate are fine crystallites (Delaunois, 2002 ; Narayanan, 2003) . These results were produced from cell temperature operating at 35°C 50°C, 75°C and 90°C respectively. Figure 6.21, Figure 6.23, Figure 6.25 and Figure 6.27 show XRD patternn after heat treatment at 600°C for 2h (1h ramping and 1h dwelling) for cell temperature ranging from 35°C, to 90°C.

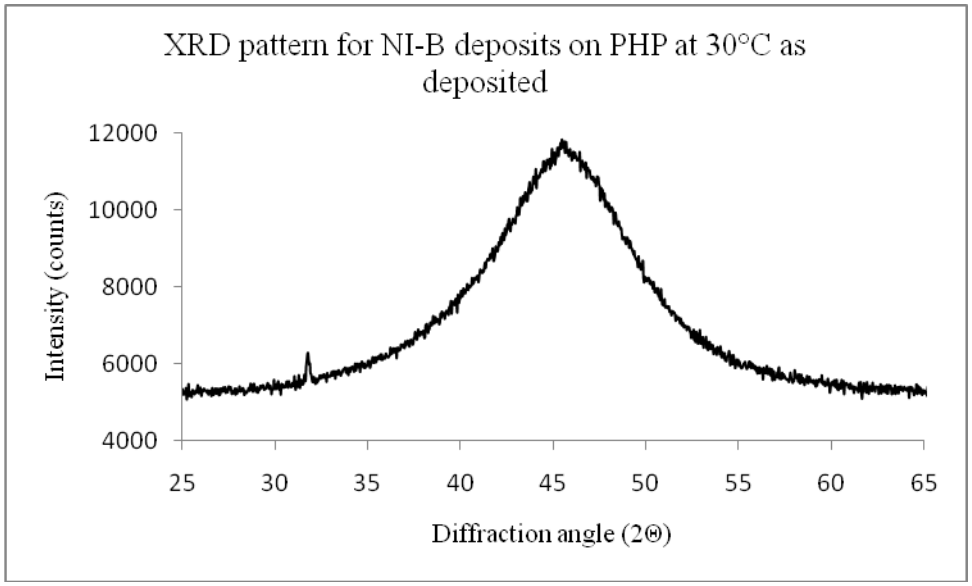

Figure 6-20: XRD pattern for Ni-B deposits on PHP before heat treatment with cell temperature at 35°C

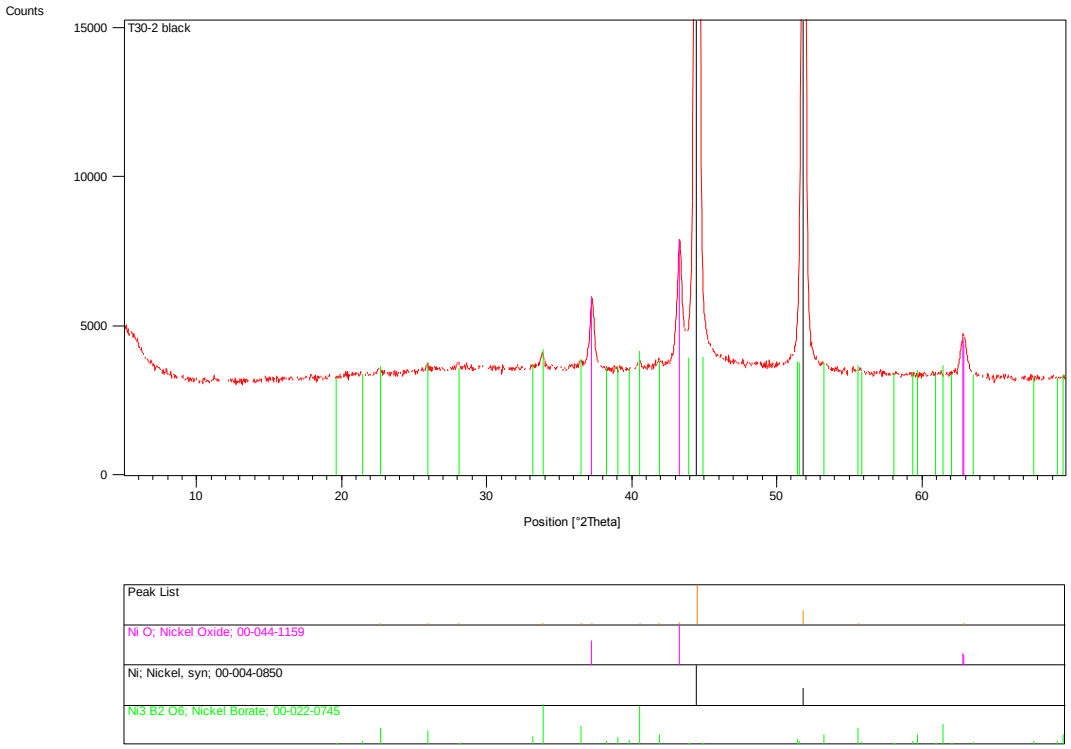

Figure 6-21: XRD pattern for Ni-B deposits on PHP after heat treatment at 600°C for 2h with cell temperature at 30°C

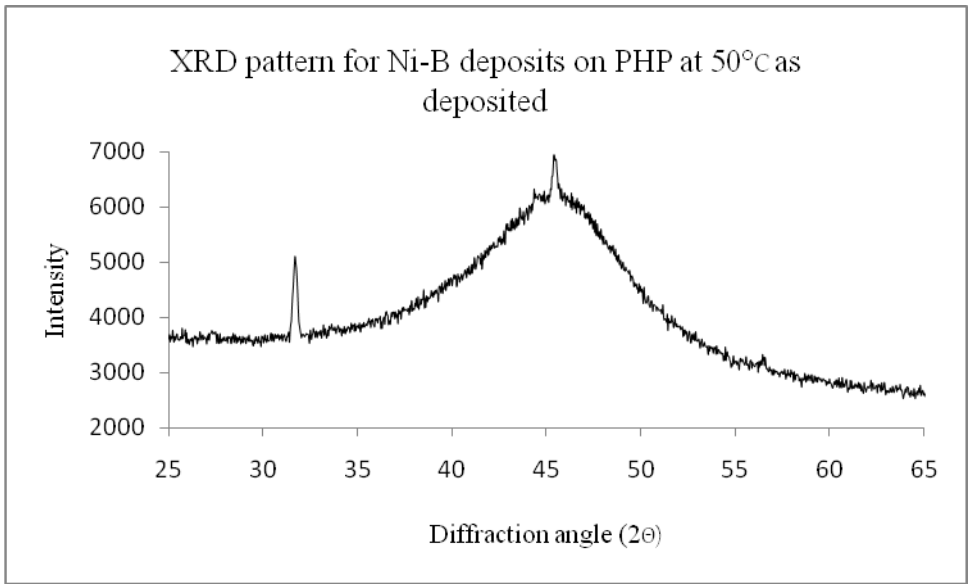

Figure 6-22: XRD pattern for Ni-B deposits on PHP before heat treatment with cell temperature at 50°C

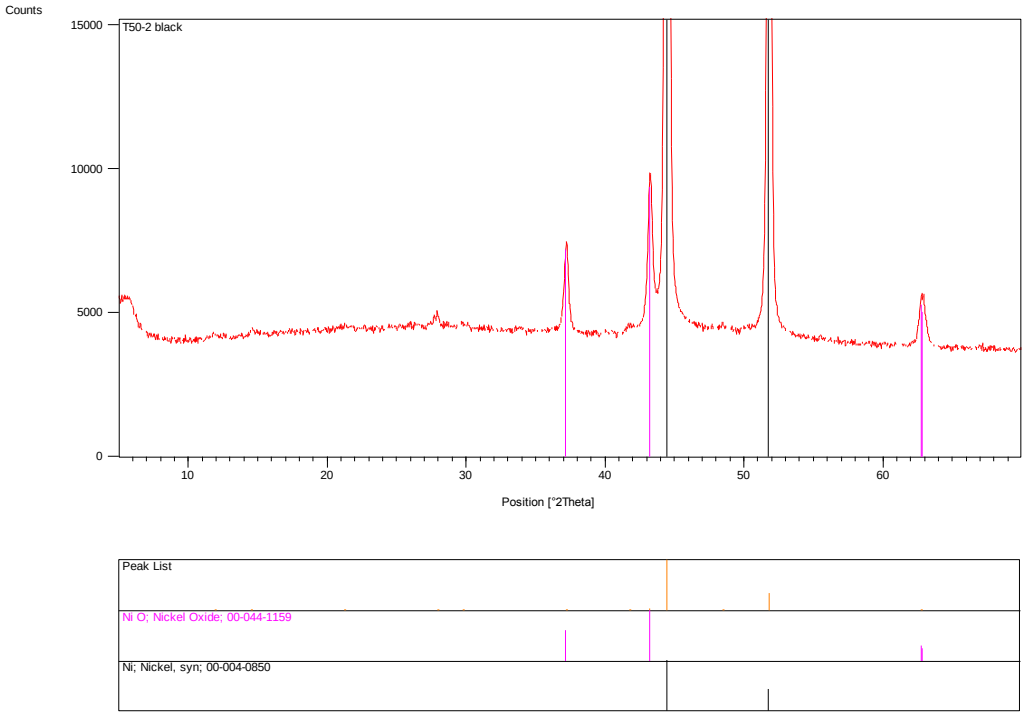

Figure 6-23: XRD pattern for Ni-B deposits on PHP after heat treatment at 600°C for 2h with cell temperature at 50°C

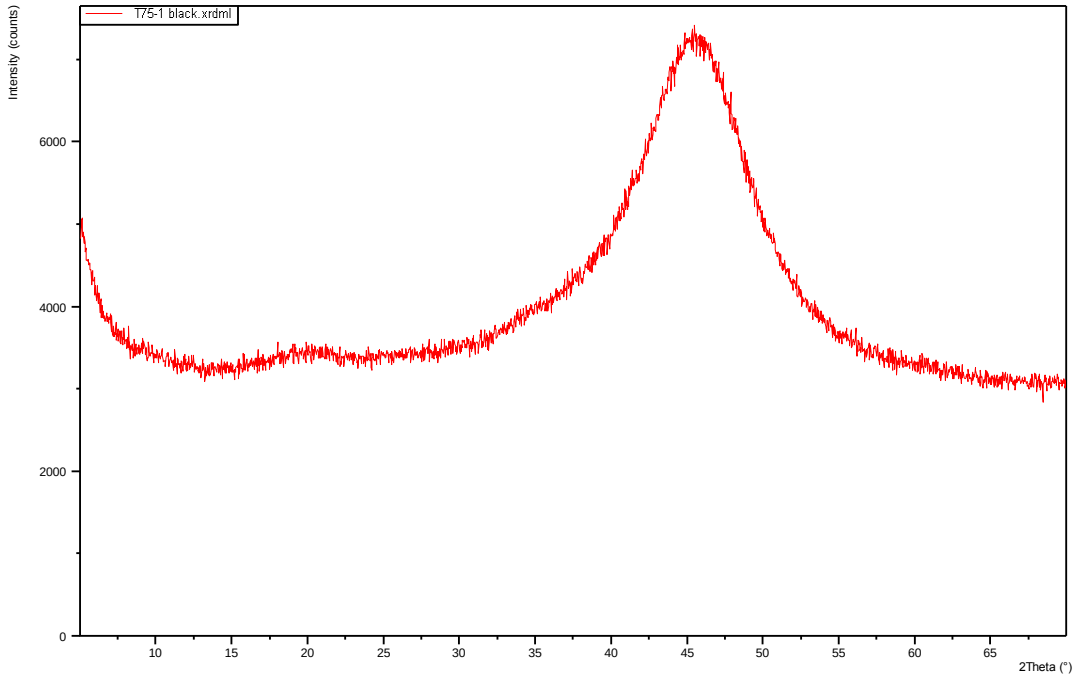

Figure 6-24: XRD pattern for Ni-B deposits on PHP before heat treatment with cell temperature at 75°C

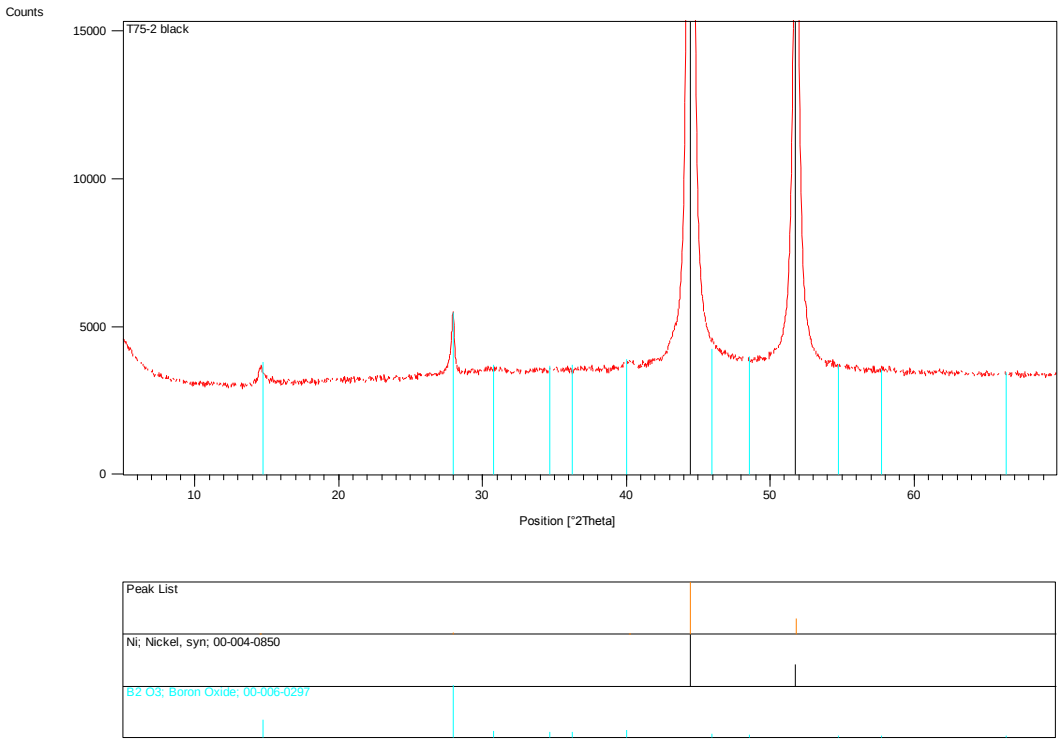

Figure 6-25: XRD pattern for Ni-B deposits on PHP after heat treatment at 600°C for 2h with cell temperature at 75°C

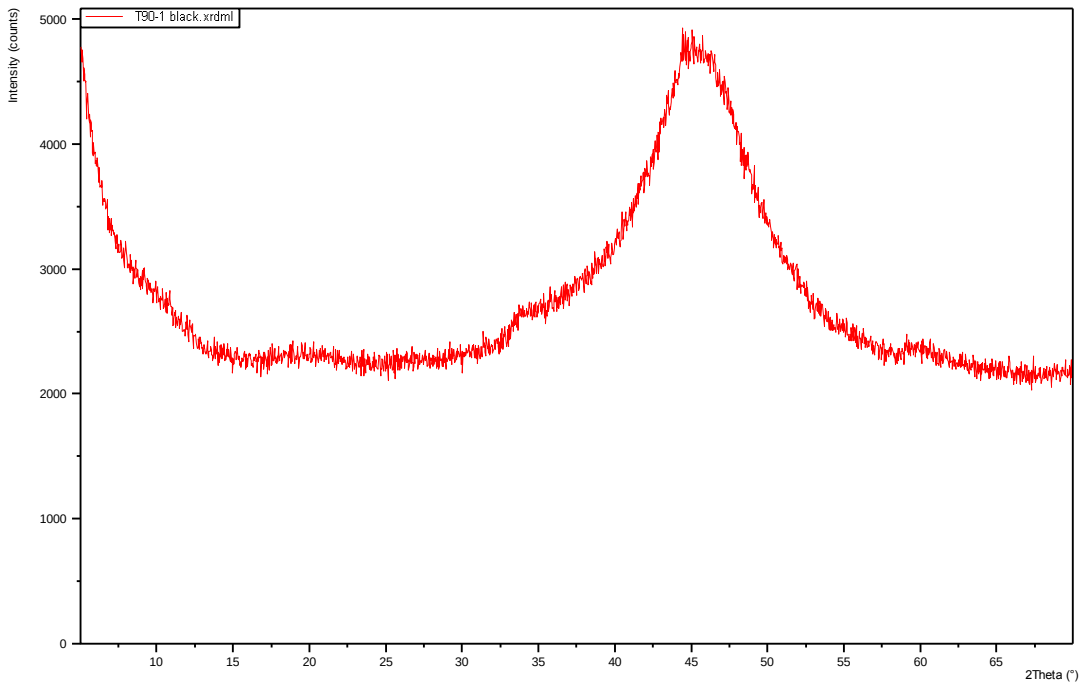

Figure 6-26: XRD pattern for Ni-B deposits on PHP as deposited condition with cell temperature at 90°C

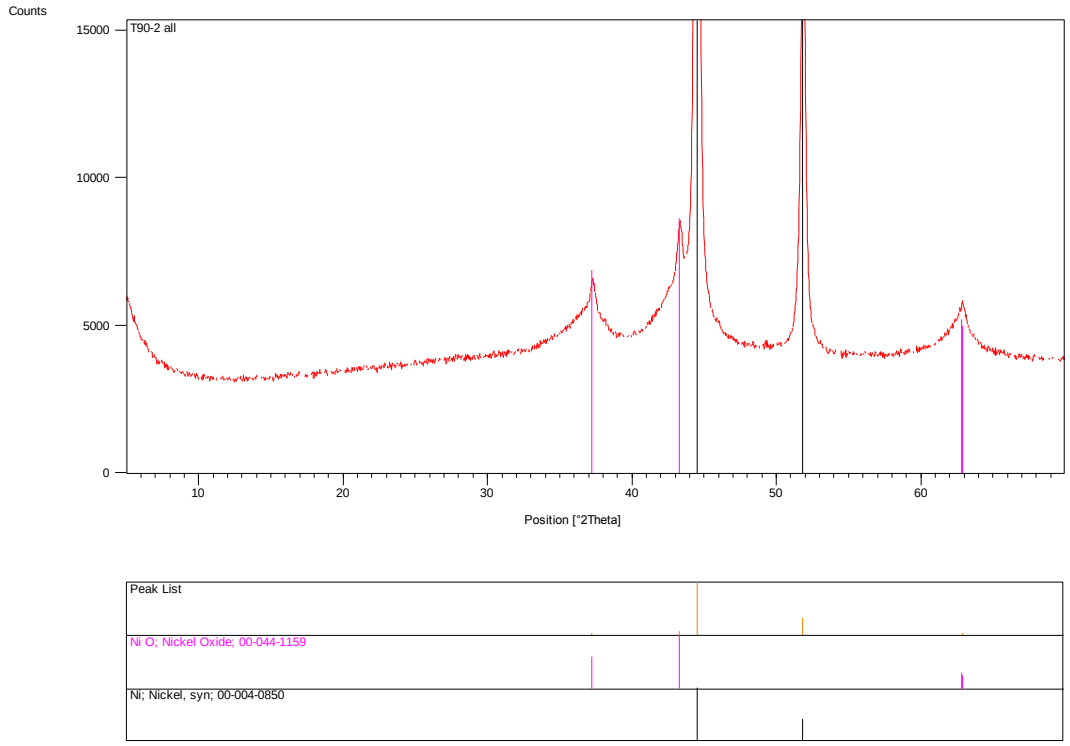

Figure 6-27: XRD pattern for Ni-B deposits on PHP after heat treatment at 600°C for 2h with cell temperature at 90°C

Electroless Ni-B deposits undergo phase transformation upon heat treatment. The Ni-B deposits for cell temperature 35°C exhibited a sharp crystallized nickel peak and contained phases dominantly Ni, nickel boride in the Ni_3B form and NiO (see Figure 6-21). However for XRD pattern for electroless Ni-B deposits heat treated at 600°C for samples deposited at higher than 30°C results in growth of crystalline nickel that indicates the absence of nickel boride phase and predominance of Ni and NiO in the deposits (see Figure 6-23, Figure 6-25 and Figure 6-27).

The XRD patterns of electroless Ni-B as deposited conditions for cell temperature 30, 50, 75 and 90 were summarized in Figure 6.28. While XRD patterns for electroless Ni-B after heat treatments were summarized in Figure 6.29. From Figure 6.24 it was observed that the diffraction pattern of the Ni-B has a single broad peak indicating

amorphous phase and evidently followed the same pattern for all different cell temperature.

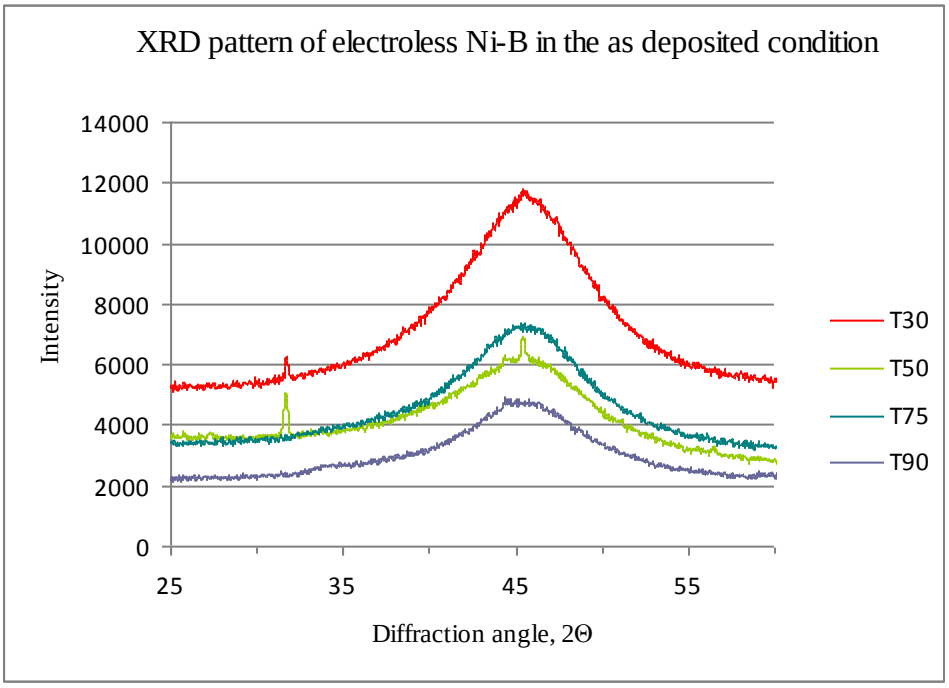

Figure 6-28: XRD of electroless Ni-B deposition at various temperatures as deposited condition.

Upon heat treatment at 600°C for 2 h, the Ni-B deposits produced a narrow peak that results in growth of crystalline nickel. The shifting of peak showed from Figure 6-29 between the cell temperatures operated at different temperatre (T30-T90) indicates strains present within the deposits. As the cell temperature decreases (at T30), the intensity of the peaks improved. Diffraction pattern shows the highest intensity with well defined sharp peak indicating high crytallinity of the Ni-B (see Figure 6-29). This means that the grain size increases with increase in the bath temperature.

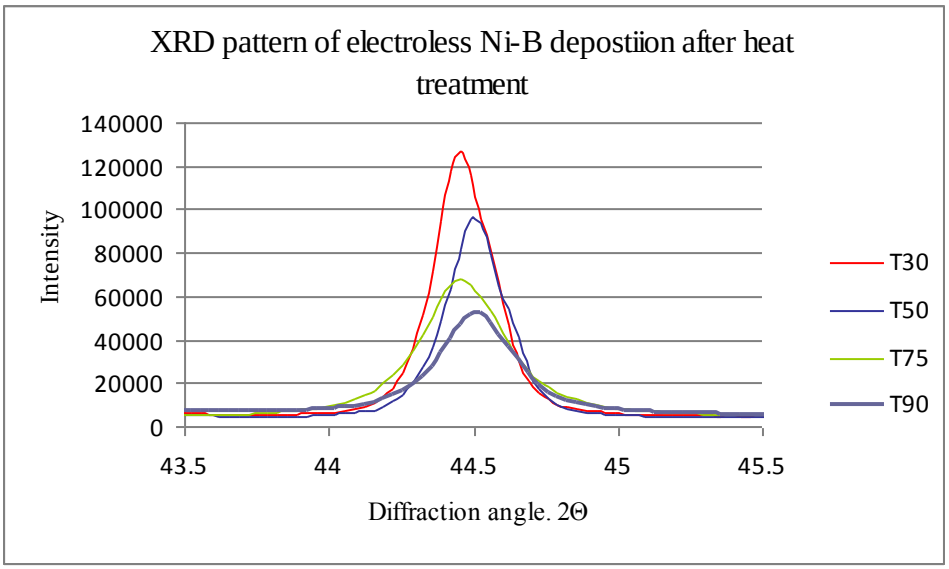

Figure 6-29: XRD patterns of electroless Ni-B deposition after heat treatment for samples deposited at various temperatures

6.3.4 Effect of Cell Temperature on Morphology

The effect of cell temperature on the macro- and nano-scale structures of Ni-B is illustrated in Figure 6.30 (a-d). As can be seen, the skeletal structures at both scales are affected by temperature. Unlike the macrostructures obtained with nickel-phosphorous systems (Calkan, 2006) (see Figure 6-30), the pores appear to be more discrete with a higher connectivity. We found that the skeletal structure and shape of PHP changes according to operating cell temperature used. After heat treatment, the shapes of PHP showed either a spherical or broken cage cell, indicating Ni-B metal deposits have strong adhesion to the strand of the PHP; although in principle there is no adhesion between an electroless metal deposit and a non-metallic substrate (Watanabe, 2004). This shows that the metal deposits were embedded and strongly anchored inside the pore of PHP. Ni-B deposits operated at cell temperature 30°C exhibited a broken cage structure with some irregular PHP shape (Figure 6.31 (a)), while Ni-B deposits operated at cell temperature 50°C remain the PHP structure with uniform and even Ni-B particle deposits (Figure 6.31 (b)). When cell temperature was operated at 75°C, the structure exhibited a spherical cage like structure and was more irregular. Also, the particles were

in closer contact (Figure 6.31) (c)). Finally, at 90°C operating cell temperature, all the Ni-B particles coalesced and the Ni-B surface became smooth while having a broken cage structure (Figure 6.31 (d).)

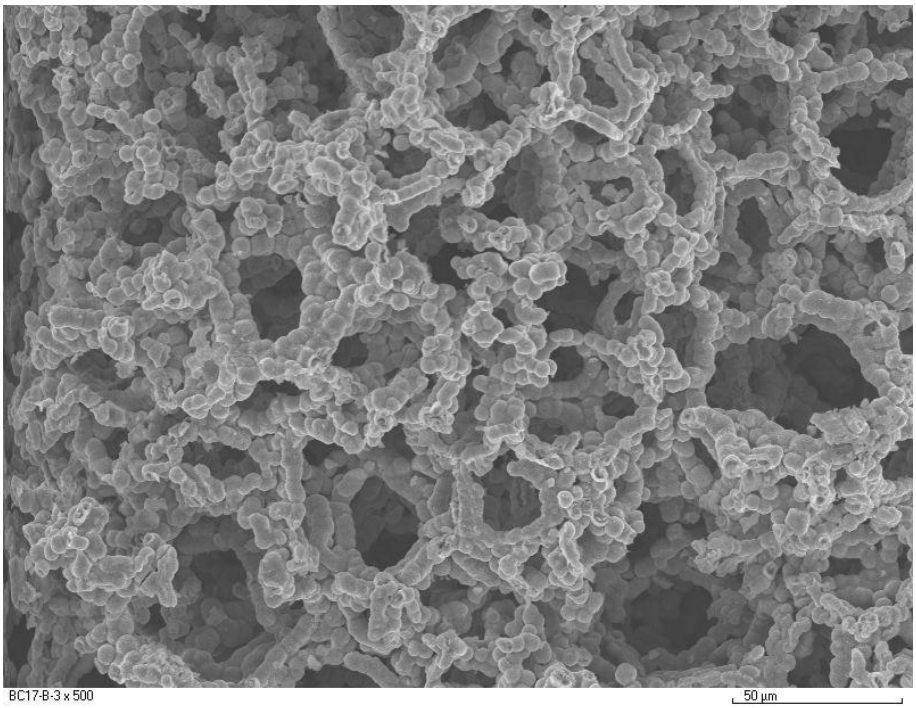

Figure 6-30: Metallised PHP using Ni-P electroless system (Calkan, 2006)

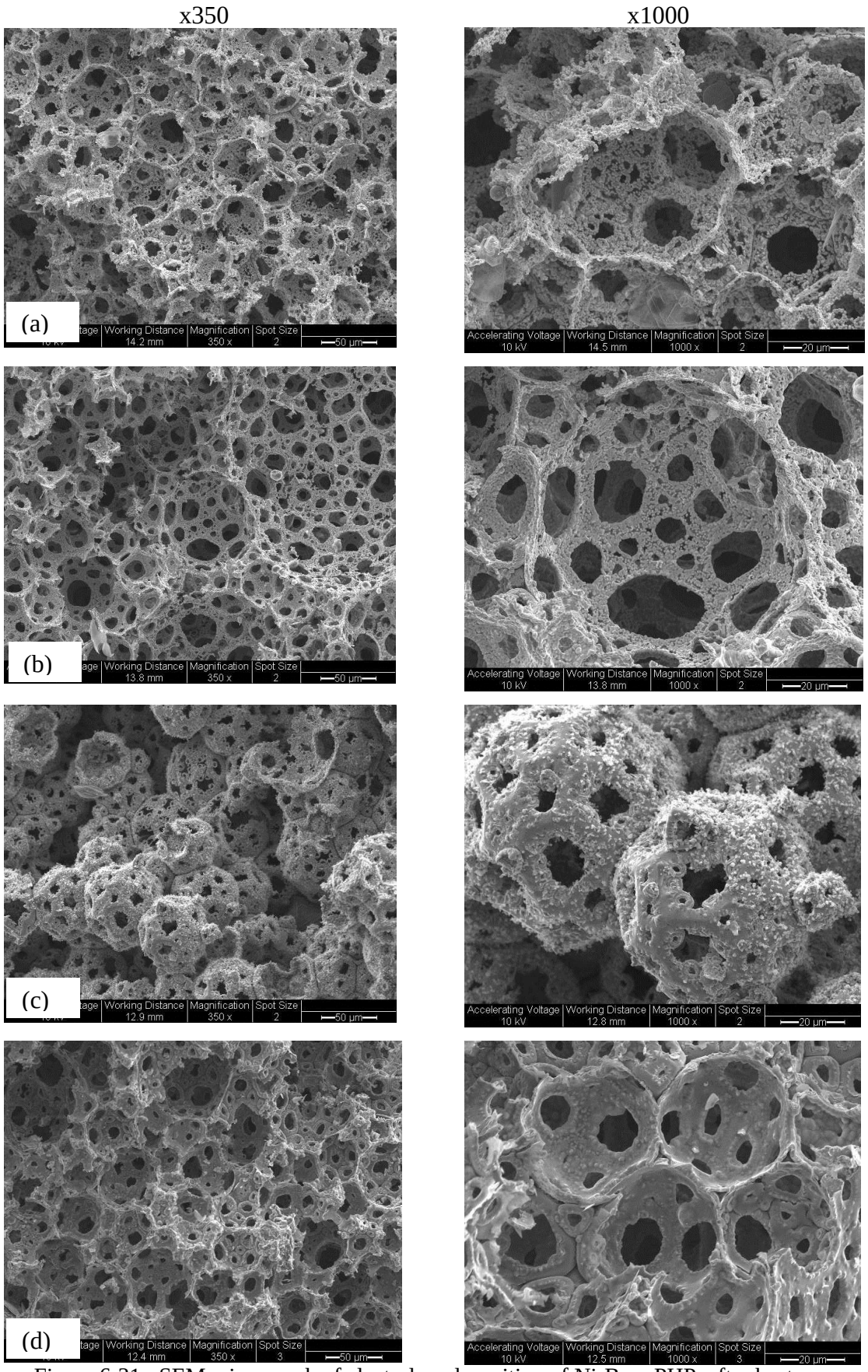

Figure 6-31: SEM micrograph of electroless deposition of Ni-B on PHP after heat treatment at 600°C at x350 and x1000 magnification a) Deposited PHP at 35°C; b) Deposited PHP at 50°C; c) Deposited PHP at 75°C; d) Deposited PHP at 90°C operated at [Ni]:[B]=1:2

6.3.5 Morphology Change with Type of Nickel Source

Two different nickel sources were used during the experiment: nickel chloride and nickel sulphate. Figure 6.32 (a)-(b) and Figure 6.33 (a)-(b) show the results from the solution using nickel chloride and nickel sulfate in Ni-B deposition with cell temperature at 50°C after heat treatment. A smaller grain size was obtained from the chloride bath compared to the sulfate bath (Table 6-6). According to (Watanabe, 2004), the morphology is affected by molecular weight of the ions. Solution containing chloride ions has small molecules while solution containing sulphate ions has molecules of a larger size. This is evident from Figure 6.18 which shows Ni-B deposits containing chloride ions have smaller grain size compared to solution containing sulphate ions which have larger grain size. Therefore it was evident that when using nickel chloride as nickel source, the grains size is smaller. (see Figure 6.32 and Table 6.6)

Table 6-6: Average grain size in relation to nickel source

Nickel Source	Average Grain size (μm)
Nickel Chloride	0.24 ± 0.08
Nickel Sulphate	0.78 ± 0.20

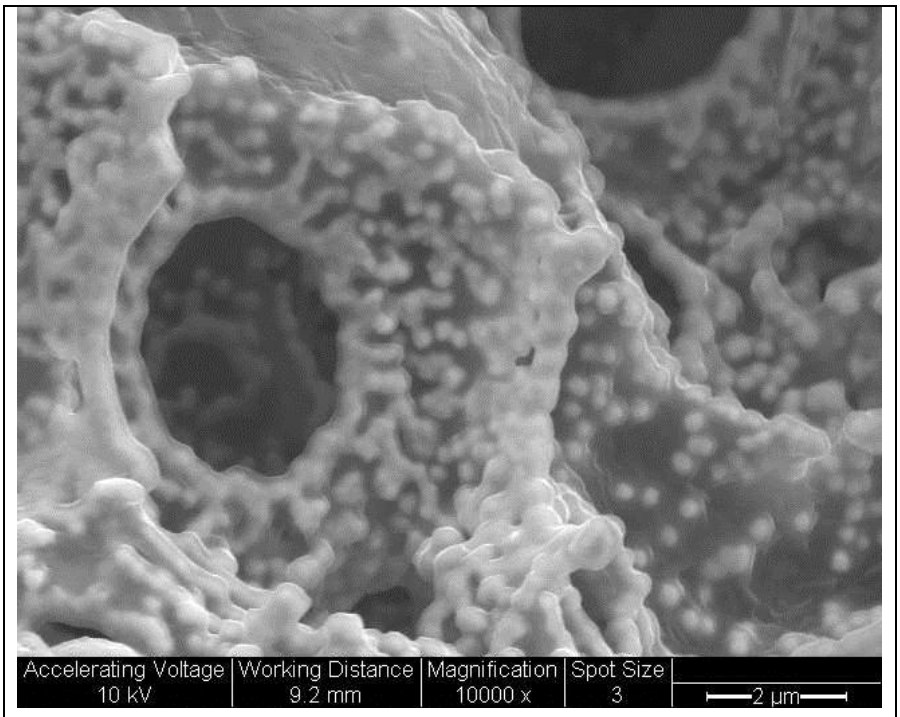

a) x10000 magnification

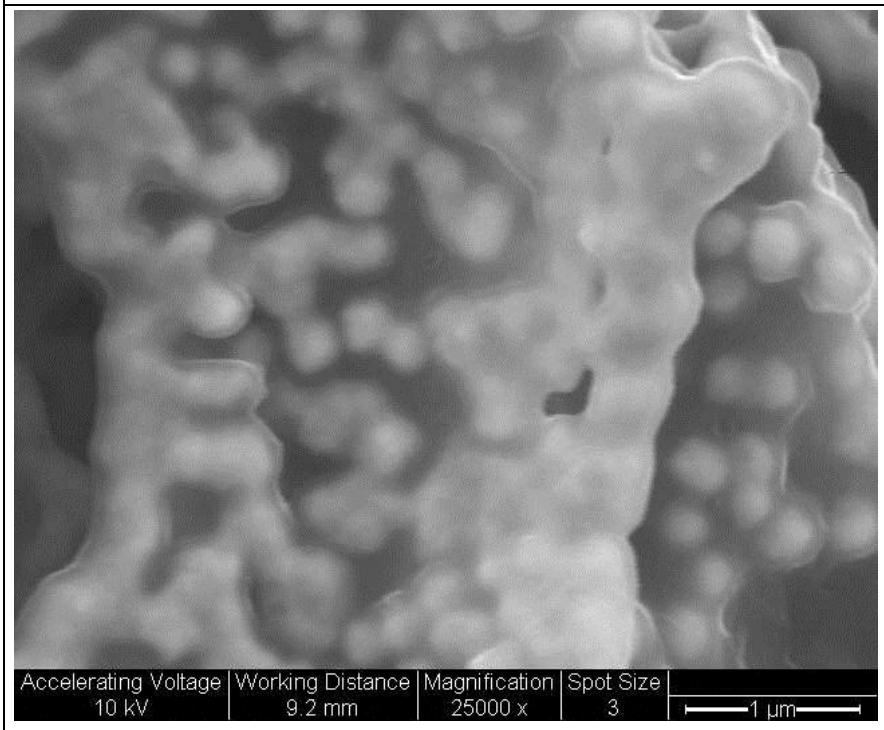

b) x 25000 magnification

Figure 6-32: SEM micrograph of Ni-B electroless deposition on PHP using Nickel chloride as nickel source a) x 10000 b) x25000

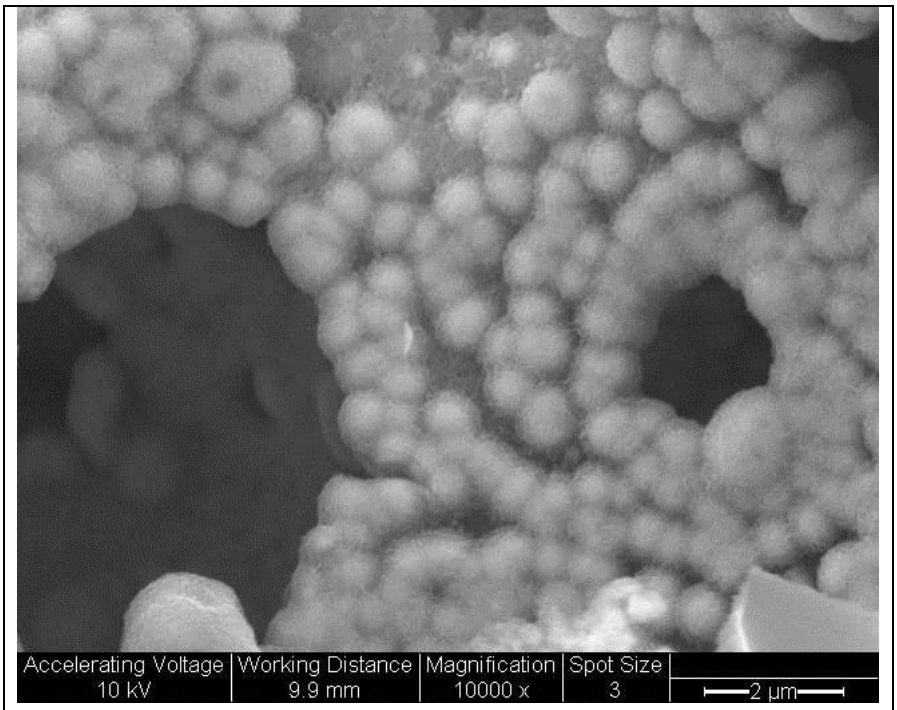

a) x10000 magnification

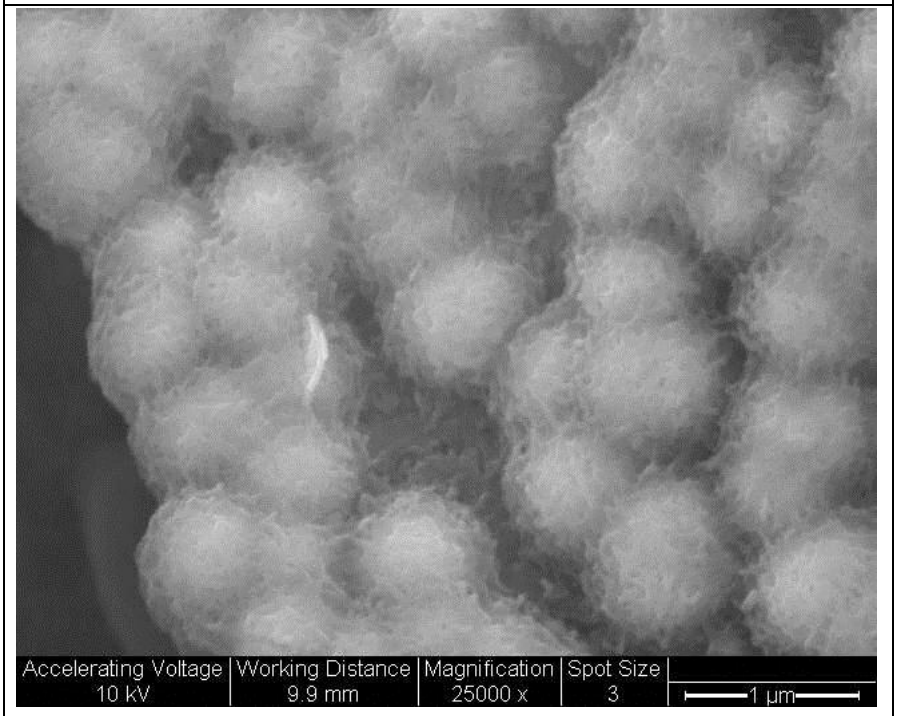

b) x 25000 magnification

Figure 6-33: SEM micrograph of Ni-B electroless deposition on PHP using Nickel sulphate as nickel source a) x 10000 b) x25000

6.3.6 Effect of Reducing Agent Used on Grain Size

The Ni-B electroless system often uses $NaBH_4$ or DMAB as reducing agents. Therefore, in this experiment the effect of the reducing agent used on grain size was investigated. For system using $NaBH_4$, 1:2 nickel to borohydrate ratio was used and cell temperature was operated at 90°C due to metal precipitation occur at this temperature. For system using DMAB 1:2 nickel to amine ratio was used and cell temperature was operated at 90°C as comparison to cell temperature in NaBH4 bath. Figure 6.34 (a)-(c) shows Ni-B deposits on PHP using $NaBH_4$ and Figure 6.35 (a) –(c) shows Ni-B deposits on PHP using DMAB. It was observed that Ni-B deposit from $NaBH_4$ exhibited grain size ca 300nm (Figure 6.34 (c). When DMAB was used as the reducing agent, grain size was reduced to ca 140nm (Figure 6.35 (c)).

Table 6-7: Average grain size in relation to reducing agent used

Nickel Source	Average Grain size (μm)
Sodium Borohydride	0.30 ± 0.16
Dimethylamine Borane	0.14 ± 0.20

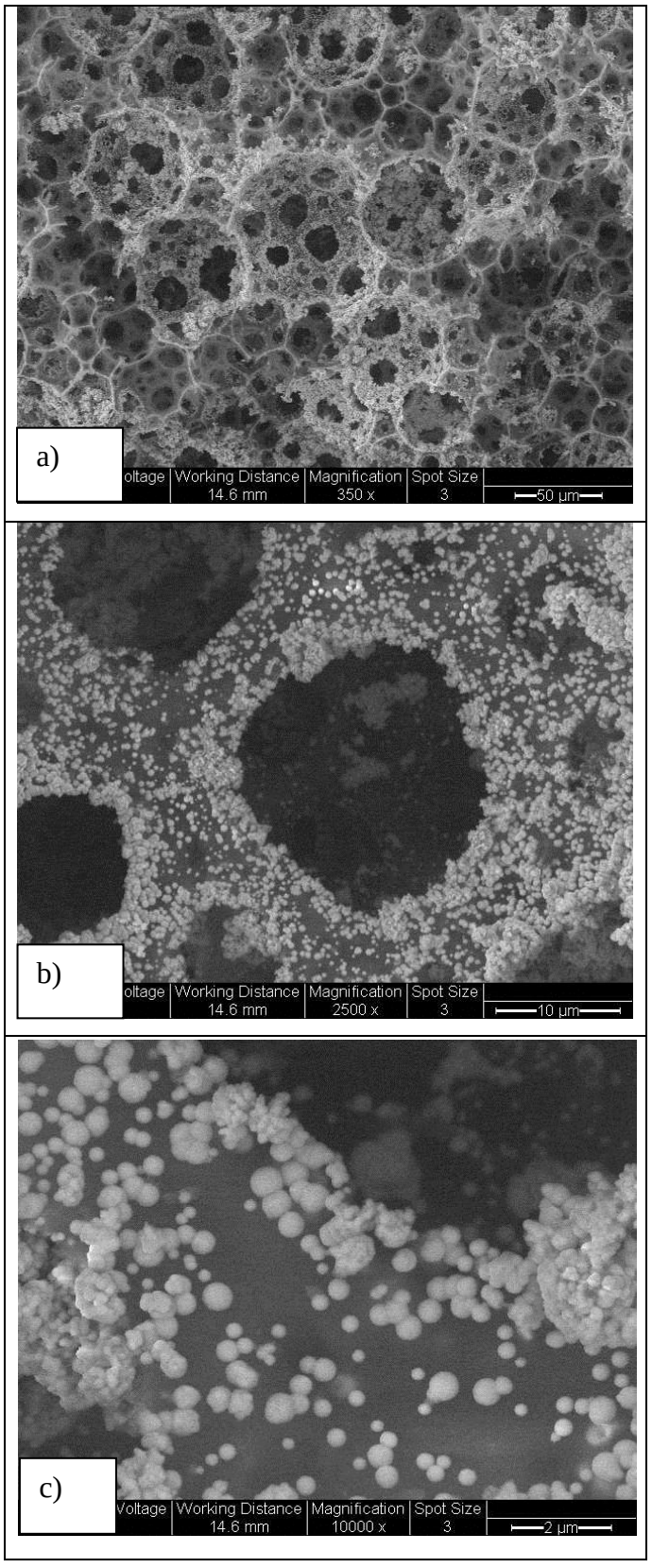

Figure 6-34: SEM micrograph of Ni-B electroless deposition on PHP using NaBH4
a) General view of Ni-B deposits on PHP using NaBH4 as reducing agent b) Detail Ni-B grain size structure c) distribution of metal grain on PHP at higher magnification

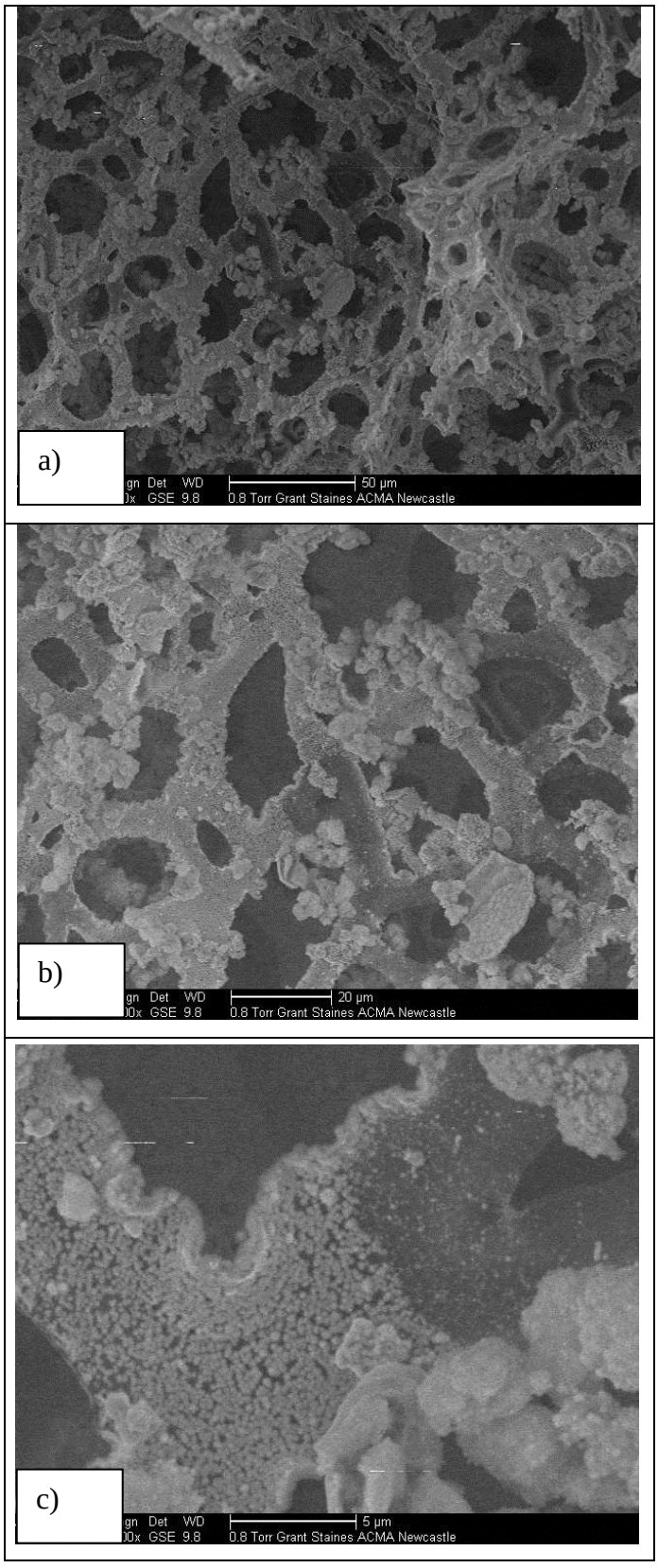

Figure 6-35: SEM micrograph of Ni-B electroless deposition on PHP using DMAB a) General view of Ni-B deposits on PHP using DMAB as reducing agent b) Detail Ni-B grain size structure c) distribution of metal grain on PHP at higher magnification

6.3.7 Effect of Cooling Temperature on Morphology

This experiment showed the effect of cooling temperature on surface morphology and structure of PHP. Metallised PHP with Ni-B deposits was cooled down under three different conditions after the heat treatment process. In the first experiment, PHP was immersed immediately in deionised water at room temperature, as shown in Figure 6.36 (a). When metal is subjected to cooling it goes through a transformation phase. It has been confirmed that the cooling (heating) rate can affect the temperature of phase transformation greatly; hence, it can cause a change in system enthalpy (Wong and Ren, 2004). A sudden reduction in temperature caused the grains to agglomerate, producing a bulk grain structure (Figure 6-36). On the other hand, the rapid cooling by quenching destroyed the grains as well as the very few remaining pores present after the heat treatment. Figure 6.36 clearly shows that the structure was composed of thick pore-free strands with irregular shapes, instead of spherical grains. Cooling gradually at room temperature or cooling gradually in the oven, however, maintained the original PHP structure. Figure 6.37 and Figure 6-38 presents the SEM micrograph of the fused metal grains. As can be seen, the particles were close together but did not agglomerate as in the first experiment. However, when the sample was cooled gradually in the oven the skeletal structure became a spherical cage like structure.This probably due to shrinkage affect phenomena within metal bond that formed the skeletal structure which led to formation of a spherical cage like structure.

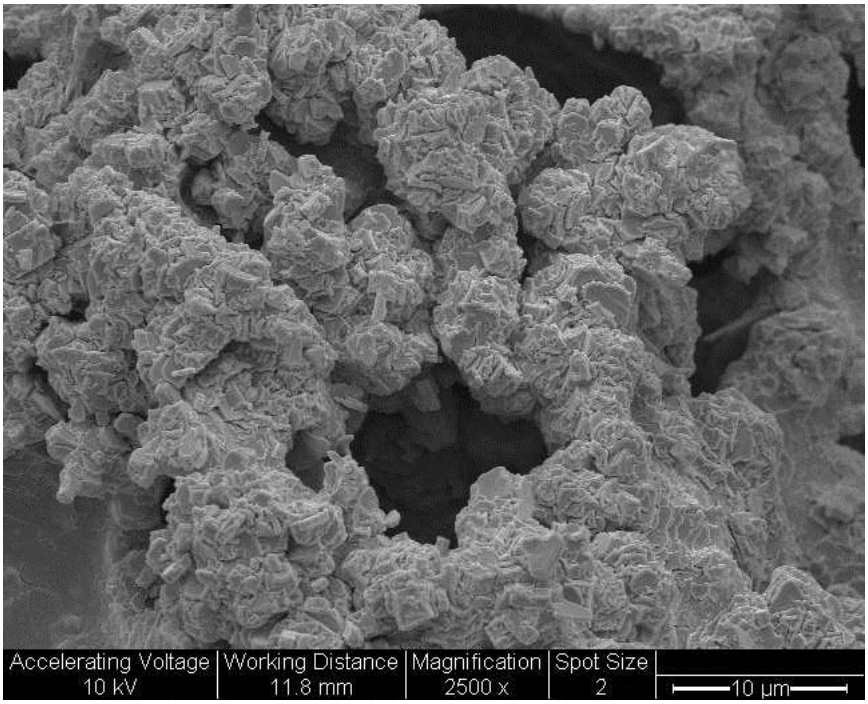

Figure 6-36: Structure change with cooling condition: Immediate cooling

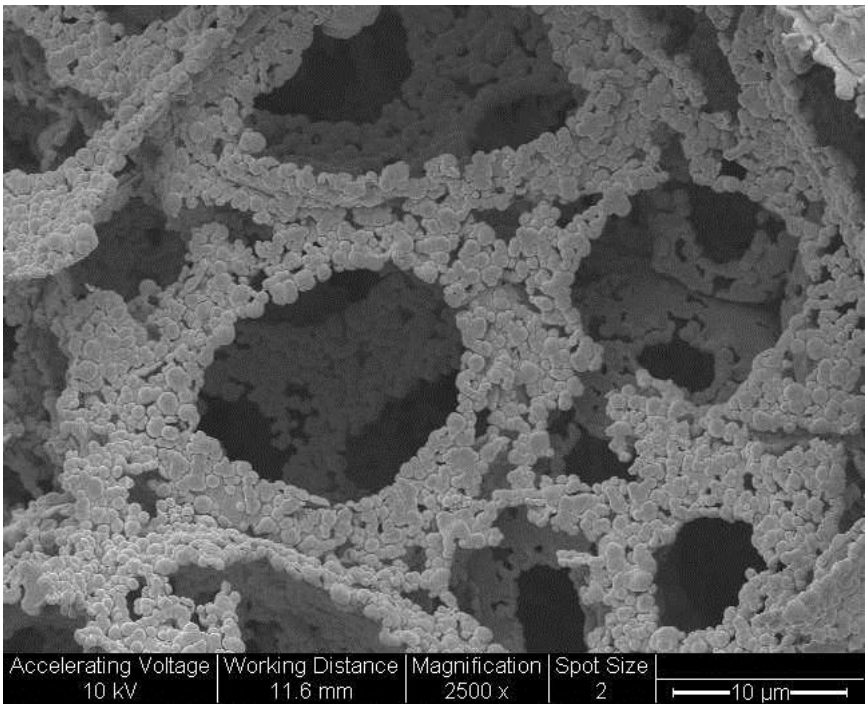

Figure 6-37: Structure change with cooling condition: Cooling at room temperature

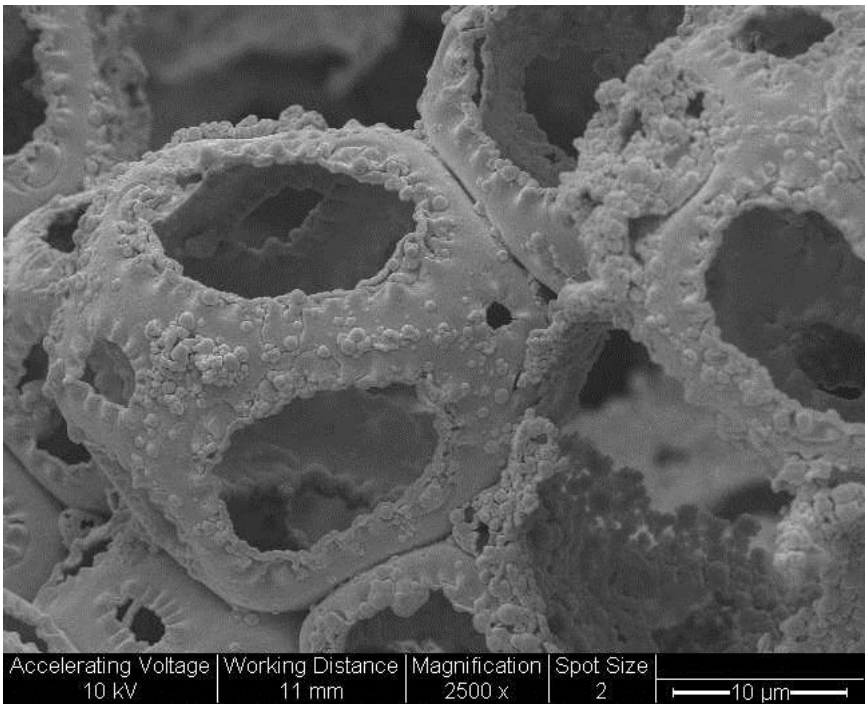

Figure 6-38: Structure change with cooling condition: Cooling gradually in oven

6.3.8 Effect of Heat Treatment on Morphology

The effects of thermal treatment on Ni-B deposits and structure of PHP was investigated. Using parallel studies, heat treatment was performed in two stages: burning of the polymer (ramping) at the required temperature for one hour and annealing (dwelling) of the resulting porous metal at the same temperature for another hour. The samples were thermally treated at 600°C, 800°C and 1000°C respectively. The experiment was conducted using Nickel sulphate as the nickel source, DMAB as the reducing agent with 1:2 Ni/B ratios and it was operated at cell temperature 50°C. Heat treatment resulted in the transformation of the amorphous phase to crystalline nickel and nickel boride phases. XRD patterns of electroless Ni-B deposits, heat treated at 600°C for 2 h, confirmed the formation of crystalline nickel and Ni_3B phases, as described in section 6.3.3. They underwent a chemical reaction during heat treatment in air, transforming from a nickel alloy to a mixture of NiO + Ni with small amounts of

Ni-B compound. Detailed analysis of the X-ray diffraction patterns of heat treated Ni–B is well reported in literature (Krishnaveni et al., 2006; Dervos et al., 2004; Delaunois and Lienard, 2002). It was observed that the metal grains fused together after the decomposing of the polymer at 600°C (Figure 6.39 (b)). The wall of the strand was intact and showed good adhesion between the particles. In contrast with samples that were heat treated at 800˚C and 1000˚C, it was found that the structure of samples collapsed compared those treated at 600˚C (Figure 6.39). Heat treatment at 800°C showed a broken structure and evidently metal fused together forming a smooth surface (.Figuren 6-40 (c)). For samples heat treated at 1000°C, it was observed that the wall had lost its integrity and the structure exhibited a more porous structure (Figure 6-41) (Contreras et al. 2006).

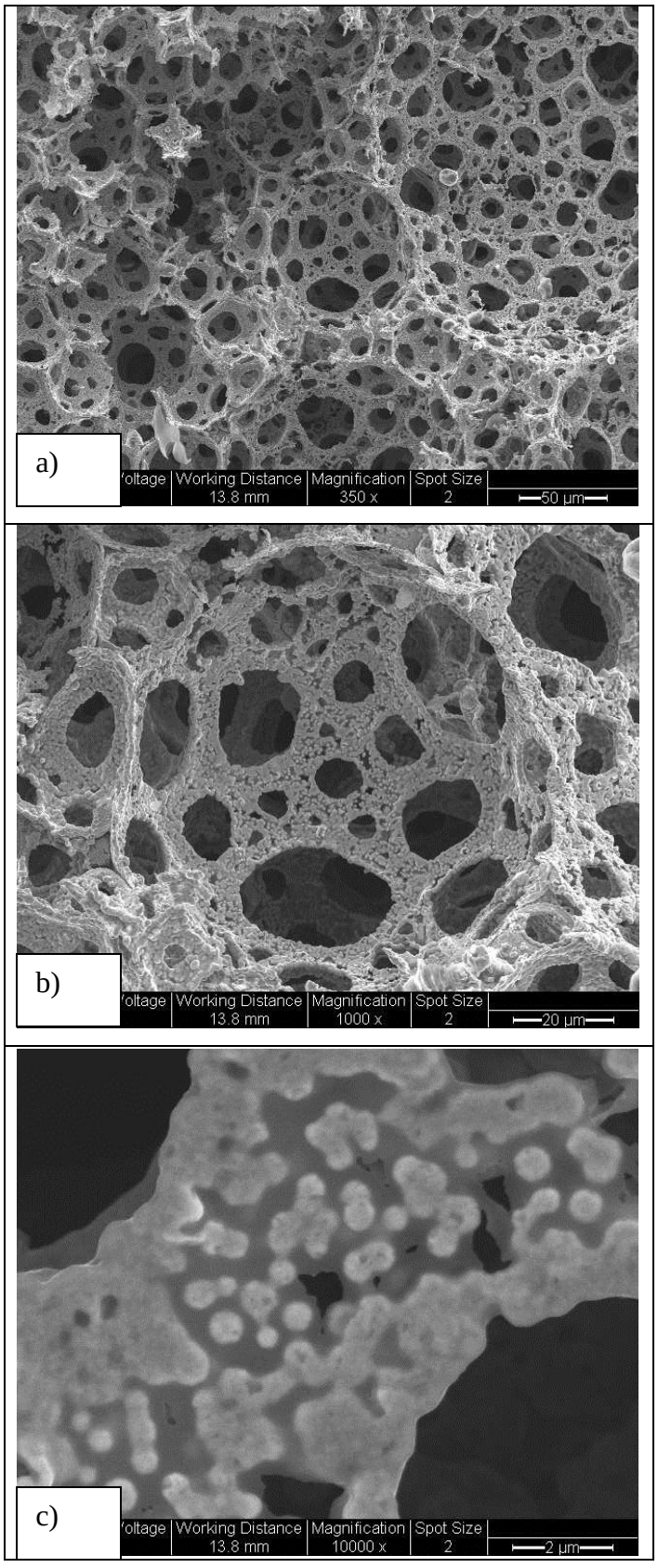

Figure 6-39: SEM micrograph of Ni-B electroless deposition on PHP after heat treatment at 600°C. a) General view of Ni-B deposits on PHP after heat treated. b) Detail structure of Ni-B deposits fused together c) metal grain fused together on PHP at higher magnification x10000

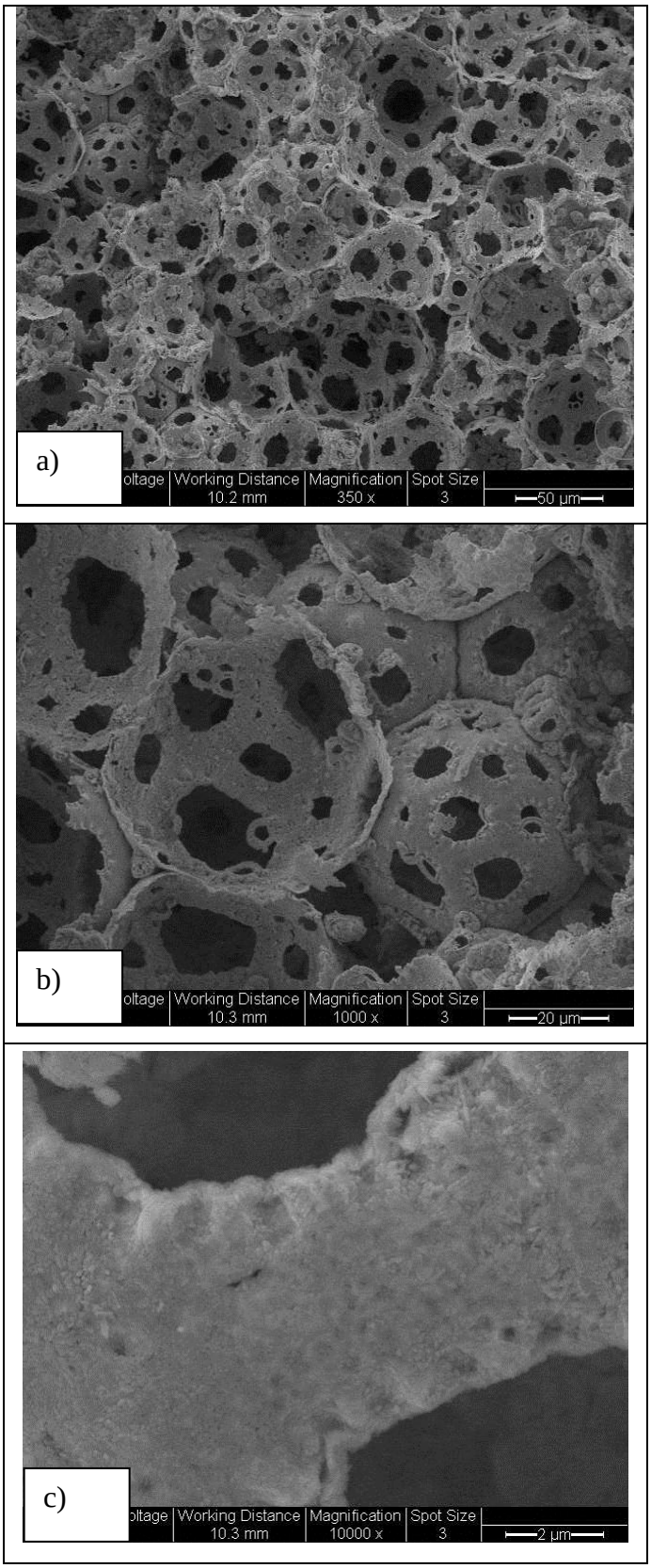

Figure 6-40: SEM micrograph of Ni-B electroless deposition on PHP after heat treatment at 800°C. a) General view of Ni-B deposits on PHP after heat treated. b) Detail structure of Ni-B deposits exhibit a spherical cage structure c) metal grain fused together on PHP at higher magnification x10000

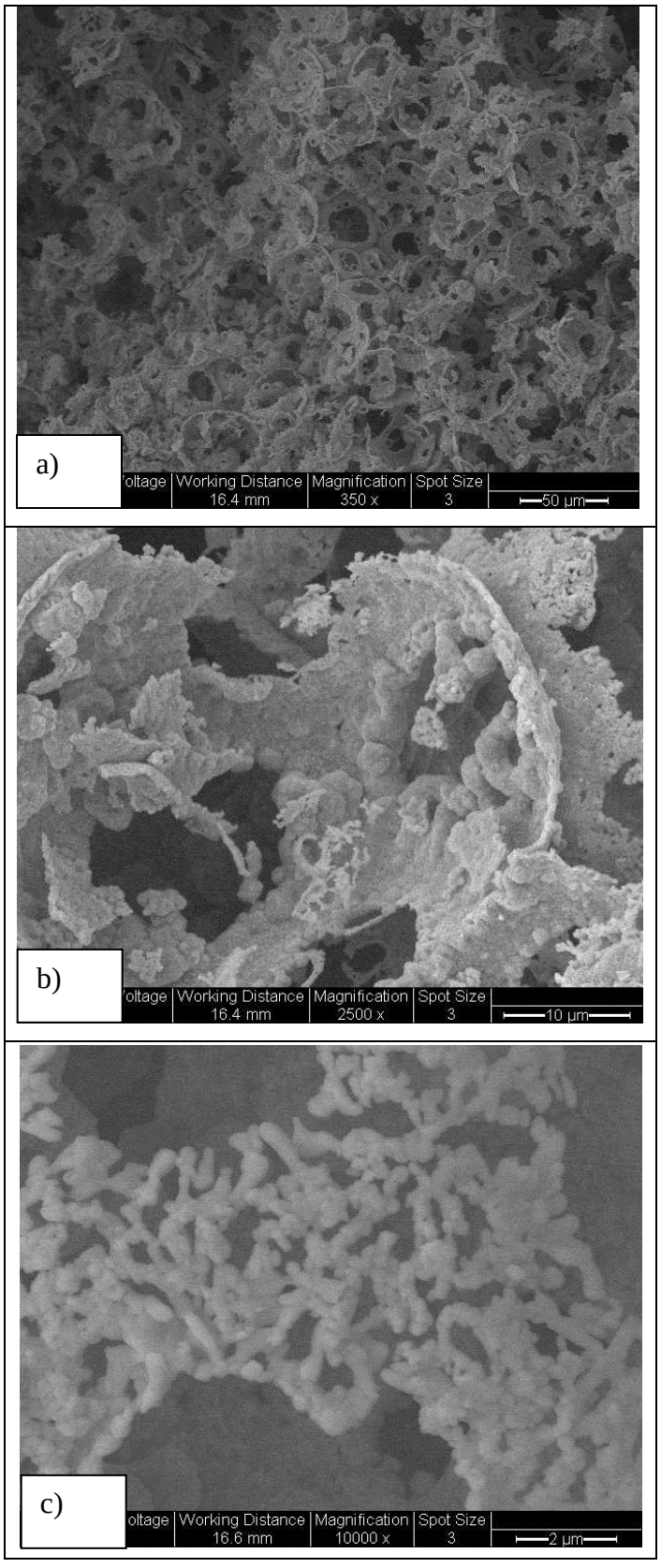

Figure 6-41: SEM micrograph of Ni-B electroless deposition on PHP after heat treatment at . 1000°C

a) General view of Ni-B deposits on PHP after heat treated. b) Detail of collapsed structure of Ni-B deposits wall c) Increase pore structure at higher magnification x 10000

6.3.9 Effect of Oxidation on PHP

This experiment was carried out to investigate the effect of oxidation on PHP when subject to heat treatment. The effect of metal deposition was investigated on compressed polymer. Compressed polymer, as described in an earlier section, was measured at 26mm diameter and compressed to ~175 µm thickness. Figure 6-42 showed the structure of compressed PHP without metal deposition from top surface structure to inner surface structure (Figure 6-42 (a) –(c)).

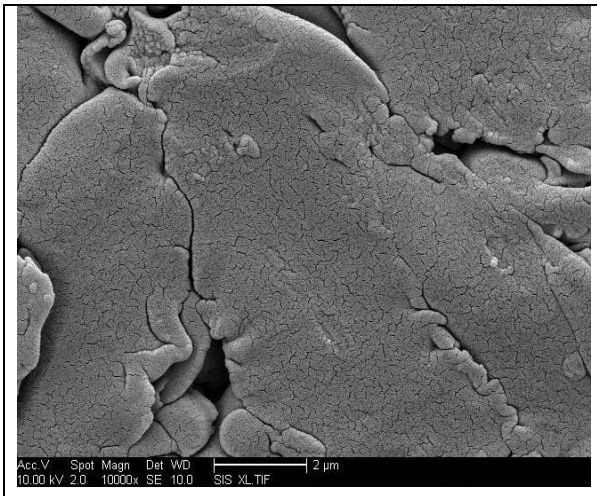

a) (a) Top surface of compressed polymer

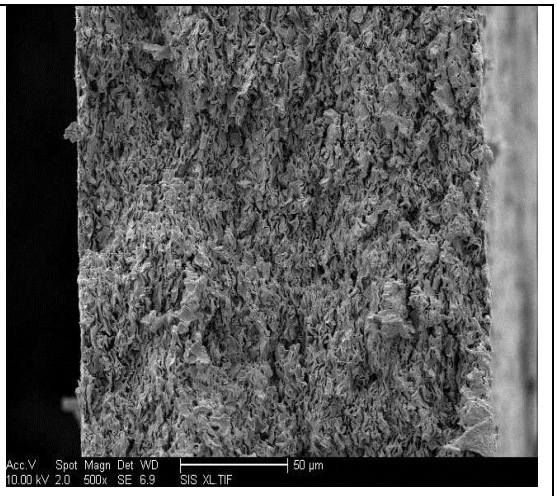

(b) Cross section of a compress polymer before metal deposition

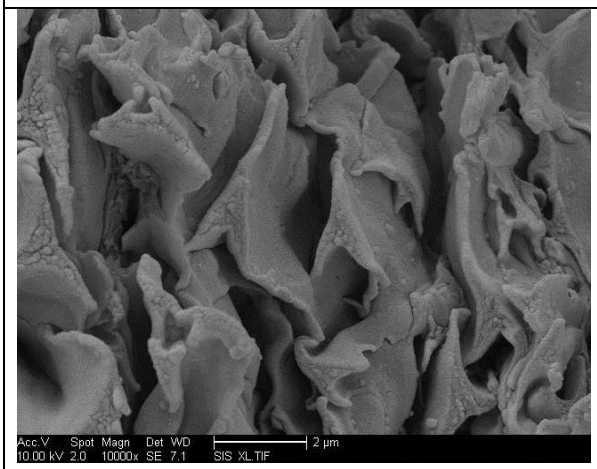

c) Inner structure of compress polymer

Figure 6-42: Compressed polymer without metal deposition

This experiment was performed using the Ni-P system and heat treatment was 600˚C for 2h. Ni-P was proposed due to the larger grain size compared to the Ni-B system to ease the analysis. Figure 6.43 a) shows the top surface of compressed PHP as deposited condition and Figure 6.43 b) shows compressed PHP sandwiched between metal deposits.

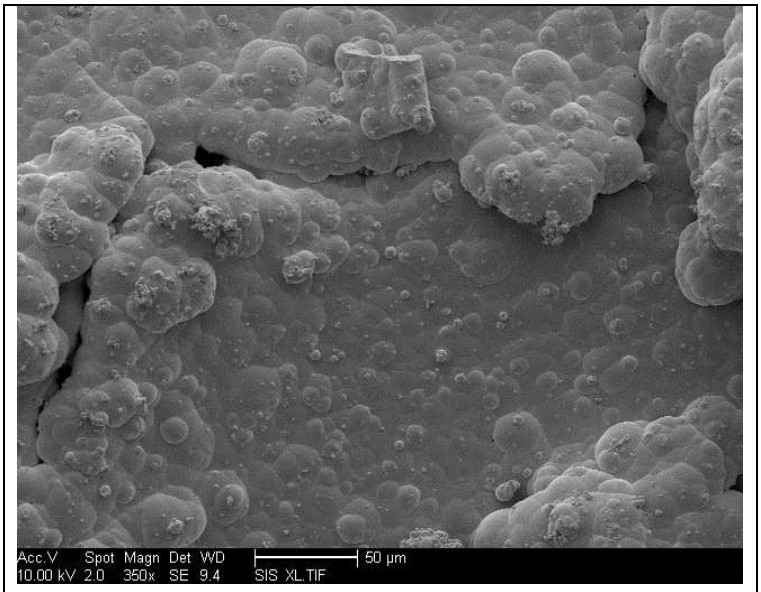

a) Top surface of compress PHP as deposited condition

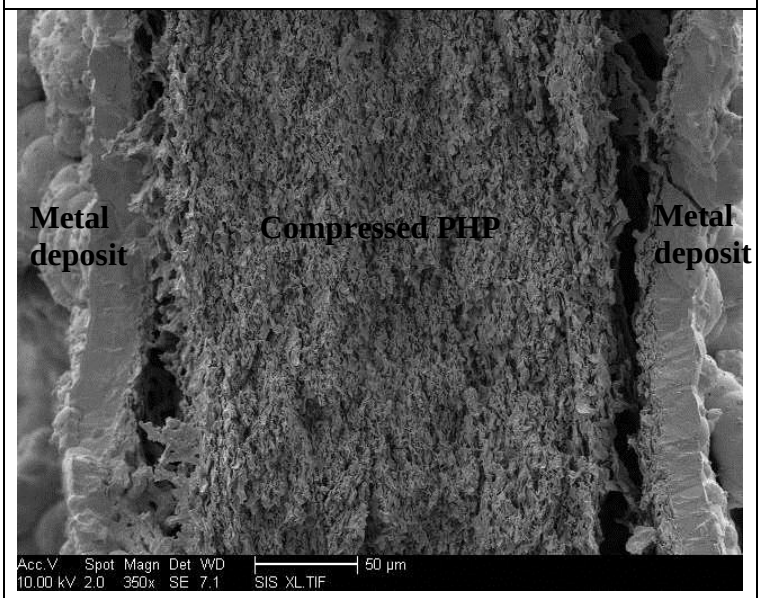

b) Compress PHP sandwiched between metal deposits

Figure 6-43: SEM micrograph of Ni-P electroless deposition on compress PHP as deposited

Figure 6-44 showed metallised compressed PHP after heat treatment. Figure 6-44 (a) showed metal deposits agglomerate to form layer of metal deposits. Figure 6.44 (b) showed metallised compressed PHP resulted from decomposition of PHP. The gap in between metal deposits was from decomposition of compress PHP that left an empty space.

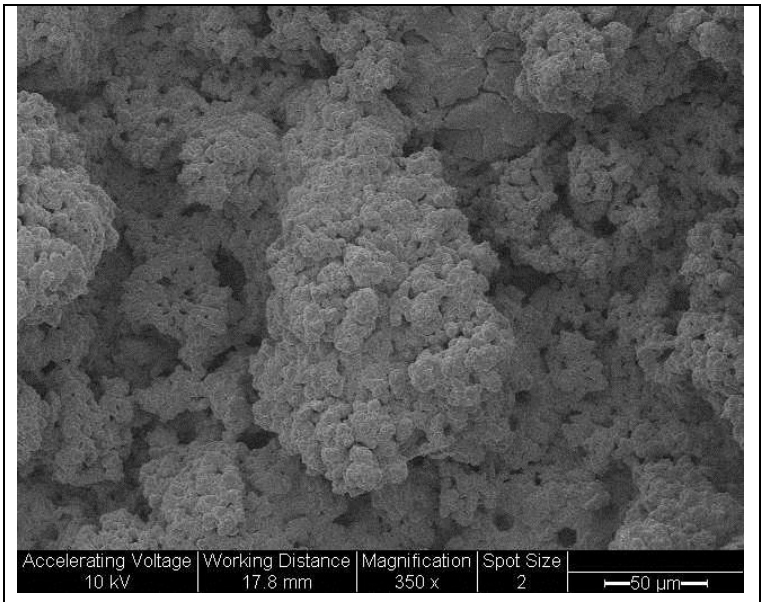

a) Top surface of compress PHP after heat treatment

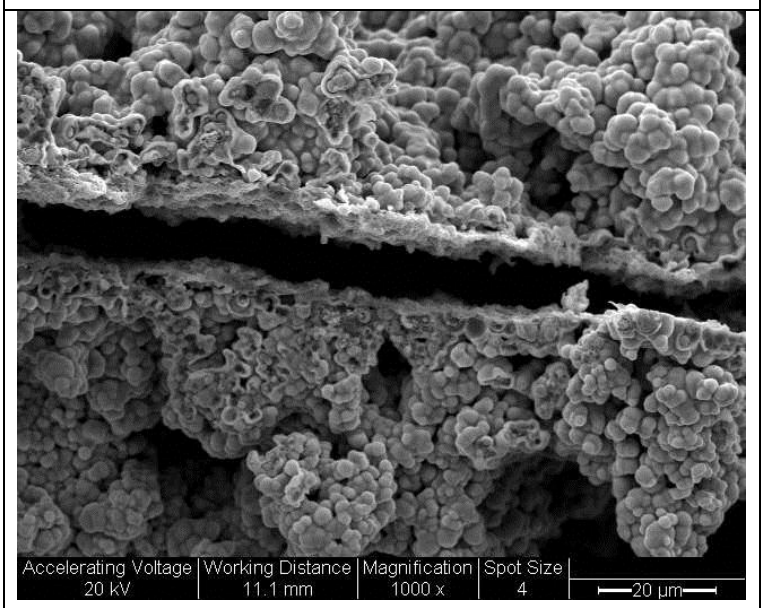

b) Cross section of metallised compressed polymer after heat treatment

Figure 6-44: SEM micrograph of Ni-B electroless deposition on compress PHP after heat treatment

Using the same composition for deposition solution, it was observed that metal deposition on a flat surface was different to that of a porous material. Relatively thicker and denser agglomerates were observed on compressed PHP, indicating that a non-free flow solution created coalesces of grains particles vigorously. Metals were deposited only on the surface rather than penetrating through the pore, as shown in Figure 6.45. It was observed that metal deposited on compressed PHP exhibited smaller grain size, ~1-3 µm, as compared to metal deposited on porous PHP (Figure 6-46). Magnified image of the metal grain on compress PHP showed sharp peak structure and less porous (Figure 6.45 (b) while metal grain deposited on PHP showed a smooth surface structure and more porous (Figure 6.46 (b)).

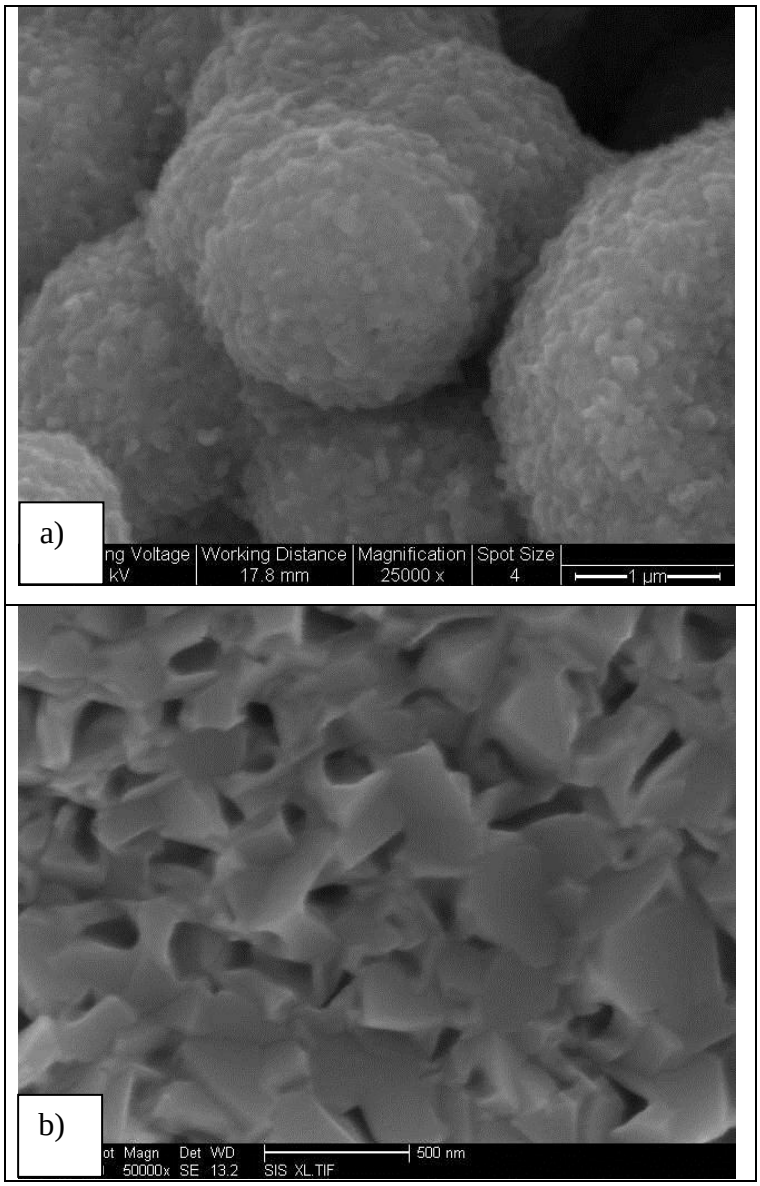

Figure 6-45: SEM micrograph of metal grains on compress PHP

a) SEM micrograph of grain structure

b) Grain structure at higher magnification

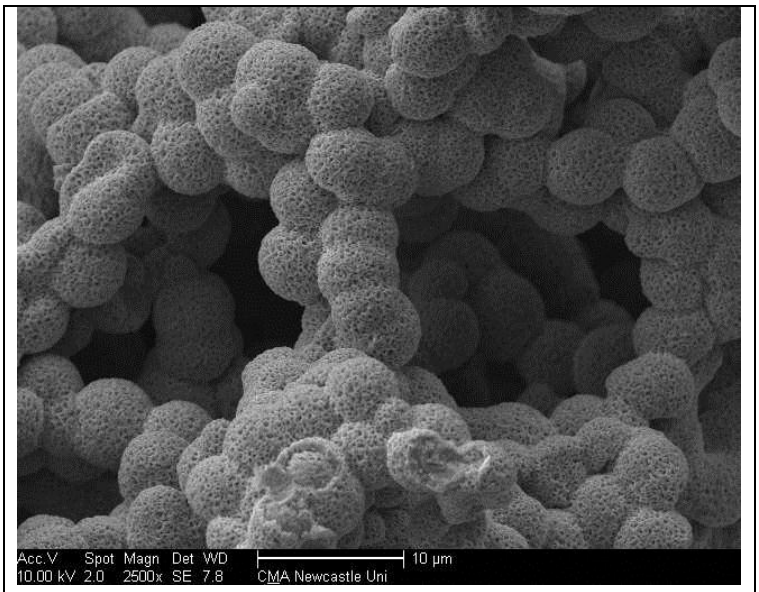

a) SEM micrograph of grain structure

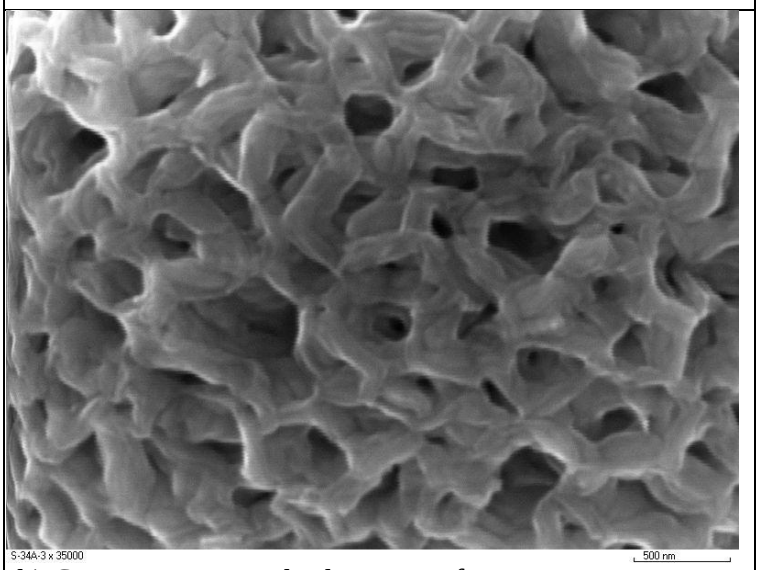

b) Grain structure at higher magnification

Figure 6-46: SEM micrograph of metal grains on PHP (Calkan, 2006)

a) SEM micrograph of grain structure

b) Grain structure at higher magnification

On the other hand, the inner structure exhibited a different structure whereby grains coalesced together to obtain a smooth and even structure. This indicated that the structure obtained from porous PHP was a result of carbon being oxidised to form CO which reacted with Ni to produce the porous structures, as seen in Figure 6.47 (a)-(b). Some of the oxygen must be used to oxidise Ni and P. Since far more fine structures were obtained using compressed PHP, it may explain the reason for structure formation on non compress PHP. (See Appendix C for more images)

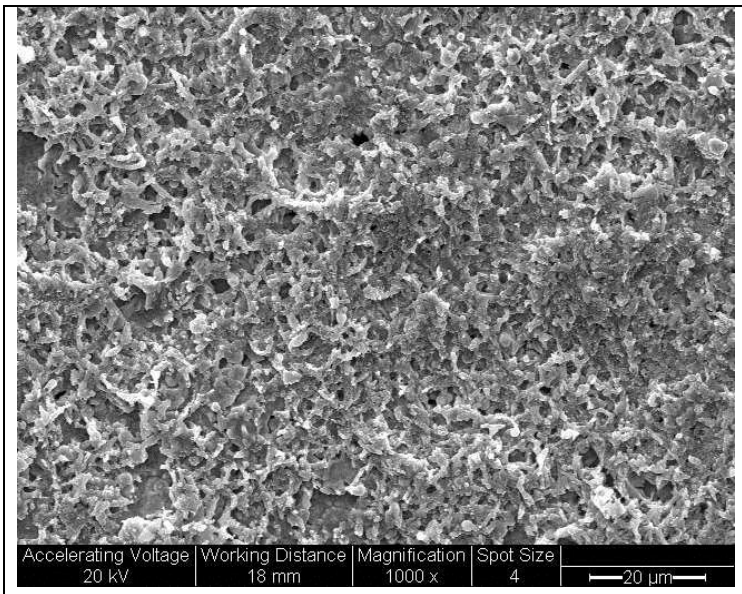

a) Overall image of grain structure on inner surface of compresss PHP

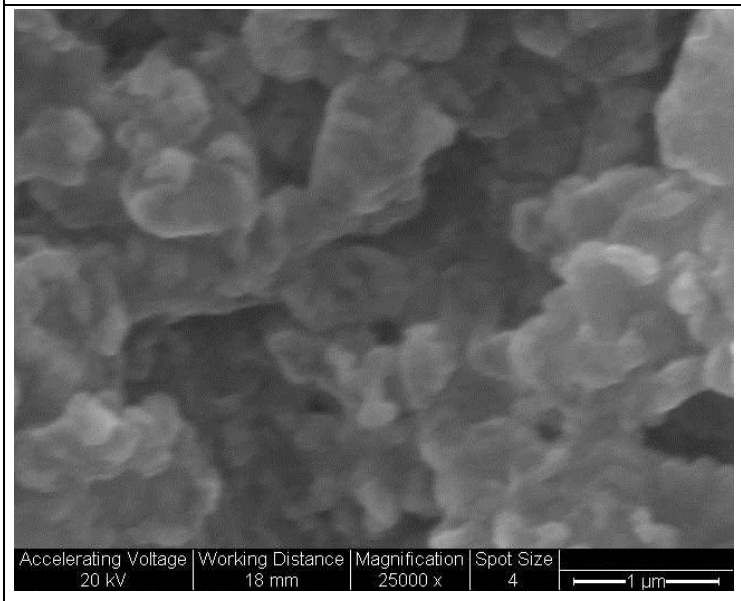

b) Grain structure at higher magnification x25000

Figure 6-47: SEM micrograph of Inner surface of compressed PHP

Results from EDX spectra have shown that CO content is higher at the inner surface (Figure 6-48 and Figure 6-49), suggesting that the compressed PHP decomposition was done in a confined environment (see Table 6.8).

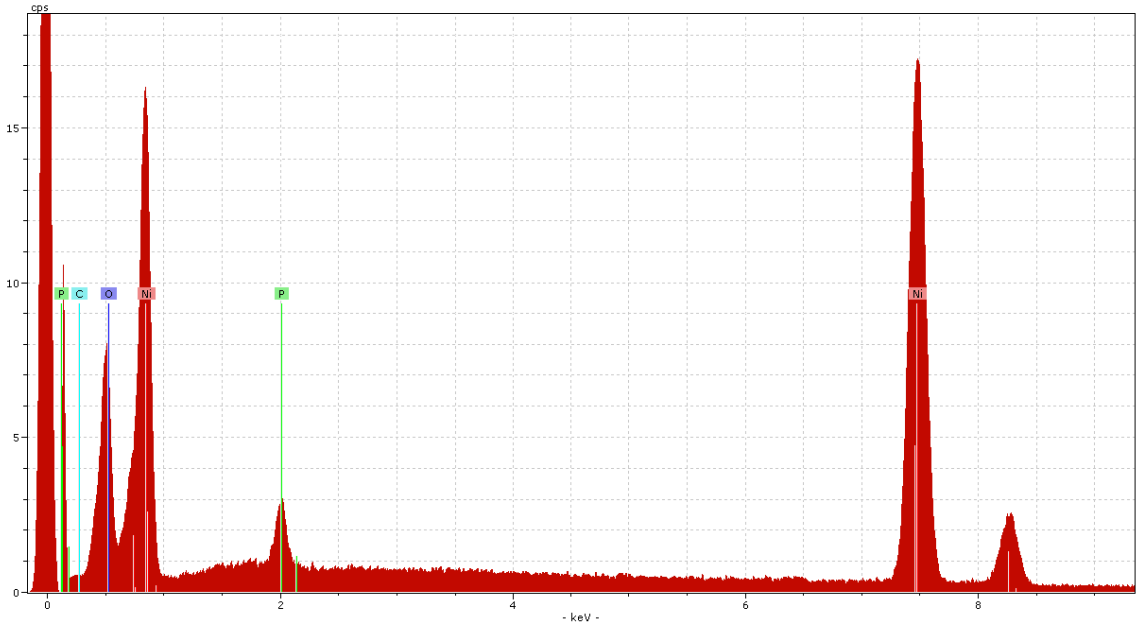

Figure 6-48: EDX spectra for top surface of metallised compressed polymer

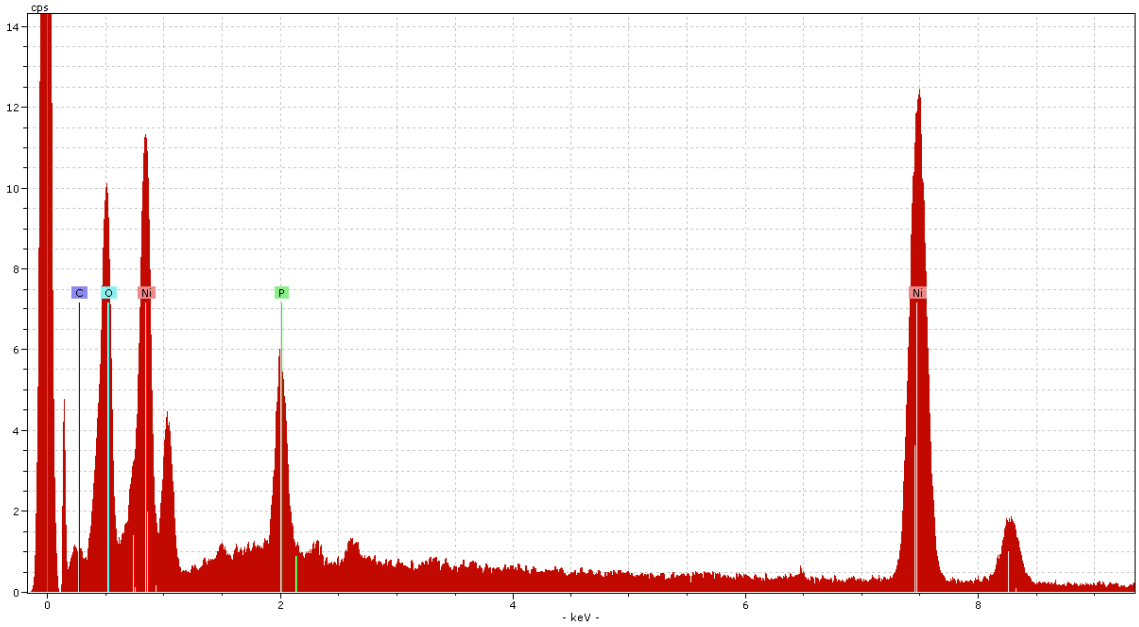

Figure 6-49: EDX spectra for inner surface of metallised compressed polymer

Table 6-8: EDX spectra for top and inner surface of compress PHP

Spectra	Nickel (at%)	Phosphoros (at%)	Carbon (at%)	Oxygen (at%)
Top surface	34.49	1.33	9.22	54.96
Inner surface	21.85	3.33	12.64	62.18

6.4 Ni-B Deposition on Other Template Material

In addition to having well defined and controlled metal deposition on PHP, other template systems were also performed in this research. The reason was to determine economically cheap material and production with high temperature stability suitable for high/strong catalytic activity systems. Initial indications showed that fibrous materials are much easier to produce and to deposit, making them more suitable for certain applications such catalyst for ozone decomposition or for purifying of exhaust gases. Therefore, for a given system (either Ni-P or Ni-B) we investigated various fibrous systems including carbon felt, cotton wool and glass wool. Process conditions were performed similar to metallization on PHP. However, depending on the density of the respective materials, template samples were fabricated and adjusted to suit the deposition cell. Each template was fabricated having a size of 25mm diameter and 4mm thickness.

6.4.1 Nylon Fibre

This experiment covered the metallization of nylon fibre by flow through electroless deposition. Previous studies have revealed that to metalize non-conductive materials, the materials need to be pretreated with conducting material. However, results have showed that the metal deposits only on the surface and does not sufficiently penetrate and cover all areas. Therefore, this experiment consisted of a process of metallization of fibrous material where the internal structure of the material was totally covered by metal. Figure 6.50 (a) presents an SEM micrograph of fibrous material without metal

deposition. A 600 ml Ni-B deposition solution was used and metals were deposited using a flow through electroless deposition method at cell temperature 50°C with [Ni]:[B]=1:2. It was observed that Ni-B metal deposited uniformly, which was similar to metal deposits on PHP, as shown in Figure 6.50 (b).

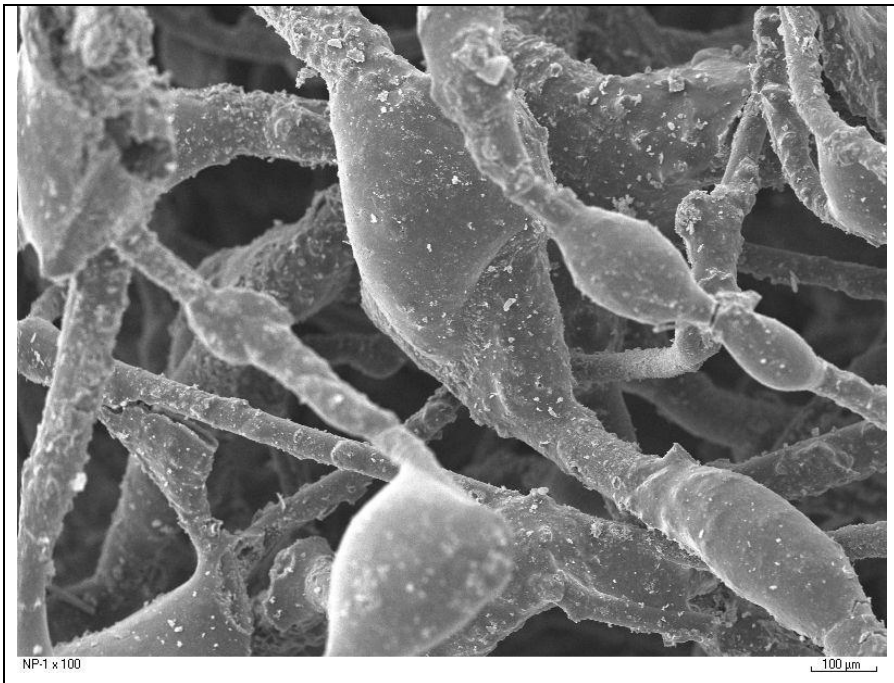

a)

Continue next page

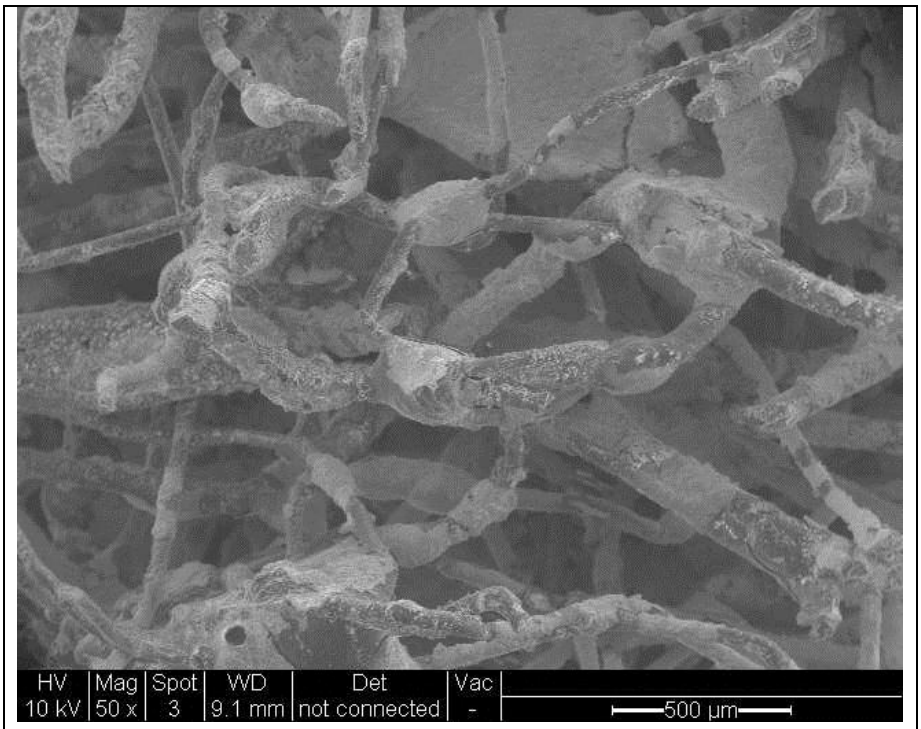

b)

Figure 6-50: SEM micrograph of nylon fibre a) nylon fiber without metal deposition

b) Ni-B deposits on fibrous material as deposited condition

When fibrous material was fully metalized, it was heat treated at 600°C for 2h. Figure 6.51 shows a general view of metal deposition after heat treatment. The results reveal that metal grain fused together to form a smooth surface (Figure 6.52) which differs from metal deposition on PHP.

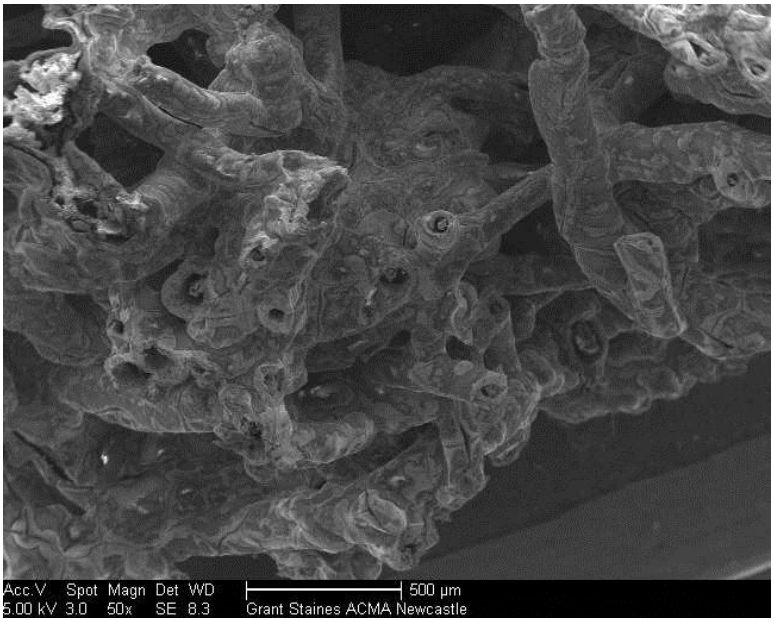

Figure 6-51: General view of Ni-B deposits on fibrous material heat treated at 600°C for 2h

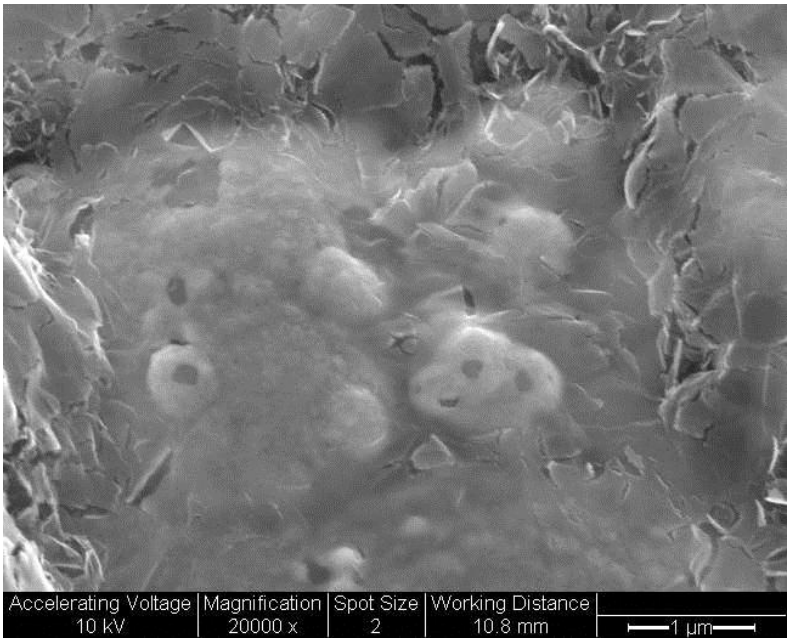

Figure 6-52: Surface detail structure on fibrous material after being heat treated

Figure 6.53 presents a cross section of a broken part of fibrous material. Heat treatment at 600°C had totally decomposed the template (nylon fibre), hence leaving a capillary.

The capillary produced by the removal of the fibrous material had a diameter of ~40-50µm, which is similar to the diameter of the material. Using 600ml deposition solution, 35-40 µm of metal deposits were produced around the fibrous material. It was observed further at the inner structure of the metal deposits and it was found that the metal deposited uniformly layer by layer and was formed from a 50nm-200nm nano size grain structure (Figure 6.54). (See Appendix C for more images)

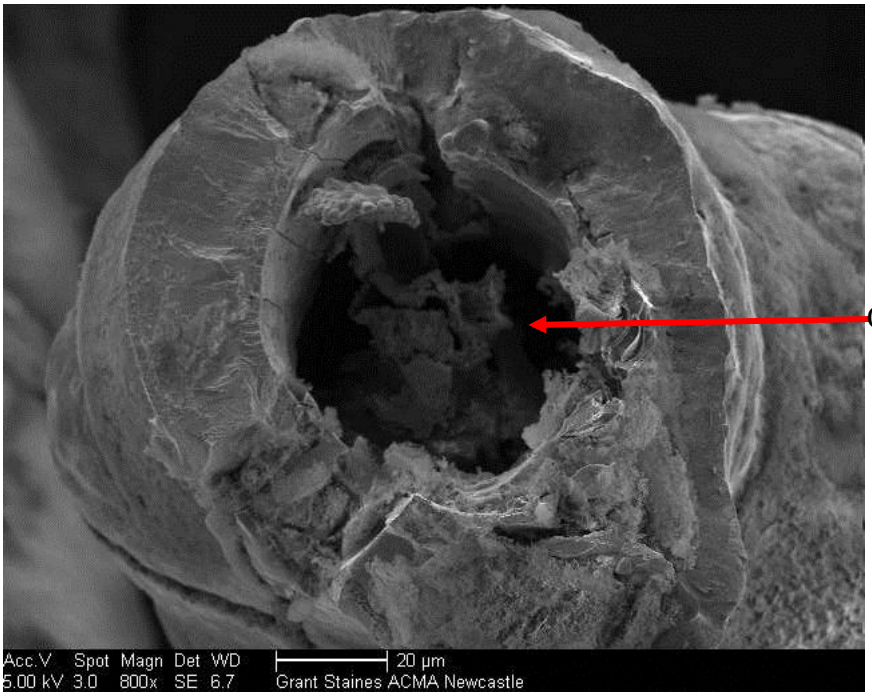

Figure 6-53: Image of a broken part from metalized fibrous material

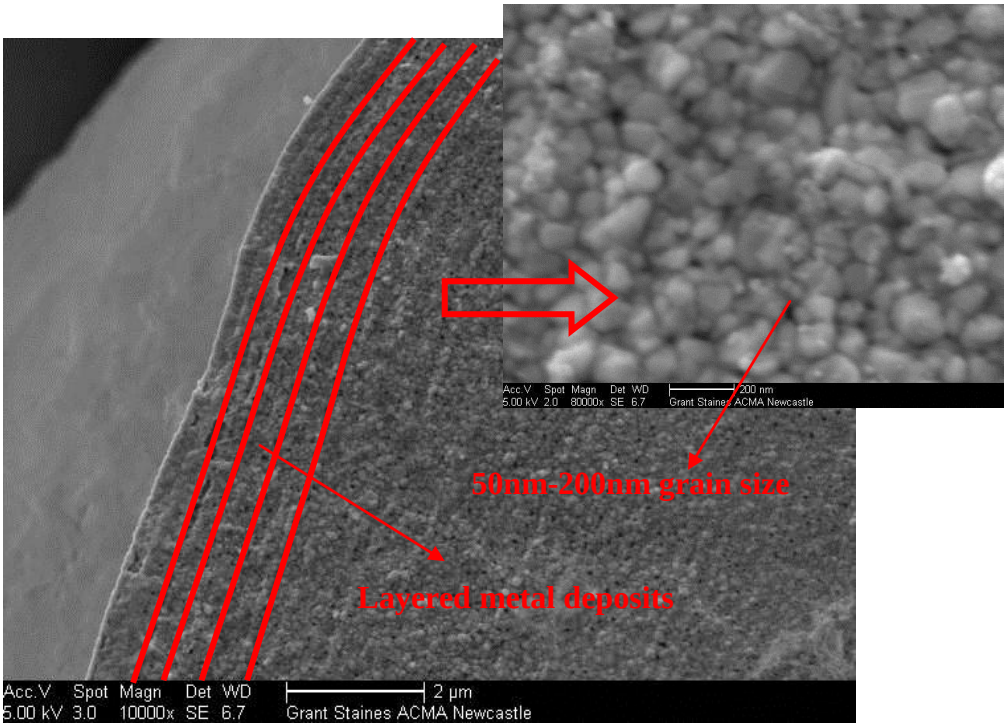

Figure 6-54: Inner structure of Ni-B metal deposition consists of fine grain size.

6.4.2 Carbon Felt

In this experiment, we investigated using carbon felt as a substrate for solution deposition of continuous Ni-B on fibres. The procedure used for Ni-B deposits is as describe in earlier section using 600 ml metal deposition solution by a flow through electroless deposition method at 50°C and heat treated at 600°C and 1000°C for 2h to decompose the felt. A continuous metal deposit was formed within the carbon felt disk. Figure 6.55 shows the carbon felt without metal deposition.

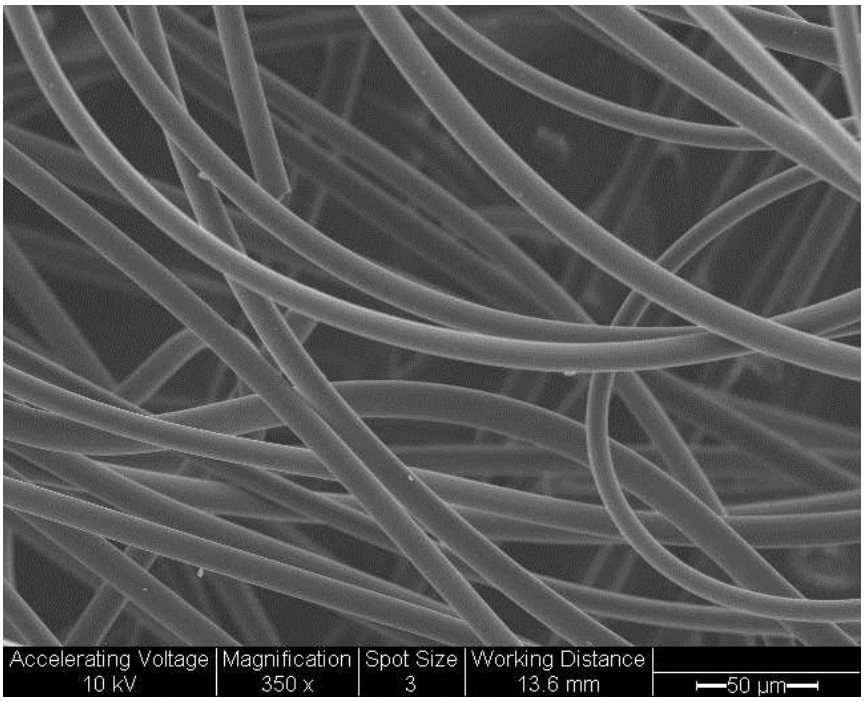

Figure 6-55: Carbon felt without metal deposition

A metalized felt was produced after the reduction of nickel salt, shown as deposited in Figure 6.56 and Figure 6.57. It was observed that the grain deposited uniformly around the felt.

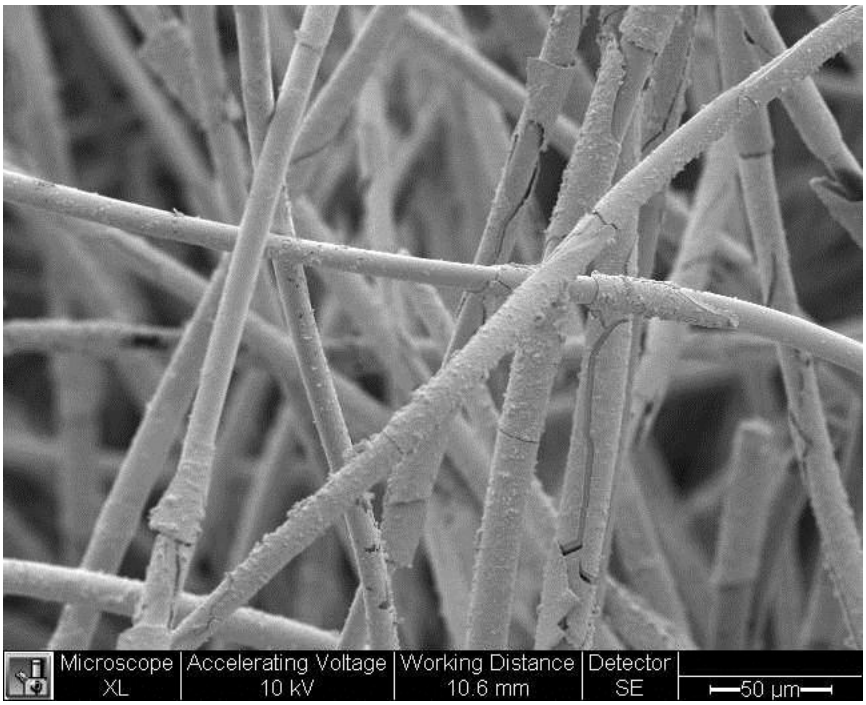

Figure 6-56: Metalized carbon felt before heat treatment

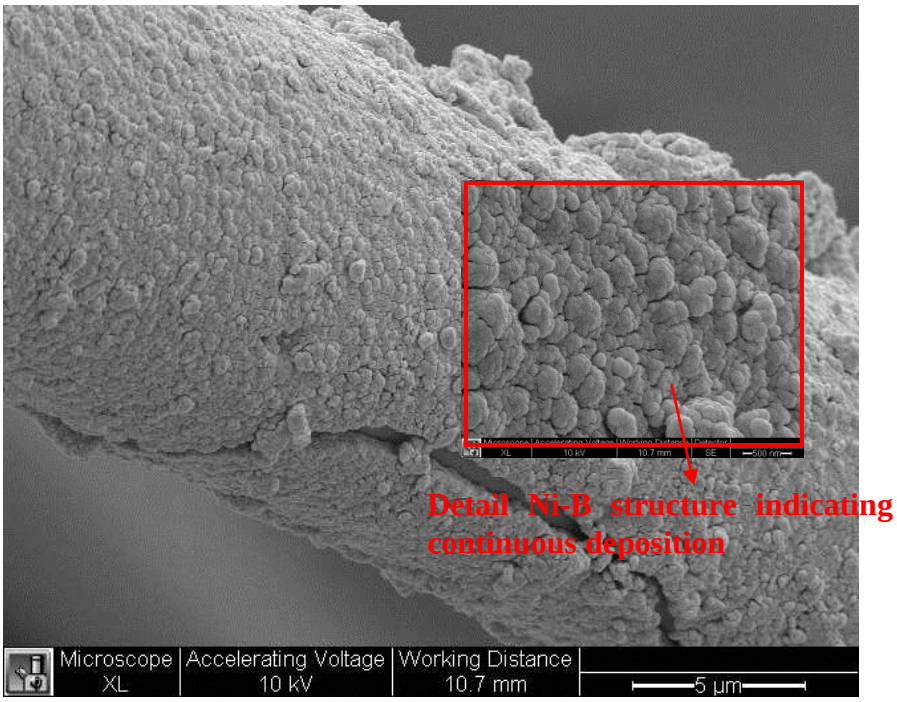

Figure 6-57: Ni-B deposited on carbon felt

When the felt was fully metalized, it was dried and heat treated at 600°C and 1000°C respectively. Carbon felt treated at 600°C exhibited a crystal like grain structure (see Figure 6-58), while metalized felt treated at 1000°C exhibited grains that were fused together to obtain a smooth structure (Figure 6.59).

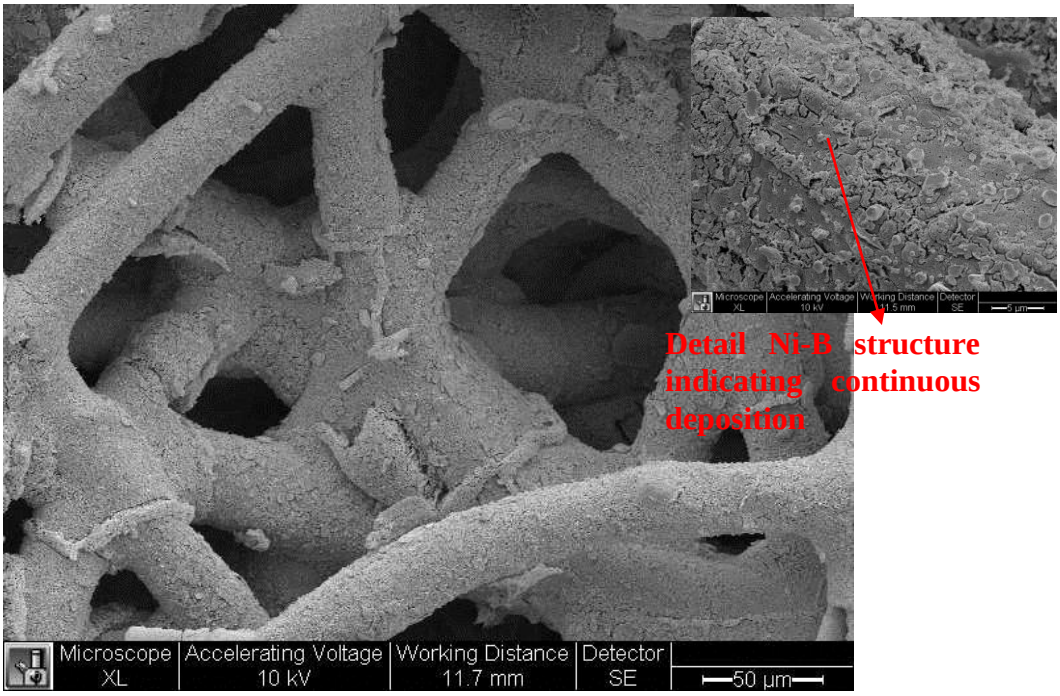

Figure 6-58: Metalized carbon felt after heat treatment at 600°C for 2h

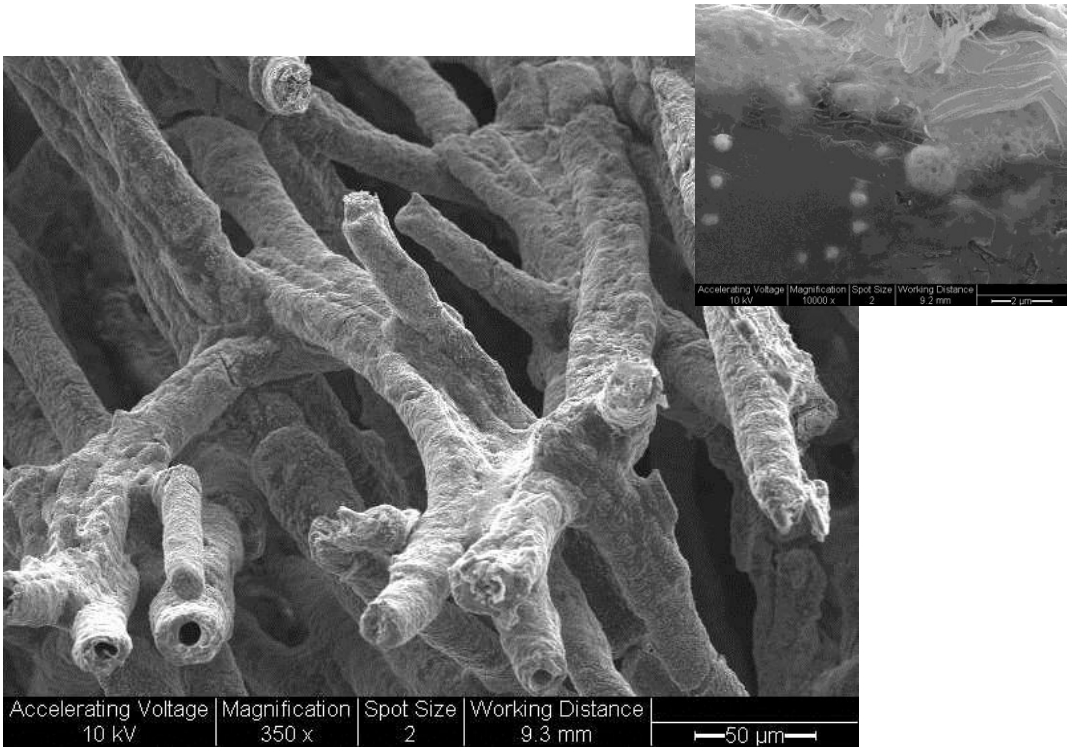

Figure 6-59: Metallised carbon heat treated at 1000˚C for 2h

Heat treatment at 1000˚C totally decomposed the material, hence leaving a capillary (see Figure 6.60). The capillary produced by the removal of the carbon felt had a diameter of ~10µm, which was slightly reduced in size from the original felt (carbon diameter is around 30-35 µm). Using 600ml of deposition solution produced 5-10 µm of metal deposits around the carbon felt

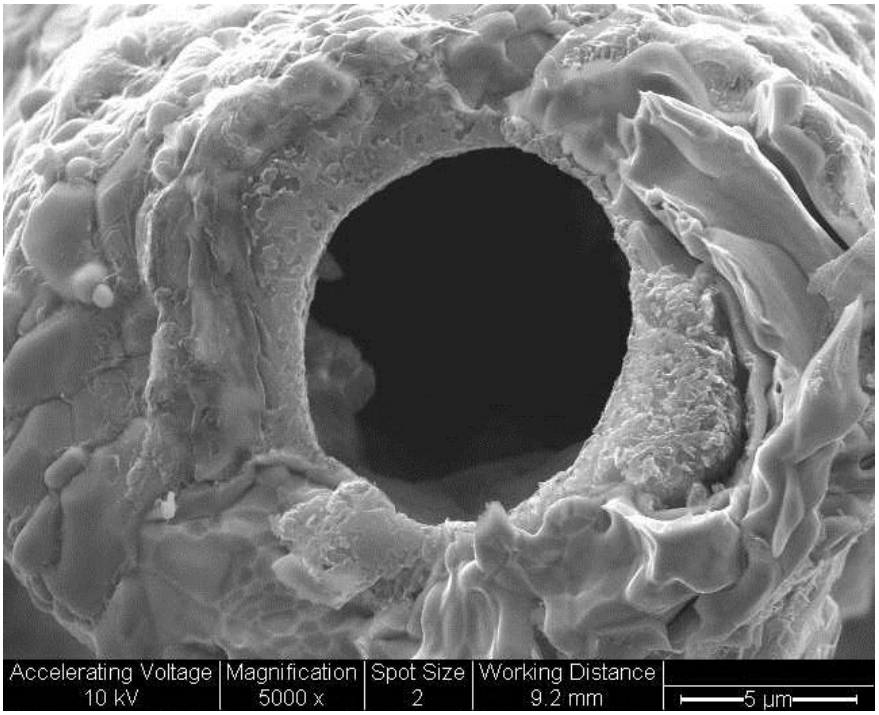

Figure 6-60: Capillary formation after heat treated at 1000°C for 2 h

6.4.3 Cotton Wool

Another potentially useful template material used in this research was cotton wool. A common problem in the use of such substrate is the lack of ability to deposit metal on the cotton filaments; such contact made can eventually provide properties such as high strength filaments.

This experiment showed that the method used is suitable for metalizing a broad range of porous substrates, including synthetic and natural fabrics such as cotton wool. Figure 6.61 shows a general view of cotton wool without metal deposits. The procedure used for Ni-B deposits consists of metal depositing using 600 ml of deposition solution by a flow through electroless deposition method at 50°C, and heat treated at 600°C.

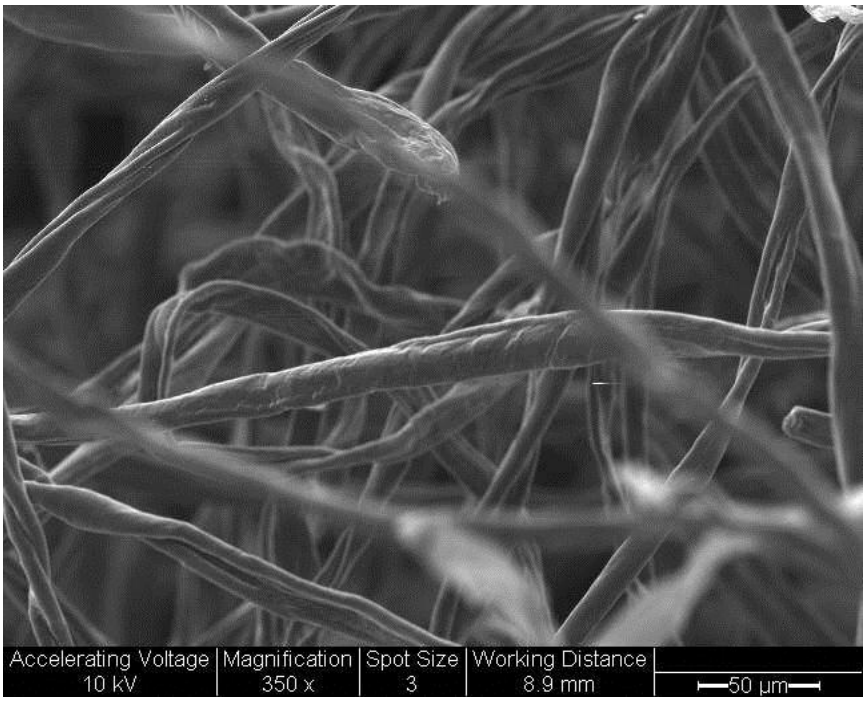

Figure 6-61: Cotton wool without metal deposition

After being heat treated, the structure exhibited fusion of grains together to form a smooth structure (Figure 6.62). Unlike carbon felt, the smooth surface was achieved when heat treated at 600°C.

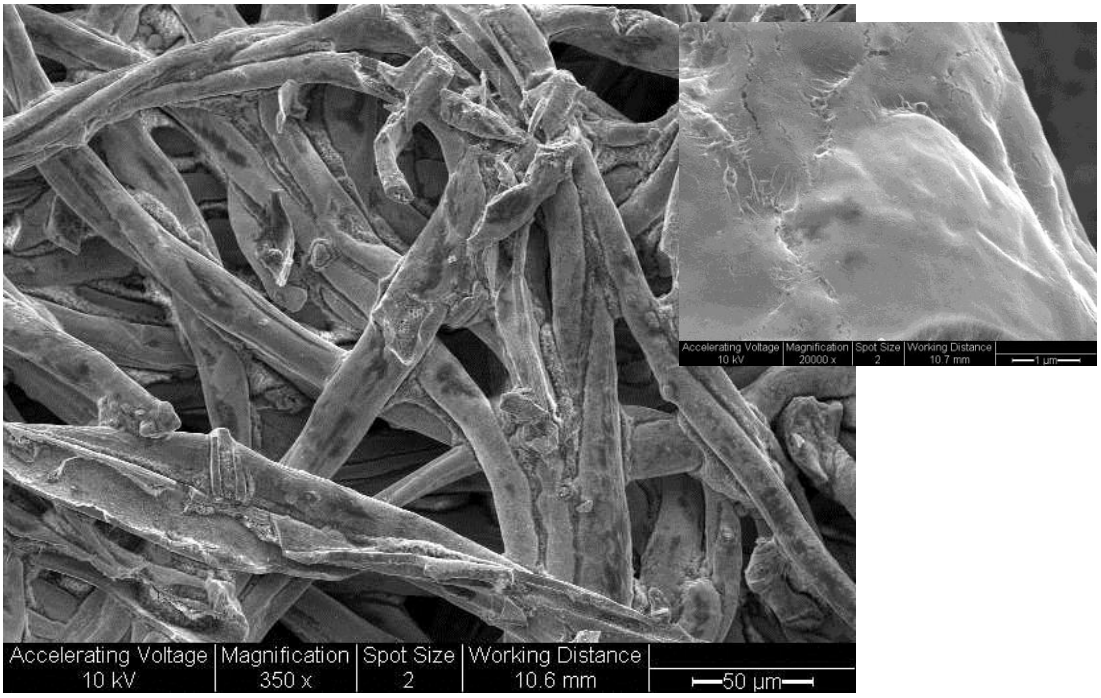

Figure 6-62: Metalized cotton wool after heat treatment at 600˚C for 2 h

Figure 6.63 illustrates metal deposited on the filament of cotton wool. The thickness of metal deposition was observed to be ~2µm without affecting the structure of the cotton filaments.

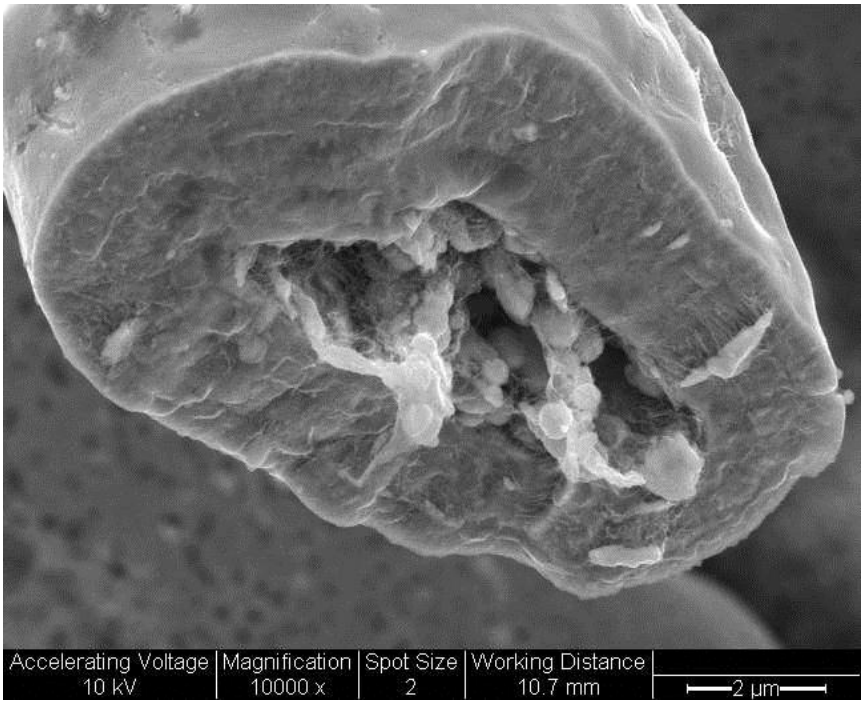

Figure 6-63: Detail structure of broken part

6.4.4 Glass Wool

Metallization of glass wool was performed by depositing Ni-B on glass wool. Figure 6.64 shows a general view of glass wool without metal deposition.

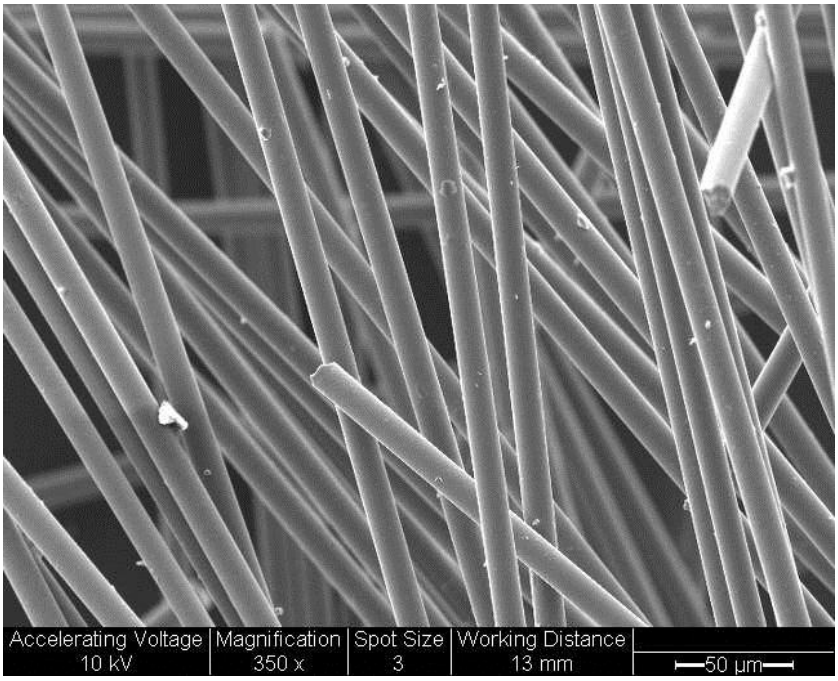

Figure 6-64: General view of glass wool without metal deposition

A 600ml metal deposition solution was used to completely cover the wool with metal deposits. The results for metalized glass wool can be seen in Figure 6.65. Grain structure growth on glass wool was observed to be similar to that described in the previous section (6.4.2).

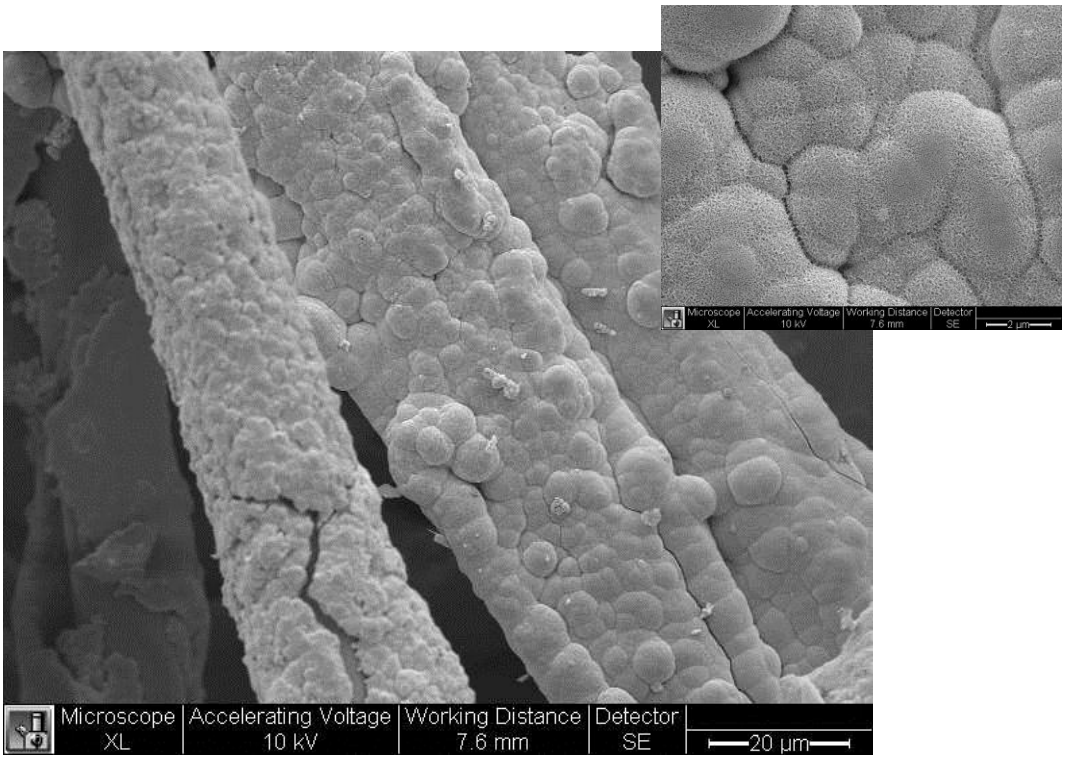

Figure 6-65: Metalized glass wool with detail deposited grain structure

Grain structure exhibited a continuous and uniform structure. Thickness of metal deposits around the glass wool was 2- 3 µm (see Figure 6.66).

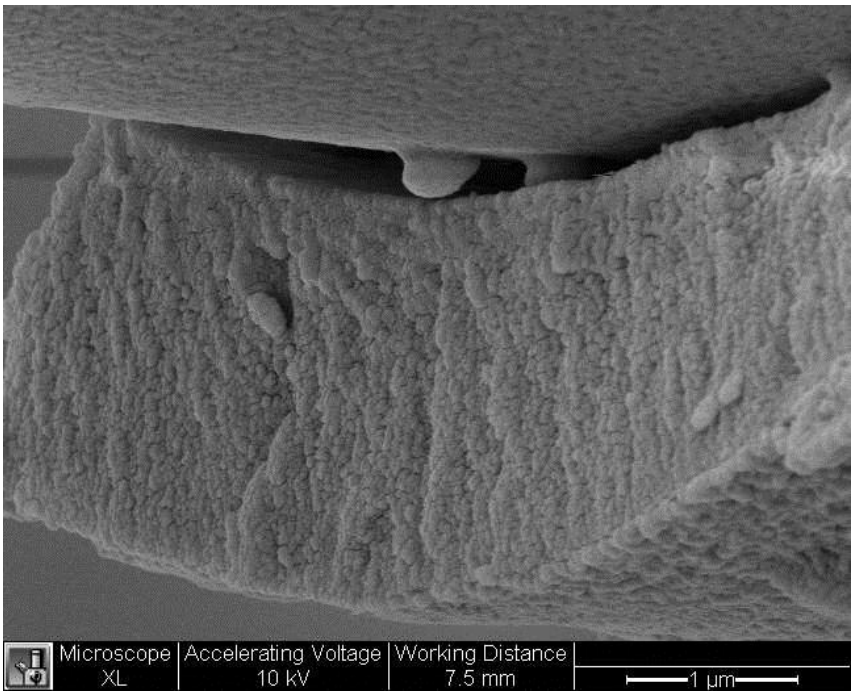

Figure 6-66: Thickness of metal deposit on glass wool

The deposited glass wool was heat treated at 600˚C for 2 h after the metal deposition was completed. Figure 6.67 shows a general view and detailed structure appearance of glass wool that was heat treated. The structure was found to be similar to the structure described in section 6.4.2 when heat treated at 600˚C, with grains coalescing together to form a smooth surface. A crystal like structure was also exhibited.

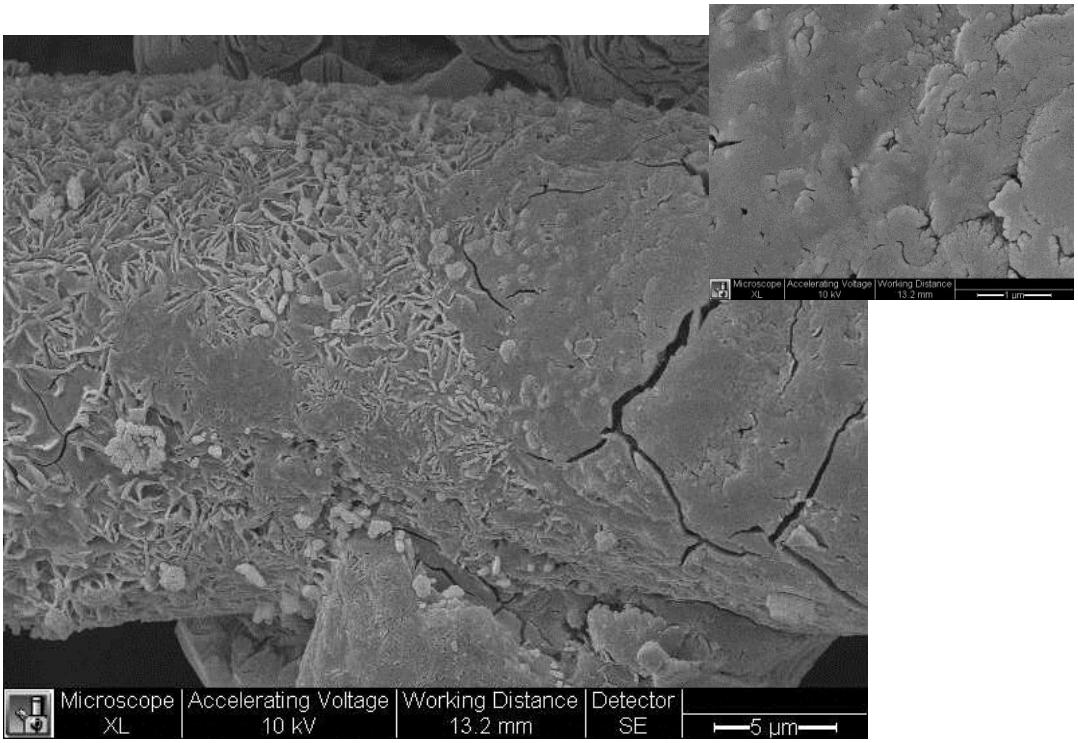

Figure 6-67: Metalized glass wool after heat treatment at 600° for 2 h

6.4.5 Summary

- Increasing the Ni-B ratio from 1:5 to 1:2 by maintaining the pH and operating temperature led to reduction of grain size from 0.5µm to 0.25µm. Increasing the operating temperature (in the range of 35°C to 90°C), on the other hand, led to increased grain size (from 0.15µm to 2µm) where resultant deposits were associated with increased deposition rate. The use of a nickel source and reducing agent had a significant affect on grain size. Grain size from nickel

chloride was observed to be smaller than from nickel sulphate (from 0.25µm to 1 µm). DMAB also displayed a smaller grain size (0.25µm) compared to $NaBH_4$ (0.3µm). All experiments were carried out using 600ml of bath solution. A summary of grain size and operating parameters as deposited metal is shown below:

Table 6-9: Relationship between Grain size and Operating Parameters

Operating parameters	Grain size (µm)
Ni-B ratio	
[Ni]:[B]=1:2	0.15±0.02
[Ni]:[B]=1:5	0.40±0.06
Operating temperature °C	
90	2.00±0.38
75	0.60±0.09
55	0.40±0.04
35	0.26±0.01
Nickel Source	
Nickel Chloride	0.24±0.08
Nickel Sulphate	0.78±0.20
Reducing Agent	
DMAB	0.30±0.16
$NaBH_4$	0.30±0.16

- It was discovered that by utilizing the flow through electroless method to metalise varies porous materials, it is possible to control the thickness (depending on the parameters) of the deposited layer and the problem of pore plug up can be avoided, thus retaining permeability. Therefore, it is suitable for metal deposit over a broad range of porous materials, including synthetic and natural fibres. Accordingly, the bath solution can penetrate deep into the substrates, producing a control and homogenous deposited metal that covers the

entire surface of individual fibres in the thin metal layer (approximately 35µm, which is significant for providing wear and tear). As a result, the porosity of the substrate is essentially unaffected. In other words, without plugging the pore the final product acquires the desired application. After heat treatment the structure retained its original properties, but yielded smoother continuous metal grains. Capillary formation was observed due to the decomposition of the substrates, which could have enhanced surface area. It is apparent that the metal deposited porous material in this research has the potential for catalytic application.

- As deposited metal deposits exhibited a spherical shape with continuous re-nucleation characteristic of the electroless deposition process covering the strands of template. An amorphous peak was observed from the XRD result showing the presence of the template and metal deposits.

- Heat treatments of as deposited metal deposit resulted in a change of morphologies showing transformation of amorphous structure into crystalline phases with Ni or NiO as the dominant phases. Samples were heat treated at 600°C for two hours duration, producing gradual surface levelling and coalescence of grain particles. The samples were also thermally treated at 800˚C and 1000˚C respectively. Although heat treatment at 800°C produced metal deposits that were fused together, the wall of samples could not be compromised and a similar effect was observed after further heat treatment at 1000°C. The wall lost its integrity due to the formation of a more porous structure.

- It is possible to conclude that the effect of normalizing heat treated samples is that the as deposited metal fine grained structure is changed to a coarse structure. Normalizing at room temperature presents a better compromise between immediate cooling and cooling gradually in the oven.

- The relative strength of the materials was observed qualitatively depending on the nature of the substrates. The strength of the material were tested manually and was proved to be destictively strong. Table 6-10 presents the qualitative relative strength of samples used in this research. Therefore all samples used are reliable except cotton wool.

Table 6-10: Strength Relation to nature of substrate

Substrate	Strength
PHP 1	Strong
PHP 2	Strong
PHP 3	Strong
PHP 4	Strong
Fibrous Material	Strong
Carbon Felt	Very Strong
Cotton Wool	Weak
Glass Wool	Very Strong

6.5 Effect of Silanation

Various attempts have been made to improve the film adhesion of non-metallic substrate using surface treatment techniques. Among them is surface treatment by application of silane coupling agent, or adhesion promoter. These are applied to achieve the chemical reaction between adhesive and substrate. Silanes are silicon based chemical that contain two type of reactivity; inorganic and organic in the same molecule. The general structure of silane is Y-Si $(OR)_3$ where OR is a hydrolyzable group such as methoxy, ethoxy or acetoxy and XY is an organofuntional group such as amino, methacryloxy, epoxy and so forth. In this case silane acts as adhesion between PHP, silica colloid and metal deposits.

6.5.1 Silanization of PolyHIPE Polymer through Surface Treatment

The effect of metal deposition on silanated PHP with silica colloid was studied. A silane coupling agent was deposited with styrene end chain. The silanes were selected to have hydrolysable groups and silanation was carried out using an ethanol-water solution of the silanes and by immersing the PHP directly into the solution at room temperature (24°C). The amount of silane used was that required to produce minimum uniform coverage on the PHP. The silanation process was carried out on PHP with silica fillers, coded as PHP4. The experiment was performed using a Ni-B system, with nickel chloride as the nickel source and DMAB as the reducing agent. Metal deposition was realised by electroless deposition flow through, operated at cell temperature 50°C. An initial experiment was carried out without silanation and the results showed that the PHP crumbled; indicating that no bonding occurred between the metal and silica Figure 6.68 shows the results of unfunctionalised PHP.

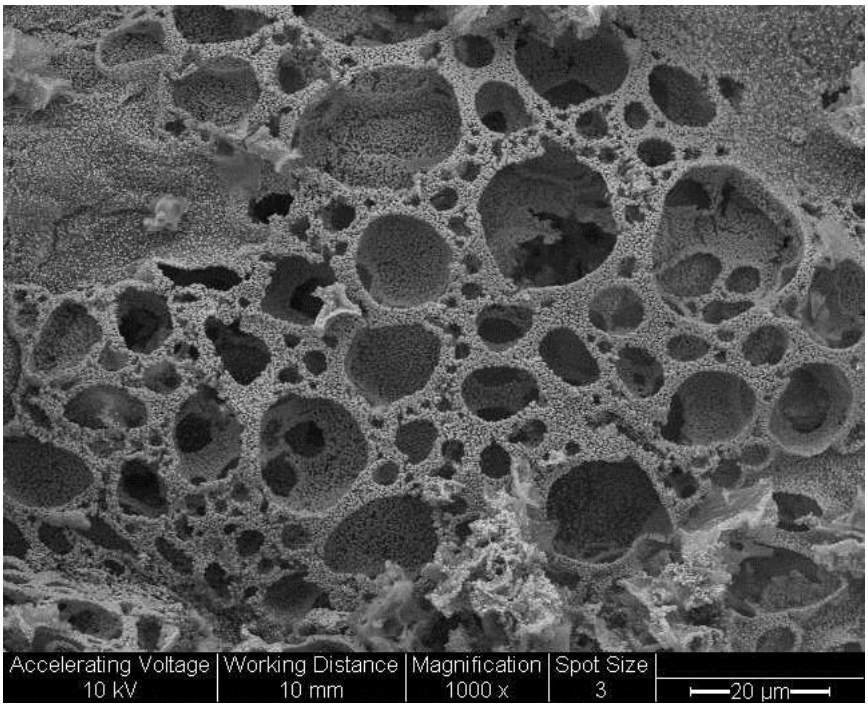

Figure 6-68: General view of Ni-B metal deposited on PHP + silica without silanation after heat treatment

The results in Figure 6.69 prove that metal and silica do not incorporate each other to obtain a metalized porous structure. As seen from SEM image in Figure 6.69, the white dot indicating the silica particle (see magnified SEM image from Figure 6.69) while metal exhibited grain structure that fused together. However silica and metal did not incorporate to one another and lose their connectivity during morphology formation. Hence, the wall collapsed leaving silica and metal separated.

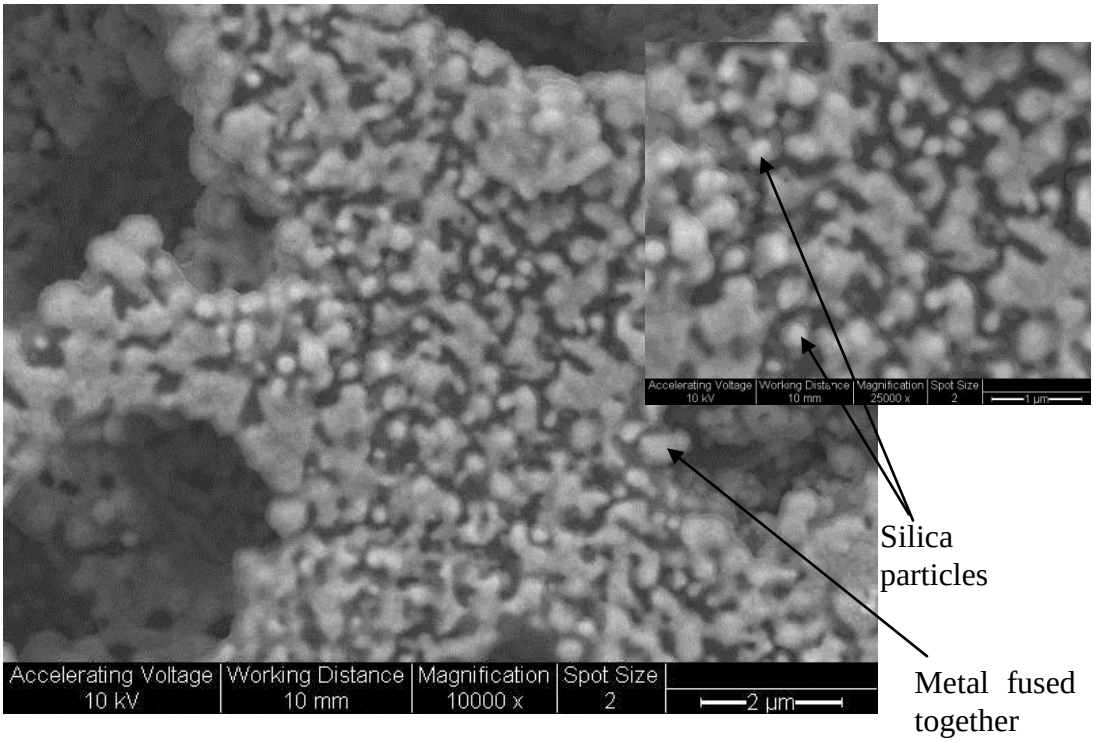

Figure 6-69: Ni-B metal deposited on PHP + silica after heat treatment at 600°C for 2h without silanation

To overcome this problem, silanation was carried on the templates as described in section 5.4. Similar procedure was performed to metallise the functionalized PHP as described in section 5.3. Metal was successfully deposited and metal covered the whole PHP disk. The results for functionalised PHP are shown in Figure 6.70 and Figure 6.71. Metal and silica were found incorporated on one another, hence obtaining an intact and strong disk.

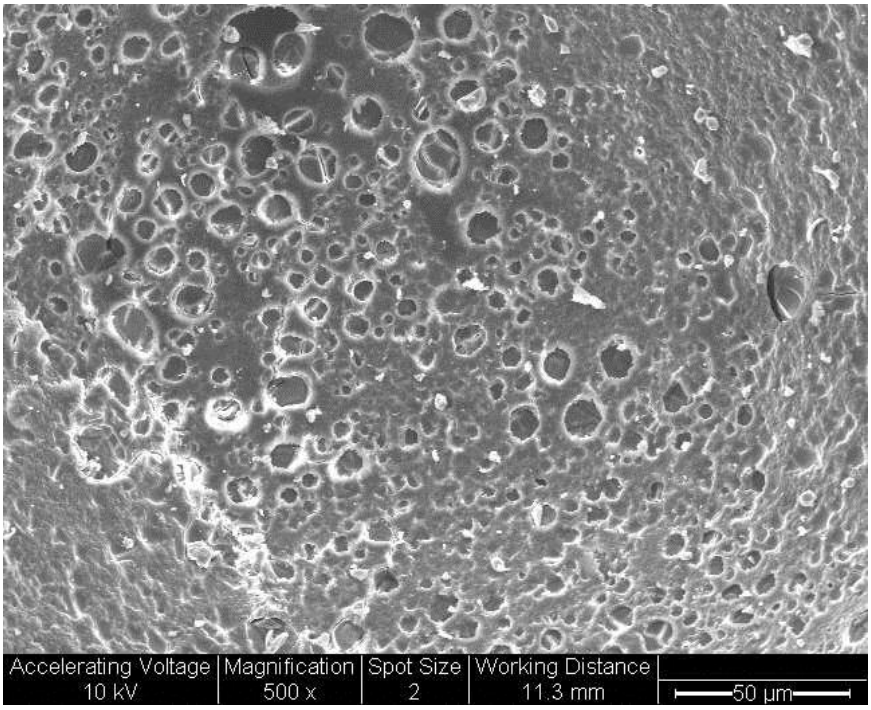

Figure 6-70: General view of Ni-B deposited on functionalized PHP4

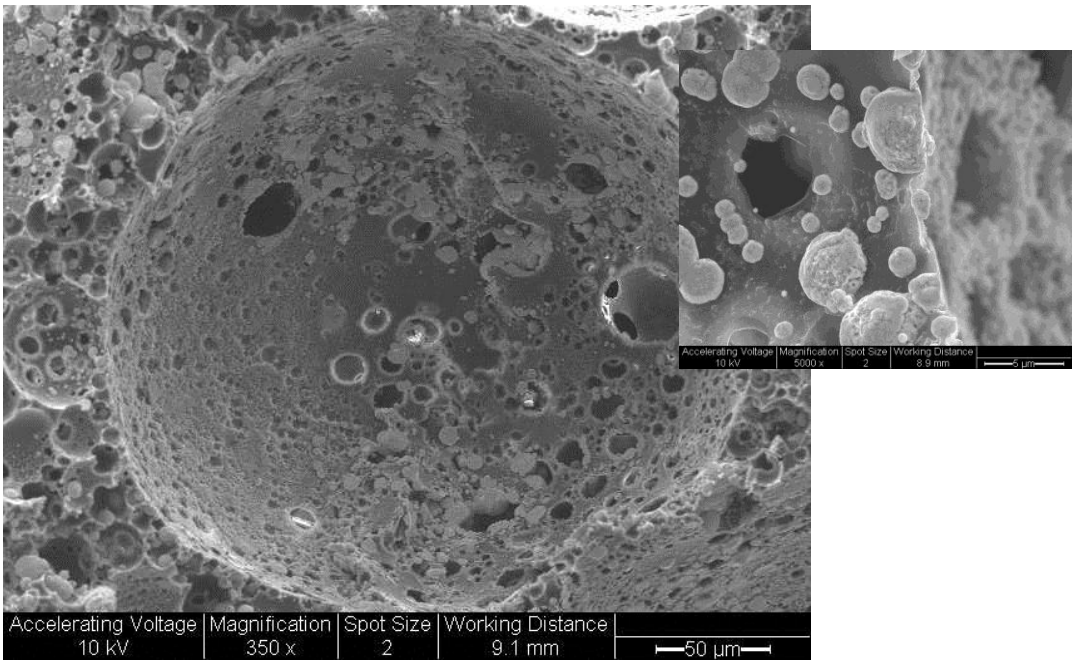

Figure 6-71: Higher magnification of Ni-B deposited on functionalized on PHP 4

The results from the EDX spectra analysis revealed the cooperation of these two materials. Two type of EDX analysis were carried out i) an individual spot analysis and ii) an average area analysis. For an individual spot analysis, two different spot (point 0 and point 1) were analysed from the associated SEM micrograph (Figure 6.72). The elemental composition analysis showed the presence nickel and silica in both spot which implies the coorporation of both metal and silica. This analysis technique confirmed that silica colloidal and silanization had proven as factors for enhacing material strength as well as bonding enhancer. Figure 6.73 and Figure 6.74 showed the spectra image of point 0 and point 1 respectively and Table 6-11 summarised the findings of nickel and silica composition.

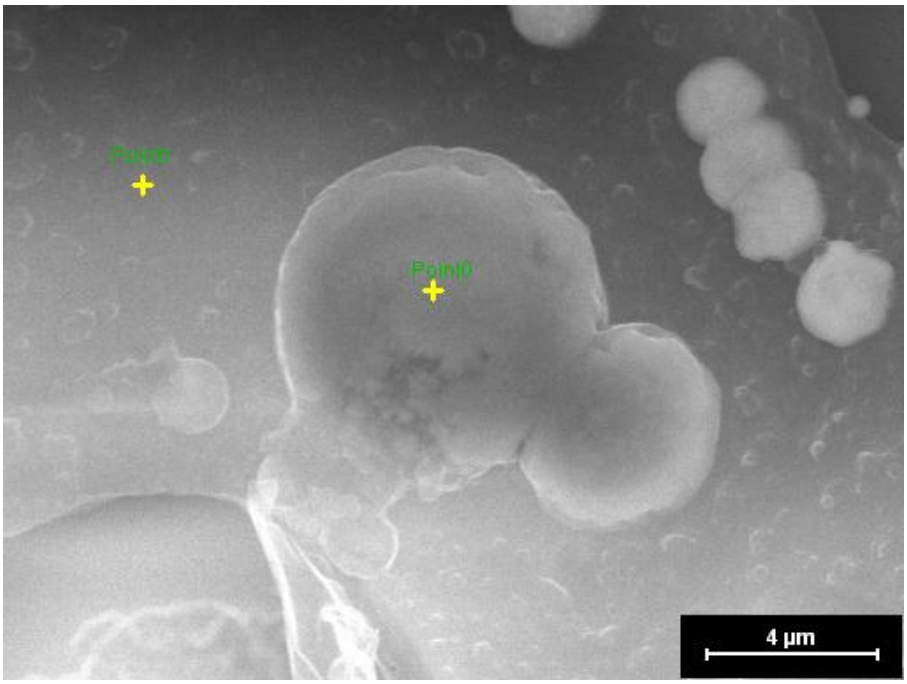

Figure 6-72: EDX spectra image of functionalized PHP4 at point 0 and point 1

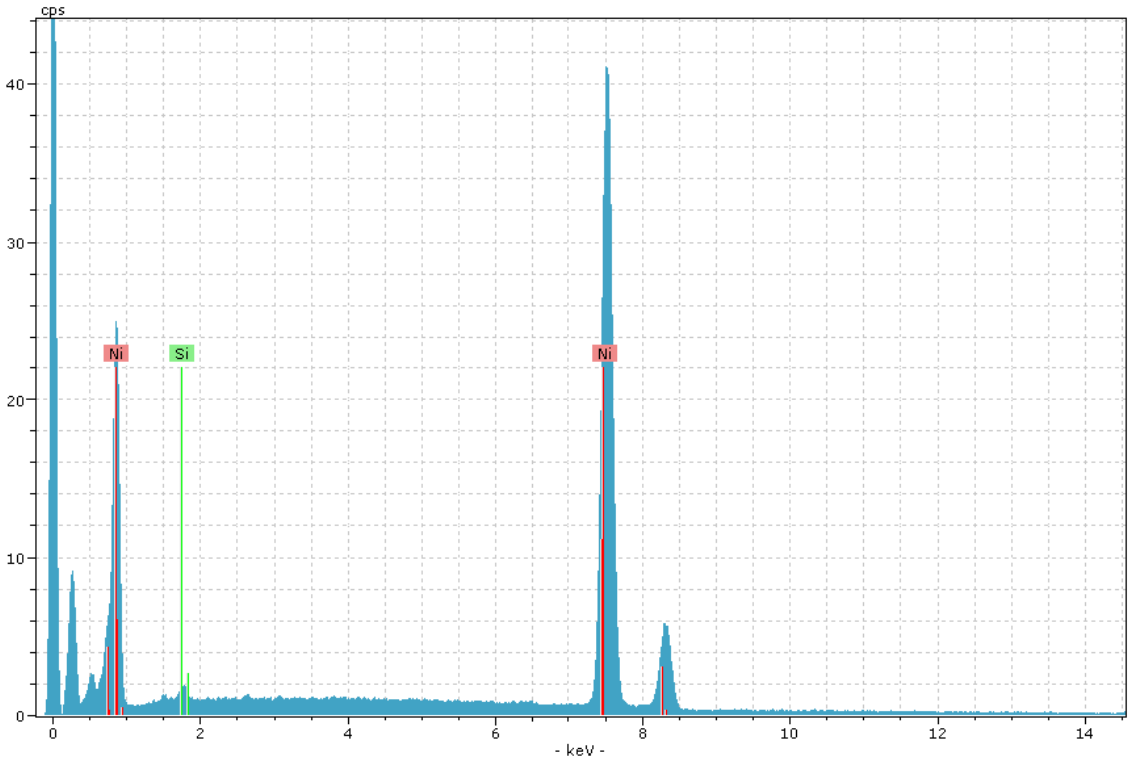

Figure 6-73: EDX spectra image of functionalized PHP at point 0

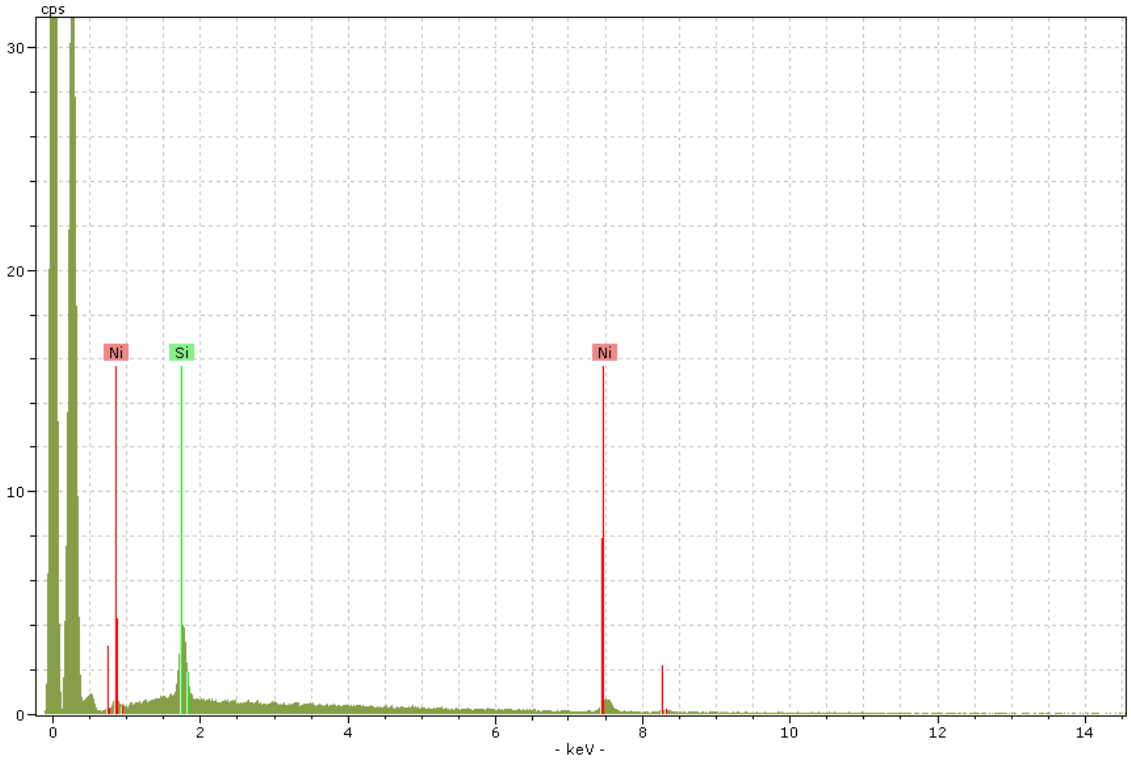

Figure 6-74: EDX spectra of functionalized PHP at point 1

Table 6-11: EDX spectra for point 0 and point 1 of functionalized PHP

Spectra	Nickel (%)	Silica (%)
Point 0	99.42	0.58
Point 1	52.81	47.19

More than one EDX spectra was performed at other site (Figure 6-7) (see Figure 6.76 and 6.77 for EDX spectra) and Table 6-12 for summarized composition of the findings.

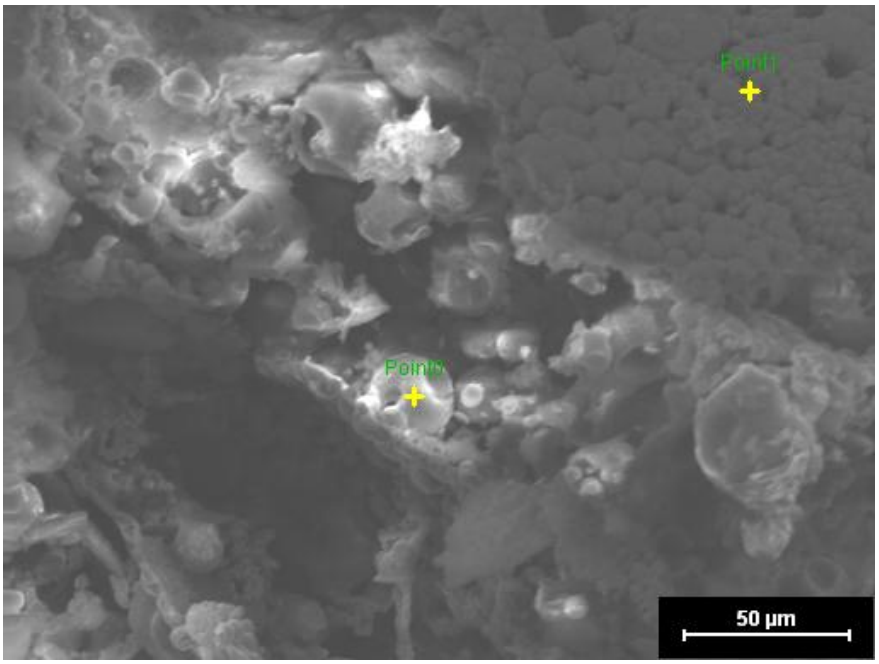

Figure 6-75: EDX spectra image of functionalized PHP at point 0 and point 1

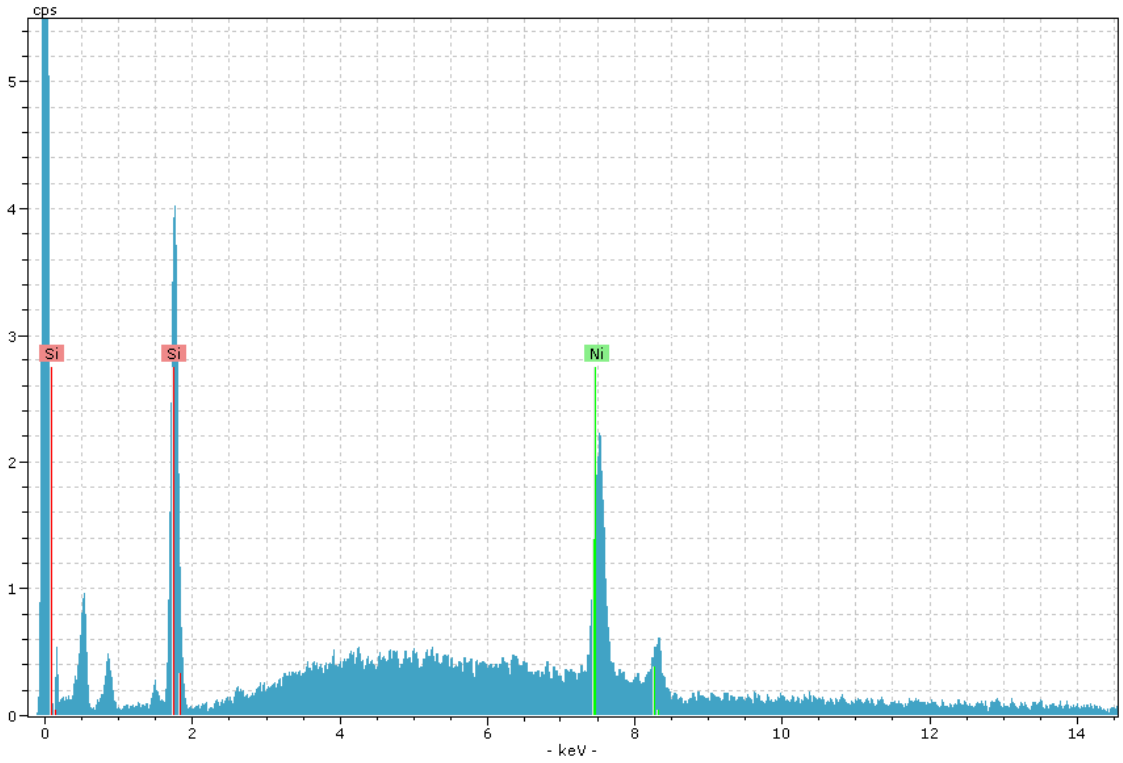

Figure 6-76: EDX spectra image of functionalized PHP at point 0

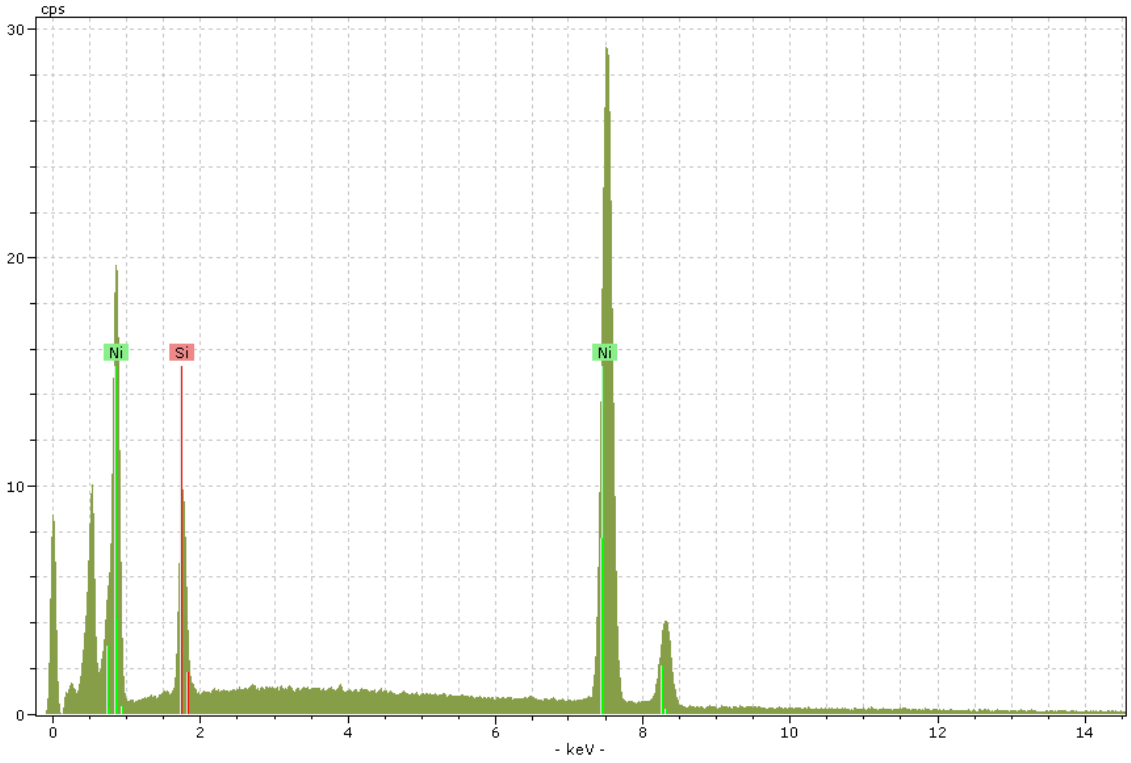

Figure 6-77: EDX spectra image of functionalized PHP at point 1

Table 6-12: EDX spectra for point 0 and point 1 of functionalized PHP

Spectra	Nickel (at%)	Silica (at%)
Point 0	18.48	81.52
Point 1	88.59	11.41

Figure 6-78 illustrates the associated SEM micrograph of Ni-B depositon on PHP4 for the area analysis. EDX analysis was performed over the area. It detected the presence of nickel and silica as showed in EDX spectra image (Figure 6.79). The composition was summarised in Table 6-13.

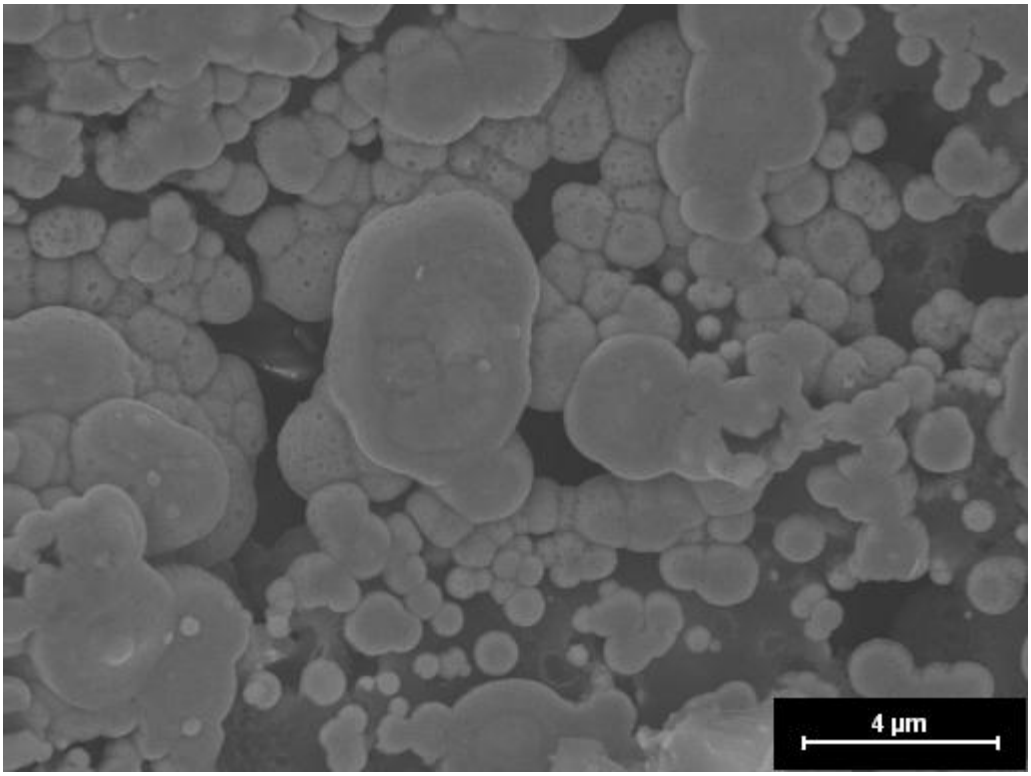

Figure 6-78: EDX spectra image of functionalized PHP at a specific area

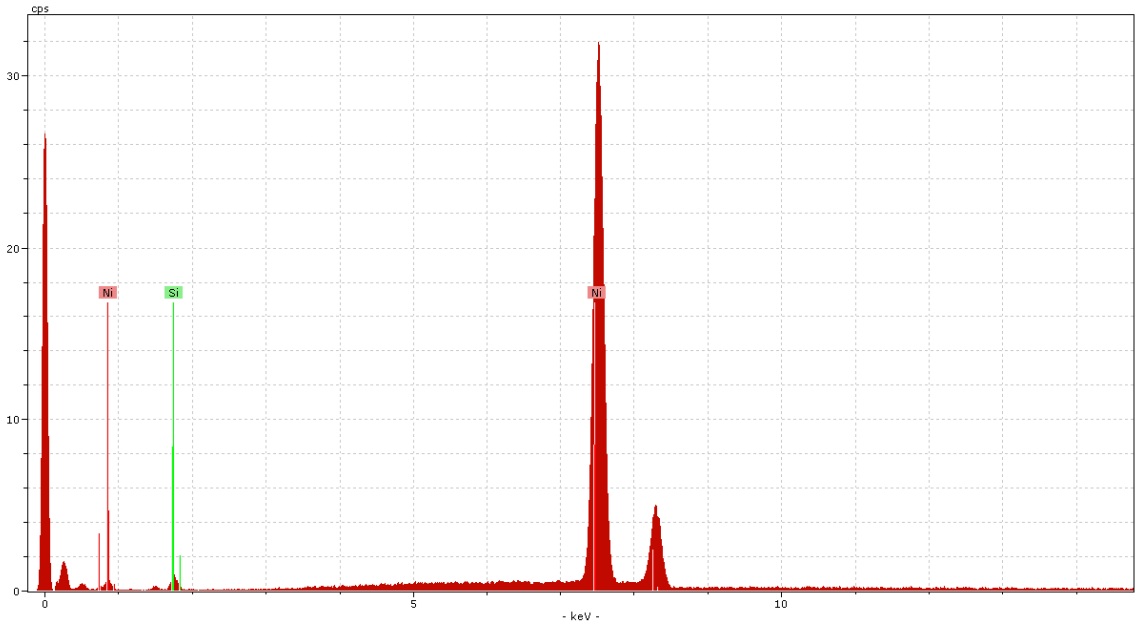

Figure 6-79: EDX spectra of functionalized PHP at a specific area

Table 6-13: PHP at a specific area

Spectra	Nickel (at%)	Silica (at%)
Area	95.23	4.77

In order to explain the establishment of metal bondage and template, Figure 6.80 illustrated the schematic diagram of the silanization process and succession of metal deposition. In this method, the surface is treated with a solution of a silane, with a vinyl group in an organic solvent. As a result of chemical modification of surfaces via silanization, a monomolecular silane layer is formed on the SiO_2 surface (Weetall, 1970) thus allowing metal to deposit on it.

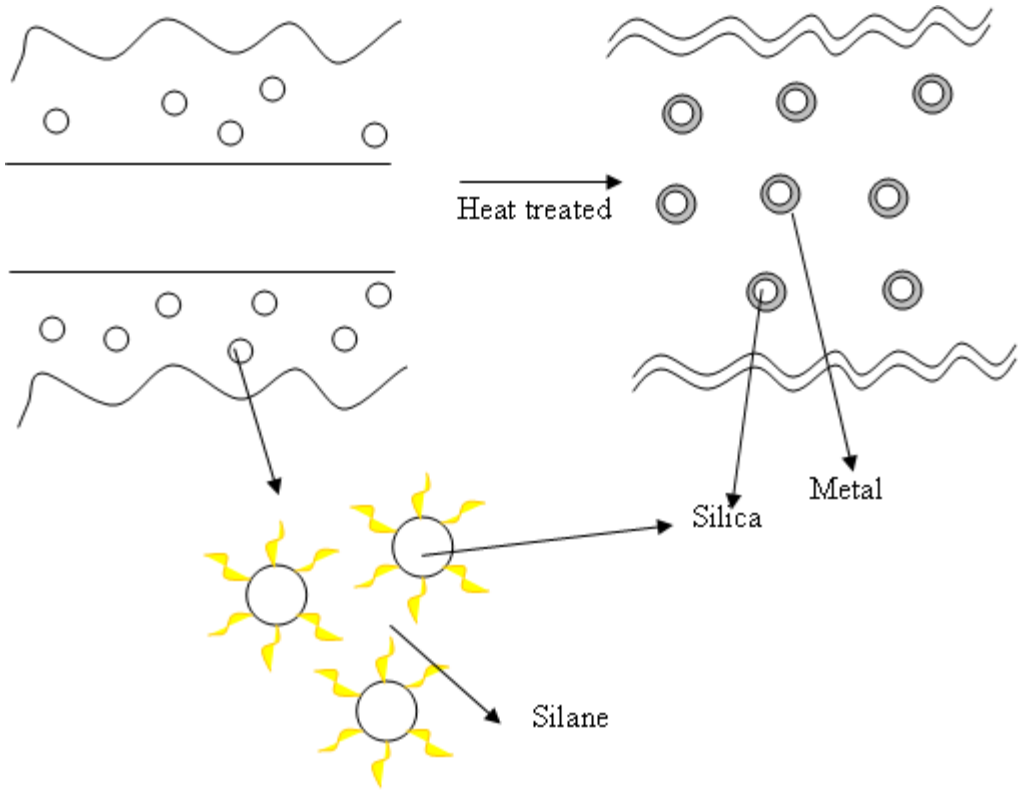

Figure 6-80: Mechanism of deposited metal on silanated PHP+Silica

6.5.2 Silanization of PolyHIPE Polymer through Cross Linking

This section provides the use of silane coated colloidal silica to obtain a micro-porous silica coated polymer. Silane coated PolyHIPE Polymer with colloidal silica using reactive vinyl trimethoxysilane as a co-monomer in the oil phase of the HIPE, when successfully performed, can be used as a template for further modifications, including silica supported catalysts.

Since some organically reactive silanes particularly vinylsilane do not have a space group, a hydrogen atom on silicon will easily add across a carbon-carbon double bond to form a very stable silicon-carbon bond and making it useful for cross linking reaction (Witucki, 1993). However this work is the subject of on going research.

The mechanism of how the reaction between DVB and Styrene for the formation of the normal polyHIPE takes place is shown as follows:

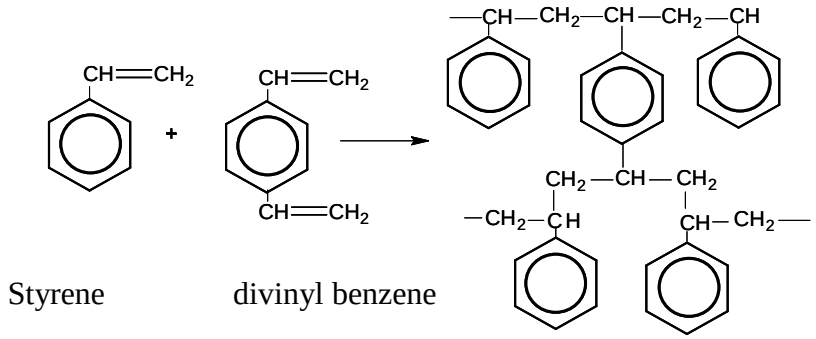

Figure 6-81: Formation of PolyHIPE polymer using DVD and Styrene

The incorporation of vinyl trimethoxysilane into the oil phase during the polymerization process has led to a change in the morphology and structure of the produced polymer, as shown in both the following equation and SEM images.

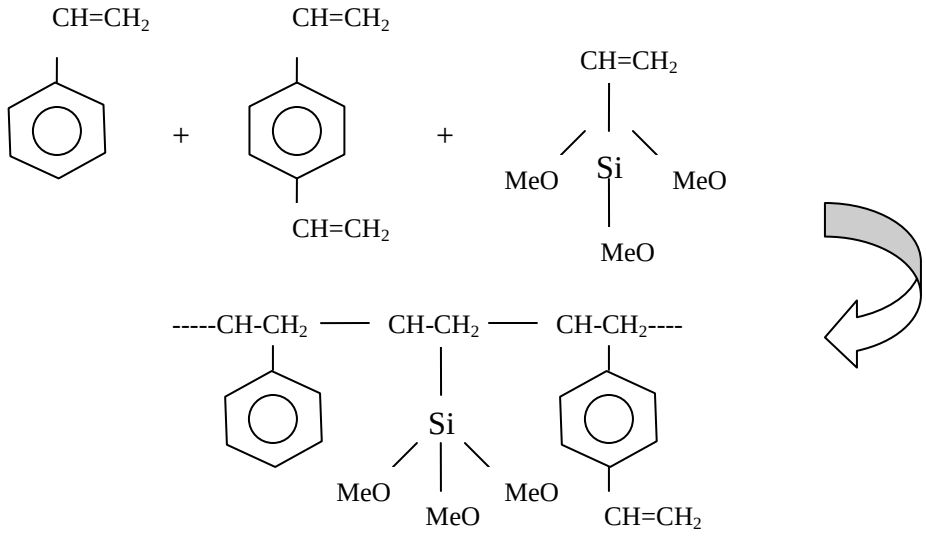

Figure 6-82: Formation of silane coated PolyHIPE polymer with colloidal silica by reactive intermediate

The different surface morphology and non-porous surface shown in the SEM analysis images can be explained to be a result of the presence of a Si atom as a central atom. Due to the highly electron withdrawing character of the methoxy groups attached to the Si atom, a highly partial positive charge is located for silicon metal, and of course methoxy groups are negatively charged. Also, due to the high electron density and electron withdrawing nature of benzene rings, they hold a partially negative charge. This consequently leads to polar attraction between both the Si metal atom and aromatic benzene rings, thus the molecules become closer. The closer the molecules, the less porous structure obtained but physically stronger polymers produced.

6.5.3 Glass Wool

This study was designed to prove that surface treatments consisting of silanation of glass wool can improve the bond strength of metal to glass wool. Statistical analysis elsewhere showed that silanation resulted in significantly higher bond strength. In this experiment metal deposition on glass wool in three different conditions we investigated. First glass wool without silanation, second the silanation of glass wool in water, and third silanation of glass wool in ethanol. Figure 6.83 showed SEM micrograph of glass wool as received. An SEM micrograph revealed that metal deposition on glass wool without treatment seemed to be broken, indicating a weak bond between metal and wool (Figure 6.84).

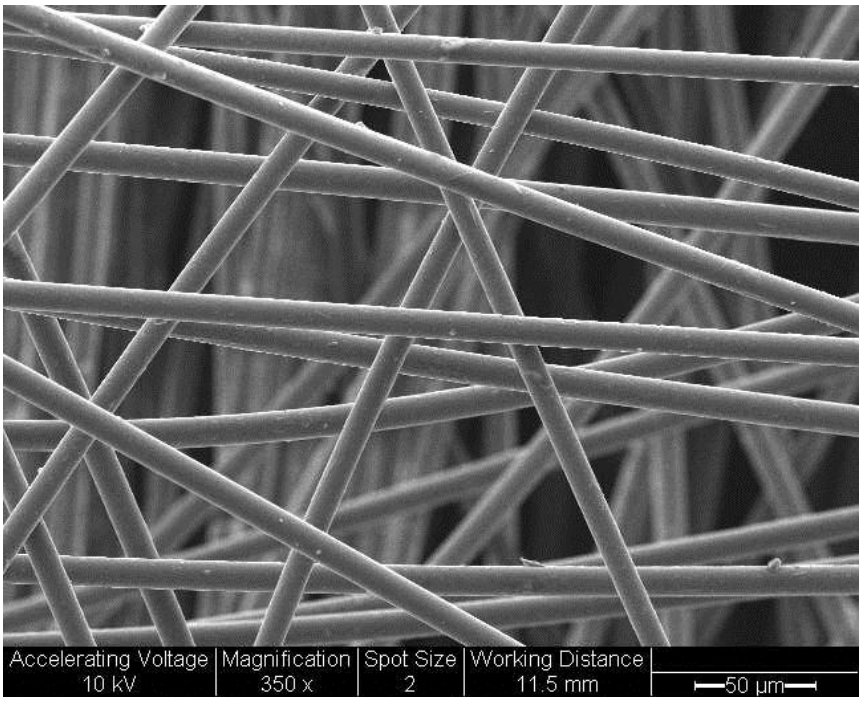

Figure 6-83: Micrograph of as-received Glass wool (x 350 magnifications)

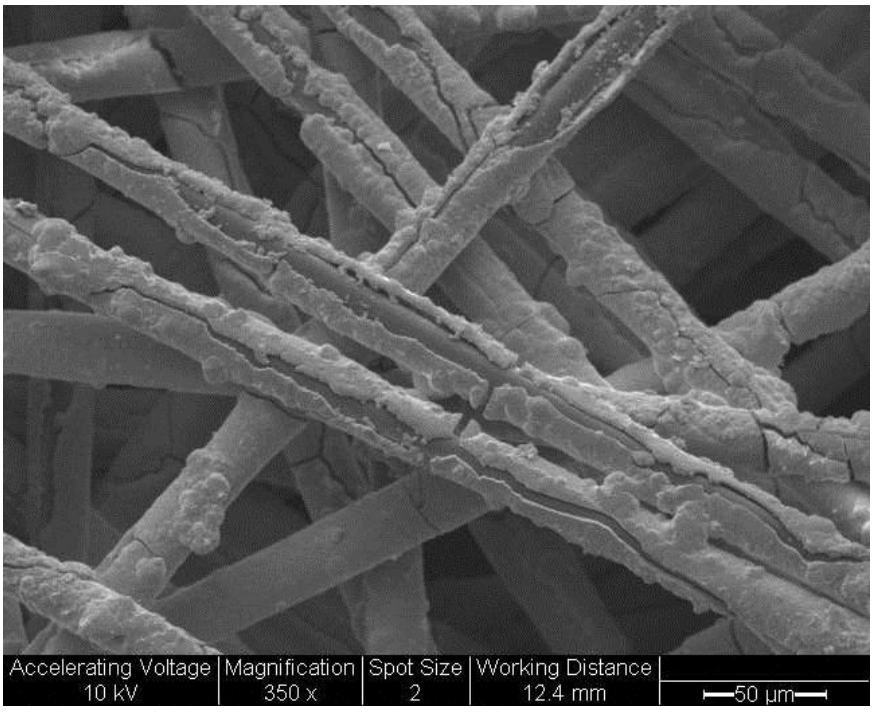

Figure 6-84: Glass wool without sitlane treatment

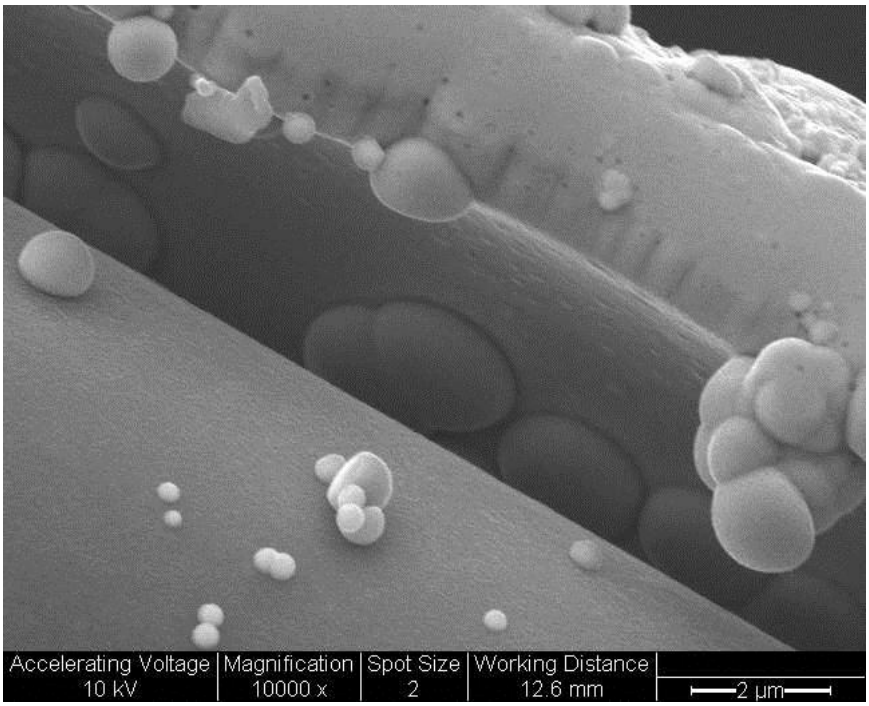

Figure 6-85: Weak bondage seen in gap between glass wool and metal

As in Figure 6.85 a large gap of about 1-3µm occurred on the surface of the glass wool. With no silane treatment gap exist between the surface of glass wool and metal deposits. These gaps are predetermining fracture points resulting in a low mechanical stability of the samples. Figure 6.86 and Figure 6.87 illustrate the SEM micrograph of glass wool after heatment. When the samples were heat treated, metal and glass wool exhibited a strong bond indicating that the silanation process was successful in enhancing bondage between metal and glass wool. The strength is manually tested and proved that the silanated glass wool was distinctively strong.

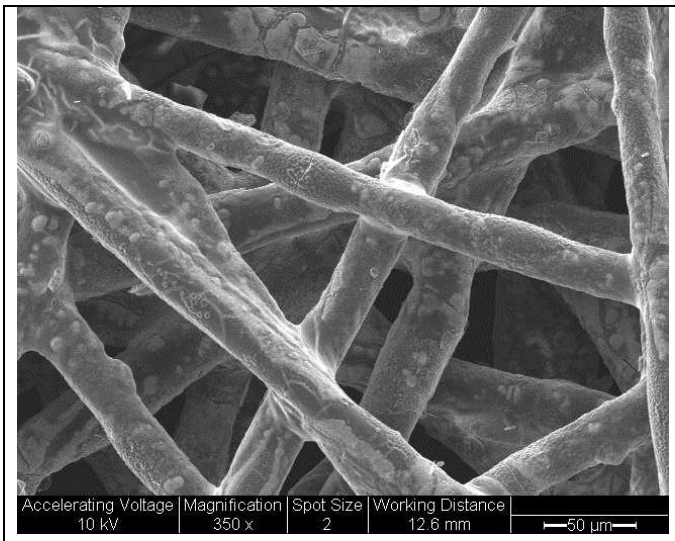

Figure 6-86: Glass wool after heat treatment and before silanation

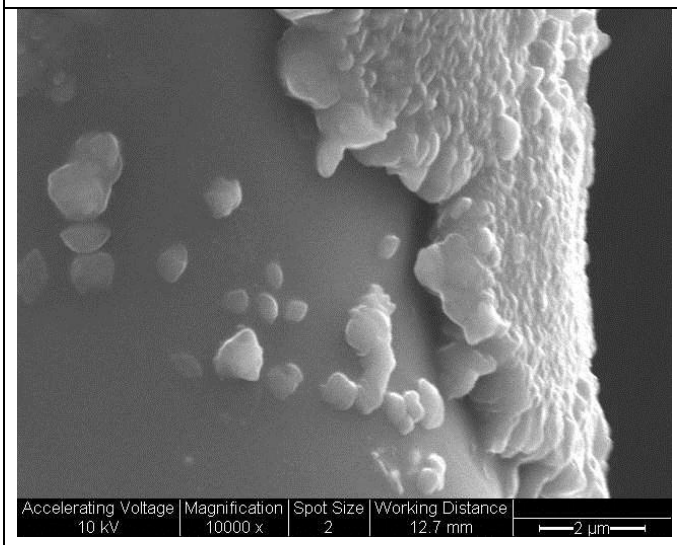

Figure 6-87: Closed-up image of glass wool after heat treatment and before silanation

6.5.3.1 Silanation of Glass Wool in Water

This experiment dealt with silanation of glass wool in water. After the silanation process it was observed that the glass wool disc was rigid. An average glass wool disk (4mm thick and 26 mm in diameter) were weighed. ±0.08 g before silanization and it

made up to 40 times of its original weight of metal deposits and generally reaching a final disk weight of around ±2.33g before metal deposition. The silanised glass wool is shown in Figure 6.88. SEM evaluation revealed that the surface morphology was modified following the treatment when compare to as received glass wool (Figure 6.83). Silane seems to penetrate around the glass wool and promoted surface modification. Relatively a rough surface area was produced.

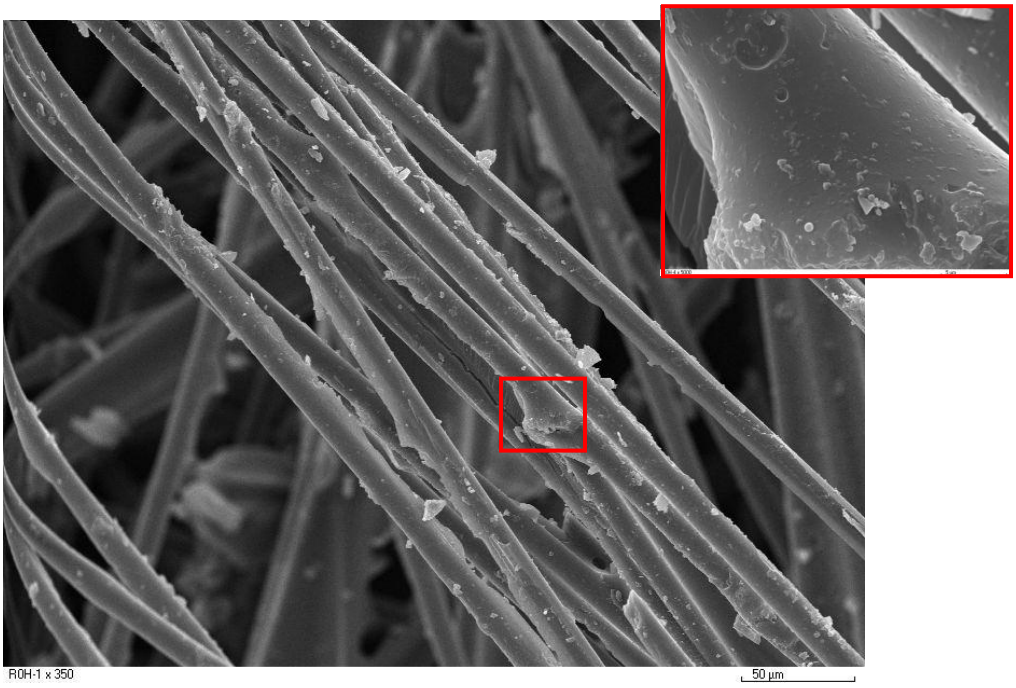

Figure 6-88: Silanated glass wool in water

When Ni-B deposited on the surface of silanated glass wool, less fraction was observed indication of better bondage between the glass wool and metal deposits (Figure 6.89).

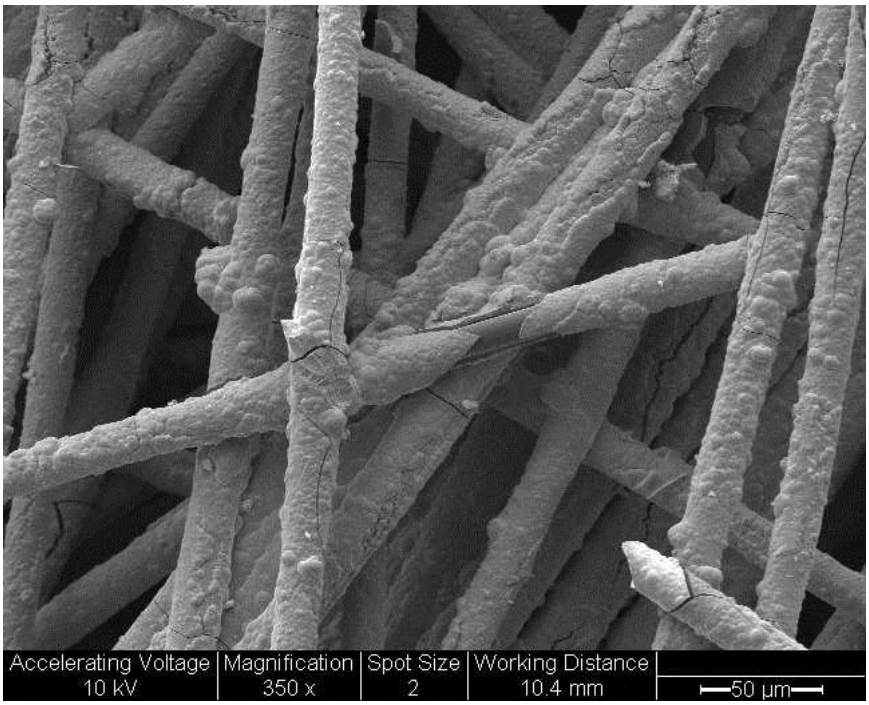

Figure 6-89: Ni-B deposits on glass wool silanated in water

Figure 6.90 revealed the Ni-B a deposit on glass wool silanised in water and it was that the gap of less than 1 µm which is far less from the untreated glass wool. The heat treated silansised glass wool with Ni-B deposit displaying morphology of a smooth surface (Figure 6.91)

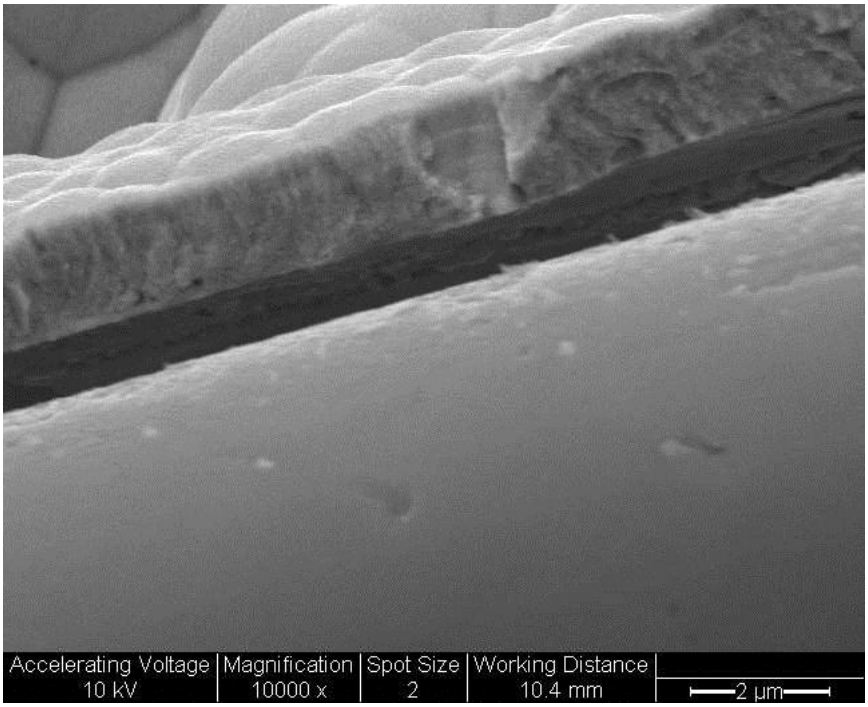

Figure 6-90: Gap between glass wool and metal in treated glass wool

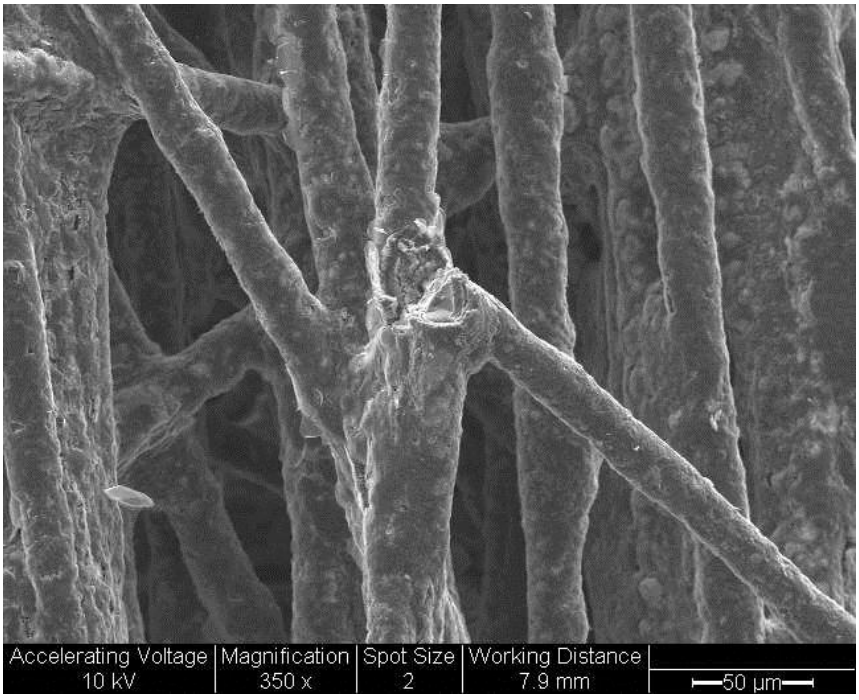

Figure 6-91: Ni-B deposits of glass wool Silanated in water after heat treatment

Eventually, Figure 6.92 revealed the increase bondage occurs between Ni-B deposits and silane treated glass wool. It was observed that gap was not presence.

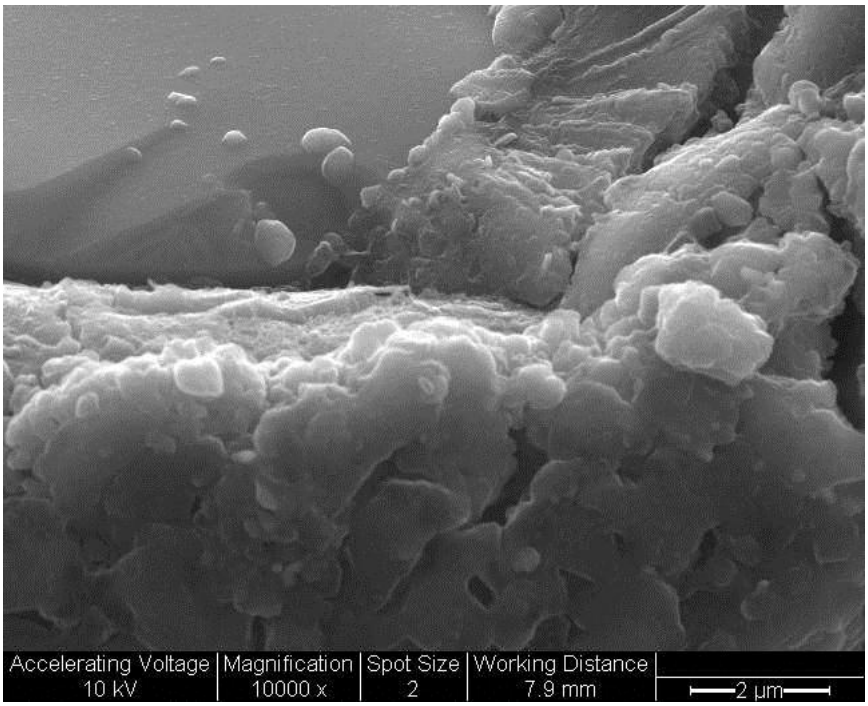

Figure 6-92: Bondage between metal and glass wool after silanation and heat treatment at 600˚C

6.5.3.2 Silantion of Glass Wool in EtOH

This experiment presented the experiment of glass wool treated with silane in EtOH. The silanation resulted in the formation of a hard outer layer or crust on the substrate.Weight after silanization was ±3.08g compared to ±0.08g from the as received glass wool disk (26mm diameter and 4mm thickness) Figure 6-93 shows glass wool silanated in EtOH. It was observed that silane deposition on glass wool in EtOH exhibited a more bulky and rough surface deposition than in water. Solvent play an important role in silanation. A small amount of solvent may be beneficial in promoting silane wetting. Ethanol evaporates easily without affecting the reactivity of silane.

Therefore ethanol/water based silane had a more stable behaviour, probably due to mixing ratio of the two solvent components.

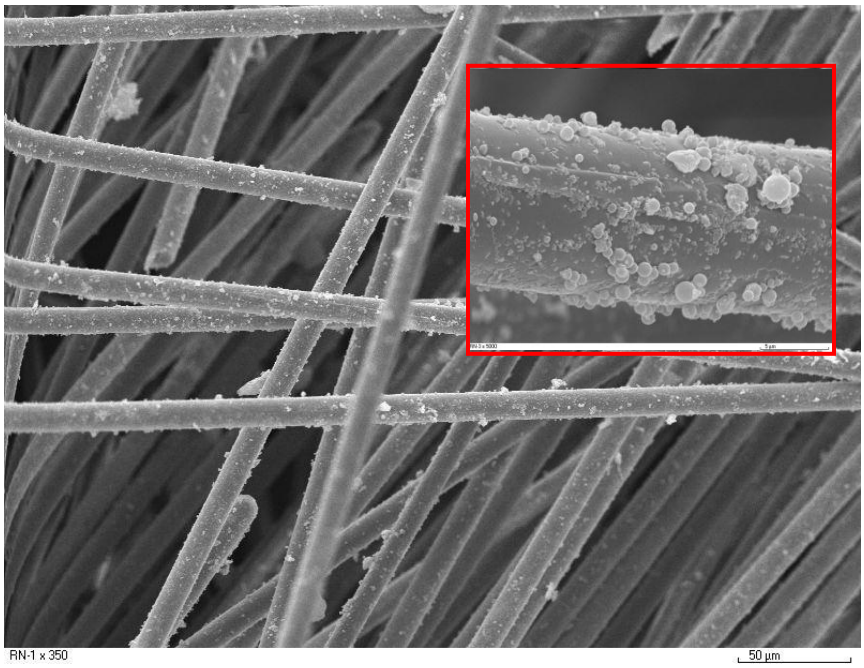

Figure 6-93: Silanated glass wool in EtOH

Although these had a stable behaviour, silane in aqueous had a longer wearing surface result. These explain the structure of Ni-B deposit which exhibit more fracture points than section 6.5.3.1 (see Figure 6-94).

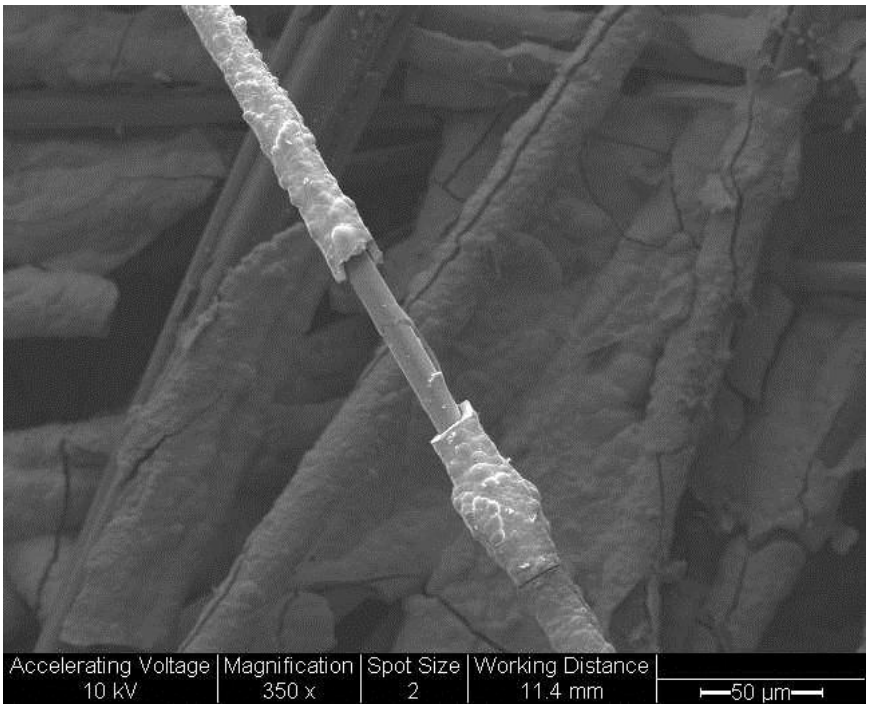

Figure 6-94: Deposited Silanation of glass wool in EtOH

Figure 6.95 revealed the Ni-B a deposit on glass wool silanised in EtOH and it was that the gap of less than 1 µm which is far less from the untreated glass wool. The heat treated silansised glass wool with Ni-B deposit displaying morphology similar to those in section 6.5.3.2.1 (Figure 6.96). Consequently, the bondage between glass wool and metal deposits was proved successful (Figure 6.97)

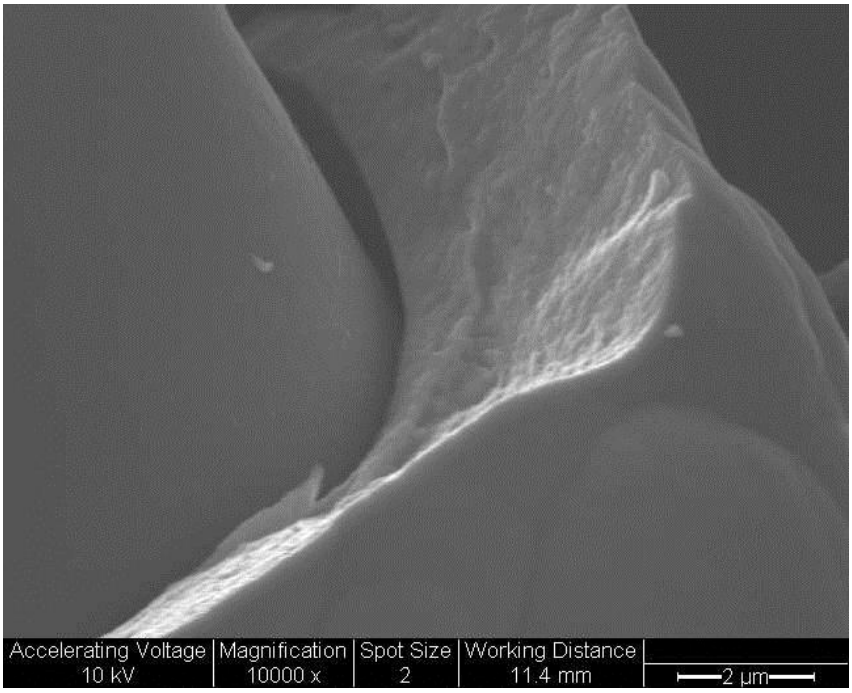

Figure 6-95: Gap between glass wool and metal in a Ni-B deposit on silane treated glass wool.

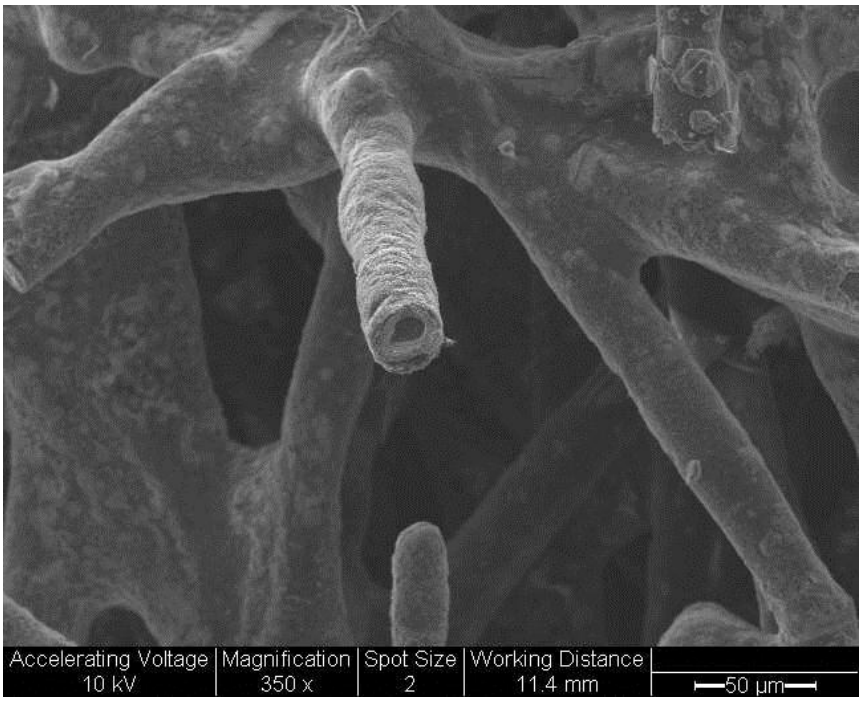

Figure 6-96: After heat treatment

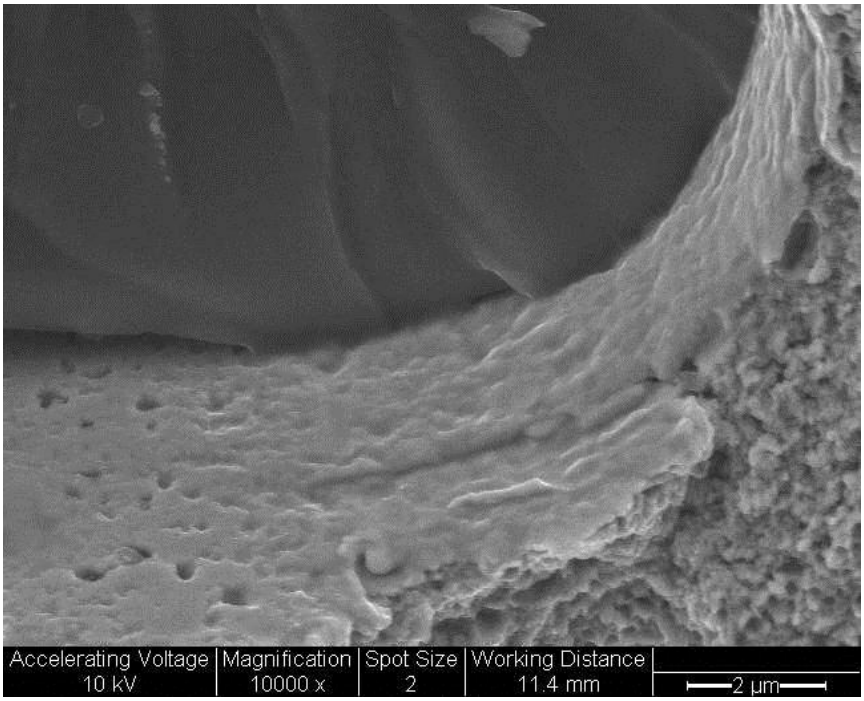

Figure 6-97: Bondage between glass wool and metal after silanation in etanol and after being heat treated

Finally this study shows that a simple, fast and inexpensive procedure using silane in water and silane in EtOH may serve to increase bonding interaction between glass wool and Ni-B deposits. However this study is not able to reveal which of the two methods preferred as more compatible.

The mechanism of metal deposited on silanized glass wool is illustrated in the schematic diagram below (Figure 6-98). This can be explained by the silicon Si $(OH)_2$ which was incorporated with the glass wool reacting with vinytrimethylsilane through substitution reaction to create a Si-O-Si bond. The methoxy group attached to it has a lone pair of electrons obtained from oxygen, hence attracting metal from the deposition solution.

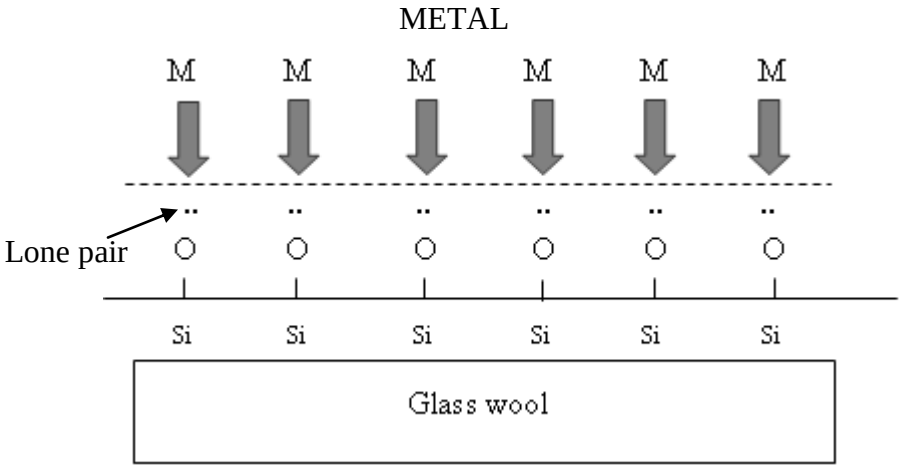

Figure 6-98: Schematic diagram of metal deposits on glass wool with silanation

6.5.4 Summary

- Through the silanization process, this work has revealed a polymer-silica metal/alloy system formed as a composite. The resulting composite is porous, whereby walls are made of silica particles and protected from collapse by the porous catalytic metal/alloy structure.

- This research has successfully proven a method for improving the adhesion of metal deposit to glass wool. It involved silanation of glass wool for a period of time sufficient to form a substantially continuous film, and subsequently metal depositing of the substrate by a flow through electroless method. After the heat treatment, improved adhesion was noted for all samples (see Appendix C for comparison images between treated and non treated glass wool). It may involve both mechanical and chemical interactions with the substrate surface under certain circumstances.

CHAPTER 7

CONCLUSION

7.1 Conclusion

In conclusion, template method of producing nanostructure macro porous materials prepare in this research was successfully developed. Instead of involving complex chemical procedure, the method described is basically simple and versatile allowing one to fabricate a hierarchical pore structure. Preparation of nanastucture macro porous materials described has much potential especially process requiring nanostructure material and has many advantages over the existing method. Generally the success of this research has showed that:

- Method used took less time than existing method
- Morphorlogy can be controlled for respective application
- The experimental set-up is simple and technically inexpensive
- The experimental procedure used in this study is not labour intensive

As a comparison, some of the porous material produced by commercially available under names:

- METAPORE® (by SORAPEC in France)
- CELMET® (by Sumitomo Electric Industries in Japan)
- RETIMET® (by Dunlop in United Kingdom)
- RECEMAT® (by SEAC in The Netherlands)

These highly porous metallic foams are generally used as matrix material for electrodes. RECEMAT® (Recemat International, Standard Specification, RECEMAT, 1998-2006)

is reported to have densities from 0.4 to 0.45 g/cm^3 in nickel foams and from 0.6 to 0.65 g/cm^3 in nickel-chromium foams. The specific surface area ranges between 500 and 5600 m^2/m^3, where estimated average cell diameter is in the range of 0.4 to 2.3 mm.

These proved that the material produced in this research is comparable to commecialised material available. Below are comparison between commercial material and nanostructure macro porous material obtained from this research.

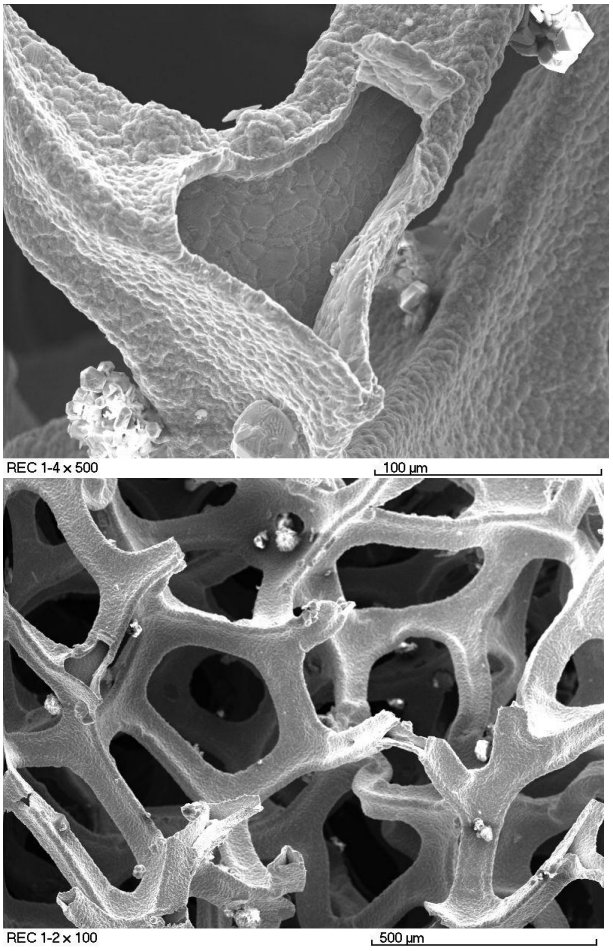

Figure 7-1: SEM micrograph of RECEMAT

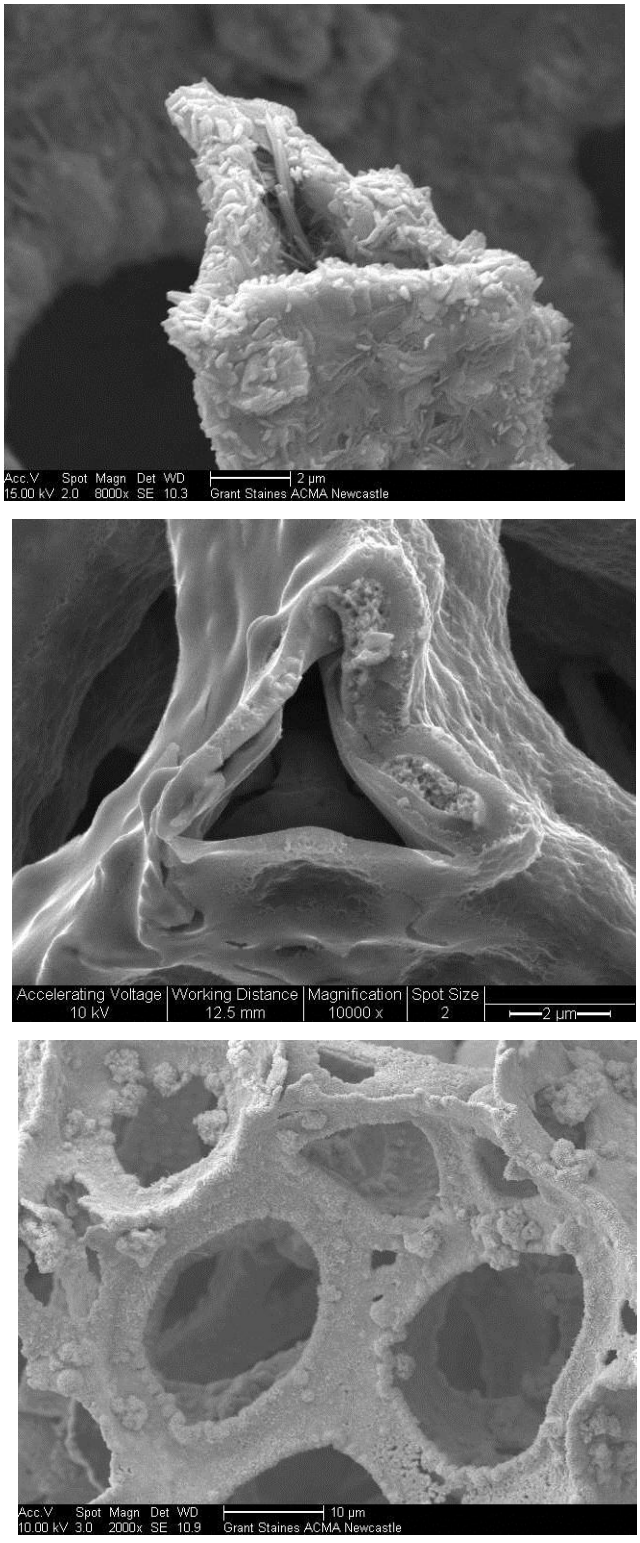

Figure 7-2: SEM micrograph of material obtained from this research.

7.2 Future Work

Following the investigations described in this thesis, a number of works could be taken up that would help expand and strengthen the results, involving the fabrication of hierarchical catalytic structured studies. The results in this thesis also provide a strong foundation for future work to consider the application of the fabricated nano-structured macro porous materials.

- PolyHIPE with colloidal silical used in this research have shown a potential characteristic of future catalysts with high surface area, enhanced mechanical properties and hierarchical pore structure. Several studies have shown that elastomeric polyHIPE can be reinforced through the synthesis of nanocomposites using several different routes, including the addition of co-monomers such as vinyltrialkoxysilane, polyhedral oligomeric silsesquioxane (POSS) bearing vinyl groups, or vinyl silsesquioxane (VSQ) (Normatov and Silverstein, 2007) . Methacryloxypropyltrimethoxysilane was also used as a co-monomer to produce an open-cell structure (Tai et al., 2001a). Nevertheless none has been used to further incorporate metal, as described in this work, to obtain a polymer-silica meta/alloy system. The deposition of silane used as a surface treatment enabled it to grow within the surface of the substrate by submerging the substrate in the silane solution. The bonding between silane and substrate occurred due to the presence of Si-O-Si bond. Thorough investigation should be made on silanization of these materials through cross link in oil phase. When silane is incorporated during the preparation of emulsion, the functional group attaches to a molecule of an organic compound via a chemical bond. Further investigation should also be carried to find out the significance of using types of Benzil and methods of silanization (either in water or EtOH)
- The experimental work in this thesis has only considered the deposition of Ni-B and Ni-P system. Other systems may respond differently to the method used. This aspect should be explored and is expected to be successful on any system with the right operation conditions and composition.

- Although characterizations of porous materials have been performed in this thesis, and since the materials fabricated have a great potential for catalytic applications, it is necessary to identify the state of the active catalysts in this research that can then be correlated with reaction rates, selectivity and in terms of deactivation.

- Moulijn and Kapteijn (2005) have recently reported that structured catalysts in the form of monolith make multiphase catalytic reactors more efficient. PolyHipe polymers and other porous materials used in this research were produced as discs having a 25 cm diameter and 0.4 cm thickness. It would be of interest to fabricate the materials produced in this research in monolithic form, as this would result in several potential applications in the chemical process industry and oil refinery industry.

It is important to know whether the knowledge that has been gathered is solid enough so as to continue constructing from it. It is believed that the goals have been accomplished and it is hoped that this thesis has contributed not only to present research but also future research in this field.

REFERENCES

1. Agarwala, R. C. and Agarwala, V. (2003) 'Electroless alloy/composite coatings: A review', *Sadhana - Academy Proceedings in Engineering Sciences*, 28, (3-4), pp. 475-493.
2. Akay, G. (1998) 'Flow-induced phase inversion in the intensive processing of concentrated emulsions', *Chemical Engineering Science*, 53, (2), pp. 203-223.
3. Akay, G. (2003) 'Flow induced phase inversion phenomenon in process intensification and micro-reactor technology', *Abstracts of Papers of the American Chemical Society*, 226, pp. U45-U46.
4. Akay, G. (2006) 'Bioprocess and Chemical Process Intensification', in Lee, S. e.(ed), *In: Encyclopedia of Chemical Processing.*NY: Marcel Dekker.
5. Akay, G., Bhumgara, Z. and Wakeman, R. J. (1995) 'Self-Supported Porous Channel Filtration Modules - Preparation, Properties and Performance', *Chemical Engineering Research & Design*, 73, (A7), pp. 782-797.
6. Akay, G., Birch, M. A. and Bokhari, M. A. (2004) 'Micro Cellular PolyHIPE Polymer Supports Osteoblast Growth and Bond Formation ', *Biomaterials*, 25, (18), pp. 3991-4000.
7. Akay, G., Bokhari, M. and Birch, M. (2003) 'Polyhipe polymer: A novel scaffold for in vitro bone tissue engineering', in *Tissue Engineering, Stem Cells and Gene Therapies.* Vol. 534 New York: Kluwer Academic/Plenum Publ, pp. 247-254.
8. Akay, G., Bokhari, M.A., Byron, V.J., and Dogru, M. (2005) 'Development of nano-structured micro-porous materials and their application in bioprocess - chemical process intensification and tissue engineering', in Galan, M. A. a. D. V., E.M. [editors](ed), *In:Chemical Engineering Trends and Developments,*.London: Wiley.
9. Akay, G., Brown, I. J., Sotiropoulos, S. and Lester, E. (1998) 'Nickel incorporation into a hollow fibre microporous polymer: a preparation route for novel high surface area nickel structures', *Materials Letters*, 35, (5-6), pp. 383-391.
10. Akay, G., Dogru, M., Calkan, B. and Calkan, O. F. (2005) 'Flow-induced phase inversion phenomenon in process intensification and microreactor technology - Preparation and applications of nanostructured microporous polymers and metals', in Wang, Y. and Holladay, J.(eds) *Microreactor Technology and Process Intensification.*Oxford: Oxford University, pp. 286-308.
11. Akay, G., Downes, S. and Price, V. J. (2002) *Method for separating oil in water emulsion*. EP 1 307 402.
12. Akay, G., Erhan, E. and Keskinler, B. (2005) 'Bioprocess intensification in flow-through monolithic microbioreactors with immobilized bacteria', *Biotechnology and Bioengineering*, 90, (2), pp. 180-190.

13. Akay, G., Noor, Z. Z. and Dogru, M. (2005) 'Process intensification in water-in-crude oil emulsion separation by simultaneous application of electric field and novel demulsifier adsorbers based on polyhipe polymers', in *Microreactor Technology and Process Intensification.* Vol. 914 Washington: Amer Chemical Soc, pp. 378-392.
14. Akay, G., Noor, Z.Z, Calkan, O.F., Ndlovu, T.M and Burke, D. (2006) *Microwave Functionalisation of PolyHIPE*
15. Akay, G. and Tong, L. (2000) 'Intensive structuring: Intensive processing of microstructured materials by flow induced phase inversion', *Chemical Engineering & Technology*, 23, (3), pp. 285-288.
16. Akay, G. and Tong, L. (2001) 'Preparation of colloidal low-density polyethylene latexes by flow-induced phase inversion emulsification of polymer melt in water', *Journal of Colloid and Interface Science,* 239, (2), pp. 342-357.
17. Akay, G. and Vickers, J. (2003) *Method of Separating Water-in-Oil Emulsions*. WO 02/10070.
18. Allen, R. M. and Vance Sande, J. B. (1982) 'The Structure of Electroless Ni-P films as a Function of Composition', *Scripta Metallugica*, 6, (10).
19. Allen, R. M. and VanderSande, J. B. (1982) *Proceedings - Electron Microscopy Society of America.*
20. Arabani, M. R. and Vaghefi, S. M. M. (2006) *"Proceedings - 15th IFHTSE - International Federation for Heat Treatment and Surface Engineering Congress 2006".*
21. Aronson, M. P. and Petko, M. F. (1993) 'Highly Concentrated water-in-oil Emulsion: Influence of Electrolyte on their Properties and Stabilities', *Journal of Colloid Interface Science,* 159, pp. 134.
22. Athavale, S. N. and Totlani, M. (1981) 'Electroless Nickel Coatings on Copper Electrode for Wear and Corrosion-Resistance', *Journal of the Electrochemical Society of India*, 30, (1), pp. 8-10.
23. Backovic, N., Janc?ic, M. and Radonjic, L. J. (1979a) 'Study of electroless Ni-P deposition on aluminium', *Thin Solid Films,* 59, (1), pp. 1-12.
24. Backovic, N., Jancovic, M. and Radonjic, L. J. (1979b) 'Study of electroless Ni-P deposition on aluminium', *Thin Solid Films*, 59, (1), pp. 1-12.
25. Balaraju, J. N., Jahan, S. M., Anandan, C. and Rajam, K. S. (2006) 'Studies on Eletroless Ni-W-P and Ni-W-Cu-P alloy coatings using chloride-based bath', *Surface and Coatings Technology,* 200, (16-17), pp. 4885.
26. Balaraju, J. N. and Rajam, K. S. (2005) 'Electroless Deposition of Ni-Cu-P, Ni-W-P and Ni-W-Cu-P Alloys', *Surface and Coatings Technology,* 195, (2-3), pp. 154.
27. Bandrand, D. W. (1994) *Electroless Nickel Plating.* ASM.
28. Banhart, J. (2001) ' Manufacture, characterisation and application of cellular metals and metal foams', *Progress in Materials Sci,* 46, (6), pp. 559-632.
29. Barbetta, A. and Cameron, N. (2004) 'Morphology and Surface Area of Emulsion-Derived (PolyHIPE) Solid Foams Prepared with Oil-Phase Soluble Porogenic Solvents:Span 80 as Surfactant', *Macromelecules,* 37, pp. 3188-3201.
30. Barbetta, A., Cameron, N. and Cooper, S. J. (2000) 'High internal phase emulsions (HIPEs) containing divinylbenzene and 4-vinylbenzyl chloride and the morphology of the resulting PolyHIPE materials', *Chem. Commun.*, pp. 221-222.

31. Barby, D. and Haq, Z. (1982) Eur Pat 0,060,138.
32. Barby, D. and Haq, Z. (1985) *Low Density Porous Cross-linked Polymeric Materials and their Preparation and use as Carries for including Liquids.* 4,522,955.
33. Baudrand, D. (1995) 'Electroless Plating Process', *Metal FINISHING* pp. 55-57.
34. Bera, D., Kuiry, S.C. and Seal, S. (2004) 'Synthesis of Nanostructured Materials using Template-Assisted Electrodeposition', *JOM,* 56, (1), pp`49-53.
35. Bertin, E. P. (1975) *Principles and Practice of X-ray Spectrometric Analysis.* New York: Plenum Press.
36. Bhumgara, Z. G. (1995a) 'PHP Foams Materials as Filteration Media', *Filtration and Separation,* 32, pp. 245-251.
37. Bhumgara, Z. G. (1995b) *Study of Development of PolyHIPE Foam Material for use in Separation Process* thesis. University of Exeter.
38. Binks, B. P. and Lumsdon, S. O. (1999) 'Stability of oil-in-water emulsions stabilised by silica particles', *Phys. Chem. Chem. Phys.,* 1, pp. 3007-3016.
39. Bladergroen, B. J., Maluleke, A. and Linkov, V. M. (2003) 'Electroconductive Coatings on Porous Ceramic Supports', *Journal of Applied Electrochemistry,* 33, (6), pp. 475.
40. Bokhari, M. (2003) *Bone Tissue Engineering using Novel Microcellular Polymer* thesis. University of Newcastle upon Tyne.
41. Bokhari, M., Birch, M. and Akay, G. (2003) 'Polyhipe polymer: A novel scaffold for in vitro bone tissue engineering', in *Tissue Engineering, Stem Cells and Gene Therapies.* Vol. 534 New York: Kluwer Academic/Plenum Publ, pp. 247-254.
42. Bokhari, M. A., Akay, G., Zhang, S. G. and Birch, M. A. (2005) 'Enhancement of osteoblast growth and differentiation in vitro on a peptide hydrogel - polyHIPE polymer hybrid material', *Biomaterials,* 26, (25), pp. 5198-5208.
43. Bouanani, M., Cherkaoui, F., Fratesi, R., Roventi, G. and Barucca, G. (1999) 'Microstructural Characterisation and Corrosion Resistance of Ni-Zn-P Alloys Electrolessly Deposited from a Sulphate Bath', *Journal of Applied Electrochemistry,* 29, (5).
44. Bragg, L. (1975) *The Development of X-ray Analysis.* London: G,Bell & Sons
45. Brown, I., J., Clift, D. and Sotiropolous, S. (1999) 'Preparation of Microporous Nickel Electrodeposits using a Poymer Matrix', *Materials Research Bulletin,* 34, pp. 1055-1064.
46. Butler, R., Davies, C. M. and Cooper, A. I. (2001) 'Emulsion Templating', *Adv. Mater,* 13, pp. 1459.
47. Byron, V. (2000) *The Development of Microcellular Polymers as a Support for Tissue Engineering* thesis. Newcastle University.
48. Calkan, B. (2006a) *Preparation of Novel Nano-structured Macro- and Meso-Porous Metal Foams for Process Intensification and Miniaturisation* thesis. University of Newcastle upon Tyne
49. Calkan, B., Akay, G. and Dogru, M. (2005) 'Nano-structured Micro-porous Catalysts for Intensified Catalysts*', 7th World Congress of Chemical Engineering.* Glasgow, Scotlant, IChemE.

50. Calkan, O. F. (2005) 'Nano-structured Electrically Conductive Polymers: Fabrication and Application', *7th World Congress of Chemical Engineering* Glasgow, Scotland, IChemE.
51. Calkan, O. F. (2006b) *Development of an Intensified Gasification System.* thesis. University of Newcastle upon Tyne.
52. Cameron, N. (2003) 'In Monolithics Materials', in *Journal of Chromatography Library.* Vol. 67 Burlington: Elsevier, pp. 255-276.
53. Cameron, N. and Barbetta, A. (2000) 'The Influence of Porogen Type on the Porosity, Surface Area and Morphology of poly(divinylbenzene) PolyHIPE Foams ', *Journal of Mater. Chem.*, 10, pp. 2466-2472.
54. Cameron, N. and Sherington, D. C. (1997) 'Preparation and Glass Transition Temperatures of Elastomeric PolyHIPE materials', *Journal of Mater. Chem.*, 7, (11), pp. 2209-2212.
55. Cameron, N. R. (2005) 'High Internal Phase Emulsion Templating as a Route to Well-Defined Porous Polymers', *Polymer*, 46, (5), pp. 1439-1449.
56. Cameron, N. R. and Sherrington, D. C. (1997) 'Synthesis and Characterisation of Poly(aryl ether sulfone) PolyHIPE Materials', *Makromolecules* 30, pp. 5860-5869.
57. Cameron, N. R., Sherrington, D.C, Ando, I. and Kurosu H. (1996a) 'Chemical Modification of Monolithic Poly(Styrene-Divinylbenzene) PolyHIPE Materials', *Journal of Mater. Chem.*, 6, (5), pp. 719-726.
58. Cameron, N. R., Sherrington, D.C., Albiston, L. Gregory, D.P. (1996b) 'Study of the Formation of the Open Cellular Morphology of Poly(Styrene/Divinylbenzene) PolyHIPE Materials by Cryo-SEM', *Colloid Polymer Science*, 274, pp. 592-595.
59. Carn, F., Colin, A., Achard, M.-F., Deleuze, H., Sellier, E., Birot, M. and Backov, R. (2004) 'Inorganic monoliths hierarchically textured via concentrated direct emulsion and micellar templates', *Journal of Materials Chemistry*, 14, (9), pp. 1370-1376.
60. Che, G., Lakshmi, B. B., Martin, C. R., Fisher, E. R. and Ruoff, R. S. (1998) 'Chemical Vapor Deposition Based Synthesis of Carbon Nanotubes and Nanofibers Using a Template Method', *Chemistry of Materials*, 10, (1), pp. 260-267.
61. Chen, B. H., Hong, L., Ma, Y. and Ko, T. M. (2002) 'Effects of surfactants in an electroless nickel-plating bath on the properties of Ni-P alloy deposits', *Industrial and Engineering Chemistry Research*, 41, (11), pp. 2668-2678.
62. Chen, Y., Kang, E. T., Neoh, K. G. and Huang, W. (2001) 'Electroless metallization of glass surfaces functionalized by silanization and graft polymerization of aniline', *Langmuir*, 17, (23), pp. 7425-7432.
63. Chiu, J. J., Pine, D. J., Bishop, S. T. and Chmelka, B. F. (2004) 'Friedel-Crafts alkylation properties of aluminosilica SBA-15 meso/macroporous monoliths and mesoporous powders', *Journal of Catalysis*, 221, (2), pp. 400-412.
64. Clegg, W. (1998) *Crytal Structue Determination.* London: Oxford Science Publication.
65. Colombo, P. (2008) 'Microporous Ceramic for Preceramic Precursors ', *Journal of The European Ceramic Society*, 28, (7), pp. 1389-1395.
66. Contreras, A., León, C., Jimenez, O., Sosa, E. and Pérez, R. (2006) 'Electrochemical behavior and microstructural characterization of 1026 Ni-B coated steel', *Applied Surface Science*, 253, (2), pp. 592-599.

67. Cooper, A. I. and Holmes, A. B. (1999) 'Macroporous Polymer Monolith', *Adv. Mater,* 11, pp. 2170.
68. Coppens, M. O., Froment, G.F. . (1997) 'The effectiveness of mass fractal catalysts', *Fractals,* 5, (3), pp. 493-505.
69. Coppens, M. O., Maschmeyer, J. T. (2001) 'Synthesis of hierarchical porous silica with a controlled pore size distribution at various length scales', *Catalysis Today,* 69, (1-4), pp. 331-335.
70. COULTER-manual. (1996) *COULTER^TM SA 3100^TM Series Surface Area and Pore Size Analysers.* Miami, Florida: Coulter Corporation.
71. Danumah, C., Vaudreuil, S., Bonneviot, L., Bousmina, M., Giasson, S. and Kaliaguine, S. (2001) 'Synthesis of macrostructured MCM-48 molecular sieves', *Microporous and Mesoporous Materials,* 44-45, pp. 241-247.
72. Davis, S. A., Burkett, S. L., Mendelson, N. H. and Mann, S. (1997) 'Bacterial templating of Ordered Macrostructures in Silica-surfactant mesophases', *Nature,* 385, (6615), pp. 420-.
73. Delaunois, F. and Lienard, P. (2002) 'Heat treatments for electroless nickel-boron plating on aluminium alloys', *Surface and Coatings Technology,* 160, (2-3), pp. 239-248.
74. Delaunois, F., Petitjean, J. P., Lienard, P. and Jacob-Duliere, M. (2000) 'Autocatalytic electroless nickel-boron plating on light alloys', *Surface and Coatings Technology,* 124, (2-3), pp. 201-209.
75. Deleuze, H., Desforges, A., Mondain-Monval, O. and M, O. (2002) 'Systhesis and Functionalisation of PolyHIPE beads', *Reactive and Funtional Polymers,* 53, pp. 183-192.
76. Dennis, J. K. and Such, T. E. (1972) *Nickel and Chromium Plating.* London: Newnes-Butterworth.
77. Dervos, C. T., Novakovic, J. and Vassiliou, P. (2004a). Electroless Ni-B and Ni-P coatings with high-fretting resistance for electrical contact applications.
78. Dervos, C. T., Novakovic, J. and Vassiliou, P. (2004b) 'Vacuum heat treatment of electroless Ni-B coatings', *Materials Letters,* 58, (5), pp. 619-623.
79. Dervos, C. T., Novakovic, J. and Vassiliou, P. (2005). 'Electroless Ni-B Plating with for electrical contact applications'. *Rev. Metal Madrid Vol. Extr.,* pp 232-238.
80. Di Giampaolo, A. R., Ordonez, J. G., Gugliemacci, J. M. and Lira, J. (1997) 'Electroless nickel-boron coatings on metal carbides', *Surface and Coatings Technology,* 89, (1-2), pp. 127-131.
81. Dogru, M. and Akay, G. (2004) *Gasification.* PCT/GB2004/004651
82. Doong, J. C. and Duh, J. G. (1993) 'Effects of pH values in electroless Ni plating on mild steel with TiN coating', *Surface and Coatings Technology,* 58, (1), pp. 19-28.
83. Dressick, W., Dulcey, C. S., Geoger Jr, J. H., Calabrese, G. S. and Calvert, J. M. (1994) 'Covalent Biding of Pd Catalyst to Ligating Self Assembly Monolayer Film for Selective Electroless Metal Deposition', *Journal of Electrochem Soc,* 141, (1), pp. 210-220.
84. Duncan, R. N. and Arney, T. L. (1984) 'Operation and use of Sodium Borohydribe-Reduced Electroless Nickel', *Plating Surface Finish,* 71, (12).

85. Duran, A., Castro, Y., Aparicio, M., Conde, C. and de Damborensa, J. J. (2007) 'Protecting and Surface modification of Metal with sol-gel coating', *International Material View*, 52, (3), pp. 175-192.
86. Durkin, B. and Steinecker. (2004) *Electroless Deposition.* John Wiley & Sons, Inc.
87. Dyson, D. J. (2004) *X-ray and Electron Diffraction Studies in Materials Science.* London: Maney Publishing.
88. Edwards, D. J., Gregory, D. P. and Sharpies, M. (1987) *Low Density Porous Elastic Crosslinked Polymeric Materials and their Preparation*. European Patent 0,239,360.
89. Elmes, A. R., Hammond, K. and Sherington, D. C. (1988) *Porous Materials and its Preparation* European Patent 0,289,238
90. Erhan, E., Yer, E., Akay, G., Keskinler, B. and Keskinler, D. (2004) 'Phenol degradation in a fixed-bed bioreactor using micro-cellular polymer-immobilized Pseudomonas syringae', *Journal of Chemical Technology and Biotechnology*, 79, (2), pp. 195-206.
91. Fan, H. F., Yan, H. J., Zhang, Y., Liu, Z. L. and Wang, L. (2008) 'Effects of heat treatment on properties of Ni-P coating on titanium alloy', *Cailiao Rechuli Xuebao/Transactions of Materials and Heat Treatment*, 29, (4), pp. 153-156.
92. Farr, J. P. G. and Noshani, A. (1996) 'Some Properties of Electroless Ni-P, Co-P and Ni-Co-P Deposits', *Tran Inst Met Finish*, 74.
93. Fellner, P. and Phuong Ky, C. (1996) 'Ni---B and Ni---Si composite electrolytic coatings', *Surface and Coatings Technology*, 82, (3), pp. 317-319.
94. Fields, W. D., Duncan, R. N. and Zickgraf, J. R. (1982) 'Electroless Nickel Plating', in *Metal Handbook - Surface Cleaning, finishing and Coating.* Vol. 5 United States: ASM Handbook Committee.
95. Fils, J. and Kanova, M. (2006) 'Electrochemical and surface Analytical Study of Vinyl-triethoxy Silane Films on Iron for Exposure to Air', *Eletrochimica Acta*, 51, (11), pp. 2338-2345.
96. Flacker, A., Gozzi, A. C., Rautemberg Finardi, M. and Fissore, A. (1995) *Preparation of Alumina Seramic Surface for electroless and Electrochemical Metal Deposited*.
97. Fuat, A. and Akay, G. (2006) 'Water Treatment by Microreactor', *CHISA 2006.* Prague, pp.
98. Garratt-Reed, A. J. a. B., D.C. (2003) *Energy Dispersive X-ray Analysis in the Electron Microscope* Oxford: Bios Scientific Publishers.
99. Gheorghiu, S. and Coppens, M. O. (2004) 'Optimal Bimodal pore network for heterogeneous', *AIChE Journal*, 50, (4), pp. 812-620.
100. Gitli, T. and Silverstein, M. S. (2008) 'Bicontinueos Hydrogel-Hydrophobic Polymer System through Emulsion Templated Simultaneous Polymerisation', *Soft Matter*, 4, (12), pp. 2475-2487.
101. Goldstein, J. I., Newbury, D. E., Echlin, P., Joy, D.C., Romig, A.D. Jr., Lyman, C.E., Fiori, C., Eric, E. (1992) *Scanning Electron Microscopy and X-ray Microanalysis.* New York: Plenum Press.
102. Gorbunova, K., Ivanov, M. and Moissev, V. P. (1973) 'Electroless Deposition of Nickel-Boron Alloys Mechanism of Process, Structure, and Some Properties of Deposits', *Journal of Electrochem Soc*, 120, (5), pp. 613-618.

103. Goyal, S. (2006) 'Silane: Chemistry and Application', *The Journal of Indian Prosthodontic Society*, 6, (1), pp. 14-18.
104. Gregory, D. P., Sharpies, M. and Tucker, I. M. (1989) Eur Pat Appl 299762.
105. Grosse, M., Lamotte, M., Birot, M. and Deleuze, H. (2007) 'Preparation of Microcellular Polysiloxane Monoliths', *Journal of Polymer Science*, 46, (1), pp. 21-32.
106. Gu, C., Lian, J., Li, G., Niu, L. and Jiang, Z. (2005) 'High corrosion-resistant Ni-P/Ni/Ni-P multilayer coatings on steel', *Surface and Coatings Technology*, 197, (1), pp. 61-67.
107. Haibach, K., Menner, A., Powel, R. and Bismarck, A. (2006) 'Tailoring Mechanical Properties of Highly Porous Polymer Foams: Silica Particle Reinforced Polymer Foams via Emulsion Templating ', *Polymer*, 47, (13), pp. 4513-4519.
108. Hainey, P., Huxham, I., B, R. M., Sherington, D. C. and Tetley, L. (1991) 'Systhesis and Ultrastructural Studies of Styrene-Divinylbenze PolyHIPE Polymers', *Macromelecules*, pp. 117-121.
109. Hamid, Z. A. (2003) 'Mechanism of Electroless Deposition of Ni-W-P Alloys by Adding Surfactant', *Surface Interface Anal*, 35.
110. Hamid, Z. A., Ghanem, W. A. and El Enin, S., A.A. (2005) 'Process Aspects of Electroless Deposition for Nickel-Zinc-Phosphoruous Alloys', *Surf Interface Anal*, 37, (10).
111. Haq, Z. (1985) *Crosslinked Absorbent Polymeric Materials*. 4,536,521
112. Hayman, M. W., Smith, K. H., Cameron, N. R. and Przyborski, S. A. (2004) 'Enhanced neurite outgrowth by human neurons grown on solid three-dimensional scaffolds ', *Biochem Biophy Res Commun*, pp. 483-488.
113. Henry, J. R. (2007) 'Electroless (autocatalytic) Plating', *Metal FINISHING*, 105, (10), pp. 350-360.
114. Hirth, F. W. and Speckhardt, H. (1972) '. Electroless Deposition of Ni-P Coatings, Their Structure and Changes by Heat Treatment', *ABSCHEIDUNG UND AUFBAU VON Ni-P-UEBERZUEGEN-VERAENDERUNG DURCH WAERMEBEHANDLUNG*, 26, (10), pp. 1012-1018.
115. Huang, Y. S. and Cui, F. Z. (2007) 'Effect of complexing agent on the morphology and microstructure of electroless deposited Ni-P alloy', *Surface and Coatings Technology*, 201, (9-11 SPEC. ISS.), pp. 5416-5418.
116. Huczko, A. (2000) 'Template based systhesis of nano materials', *Appl Phy*, 70, pp. 365-376.
117. Hulteen, J. C. and Martin, C. R. (1997) *J. Material. Chem.*, 7, (7), pp. 1075-1087.
118. Hulteen, J. C. a. M., C. R. (1997) 'A General Template-Based Method for the Preparation of Nanomaterials', *Journal of Mater. Chem.*, 7, (7), pp. 1075-1087.
119. Ikeda, Y., Watanabe, T., Tanabe, Y. and Hosoi, J. (1983) 'Latice Images of Amorphous-Like Ni-B Films Prepared by the Electroless Plating Method', *Nippon Kinzoku Gakkai-si*, 47, (3), pp. 175-179.
120. Ikem, V. O., Menner, A. and Bismarck, A. (2008) 'High Internal Phase Emulsions Stabilized Solely by Functionalized Silica Particles', *Angew. Chem. Int. Ed.*, 47, pp. 8277.

121. Imhof, A. and Pine, D. J. (1997) 'Ordered Macroporous Materials by Emulsion Templating', *Nature*, 389, (6654), pp. 948-951.
122. Ivanov, M. (2001) 'Electroless Nickel-Boron-Phosphorus Coatings: Protective and Functional Properties', *Protect Met*, 37, (6).
123. Jackson, B., Macary, R. and Shawhan, G. (1990) 'Low Phosphorus Electroless Nickel Coating Technology', *T I Met Finish*, 68.
124. Katsuhiko, T., Ken, O., Seiji, Y., Satoshi, K. and Hideo, H. (2002) 'Bath Stability of electroless Ni-B based Coatings as a Reducing Agents and evaluation of Solder Wettability of Deposited Films', *Journal of Japan Institute of Electronic Packaging*, 5, (6), pp. 591-598.
125. Kim, D. H., Aoki, K. and Takano, O. (1995) 'Sort-Magnetic Films by Eletroless Ni-Co-P Plating', *Journal of Electrochem Soc*, 142, (11).
126. Kim, S.-H., Shin, C.-K., Ahn, C.-H. and Kim, G.-J. (2006) 'Syntheses and application of silica monolith with bimodal meso/macroscopic pore structure', *Journal of Porous Materials*, 13, (3), pp. 201-205.
127. Kiparisov, S. Y. and Vershinin, V. V. (2001) 'Structure and Magnetic Properties of the Ni-Co-P Films in the Region of Transition form the Crystalline to the Amorphous Phase', *Phys Met Metalloved*, 92, (1).
128. Klugg, H. P. and Alexander, L. E. (1974) *X-ray Diffraction Procedures.* New York: Wiley & Sons.
129. Kreutzer M.T., K., F., Moulijn, J.A., and Heiszwolf, J.J. (2005) ' Multiphase monolith reactors: Chemical reaction engineering of segmented flow in microchannels', *Chem. Eng. Sci.*, 60, (5895-5916).
130. Krishnan, K. H., Praveen, J., Ganesan, M., Kavimani, P. M., John, S. and Srinivasan, K. N. (2006) 'Electtoless Ni-P-Based composite coatings', *Materials Performance*, 45, (8), pp. 36-39.
131. Krishnaveni, K., Sankara Narayanan, T. S. N. and Seshadri, S. K. (2006) 'Electrodeposited Ni-B coatings: Formation and evaluation of hardness and wear resistance', *Materials Chemistry and Physics*, 99, (2-3), pp. 300-308.
132. Kumar, P.S. and Nair, P.K. (1994) '(Effect of Phosphorus on the relative proportions of crystalline and amorphous phases in elctroless Ni-P deposits'. *Journal of Materials Science Letters*, 13, (9), pp 671-674.
133. Li, J., Jiguang, W., Jioa, J. and Zhang, Z. (2008) 'Controlled Sysnthesis of Monolithic Hierarchical Porous Materials using wood as Template with Assistance of Supercritical Carbon Dioxide', *Industrial and Engineering Chemistry Research*, 47, (20), pp. 7680-7685.
134. Liew, M. K. H., Meihua, L. and Yong, Z. (2006) 'Preparation of Porous Materials with Ordered Hole Structure', *Advances in Colloid and Interface Science*, 121, pp. 9-25.
135. Lifshin, E. (1999) *X-ray Characterisation.* London: Wiley-VCH.
136. Lin, C.J and He, J.L. (2005) 'Cavitations Erosion Behavior of Electroless Nickel –Plating on AISI1045 Steel', *Wear 259*, pp 154-159.
137. Lindberg, R., Sundholm, G., Øye, G. and Sjöblom, J. (1998) 'A new method for following the kinetics of the hydrolysis and condensation of silanes', *Colloids and Surfaces A: Physicochemical and Engineering Aspects*, 135, (1-3), pp. 53-58.
138. Lissant, K. J. (1974) *Emulsions and Emulsions Technology Part 1.* New York: Marcel Dekker Inc.

139. Lissant, K. J. (1984) *Emulsions and Emulsions Technology, Part III.* New York: Marcel Dekker.
140. Liu, W. L., Hsieh, S. H., Tsai, T. K., Chen, W. J. and Wu, S. S. (2006) 'Temperature and pH dependence of the electroless Ni-P deposition on silicon', *Thin Solid Films,* 510, (1-2), pp. 102-106.
141. Lowell, S. and Sheilds, J. E. (1991) *Powder Surface Area and Porosity.* London: Chapman & Hall.
142. Lu, L. and Eychmuller, A. (2008) 'Ordered Macroporous Bimetallic Nanostructures: Design, Characterisation and Applicaitons', *Acc. Chem. Res,* 4, (2), pp. 244-253.
143. Maekawa, H., Esquena, J., Bishop, S., Solans, C. and Chmelka, B. F. (2003) 'Meso/macroporous inorganic oxide monoliths from polymer foams', *Advanced Materials,* 15, (7-8), pp. 591-596.
144. Makarov, V. F., Prusov, Y. V. and Lebedeva, I. O. (2005) 'Electroless deposition of nickel coatings with high phosphorus content', *Russian Journal of Applied Chemistry,* 78, (1), pp. 82-84.
145. Mallory, M. O. (1990) *Electroless Plating:Fundamentals dan Applications.* Americans Electro platers and Surface Finishers Society.
146. Martin, C. (1996) 'Membrane based Synthesis of Nanomaterials', *Adv. Mater,* 8, (8), pp. 1739-1746.
147. Martin, J. C. H. a. C. R. (1997) 'A general template-base method for the preparation of nanomaterials', *J. Mater. Chem.,* 7, (7), pp. 1075-1087
148. Mc Comas, E. (2002) *Nodular Boron Coating*. .
149. Menner, A., Salgueiro, M., Shaffer, M. S. P. and Bismarck, A. (2008) 'Nanocomposite Foams obtained by Polymerisation of High Internal Phase Emulsion', *Journal of Polymer Science PartA:Polymer chemistry,* 14, (16), pp. 5708-5714.
150. Mezzenga, R., Ruokolainen, J., Fredrickson, G. H. and Kramer, E. J. (2003) 'High Internal Phase Polymeric Emulsions by Self-Assembly of Colloidal Systems', *Macromelecules,* 36, pp. 4466-4471.
151. Mohamed, R., Noor, Z. Z., Calkan, O. F., Calkan, B., Ndlovu, T. M., Burke, D. and Akay, G. (2006) 'Development of Catalytic Micro-reactors with Ultra-high Surface Area-to-Volume Ratio for Bioprocess and Chemical Process Intensification', *CHISA 2006.* Prague.
152. Moulijn, J. A., Kreutzer, M.T., F. Kapteijin (2005) 'The Chemical Engineer,' pp. 32-34.
153. Munt, S. (2000) *Gas Adsorption and Desorption.* Beckman Coulter.
154. Nakamura, N., Takahashi, R., Suto, S., Sodesawa, T. and Yoshida, S. (2000) 'Ni/SiO2 Catalyst i Hierarchical Pore Structure Prepared by Phase Separation in sol-gel Process', *Physical Chemistry Chemical Physics s,* 21, pp. 4983-4990.
155. Narayanan, S. T. S. N., Krishnaveni, K. and Seshadri, S. K. (2003) 'Electroless Ni-P/Ni-B duplex coating: preparation and evaluation of microhardness, wear and corrsion resistance', *Mat Chem Phy,* 82, pp. 771.
156. Narayanan, S. T. S. N. and Seshadri, S. K. (2004) 'Formation and Characterisation of Borohydribe Reduced Electroless Nickel Deposits', *Journal of Alloy and Compounds,* 365, pp. 197-205.
157. Nishihara, H., Mukai, S. R., Yamashita, D. and Tamon, H. (2005) 'Ordered Macroporous Silica by Ice Templating', *Chem Mater,* 17, (3), pp. 683-689.

158. Noor, Z. Z. (2006) *Intensification of Separation Processes using Fuctionalised PolyHIPE Polymers.* thesis. University of Newcastle upon Tyne.
159. Noor, Z. Z., Akay, G., Dogru, M. and Larter, S. R. (2005) 'Process Intensification in water-crude oil separation by simulteneous application of electric field and novel micro-porous polymeric demulsifiers. *' 7th World Congress of Chemical Engineering.* Glasgow, Scotland, IChemE.
160. Normatov, J. and Silverstein, M. S. (2007) 'Porous interpenetrating network hybrids synthesized within high internal phase emulsions', *Polymer,* 48, (22), pp. 6648-6655.
161. Nuffield, E. W. (1966) *Diffraction Methods.* London: John Wiley & Sons
162. Oatley, C. W. (1972) *The Scanning Electron Microscope. Part 1. The Instrument.* London: Cambridge University Press.
163. Ocampo, F., Yun, H. S., Pereira, M. M., Tessonnier, J. P. and Louis, B. (2009) 'Design of MFI Zeolite-Based Composites with Hierarchical Pore Structure: A New Generation of Structured Catalysts', *Crystal Growth & Design,* 9, (8), pp. 3721-3729.
164. Oraon, B., Majumdar, G. and Ghosh, B. (2007) 'Parametric optimization and prediction of electroless Ni-B deposition', *Materials & Design,* 28, (7), pp. 2138-2147.
165. Oraon, B., Majumdar, G. and Ghosh, B. (2008) 'Improving hardness of electroless Ni-B Coating using Optimised Deposition Condition and Anneling', *Materials & Design,* 29, (7), pp. 1412-1418.
166. Palaniappa, M. and Seshadri, S. K. (2007) 'Hardness and structural correlation for electroless Ni alloy deposits', *Journal of Materials Science,* 42, (16), pp. 6600-6606.
167. Pierson, H. O. (1999) *Handbook of Chemical Vapour Deposition: Principle, Technology and Application.* New York: Noyes Publication.
168. Pizzi, A. and Mittal, K. L. (1994) *Handbook of Adhessive Technology.* New York: MDI.
169. Pleudemann, E. P. (1982) *Silane Coupling Agent.* New York and London: Plenum Press.
170. Plueddemann, E. P. (1983) 'Silane Adhesion Promoters in Coatings', *Prog.Org. Coat.,* 11, (3), pp. 297.
171. Prusov, Y. V. and Makasov, V. F. (2005) 'Some Properties of Chemically Deposited Ni-B Coatings', *Russian Journal of Applied Chemistry,* 78, (2), pp. 193-196.
172. Qiao, X., Xu, W., Wu, Y. and Sun, P. (1995) 'Effects of deposition process on phosphorus content in electroless Ni-P coatings', *Acta Metallurgica Sinica Series A, Physical Metallurgy & Materials Science,* 8, (2), pp. 115-117.
173. Rao, Q., Bi, G., Lu, Q., Wang, H. and Fan, X. (2005) 'Mictrostructure Evolution of Electroless Ni-B Film during its Depositing Process'. *Applied Surface Science,* 240, pp 28-33.
174. Riedel, W. (1991) *Electroless Nickel Plating.* Stevenage, Herfordshire, UK: Finishing Publications Ltd.
175. Riedel, W. and Bailer, T.O. (2005) 'Friction and Wear Reduction via a Ni-B Electroless Bath Coating for Metal Alloys'. *JOM,* pp 40-45.

176. Roger, C., Hampden-Smith, M. J., Scaefer, D. W. and Beaucage, G. (1994) 'General Route to Porous Metal Oxide via Inorganic and Organic Template', *Journal of Sol-Gel Science and Technology,* 2, (1-3), pp. 67-72.
177. Saito, T., Sato, E., Matsuoka, M. and Iwakura, C. (1998) 'Electroless deposition of Ni–B, Co–B and Ni–Co–B alloys using dimethylamineborane as a reducing agent', *Journal of Applied Electrochemistry,* 28, (5), pp. 559-563.
178. Saito, T., Sato, E., Matsuoka, M. and Iwakura, C. (1999) 'Effect heat treatment on Magnetic properties of Electroless Ni-B Films', *Plating Surface Finishing,* 86, (2), pp. 53-57.
179. Salager, J. L. (1988) *Phase Transformation and Emulsions Inversions on the Basis of Catastrope Theorry: In Encyclopedia of Emulsions Technology.* New York: Marcel Dekker.
180. Sen, T., Tiddy, G. J. T., Casci, J. L. and Anderson, M. W. (2004) 'Synthesis and Characterization of Hierarchically Ordered Porous Silica Materials', *Chemistry of Materials,* 16, (11), pp. 2044-2054.
181. Sen, T., Tiddy, G. J. T., Casci, J. L. and Anderson, M. W. (2005) 'Meso-cellular silica foams, macro-cellular silica foams and mesoporous solids: a study of emulsion-mediated synthesis', *Microporous and Mesoporous Materials,* 78, (2-3), pp. 255-263.
182. Sherington, D. C. (1991) *Makromol. Chem. Symp,* 70, pp. 303.
183. Sherrington, D. C. (1998) 'Preparation, Structure and Morphology of Polymer Supports', *Chem. Commun.*, pp. 2275-2286.
184. Shin, Y., Wang, L. Q., Liu, J. and Exarhos, G. J. (2003) 'pH-Controlled Synthesis of Hierarchically Ordered Ceramics with Wood Cellular Structures by Surfactant-Directed Sol-Gel Procedure.' *Journal of Industrial & Engineering Chemistry* 9 (1), pp. 76-82.
185. Shin, Y. Q., Wang, C. and Exarhos, G. J. (2005) 'Synthesis of SiC Ceramics by the Carbothermal Reduction of Mineralized Wood with Silica', *Adv. Mater,* 17, (1), pp. 73-77.
186. Silberzan, P., Leger, L., Ausserre, D. and Benatter, J. J. (1991) 'Silanation of Silica Surface: A New Method of Constructing Pure or Mixed Layers', *Langmuir,* 7, (8), pp. 1647-1651.
187. Silverstein, M. S. and Normatov, J. (2007) 'Nanoporous Polymer Nanocomposites Synthesized within High Internal Phase Emulsions', *Polymer,* 48, (88), pp. 25-30.
188. Sotiropolous, S., Brown, I., J., Akay, G. and Lester, E. (1998) 'Nickel Incorporation into a Hollow Fibre Microporous Polymer: A Preparation Route for Novel High Surface Area Nickel Structures', *Materials Letters,* 35, pp. 389-391.
189. Staia, M. H., Puchi, E. S., Castro, G., Ramirez, F. O. and Lewis, D. B. (1999) 'Effect of thermal history on the microhardness of electroless Ni-P', *Thin Solid Films,* 355, pp. 472-479.
190. Stankiewicz, A., Moulijn, J.A. (2004) *Re-engineering The Chemical Processing Plant,*. New York: Maecel Dekker, Inc.
191. Stevanovic, R., Stevanovic, J. and Despic, A. (1999) 'Electrochemical activation of the electroless deposition of Ni-P alloy and phase structure characterization of the deposit. Part I: Dual bath system', *Journal of Applied Electrochemistry,* 29, (6), pp. 747-752.

192. Su, B. T., Wang, K., Zuo, X. W., Mu, H. M., Dong, N., Tong, Y. C., Bai, J. and Lei, Z. Q. (2007) 'Facile Synthesis of ZnO Hollow Fibres', *Bulletin of Material Science,* 30, (6), pp. 570-574.
193. Su, Z., Hsu, S. L. and Li, X. (2002) 'Spectroscopic and thermal studies of sulfonated syndiotactic polystyrene', *Macromolecules,* 27, (1), pp. 287-291.
194. Suda, H., Watanabe, T., Misaki, Y. and Tanabe, Y. (1981) 'Amorphous Like Ni-B Alloy Prepared by Electroless Plating Method using Dimethylamine Borance as Reducing Agent', *Nippon Kinzoku Gakkai-si,* 45, (1), pp. 5-12.
195. Suryanarayana, S. (2002) 'The Structure and Properties of Nanocrytalline Mterials: Issue and Concerns', *JOM,* 54, (9), pp24-27.
196. Suzuki, K., Ikari, K. and Hiroaki, I. (2003) 'Synthesis of Mesoporous Silica Foams with Hierarchical Trimodal Pore Structure', *Journal of Mater. Chem.,* 13, pp. 1812-1816.
197. Tai, H., Sergienko, A. and Silverstein, M. S. (2001) 'Organic-inorganic networks in foams from high internal phase emulsion polymerizations', *Polymer,* 42, (10), pp. 4473-4482.
198. Thaler, W. A. (1983) 'Hydrocarbon-Soluble Sulfonating Reagents. Sulfonation of Aromatic Polymers in Hydrocarbon Solution Using Soluble Acyl Sulfates', *Macromelecules,* 16, pp. 623-628.
199. Thornton, P. R. (1968) *Scanning Electron Microscopy.* London: Chapman and Hall.
200. Tomlinson, W. J. and Wilson, G. R. (1989) 'Oxidation of electroless Ni-B and Ni-P coatings in air at 800°C to 1000°C', *J. Mat of Sc,* 21, pp. 97-102.
201. Velev, O. D., Jede, T. A., Lobo, R. F. and Lenhoff, A. M. (1998) 'Microstructure Porous Silica obtained via Colloidal Crystal Template', *Chem. Mater,* 10, (11), pp. 3597.
202. Velev, O. D. and Lenhoff, A. M. (2000) 'Colloidal Crystals as Templates for Porous Materials', *Curr Opin Colloidal Interface Sci,* 5, (1), pp. 56.
203. Wakeman, R. J. and Akay, G. (1996) 'Special topic issue - Process intensification,' *Chemical Engineering Research & Design,* 74, (A5), pp. 509-509.
204. Wakeman, R. J., Bhumgara, Z. G. and Akay, G. (1998) 'Ion exchange modules formed from polyhipe foam precursors', *Chemical Engineering Journal,* 70, (2), pp. 133-141.
205. Walker, P. (1992) *Silane and other Coupling Agent.* Ytrecht: VSP.
206. Walsh, D. C., Stenhouse, J., I, T, Kingbury, L. P. and J, W. E. (1996) 'PolyHIPE Foam: Production, Characterisation and Performance as Aerosol Filteration Materials.' *Journal of Aerosol Science,* 27, pp. S629-S630.
207. Wan, H. H. and Cheh, H. Y. (1988) 'The Current Distribution on a Rotating Disk Electrode in Galvanostatic Pulsed Electrolysis', *135,* 3, pp. 643-658.
208. Wang, Y., Tang, Y., Dong, A., Wang, X., Ren, N., Shan, W. and Gao, Z. (2002) 'Self, Supporting porous Zeolite Membranes with Sponge like Architecture and Zeolite Microtube', *Advance Materials,* 14, (13-14), pp. 994-997.
209. Warren, B. E. and Biscoe, J. B. (1938) *Journal of American Ceramic Soc,* 21, (49).
210. Watanabe, T. (2004) *Nano-plating: Microstructure Contol Theory of Plated Film and Data Base of Plate Film Microstructure.* Oxford: Elsevier.

211. Watanabe, T. and Tanabe, Y. (1975) 'Ni-B Amorphos Alloy Film Deposited by Electroless Deposition Method', *Nippon Kinzoku Gakkaishi/Journal of the Japan Institute of Metals,* 39, (8), pp. 831-836.
212. Watanabe, T. and Tanabe, Y. (1976) 'Misfit Twin Crystals in Nickel Film Deposit on (001) Iron Substrate', *JIM,* 17, (10), pp. 655-662.
213. Watanabe, T. and Tanabe, Y. (1983) 'Latice Images of Amorphous-Like Ni-B Alloy Films Prepared by Electroless Plating Method', *Transactions of the Japan Institute of Metals,* 24, (6), pp. 396-404.
214. Watanabe, T., Tanabe, Y. and Imamura, N. (1979) 'Anomalos Magnetization Temperature Characteristic in Electroless Ni-B Amorphous Ni-B Plating Films', *Memoirs of Faculty of Technology, Tokyo Metropolitan University,* (29), pp. 2859-2867.
215. Weetall, H. (1993) 'The activation of inorganic carriers by silanization', *Biosensors and Bioelectronics,* 8, (5),pp. x-xi.
216. Weightman, R. F. and Pearlstein, F. (1974) 'Hardness and Wear Resistance of Electroless Nickel-Phosphorus and Nickel-Boron Deposits', *METAL FINISHING MAGAZINE,* 72, (9).
217. William, J. M. (1988) 'Toroidial Microstructure from Water in-Oil Emulsions', *Langmuir,* 4, pp. 44-49.
218. William, J. M. (1991) 'High Internal Phase Water-in-Oil Emulsions:Influence of Surfactant and Cosurfactant on Emulsions Stability and Foam Quality', *Langmuir,* 7, (7), pp. 1370-1377.
219. William, J. M. and Wrobleski, D. A. (1989) 'Microstrucutre and Properties of some Microcellular Foams', *Journal of Material Science Letters,* 24, pp. 4062-4067.
220. Williams, J. M., Gray, A.J. and Wilkerson, M.H. (1990) 'Emulsions Stability and Rigid Foams from Styrene or Divinylbenzene Water-in-Oil Emulsions', *Langmuir,* 6, pp. 437-444.
221. Williams, J. M. and Wrobleski, D. A. (1988) 'Spatial Distribution of the Phase in Water-in-Oil Emulsions. Open and Closed Microcellular Foams from Cross- Linked Polystyrene. ' *Langmuir,* 4, pp. 656-662.
222. Witucki, G. L. (1993) 'A Silane Primer: Chemistry and Applications of Alkoxy Silane', *A Journal of Coatings Technology* 65, (822), pp. 57-60.
223. Wu, Y. C., Li, G. H. and Zhang, L. (2000) 'Wear resistance of electroless deposited Ni-P and Ni-P/SiC composite coatings on low alloy cast iron', *Surface Engineering,* 16, (6), pp. 506-510.
224. Xia, Y. N., Gates, B., Yin, Y. D. and Lu, Y. (2000) 'Monodispersed Colloidal Spheres:Old Materials with New Application', *Adv. Mater,* 12, (10), pp. 693.
225. Xianglin, Y., Shujang, D., Zhaokai, M., Jigung, L., Xiaozhang, Q., Yngfeng, L. and Zhengzhong, Y. (2008) 'Aerosol Asisted Synthesis of Silica/Phenolic Resin Composite Mesoporous hollow Spheres', *Coloid & Polymer Sc,* 286, (12), pp. 1361-1368.
226. Xu, L., Liao, J., Huang, L., Ou, D., Guo, Z., Zhang, H. and Ge, C. (2005) 'Surface bound nanoparticles for initiating metal deposition', *Thin Solid Film,* 434, pp. 121-125.
227. Yang, P., Deng, T., Zhao, D., Feng, P., Pine, D., Chmelka, B. F., Whitesides, G. M. and Stucky, G. D. (1998) 'Hierarchically Ordered Oxides', *Science,* 282, (5397), pp. 2244-2246.

228. Yin, X. J., Zhu, G. S., Yang, W. S., Li, Y. S., Zhu, G. Q., Xu, R., Sun, J. Y., Qiu, S. L. and Xu, R. R. (2005) 'Stainless-steel-net-supported zeolite NaA membrane with high permeance and high permselectivity for oxygen over nitrogen', *Advanced Materials,* 17, (16), pp. 2006-+.
229. Yokota, T., Takahata, Y., Katsuyama, T. and Matsuda, Y. (2001) 'A New Technique for Preparing Ceramic for Catalysis Support Exhibiting High Porosity and High Resistance', *Catalysis Today,* 69, (1-4), pp. 11-15.
230. Yu, J., Yu, J. C., Leung, K. P., Ho, W., Cheng, B., Zhao, X. and Zhao, J. (2003) 'Effects of acidic and basic hydrolysis catalysts on the photocatalytic activity and microstructures of bimodal mesoporous titania', *J. Catal.,* 217, (69).
231. Yuan, Z.-Y. and Su, B. L. (2005) 'Insight into Hierarchically meso-macroporous structured materials', *Journal of Mater. Chem.,* 16, pp. 663-677.
232. Zhai, S.-R. and Chang, -. S. H. (2008) 'Structureal and Catalytic Characterisation of Nanosized Mesoporous Aluminosilicatas Synthesis via a Novel Two Step Route', *Catalysis Today,* 131, (1-4), pp. 55-60.
233. Zhang, H. and Cooper, A. I. (2005a) 'Emulsion-Templated Hierarchically Porous Silica Beads Using Silica Nanoparticles as Builidng Blocks', *Industrial and Engineering Chemistry Research,* 44, pp. 8707-8714.
234. Zhang, H. and Cooper, A. I. (2005b) 'Synthesis and Application of Emulsion-Templeted Porous Material', *Soft Matter,* 1, pp. 107-113.
235. Zhao, D., Yang, P., Chmelka, F. and Stucky, G. D. (1999) 'Multiphase Assembly of Mesoporous Macroporous Membranes', *Chem Mater,* 11, (5), pp. 1174-1178.
236. Zhou, X., Lin, Q., Xiong, R., Cui, X. and Dai, G. (2005) 'Effect of flexible polymer coating on interfacial adhesion of glass fibre reinforced polypropylene', *Polymers and Polymer Composites,* 13, (6), pp. 619-625.
237. Zinck, P., Mäder, E. and Gerard, J. F. (2001) 'Role of silane coupling agent and polymeric film former for tailoring glass fiber sizings from tensile strength measurements', *Journal of Materials Science,* 36, (21), pp. 5245-5252.
238. Ziyuan, S., Deqing, W. and D, Z. (2004) 'Surface Strengthening pure copper by Ni-B Coating', *Appl Surf Sci,* 221, pp. 62.

APPENDIX A

LIST OF PUBLICATION

Akay, G., Calkan, B. and **Mohamed, R**., Hasan, H., British Patent Application Number 0818520.9 (2008), *"Preparation of Nano-Structured Micro-Porous Composite Foam"*,

Calkan, B., **Mohamed, R**., Akay, G., *Preparation of Catalyst Systems with Enhanced Accessibility Of Active Sites for Process Intensification* in 17th International Congress of Chemical And Process Engineering, Prague, Czech Republic, 2006.

Mohamed, R., Noor Z.Z., Calkan O.F., Calkan B., Ndlovu T.M., Burke D and Akay G., *Development of catalytic micro-reactors with ultra-high surface area-to-volume ratio for bioprocess and chemical process intensification* in 17th International Congress of Chemical And Process Engineering, Prague, Czech Republic, 2006

Mohamed, R., B. Calkan, K. Premasthian, A. El-Nagger, and G. Akay**.** *Preparation of nano-structured macro-porous metallic and ceramic monolithic micro-reactors for process intensification* in International Workshop on process Intensification 2008, Tokyo, Japan, 2008.

APPENDIX B

PATENT APPLICATION

Preparation of Nano-Structured Micro-Porous Composite Foam

Inventor: Akay, G., Calkan, B., **Mohamed, R**. and Hasan, H.

Application Number: 0818520.9 (2008),

APPENDIX C

PHP3

Ni-B as deposited condition

Ni-B after heat treatment 600°C

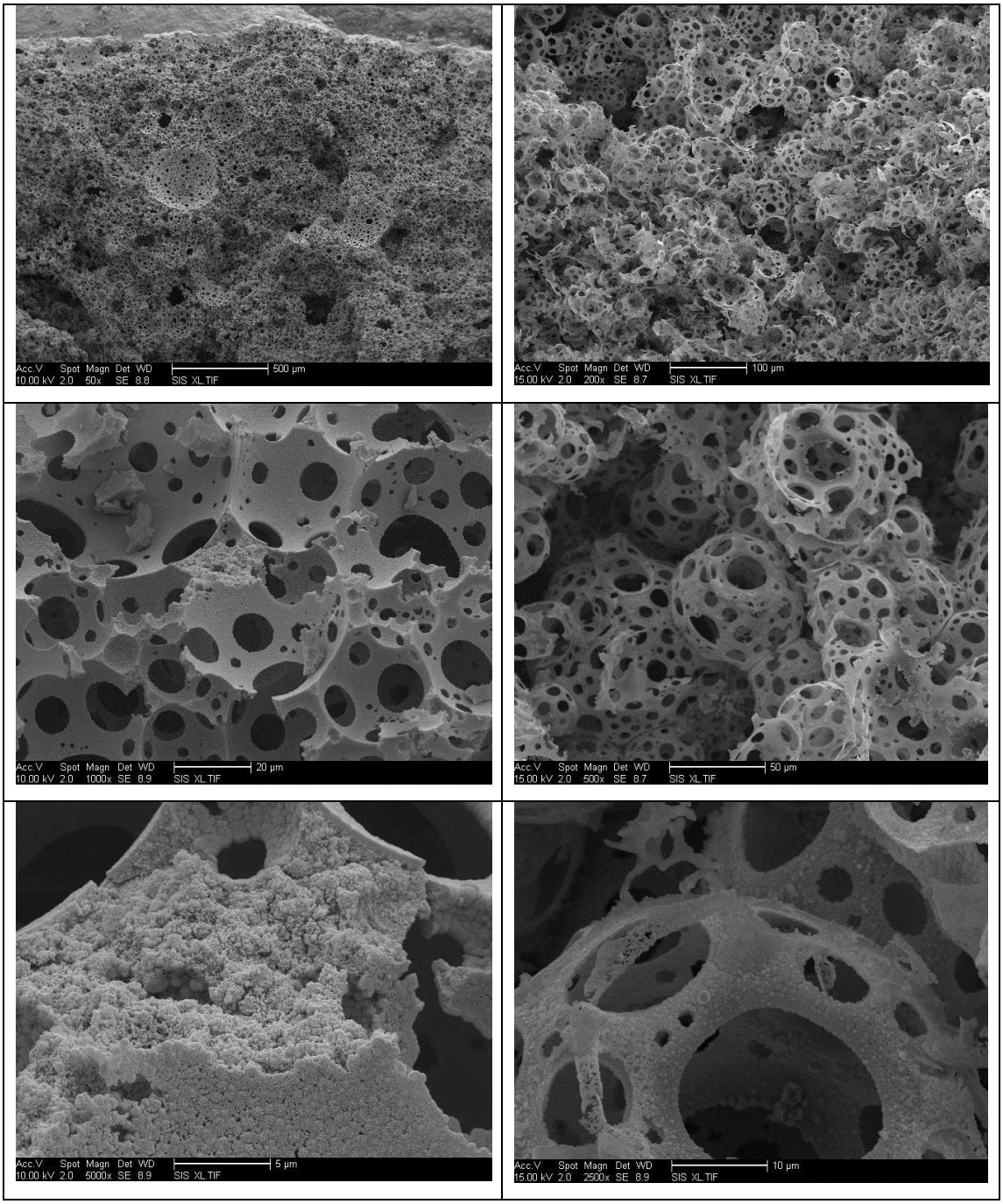

Continue next page

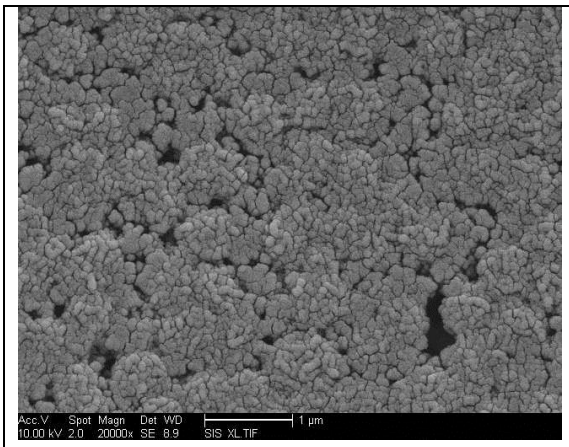

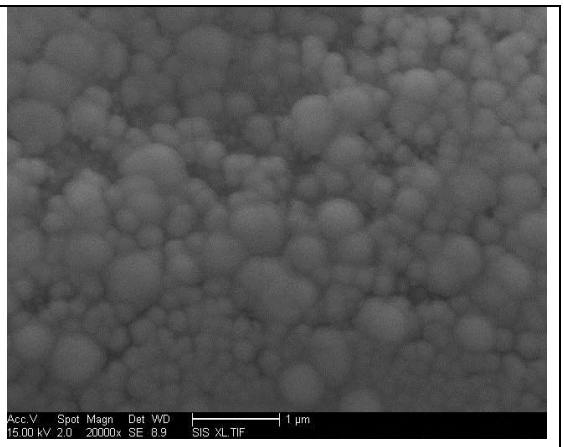

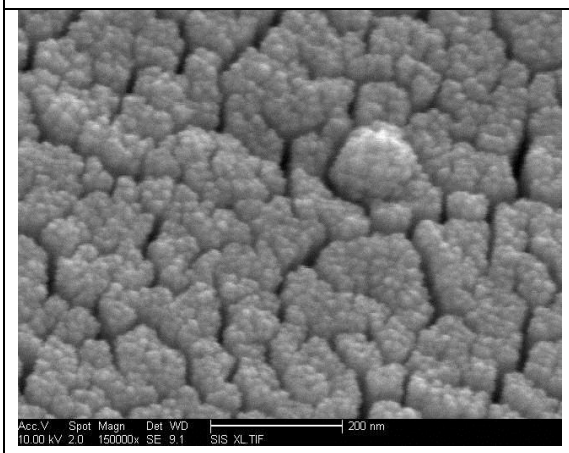

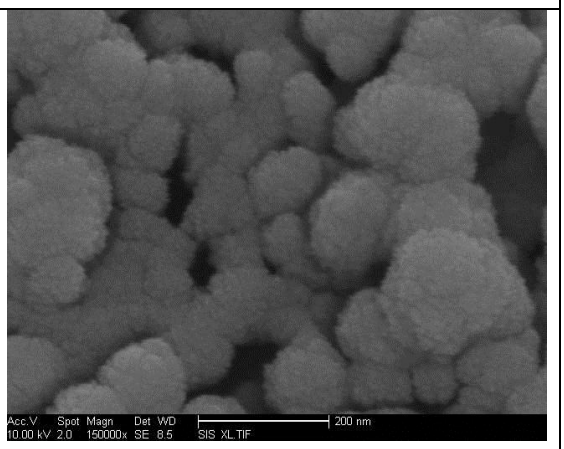

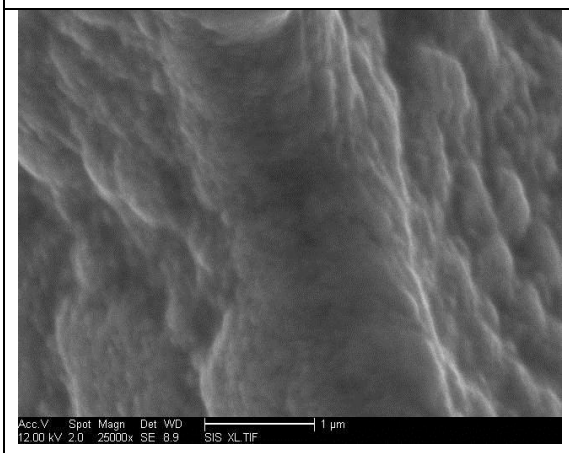

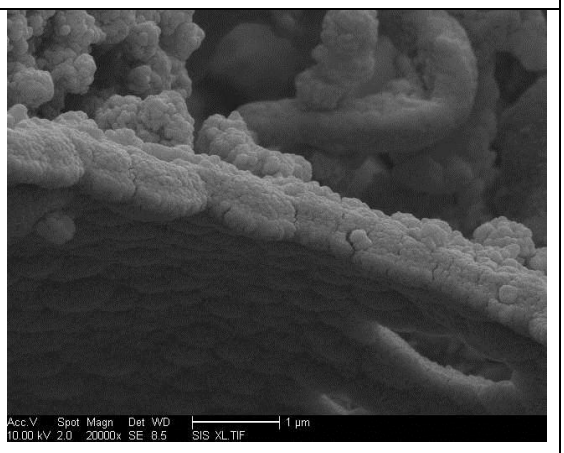

Continue next page

SEM micrograph of compress PHP

Ni-B deposits on compress PHP as deposited condition	Ni-B deposits on compress PHP after heat treatment at 600°C
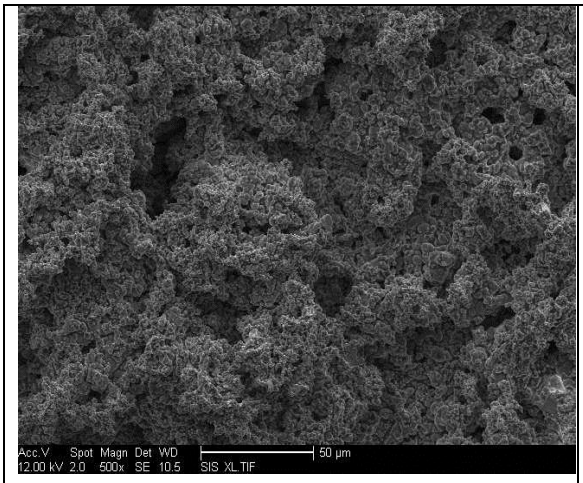	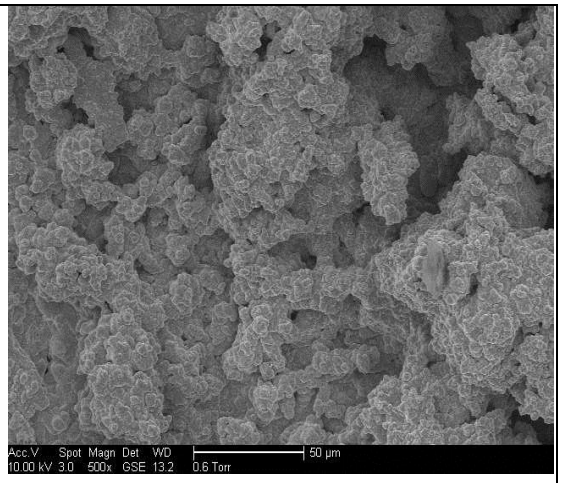
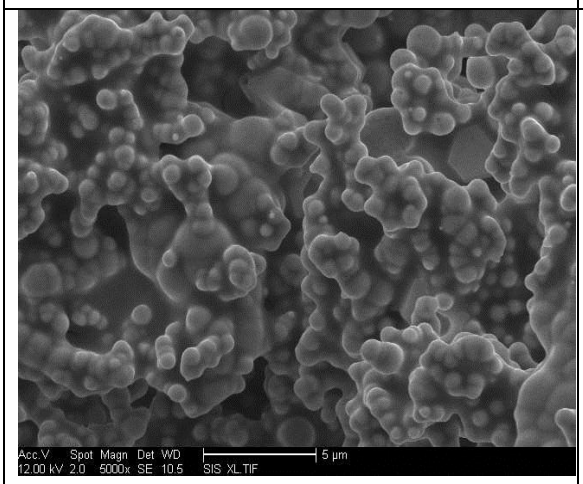	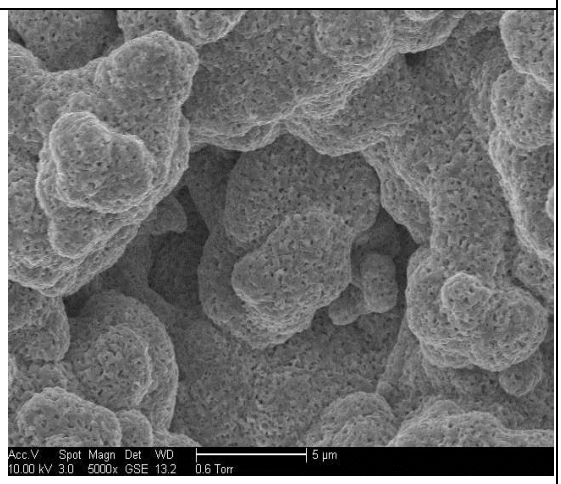
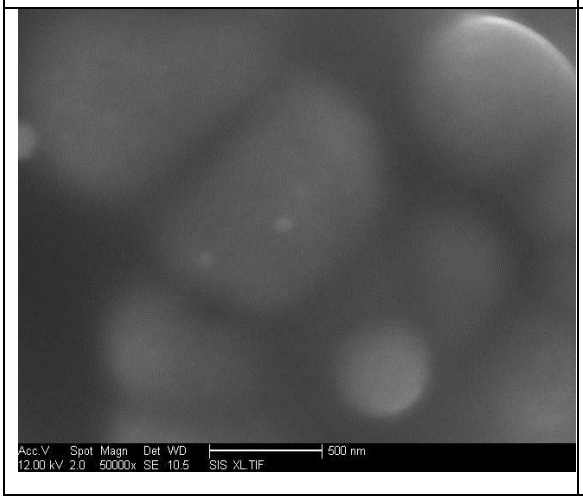	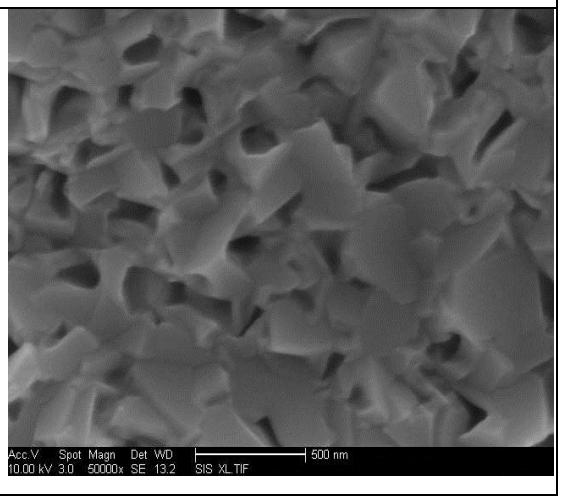

Continue next page

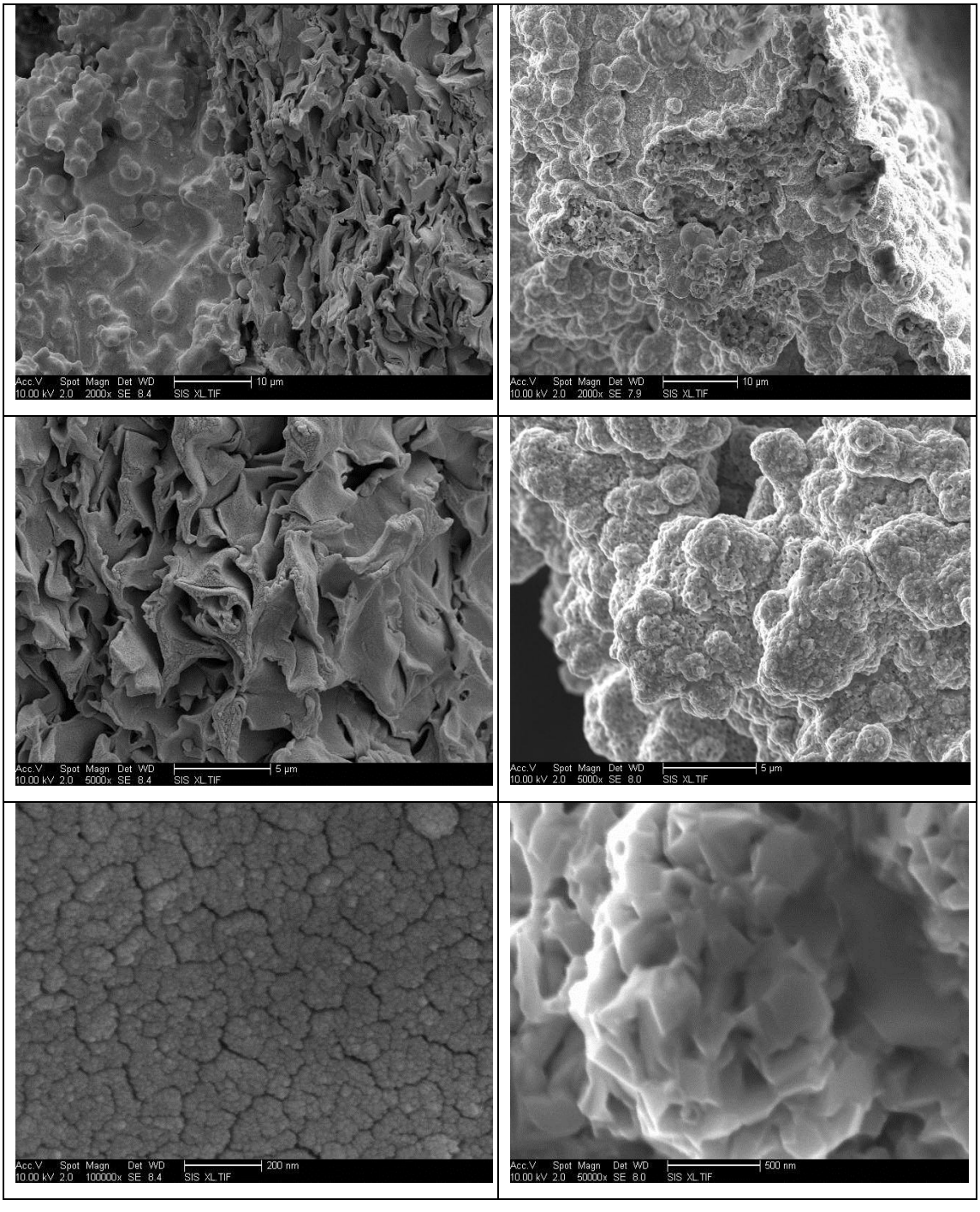
Acc.V Spot Magn Det WD 10 µm
10.00 kV 2.0 2000x SE 8.4 SIS XL.TIF
Acc.V Spot Magn Det WD 10 µm
10.00 kV 2.0 2000x SE 7.9 SIS XL.TIF
Acc.V Spot Magn Det WD 5 µm
10.00 kV 2.0 5000x SE 8.4 SIS XL.TIF
Acc.V Spot Magn Det WD 5 µm
10.00 kV 2.0 5000x SE 8.0 SIS XL.TIF
Acc.V Spot Magn Det WD 200 nm
10.00 kV 2.0 100000x SE 8.4 SIS XL.TIF
Acc.V Spot Magn Det WD 500 nm
10.00 kV 2.0 50000x SE 8.0 SIS XL.TIF

PHP at various cell temperature

Cell temperature operated at 35°C Cell temperature operated at 50°C Cell temperature operated at 75°C Cell temperature operated at 90°C

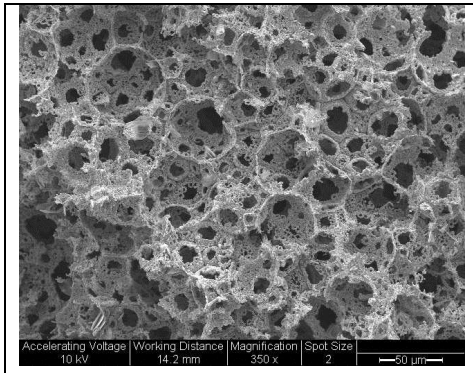

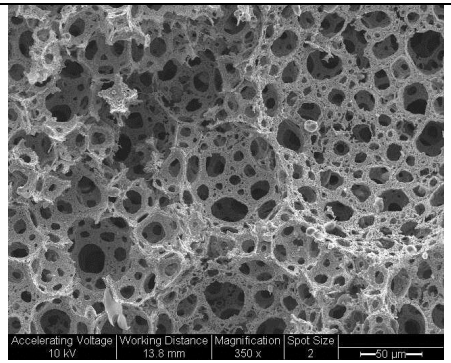

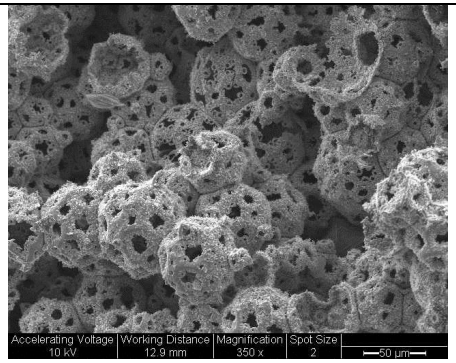

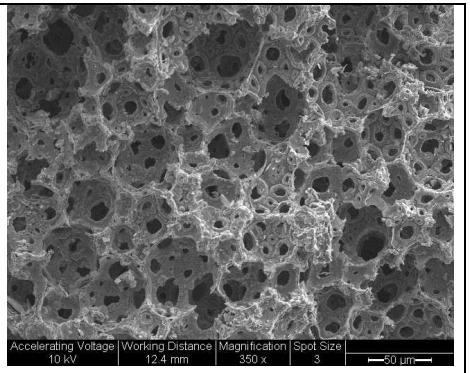

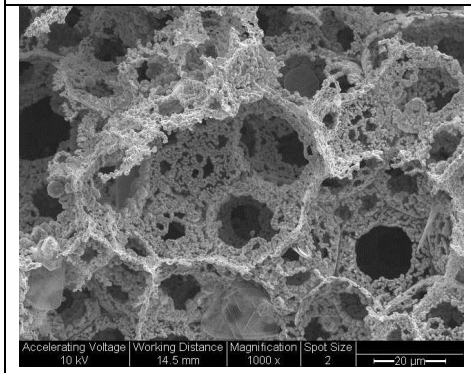

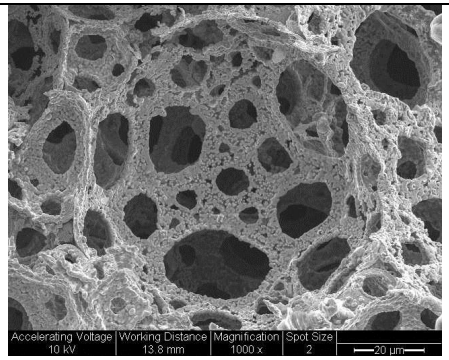

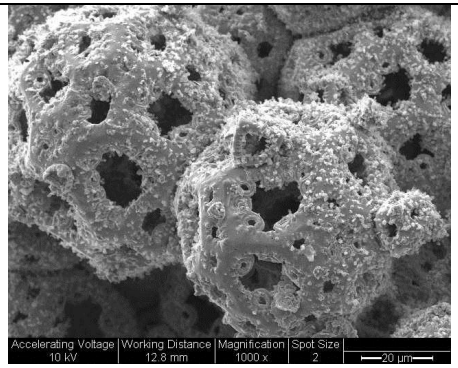

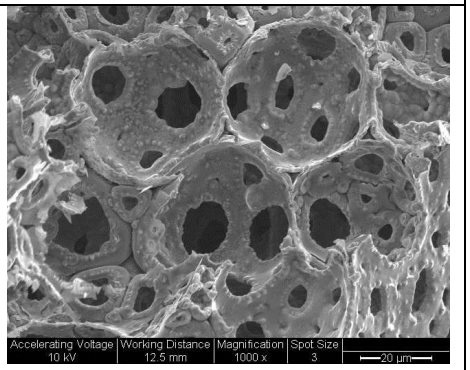

Continue next page

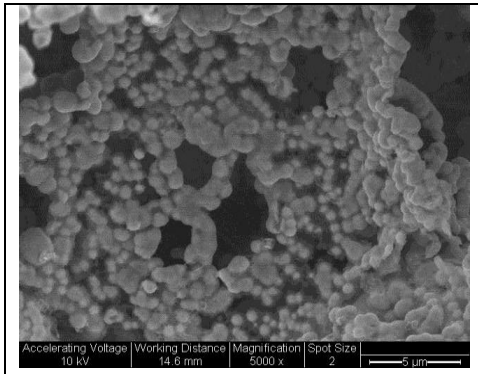
Accelerating Voltage
10 kV
Working Distance
14.6 mm
Magnification
5000 x
Spot Size
2
5 µm

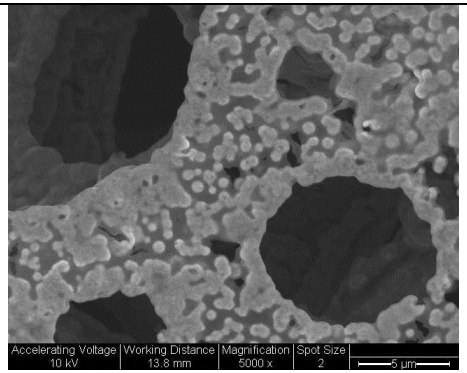
Accelerating Voltage
10 kV
Working Distance
13.8 mm
Magnification
5000 x
Spot Size
2
5 µm

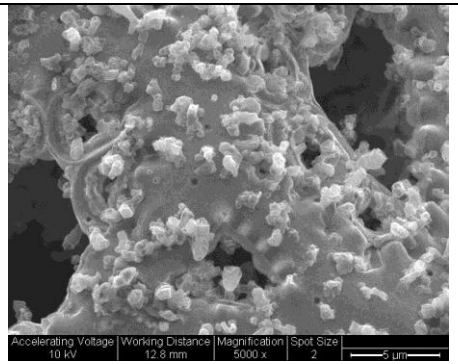
Accelerating Voltage
10 kV
Working Distance
12.8 mm
Magnification
5000 x
Spot Size
2
5 µm

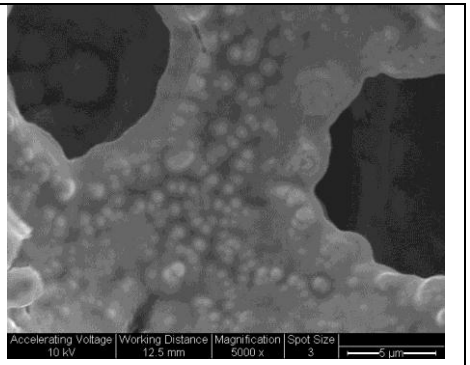
Accelerating Voltage
10 kV
Working Distance
12.5 mm
Magnification
5000 x
Spot Size
3
5 µm

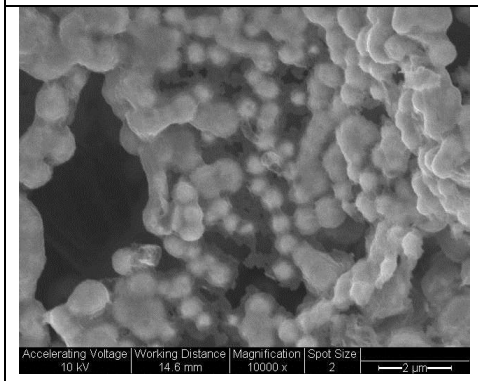
Accelerating Voltage
10 kV
Working Distance
14.6 mm
Magnification
10000 x
Spot Size
2
2 µm

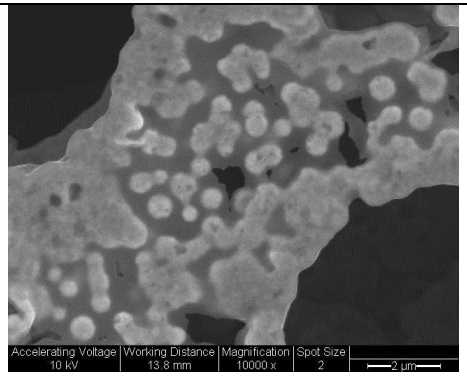
Accelerating Voltage
10 kV
Working Distance
13.8 mm
Magnification
10000 x
Spot Size
2
2 µm

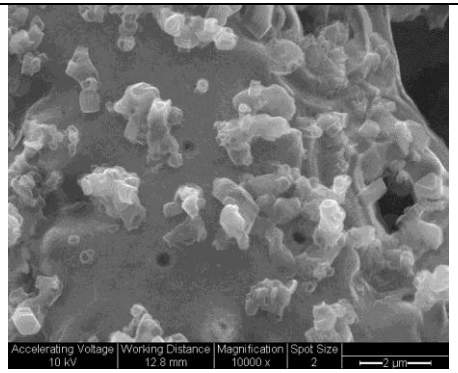
Accelerating Voltage
10 kV
Working Distance
12.8 mm
Magnification
10000 x
Spot Size
2
2 µm

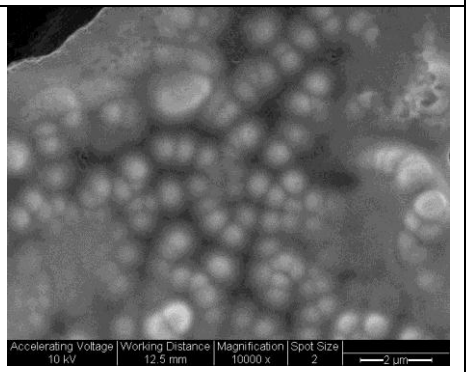
Accelerating Voltage
10 kV
Working Distance
12.5 mm
Magnification
10000 x
Spot Size
2
2 µm

SEM micrograph of Nylon Fibre as received

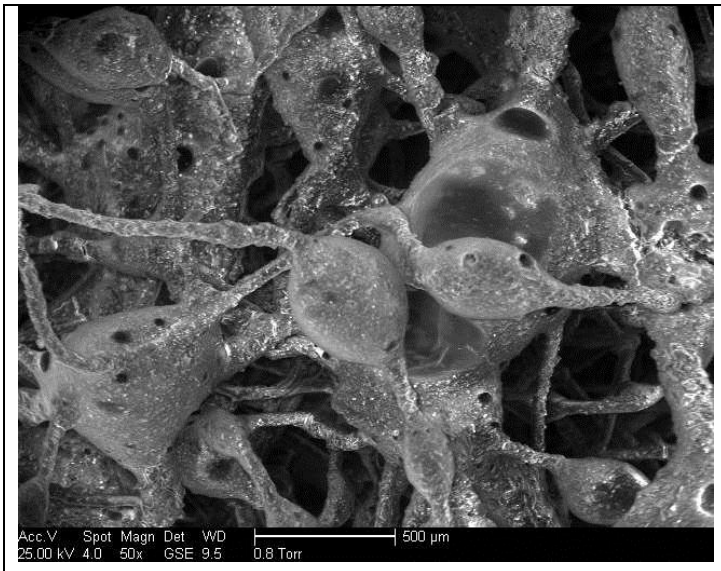

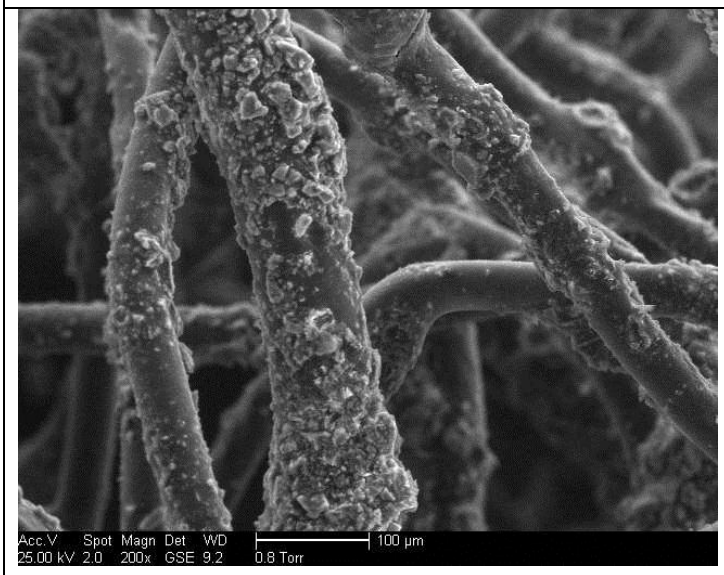

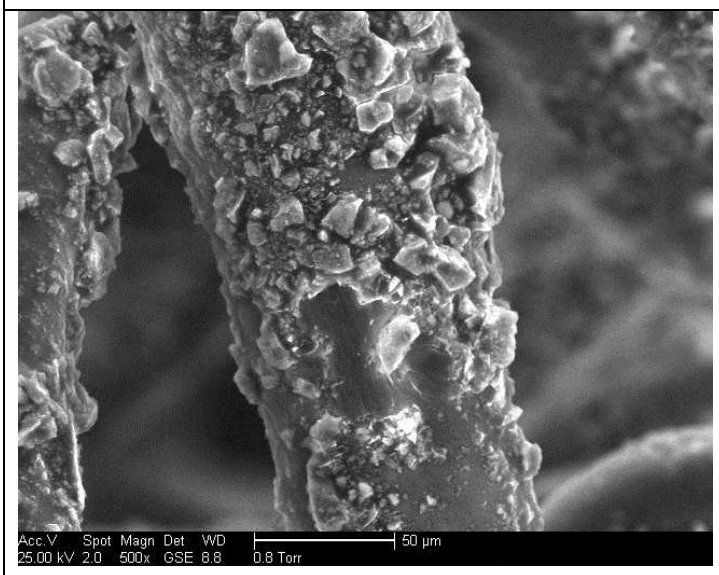

Continue next page

SEM micrograph of Nylon Fibre after heat

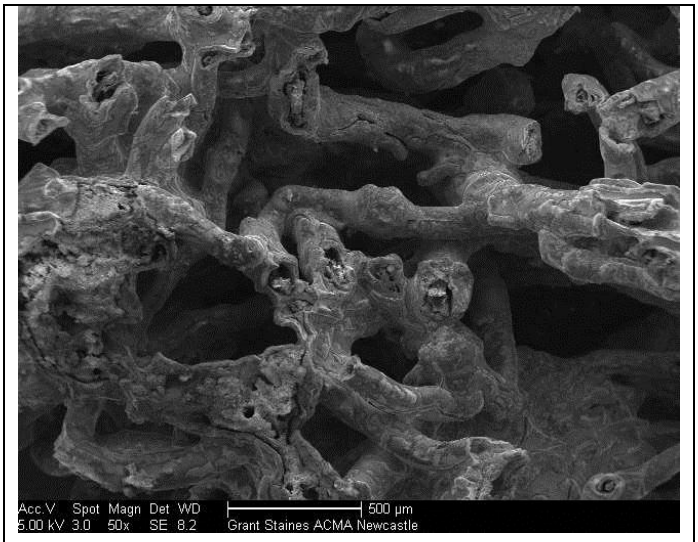

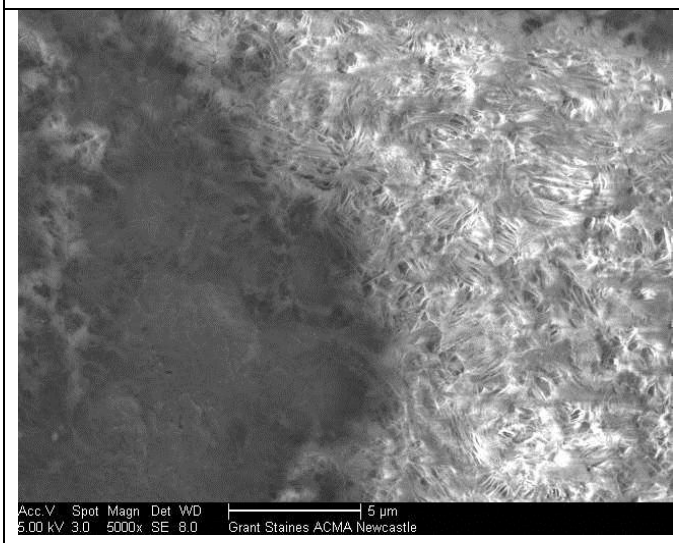

Continue next page

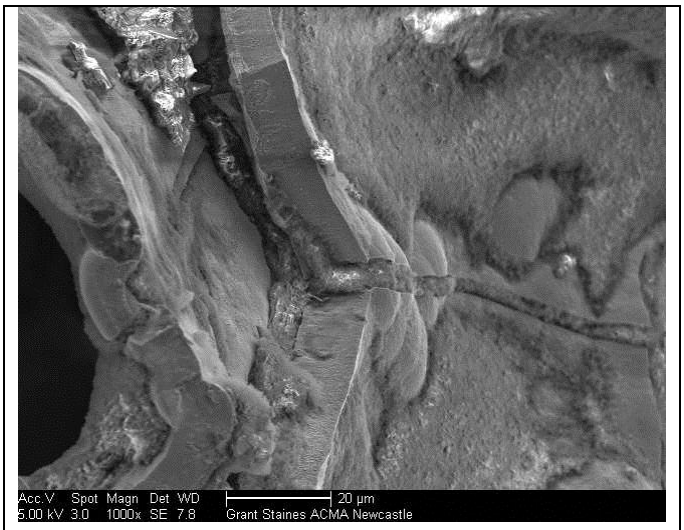

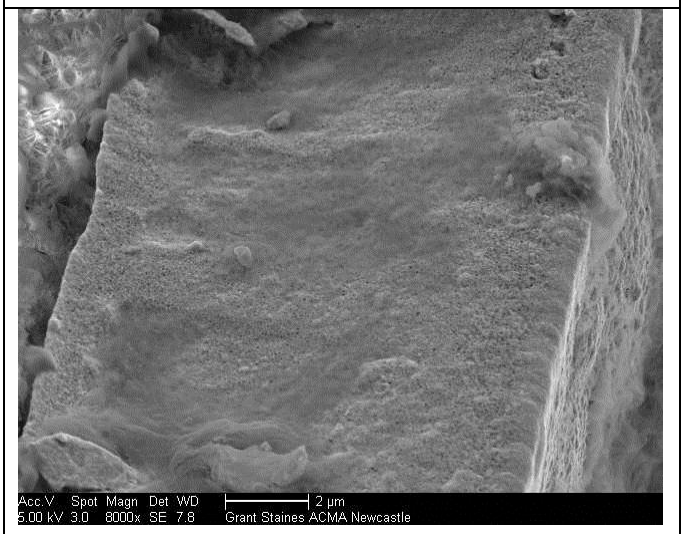

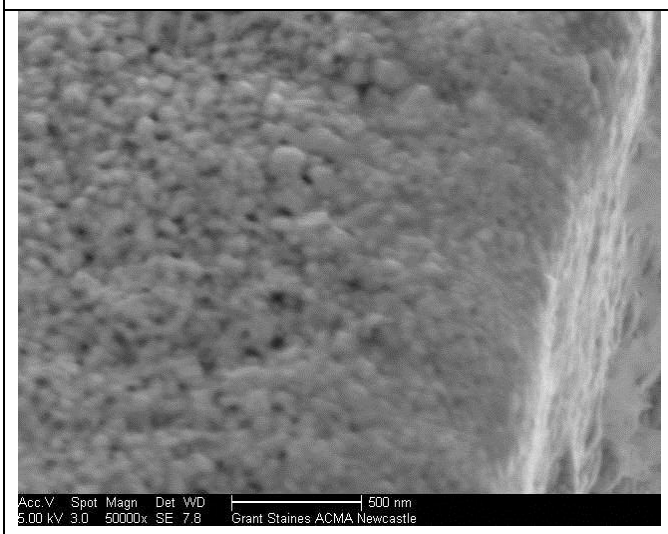

Continue next page

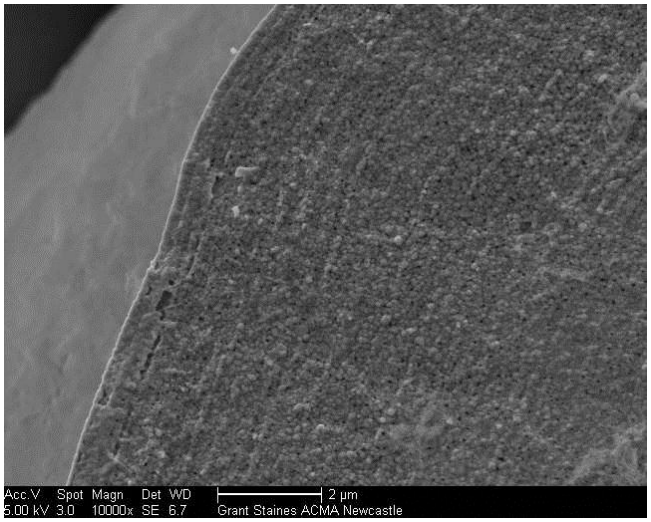
Acc.V. Spot Magn Det WD 2 µm
5.00 kV 3.0 10000x SE 6.7 Grant Staines ACMA Newcastle

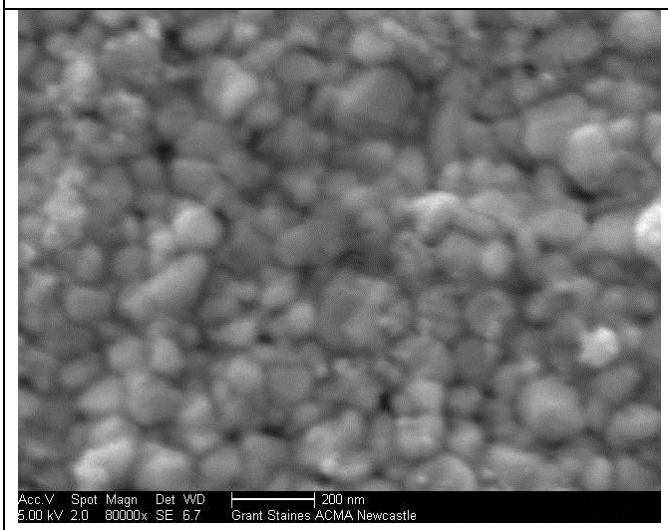
Acc.V. Spot Magn Det WD 200 nm
5.00 kV 2.0 80000x SE 6.7 Grant Staines ACMA Newcastle

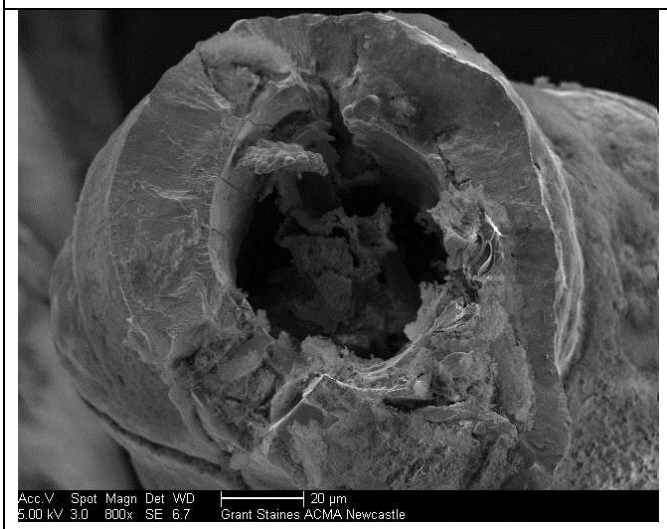
Acc.V. Spot Magn Det WD 20 µm
5.00 kV 3.0 800x SE 6.7 Grant Staines ACMA Newcastle

SEM micrograph of Carbon Felt as received

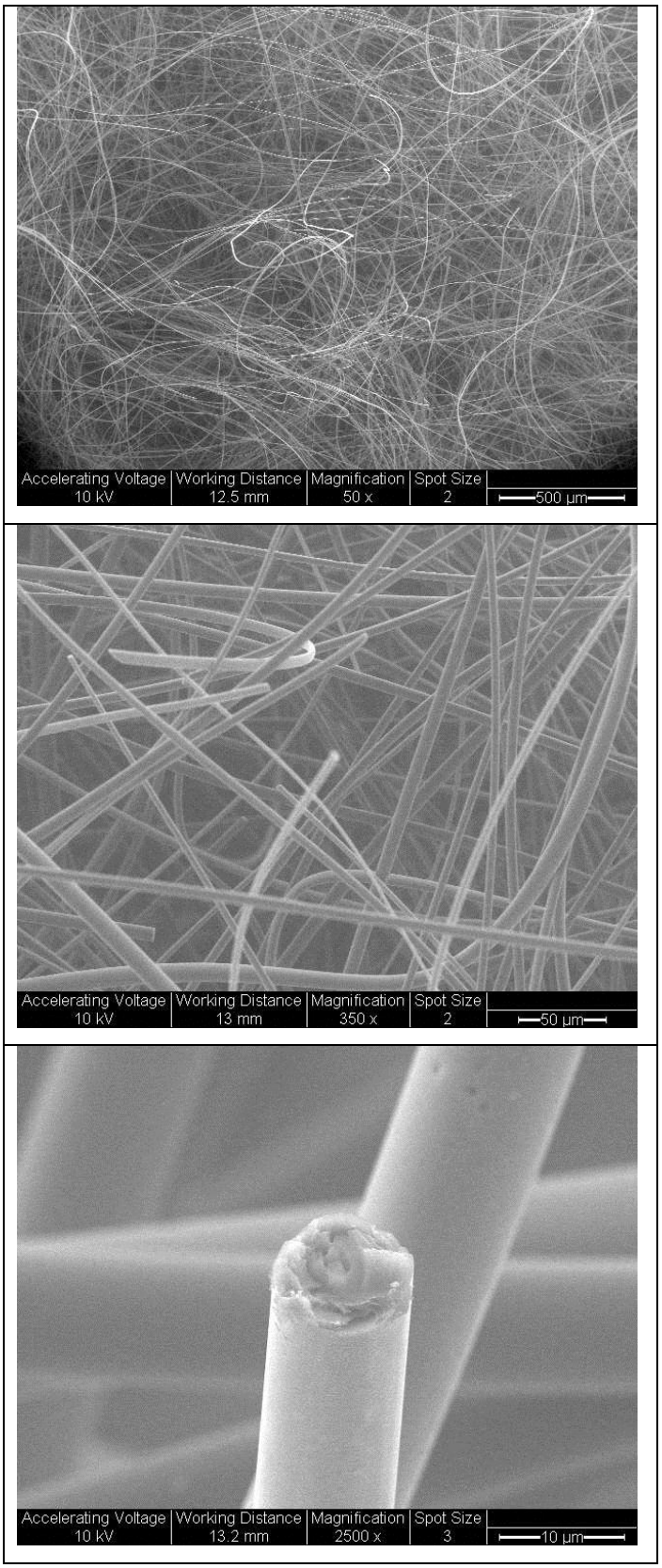

SEM micrograph of Carbon Felt as deposited condition

SEM micrograph of Carbon Felt after heat treatment

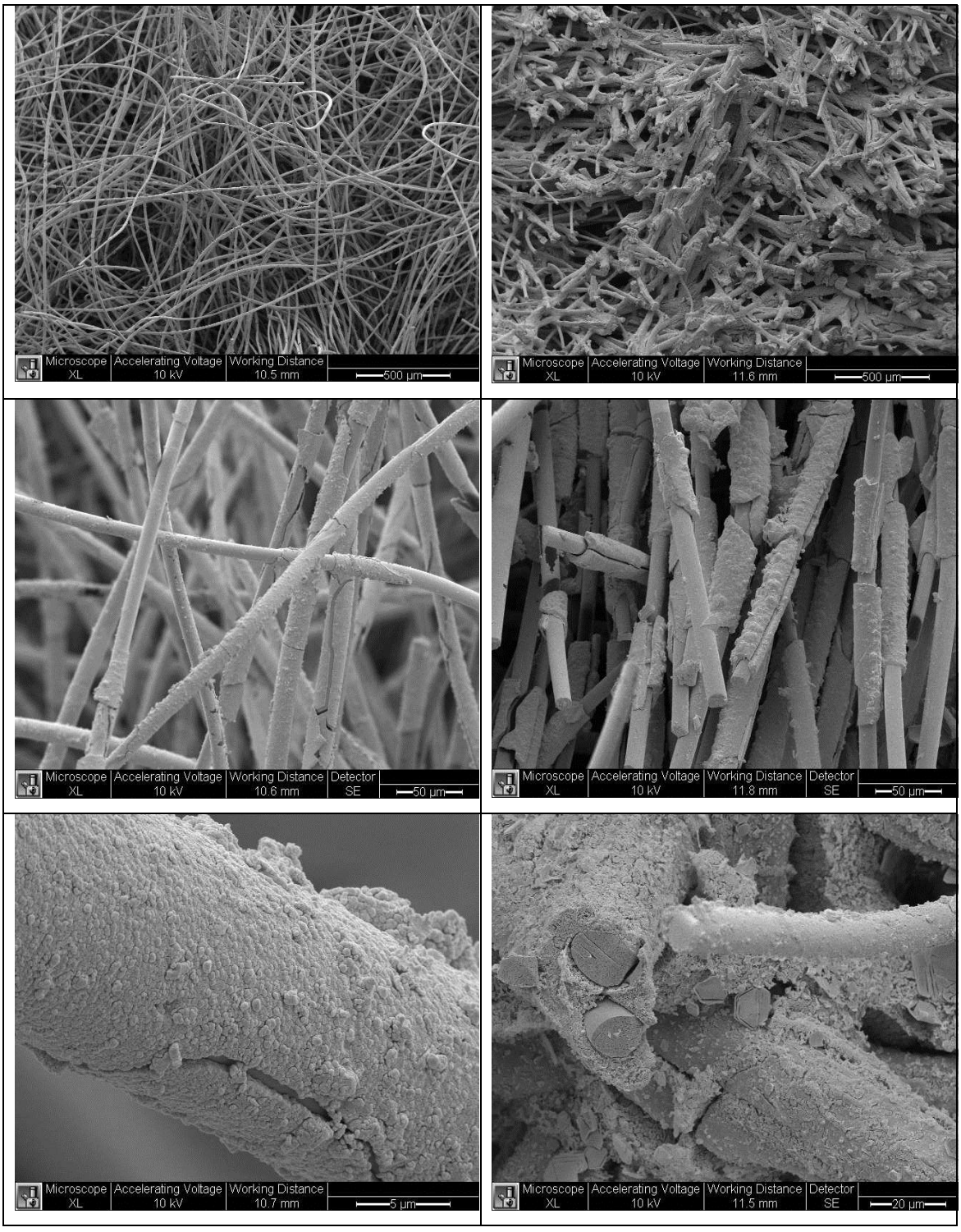

Continue next page

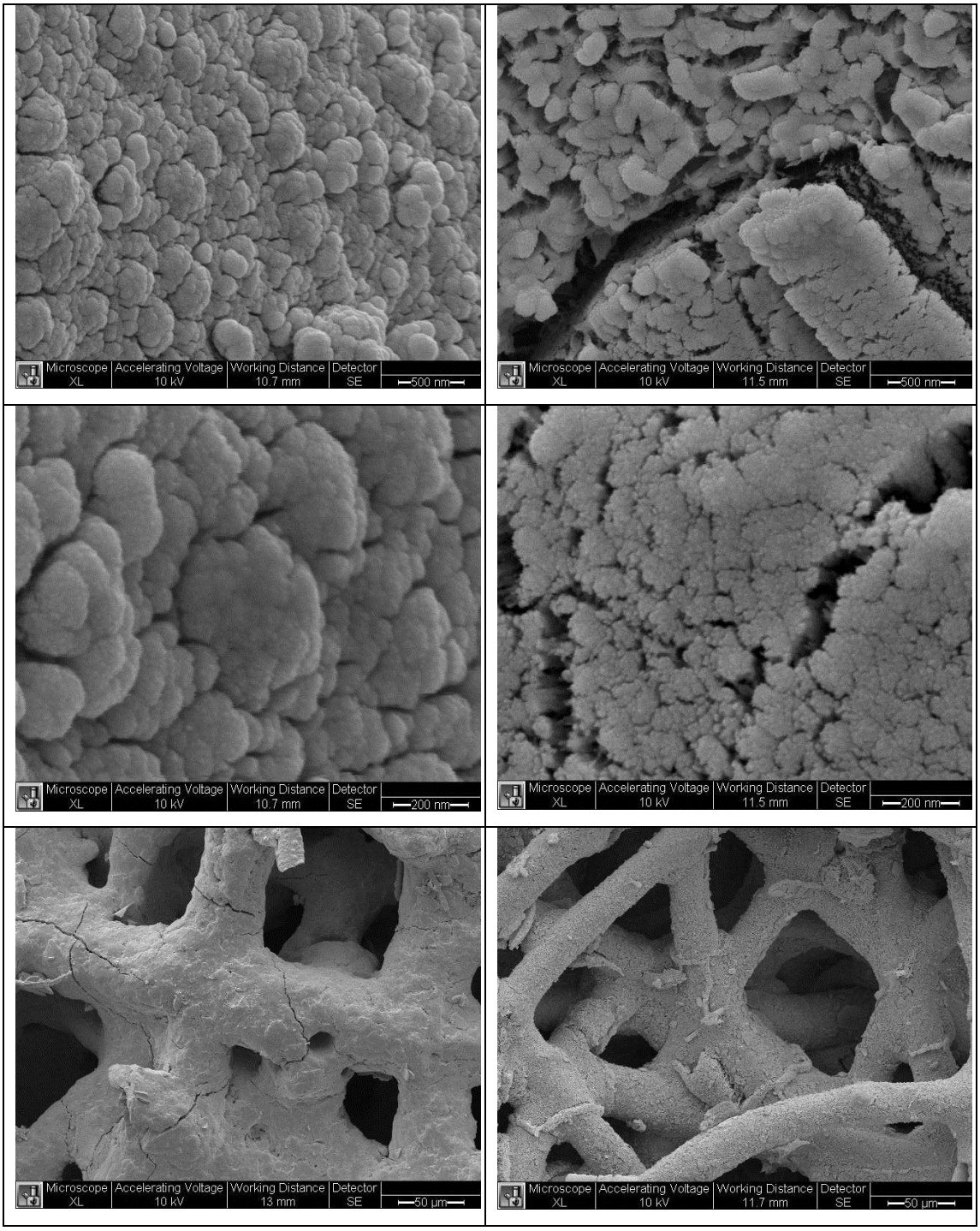

Continue next page

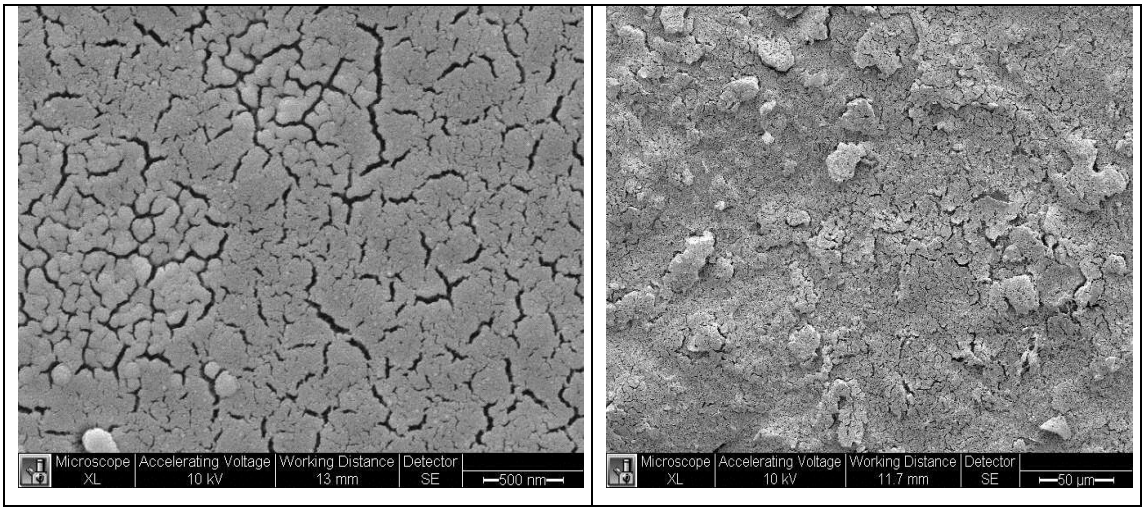

Glass Wool as Received

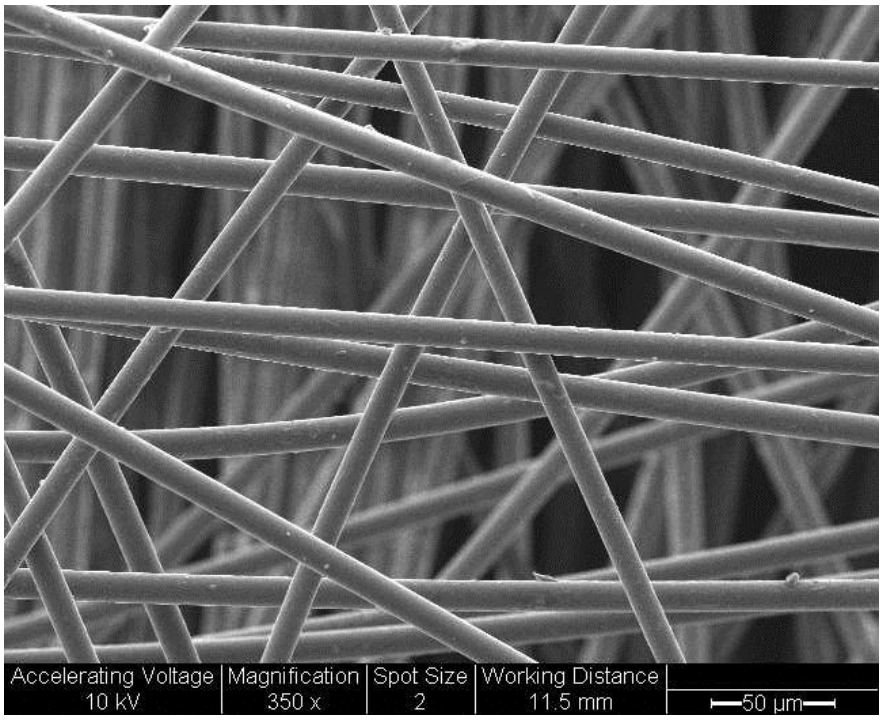

Glass Wool :non treated Ni-B deposition	Glass Wool :Silane treated in aqueous Ni-B deposition	Glass Wool :Silane treated in EtOH Ni-B deposition
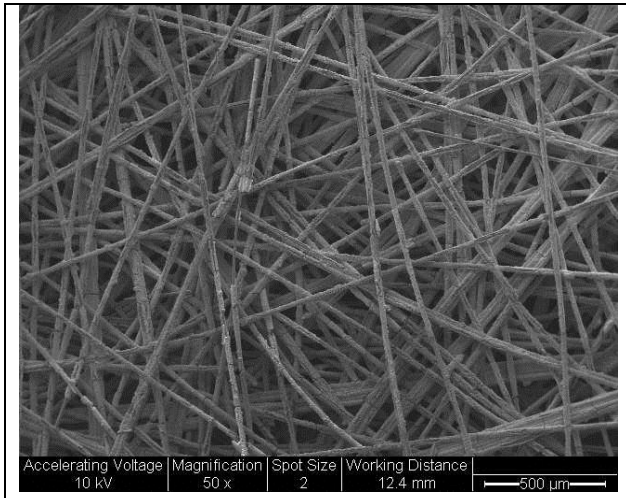	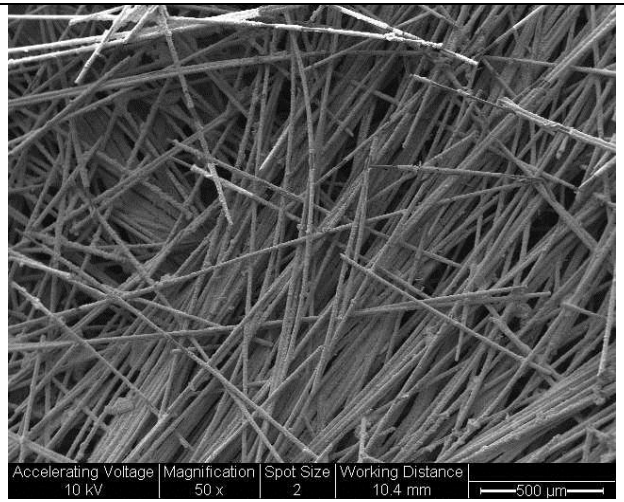	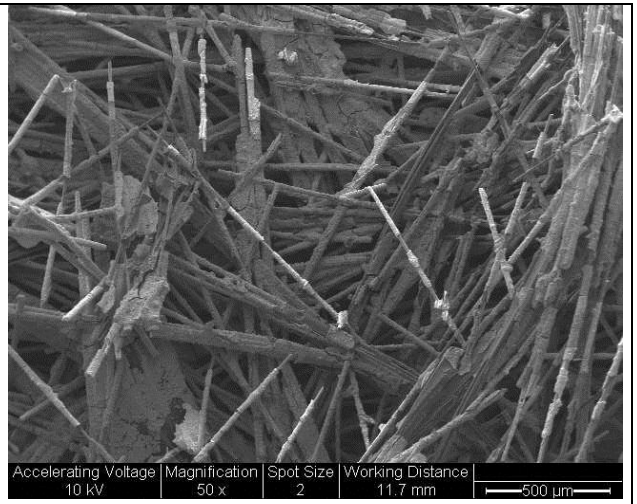
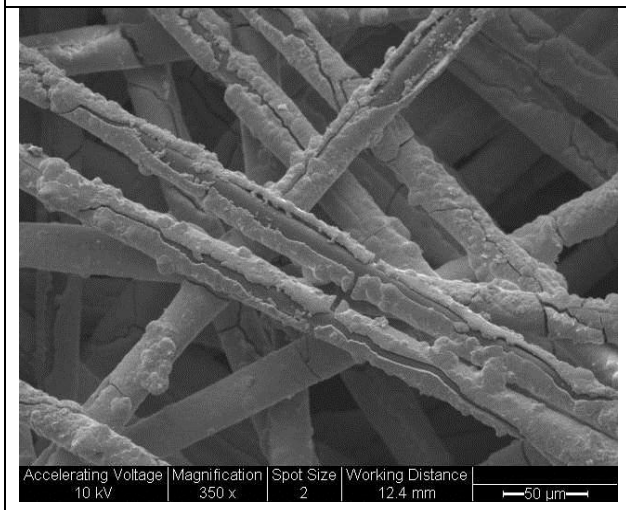	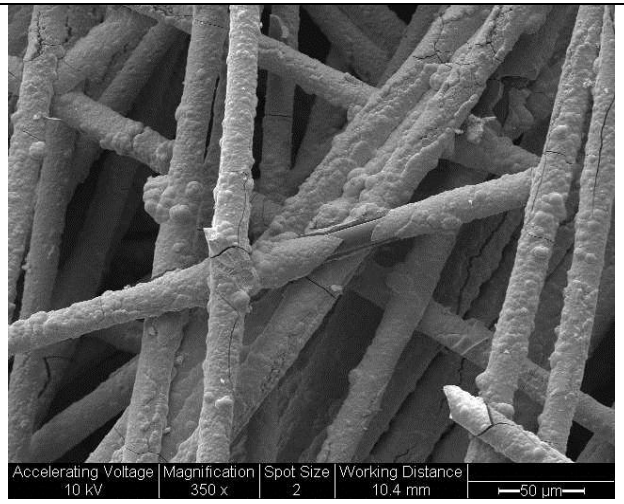	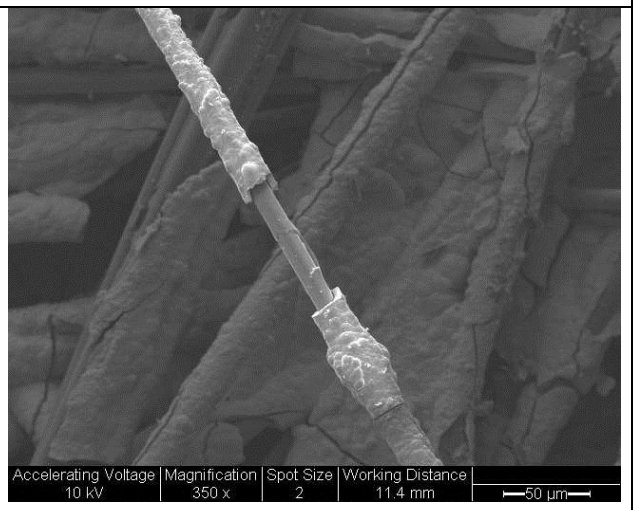

Continue next page

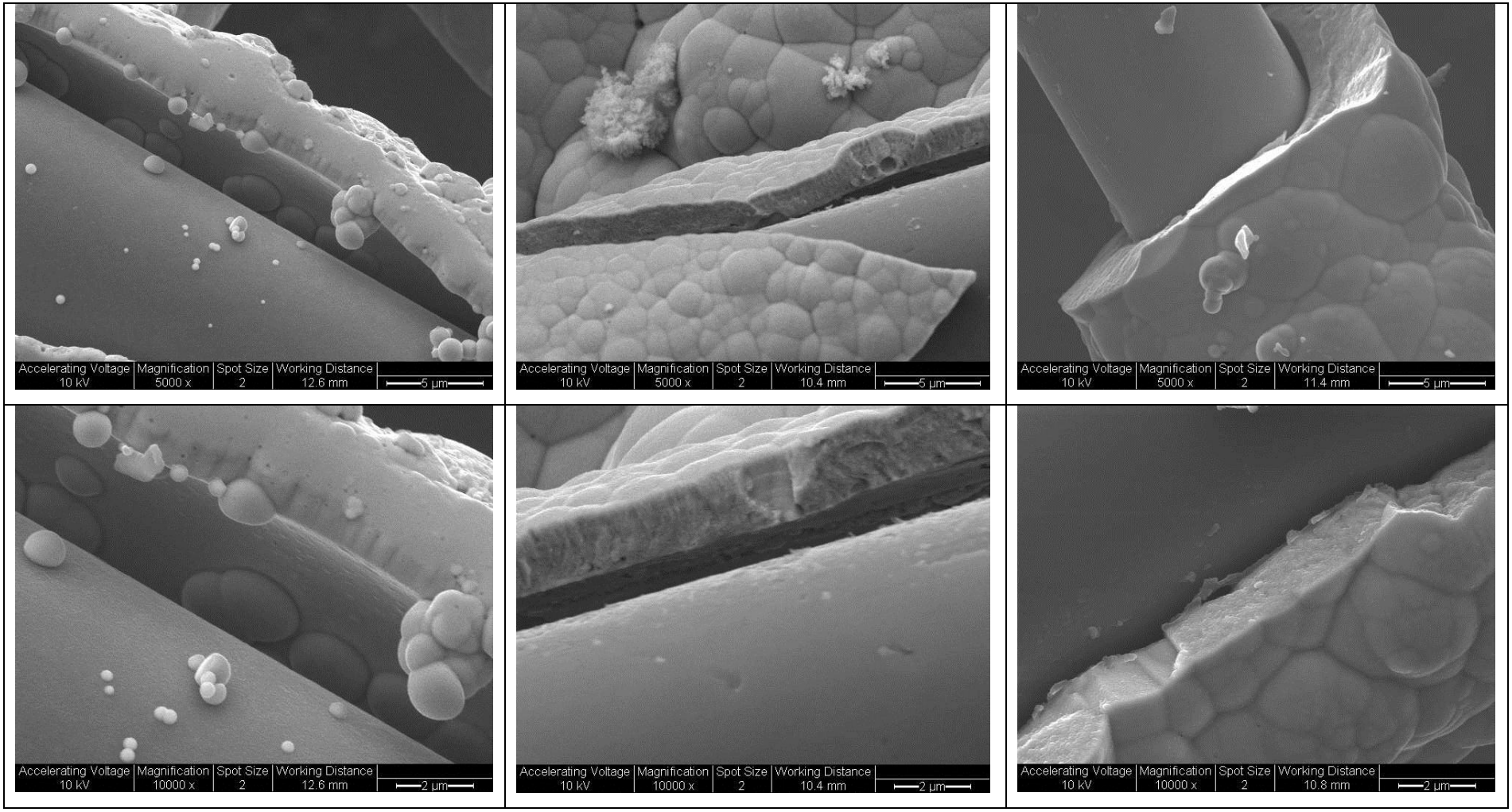

Continue next page

After heat treatment at 600°C

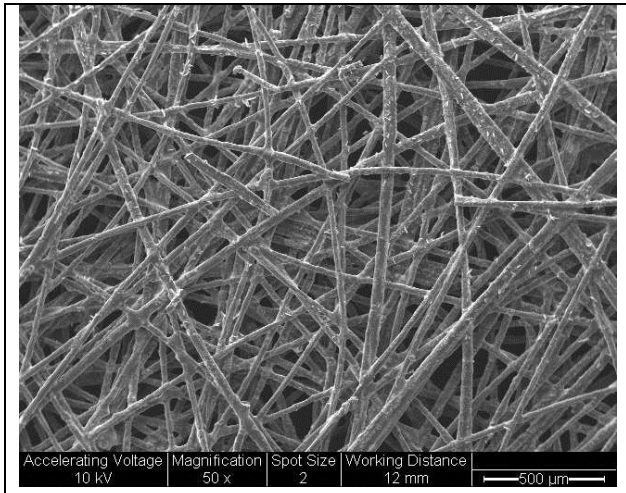

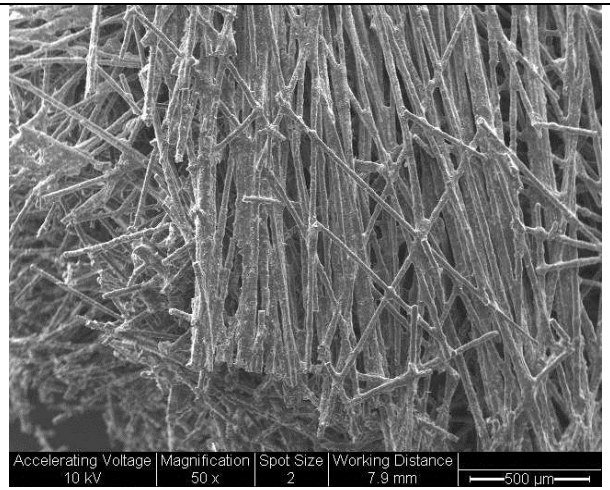

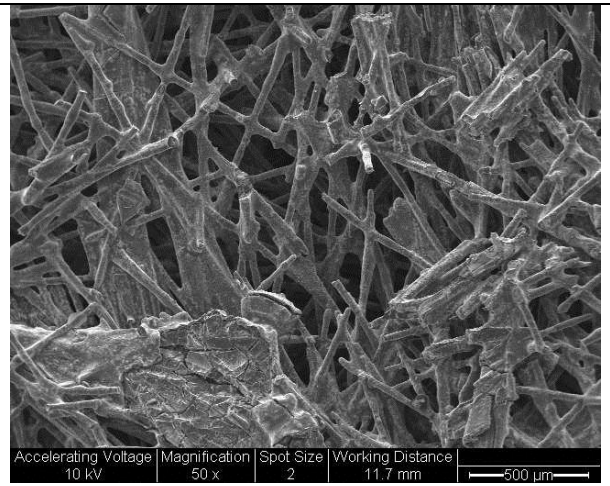

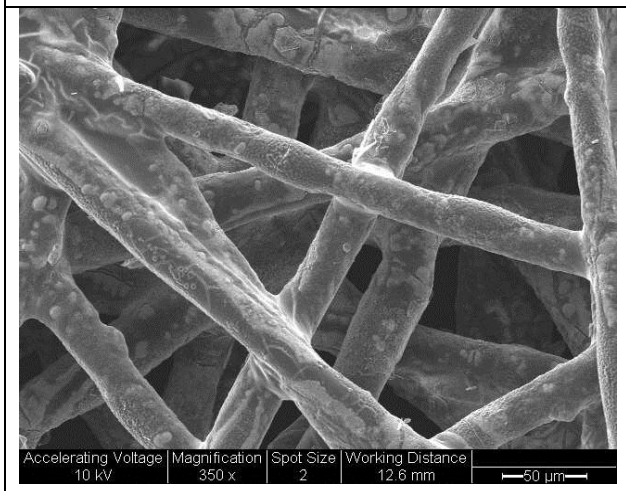

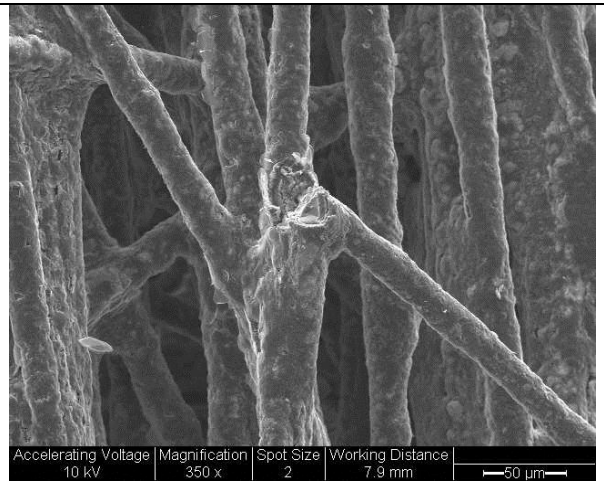

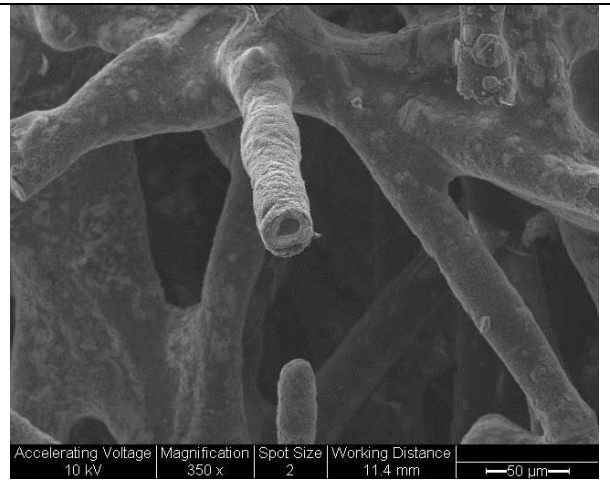

Continue next page

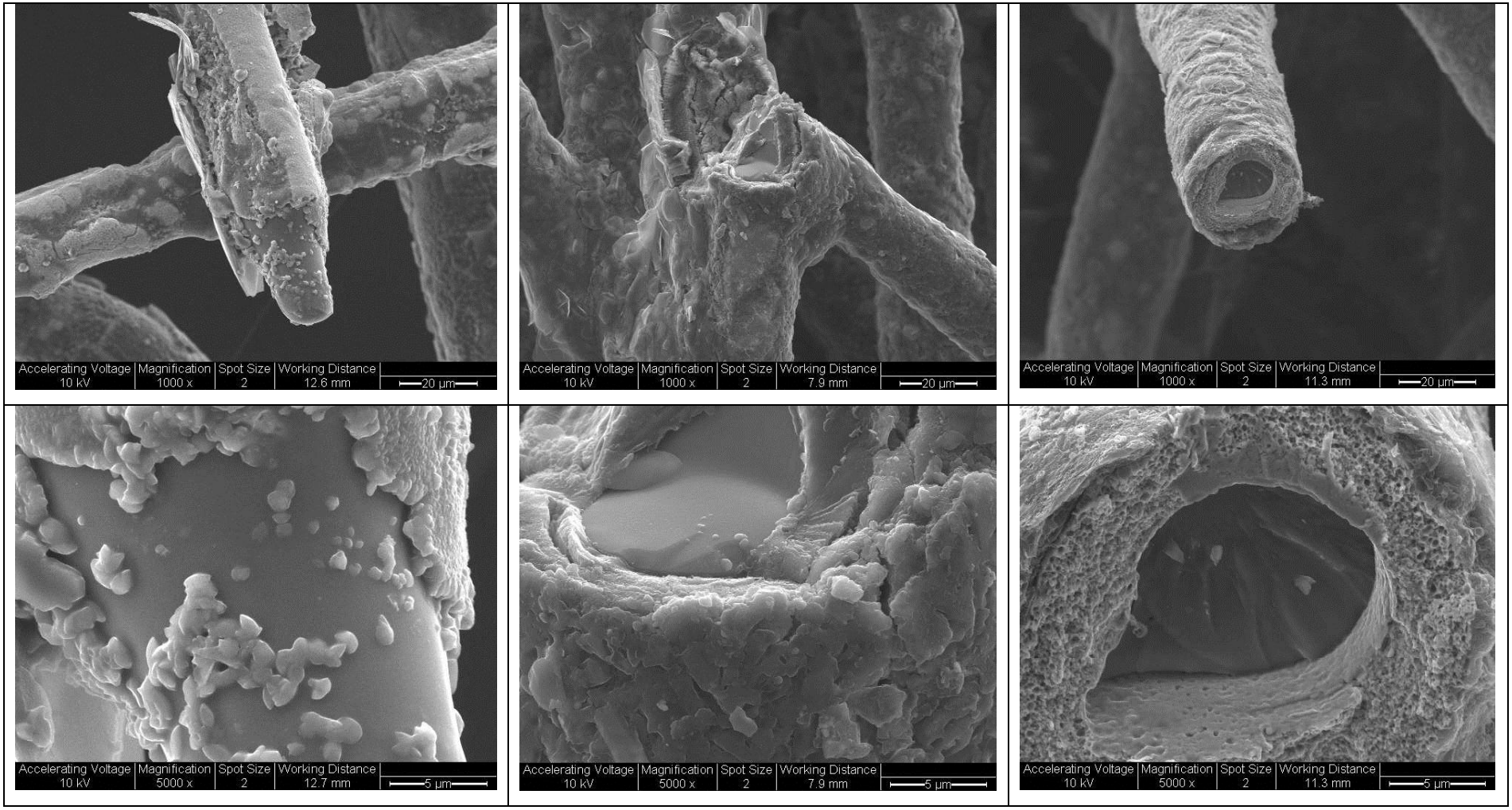

Continue next page

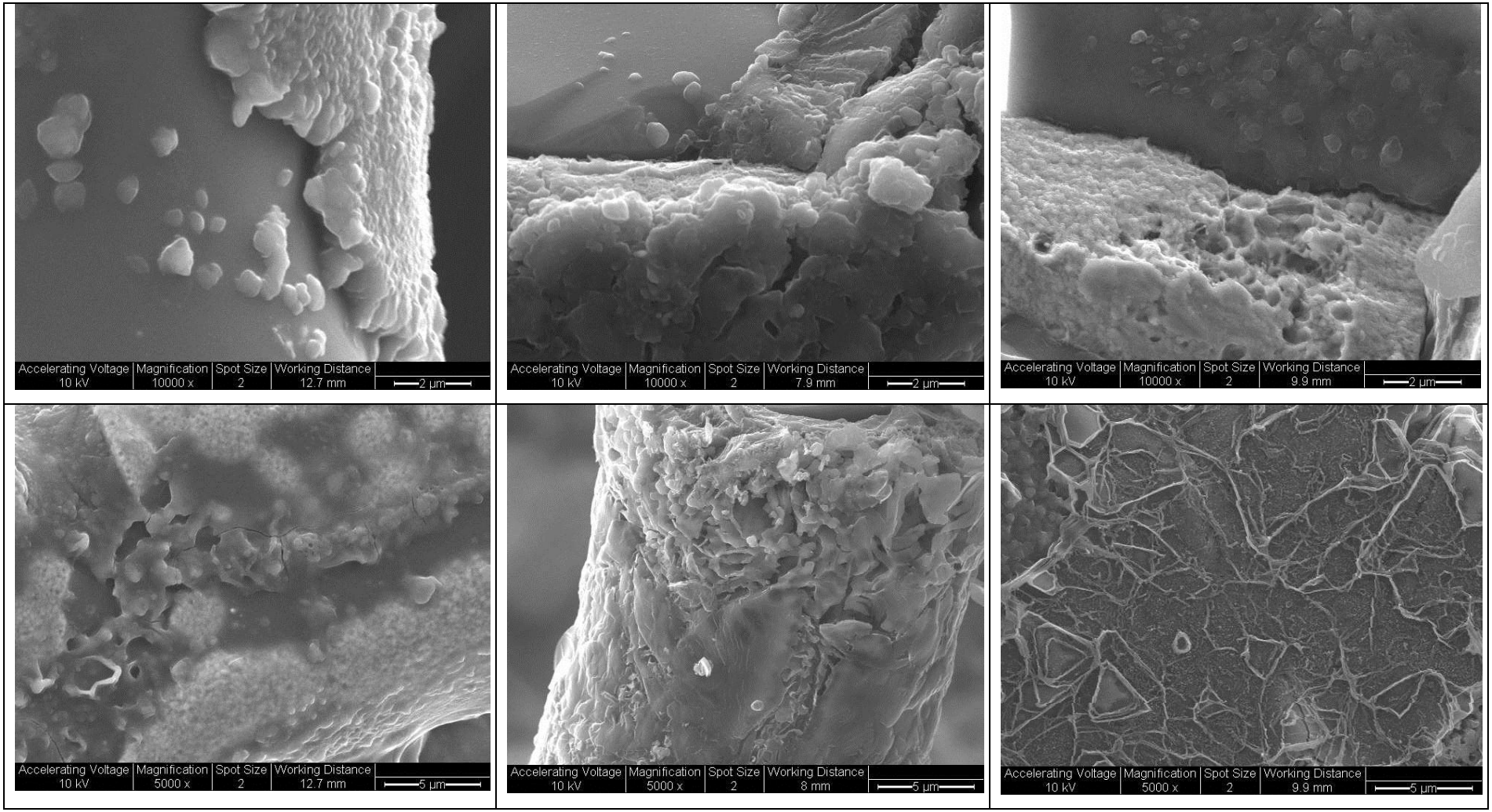
Accelerating Voltage
10 kV
Magnification
10000 x
Spot Size
2
Working Distance
12.7 mm
2 µm
Accelerating Voltage
10 kV
Magnification
10000 x
Spot Size
2
Working Distance
7.9 mm
2 µm
Accelerating Voltage
10 kV
Magnification
10000 x
Spot Size
2
Working Distance
9.9 mm
2 µm
Accelerating Voltage
10 kV
Magnification
5000 x
Spot Size
2
Working Distance
12.7 mm
5 µm
Accelerating Voltage
10 kV
Magnification
5000 x
Spot Size
2
Working Distance
8 mm
5 µm
Accelerating Voltage
10 kV
Magnification
5000 x
Spot Size
2
Working Distance
9.9 mm
5 µm